



HAL
open science

Ion specific effects on the self-assembly of cationic surfactants: experimental and computational approaches

Alla Malinenko

► **To cite this version:**

Alla Malinenko. Ion specific effects on the self-assembly of cationic surfactants: experimental and computational approaches. Chemical Physics [physics.chem-ph]. Université de Bordeaux, 2015. English. NNT: 2015BORD0065 . tel-01424142

HAL Id: tel-01424142

<https://theses.hal.science/tel-01424142>

Submitted on 2 Jan 2017

HAL is a multi-disciplinary open access archive for the deposit and dissemination of scientific research documents, whether they are published or not. The documents may come from teaching and research institutions in France or abroad, or from public or private research centers.

L'archive ouverte pluridisciplinaire **HAL**, est destinée au dépôt et à la diffusion de documents scientifiques de niveau recherche, publiés ou non, émanant des établissements d'enseignement et de recherche français ou étrangers, des laboratoires publics ou privés.

N° d'ordre :

THÈSE DE DOCTORAT

PRESENTEE A

UNIVERSITÉ DE BORDEAUX

ECOLE DOCTORALE DES SCIENCES CHIMIQUES

Par **Alla MALINENKO**

POUR OBTENIR LE GRADE DE

DOCTEUR

SPÉCIALITÉ : CHIMIE-PHYSIQUE

**Effet d'ion spécifique sur l'auto-assemblage d'amphiphiles cationiques :
des approches expérimentale et informatique**

**Ion specific effects on the self-assembly of cationic surfactants:
experimental and computational approaches**

Sous la direction de : Reiko ODA
(co-directeur : Sylvain NLATE)

Soutenue le : **12 mai 2015**

Membres du jury :

M. D. BASSANI Directeur de Recherche, CNRS, Université de Bordeaux
M. C. TRIBET Directeur de Recherche, CNRS, École Normale Supérieure de Paris
Mme. M. BLANZAT Chargée de Recherche, CNRS, Université Paul Sabatier de Toulouse
M. L. ROMSTED Professeur, Rutgers University
Mme R. ODA Directeur de Recherche, CNRS, Université de Bordeaux
M. S. NLATE Maître de Conférences, CNRS, Université de Bordeaux

Président
Rapporteur
Rapporteur
Examineur
Directrice de thèse
Co-directeur de thèse

- Acknowledgements -

These three years as a PhD student in Bordeaux were the greatest experience in my life filled with a variety of many interesting meetings and events. For the given opportunity to live unforgettable a life and scientific experience in a wonderful group I would like to thank my supervisor Reiko ODA. Thank you very much for being the driving force in my study, for leading me and even pushing when it was necessary during these three years of scientific research, for all your advises and bright ideas that made my work more interesting and versatile, for your great personality which made our international group a family. I would like to thank my co-supervisor Sylvain NLATE, who helped me to master organic synthesis and was ready to help with any questions.

This PhD thesis was created in Chimie et Biologie des Membranes et des Nanoobjets (CBMN). I would like to thank Erick DUFOURC, who is the director of the institute.

I am very grateful to all the members of the jury. I would like to thank Muriel BLANZAT and Christophe TRIBET who kindly agreed to be reviewers for this manuscript. I am also grateful to Dario BASSANI who took over the duties of the president of the jury; Larry ROMSTED who kindly agreed to be the member of jury for my thesis defense despite all the technical troubles which we had to meet and, of course, Michel LAGUERRE who was an invited member of the jury.

I would like express gratitude to all collaborators of this project who made a great contribution to this PhD helping me to combine different techniques and approaches. Especially, to Dario BASSANI who in addition to his great talent to explain and teach made each of our meetings cosy and friendly by his humor; Larry ROMSTED and his PhD student Changyao LIU who were patient in teaching me chemical trapping technique and always hospitable on the other side of the Atlantic; Michel LAGUERRE and Massimiliano PORRINI who helped me to get insight into the molecular dynamic simulations. Thank you Max for being not just a collaborator with who was nice to work, but also a good friend. I also would like to thank Stéphane MASSIP and Brice KAUFFMANN for deepening my knowledge and improving my skills in the crystallography experiments and Axelle GRELARD for being always ready to discuss and help with any questions concerning the NMR experiments.

I am happy to meet in our lab people who became my close friends and mentors. I would like separately to express my gratitude to Dima who to the end was following my work, giving me suggestions concerning the experiments and sharing his experience in writing. Also to Guillaume

- Acknowledgements -

who was always ready to help me in my research as well as my English; very often he was more excited about my results than me, it encouraged me not to give up even in hard times.

Moreover, I am thankful for the opportunity to play ping pong and relax by having very intense sets; for the all happy hours that we spent together in IECB with great food, drinks and nice company, alcohol always makes people closer. All that made my PhD life funnier, brighter and lovely.

At last but not at least I would like to thank all those with whom I was working with during these three years: Emilie POUGET, Dmitriy DEDOVETS, Jiaji CHENG, H el ene CARRIE, Guillaume LE SAUX, Alexandre CUNHA, Rajat Kumar DAS, Marie-Christine DURRIEU, Gregor KEMPER, Yutaka OKAZAKI, Laurent PLAWINSKI. Guys, each of you is a part of the great collective that made me happy to come to the lab every day. Thank you for all our talks and discussions, your advice, smiles, laugh and of course light, wonderful atmosphere at the working place.

I really appreciate the help and support of my friends and family during all my way. Thank you all. Благодарю тебя, любовь моя.

- Résumé -

La présente étude est une approche holistique axée sur l'étude des effets spécifiques d'ions sur les propriétés d'auto-assemblage d'agents tensioactifs cationiques. Nous avons étudié l'effet de divers contre-ions sur les caractéristiques d'auto-organisation de tensioactifs cationiques en solution aqueuse. Afin d'obtenir une meilleure compréhension de l'effet des interactions ioniques et moléculaires à l'interface sur les propriétés globales, nous avons utilisé des approches différentes. Nous avons combiné une étude expérimentale portée sur les propriétés en solution (concentration micellaire critique ou CMC, degré d'ionisation, nombre d'agrégation), avec des approches expérimentale (piégeage chimique) et informatique (simulations de dynamique moléculaire) centrées sur l'étude des propriétés à l'interface micelle – eau, en déterminant la concentration interfaciale des contre-ions et de l'eau. De plus, nous avons étudié l'impact de la nature du contre-ion sur la croissance des micelles par rhéologie. Enfin, outre l'examen des propriétés des tensioactifs en solution, les effets spécifiques d'ions sur les structures cristallines des agents tensioactifs gemini ont été étudiés.

Dans le premier Chapitre, nous présentons une étude bibliographique sur l'auto-assemblage de tensioactifs. En premier lieu, nous décrivons les molécules amphiphiles, leur classification et les forces motrices d'auto-assemblage. La description thermodynamique des processus de micellisation pour amphiphiles à une seule chaîne et amphiphiles gemini, avec un accent particulier sur les tensioactifs ioniques, est donnée. Afin d'élucider la façon dont les contre-ions de tensioactifs ioniques peuvent affecter leur micellisation, nous introduisons des effets ioniques spécifiques aussi appelés effets Hofmeister. Historiquement, il a pu être observé que les tentatives précédentes pour décrire les interactions impliquées dans ces phénomènes par des théories simplifiées ont leurs limites. Bien que de nouvelles forces impliquées dans l'effet ionique soient régulièrement décrites, il n'y a toujours pas de consensus quant aux les forces dominantes dans les effets ioniques spécifiques. Pour résumer les connaissances acquises à ce jour, il peut être dit qu'en plus des forces électrostatiques et de dispersion, les forces d'hydratation jouent un rôle important dans l'effet Hofmeister.

Dans le deuxième Chapitre, nous introduisons les gemini cationiques tensioactifs $C_{2}H_{4}-1,2-((CH_{3})_{2}N^{+}C_{10}H_{21})_{2}$ notée 10-2-10 gemini, et une série de contre-ions choisis pour cette étude. Pour étudier les effets spécifiques d'ions nous nous sommes concentrés sur les halogénures monoatomiques, anions inorganiques et alkyl carboxylate polyatomiques. Ici, nous donnons

également les procédures synthétiques utilisées pour obtenir 10-2-10 gemini avec les différents contre-ions.

Dans le troisième Chapitre, les propriétés physiques de la solution micellaire sont étudiées. On observe que la CMC, le degré d'ionisation et l'énergie libre de formation de micelles dépendent fortement de la nature du contre-ion et suivent la série de Hofmeister. Inversement, le nombre d'agrégation des micelles ne montre pas une dépendance importante par rapport au contre-ion. Pour les halogénures monoatomiques, une corrélation monotone entre les propriétés d'agrégation et les propriétés physiques des ions est observées. Ces propriétés sont leur taille, polarisabilité, énergie libre d'hydratation, le numéro de l'hydratation, pKa de l'acide conjugué et le nombre lyotrope. Des agents tensioactifs gemini associés à des contre-ions carboxylate d'alkyle montrent une diminution essentiellement linéaire de la CMC avec l'augmentation de la longueur de la chaîne. Ceci indique une formation d'agrégats plus favorable quand l'hydrophobicité de l'anion augmente. *A contrario*, les agents tensio-actifs avec des ions polyatomiques inorganiques ont un comportement plus complexe. Bien que toutes les propriétés ioniques influencent la CMC, l'énergie libre d'hydratation des ions a l'impact le plus clair sur la micellisation. De plus, considérant les propriétés hydrophile/hydrophobes intrinsèques des contre-ions, les surfactants associés aux ions plus hydrophobes, ayant donc un degré d'ionisation et une énergie libre d'hydratation plus faibles, favorisent la micellisation. L'inverse est constaté quand le surfactant est associé à un contre-ion plus hydrophile.

Nous avons également démontré qu'en changeant les propriétés de la tête cationique, il est possible d'influencer significativement l'ordre de la série de Hofmeister et donc les interactions responsables des effets ioniques spécifiques. Nos résultats préliminaires ont montré que, pour un gemini où le méthyle du groupe de tête est substitué par un proton, l'effet Hofmeister peut être inversé.

Afin d'obtenir une meilleure compréhension des propriétés des agrégats, les propriétés interfaciales des micelles formées ont été caractérisées en couplant une approche expérimentale avec des simulations numériques, permettant ainsi d'étudier la nature de l'interaction des contre-ions avec les macromolécules.

Le Chapitre IV décrit l'étude expérimentale des propriétés interfaciales des micelles effectuées par une technique appelée piégeage chimique. Cette méthode permet d'estimer les concentrations du contre-ion et de l'eau à l'interface micellaire. Les résultats obtenus ont démontré

que contre-ions hydrophobes et donc moins solvatés sont fortement associés avec le groupe de tête et sont situés principalement dans la région interfaciale de la micelle. D'autre part, la concentration interfaciale d'ions plus solvatés est faible et indique un plus faible degré d'interaction entre le groupe de tête le contre-ion. Ces résultats sont en bon accord avec les propriétés physiques micellaires en solution et corrèlent avec la série de Hofmeister.

Dans le cinquième Chapitre, nous introduisons une approche numérique basée sur des simulations de dynamique moléculaire (DM) afin de caractériser l'effet de la nature de l'anion sur les propriétés structurales des micelles à l'échelle atomique. Tout d'abord, les simulations de DM ont été utilisées pour enquêter sur les propriétés interfaciales des micelles en parallèle avec les expériences de piégeage chimique citées précédemment. Les résultats ont montré une bonne concordance entre les simulations et les résultats expérimentaux, les ions hydrophobes ayant tendance à s'associer fortement avec la micelle et étant principalement situés à proximité des groupes de tête, formant ainsi des paires ioniques de contact. Contre-ions hydrophiles, ayant une association plus forte avec l'eau, interagissent moins avec des groupes de tête de la micelle. En outre, il a été constaté que le contre-ion affecte les propriétés structurales des micelles, telles que la compacité, la rugosité et la sphéricité. Les simulations ont démontré que les anions hydrophobes favorisent la compacité et la sphéricité de la micelle, la stabilisant et diminuant sa rugosité. Ceci contraste avec les anions hydrophiles qui induisent une plus faible compacité micellaire et moins de stabilité. De plus, nous avons clairement montré un début de pénétration du cœur hydrophobe de la micelle par les contre-ions carboxylate d'alkyle de chaîne hydrophobe plus longue, augmentant ainsi le volume de la micelle. Il est intéressant de noter que même si la polarisabilité des ions n'a pas été considérée dans les simulations de DM, les résultats obtenus sont en bon accord avec les observations expérimentales.

Dans le Chapitre VI, les effets spécifiques d'ions dans des systèmes plus complexes ont été étudiés. Jusqu'à présent le système étudié était des micelles sphériques. Cependant avec l'augmentation de la concentration en agent tensio-actif, des micelles filandreuses enchevêtrées peuvent être formées. La viscosité augmente drastiquement à cette concentration, et rend donc possible l'étude par rhéologie des propriétés mécaniques des solutions contenant ces micelles filandreuses. Il a été montré que la nature des contre-ions affecte fortement la croissance micellaire et présente une tendance semblable à ce qui a été montré pour des micelles sphériques, suivant ainsi la série de Hofmeister. En raison de leur association avec les groupes de tête, les contre-

hydrophobes écrantent la charge micellaire et favorisent leur croissance, alors que les ions hydrophiles écrantent la charge micellaire dans une moindre mesure, induisant une croissance filandreuse à des concentrations beaucoup plus élevées. Identiquement à la CMC, l'augmentation observée de la viscosité du système qui est imputée à la croissance des micelles filandreuses, concorde bien avec l'énergie libre d'hydratation de l'anion.

Les effets spécifiques d'ions sur les propriétés d'auto-assemblage de tensioactifs gemini examinés jusqu'ici ont été faits en solution. Il était donc intéressant d'aller plus loin et d'étudier l'effet des contre-ions sur le processus la cristallisation des systèmes gemini/contre-ion.

Le Chapitre final décrit l'impact de la nature du contre-ion sur les structures cristallines de tensioactifs gemini. Il a été constaté que contrairement ce qui a été observé en solution aqueuse où l'hydratation de l'anion joue un rôle primordial, les anions ayant un rayon plus petit s'associent plus fortement avec les groupes de tête cationiques. Les résultats diamétralement opposés pour un même système, qu'il soit en solution ou à l'état solide démontrent l'importance des interactions ion-eau sur les effets spécifiques des ions.

En résumé, utilisant différentes approches, il a pu être montré les effets ionique spécifiques d'ions qui influencent le comportement des agrégats micellaires dans des solutions aqueuses, dépendent fortement de l'énergie libre d'hydratation des contre-ions. En d'autres termes, sur leurs propriétés hydrophiles/hydrophobes. Il est notable que la polarisabilité des ions, qui fournit des informations sur les forces de dispersion, et donc sur la spécificité ionique, semble moins bien concorder avec les propriétés d'agrégation. En revanche, nous observons une très bonne corrélation entre l'énergie libre d'hydratation de l'ion et les propriétés des agrégats de tensioactifs. Ces résultats suggèrent fortement que l'énergie libre d'hydratation d'ions peut fournir des informations sur les effets spécifiques d'ions en solution aqueuse. Cependant, il faut noter que les propriétés du substrat (gemini dans notre cas) doivent être prises en compte non moins rigoureusement afin de prédire entièrement les effets Hofmeister.

Mots-clés: effets spécifiques d'ions, d'auto-assemblage, tensioactifs gemini, micellisation, propriétés interfaciales, piégeage chimique, simulations de dynamique moléculaire, rhéologie, micelles, structure cristalline.

- Abstract -

The present study is a holistic approach focused on the investigation of ion specific effects on the self-assembly properties of cationic surfactants. We studied the effect of various counterions on the self-organization features of cationic surfactants in aqueous solution. In order to obtain a more comprehensive understanding of the effect of interfacial ionic and molecular interactions on aggregate properties we used different approaches. We combined an experimental study focused on the bulk solution properties (critical micelle concentration or CMC, ionization degree, aggregation number, etc.), experimental (chemical trapping) and computational (molecular dynamic simulations) approaches focused on investigating the interfacial micellar properties by analyzing the interfacial counterion and water concentrations. Moreover, the impact of counterion nature was investigated studying the growth of wormlike micelles using rheology. Besides the examination of the surfactants properties in solution, the ion specific effects on the crystalline structures of gemini surfactants were studied.

In the first Chapter we present a bibliographic study of the self-assembly of surfactants. At the beginning we introduce amphiphilic molecules, their classification and forces driving their self-assembly. The thermodynamic description of micellization process for single chain and gemini amphiphiles with particular emphasis on ionic surfactants is given. In order to elucidate how counterions of the ionic surfactants can affect their micellization, we introduce ion specific effects also known as Hofmeister effects. Following the history we can see how all previous attempts to describe the interactions involved in these phenomena by simplified theories have their limitations. Introducing new forces that might be responsible for the ion specificity was done at almost every decade, however there is still no general agreement as to which forces and ion properties drive the ion specific effects. Summarizing all knowledge obtained so far, we can say that in addition to electrostatic and dispersion forces, one should also take into account the hydration forces that play a significant role in ion specificity.

In the second Chapter we introduce the cationic gemini surfactants $C_2H_4-1,2-((CH_3)_2N^+C_{10}H_{21})_2$ denoted as 10-2-10, and a variety of counterions chosen for this study. To investigate the ion specific effects we focused on the monoatomic halides, polyatomic inorganic and alkyl carboxylate anions. Here we also give the synthetic procedures used to obtain 10-2-10 gemini with different of counterions.

In the third Chapter, the physical properties of the micellar solution are studied. It was observed that the CMC, ionization degree and free energy of micellization of the surfactants strongly depend on the counterion nature and follow the Hofmeister series. Conversely, the aggregation number of the micelles did not show a significant dependence on the counterion. We found that for monoatomic halides, the obtained properties of aggregation correlate monotonously with the physical properties of the ions such as size, polarizability, hydration free energy, hydration number, pKa of conjugated acid and lyotropic number. Gemini surfactants associated with alkyl carboxylate counterions primarily show a linear decrease in CMC with increasing chain length, indicating that with increasing hydrophobicity of the anion, aggregate formation is more favorable. On the contrary, the surfactants with polyatomic inorganic ions have a more complex behavior. We found that all properties of the ion influence the CMC values; however, the hydration free energy of the ions has the most obvious impact on the micellization behavior. Moreover, classifying anions according to their hydrophobic/hydrophilic properties, we see that: surfactants associated with more hydrophobic counterions, thus having lower ionization degree and free energy of micellization, favor surfactant micellization. Whereas surfactants with hydrophilic counterions, characterized by a high ionization degree and free energy of micellization, disfavor the formation of aggregates.

We also demonstrated that by changing the properties of the headgroup, we can significantly affect the order of Hofmeister series and hence the interactions responsible for ion specific effects. Our preliminary results showed that increasing the hardness of the cationic headgroup for gemini by replacement of one methyl by a proton, we could reverse the Hofmeister effects.

To obtain a better understanding of the properties of aggregates, the interfacial properties of the formed micelles were characterized using experimental and computation approaches. This gave us access to the information about direct interaction of ions with macromolecules.

Chapter IV describes the experimental study of the interfacial properties of the micelles done by a probing technique called chemical trapping. This method allows to estimate the ion and water concentrations within the micellar interface. The obtained results demonstrated that poorly hydrated counterions are strongly associated with the headgroup and are located primary in the interfacial region of the micelle. On the other hand, interfacial concentration of highly hydrated ions is low and indicates a low degree of counterion-headgroup binding. These results are in a good agreement with investigated micellar physical properties in bulk solution and all correlate with Hofmeister series.

In the fifth Chapter we introduce a computational approach based on molecular dynamic (MD) simulations applied to characterize the effect of anion nature on the structural properties of the micelles at the atomic level. Foremost, the MD simulations were used as computational approach to investigate interfacial properties of the micelles in parallel with experimental chemical trapping. We found that the obtained simulations are coherent with the experimental results: the hydrophobic ions tend to associate strongly with the micelle and are primarily located in the vicinity of the headgroups forming contact ion pairs. Hydrophilic counterions, having a stronger association with water, interact less with headgroups of the micelle. Furthermore, it was found that counterion nature affects the structural properties of the micelles, such as compactness, roughness and sphericity. MD simulations demonstrated that hydrophobic anions promote the compactness and sphericity of the micelle stabilizing it and decreasing its roughness. At the same time, micelles with hydrophilic anions are characterized by lower compactness and stability. Moreover, we clearly showed that alkyl carboxylate counterions with increasing chain length start to penetrate micellar hydrophobic core thereby increasing the volume of the micelle. It is interesting to note that although the polarizability of the ions was not considered in the MD simulations, obtained results are in a good agreement with experimental observations.

In Chapter VI, the ion specific effects in a system of higher complexity were studied. Until now our study was focused on spherical micelles. However with increasing surfactant concentration, large entangled wormlike micelles can be formed. Because there is a significant change in viscosity at this concentration, rheological study can be used to examine the mechanical properties of solutions containing wormlike micelles. It was shown that the nature of the counterions strongly affects the micellar growth and exhibits a similar tendency to what was shown for spherical micelles, thus following Hofmeister series. Due to their association with the headgroups, the hydrophobic counterions screen the micellar charge and favor their growth, whereas hydrophilic ions screen micellar charge to a lower extent and exhibit micellar growth at much higher concentrations. Similarly to the CMC, the observed increase in viscosity of the system, attributed to micellar growth, correlated with the hydration free energy of the anion.

The ion specific effects on the self-assembly properties of gemini surfactants discussed so far was examined in aqueous solutions. However our interest went further and we investigated the effect of counterions on the assembly process in crystals.

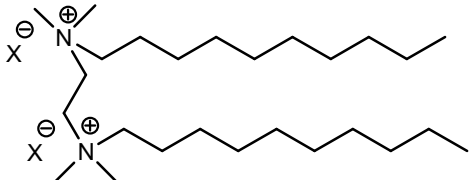
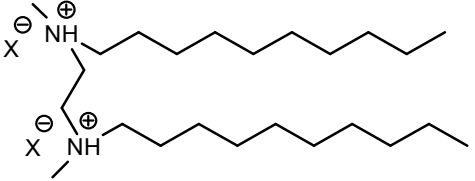
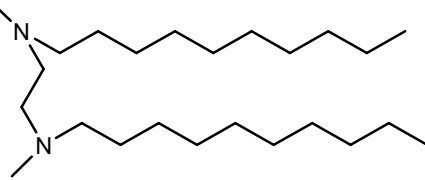
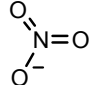
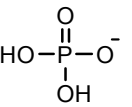
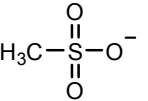
In the final Chapter we demonstrate the impact of the counterion nature on the crystalline structures of gemini surfactants. It was found that contrarily to the aqueous solution, where hydration of anion plays a primordial role, in the crystal structure the anions with smaller radius display a stronger association with the cationic headgroups. Comparison of the results obtained for the same system in aqueous solution and in solid state showed the importance of ion-water interactions in ion specific effects.

Summarizing the results obtained by different approaches, we can conclude that ion specific effects which determine the behavior of micellar aggregates of cationic quaternary ammonium gemini in aqueous solutions strongly depend on the free energy of hydration of the counterions, in others words, on its hydrophilic/hydrophobic properties. It is interesting to note that the polarizability of the ions, which provides information on the dispersion forces and thus on ion specificity, seems to correlate less with the aggregation properties. In contrast, the free energy of hydration of the ion, correlates very well with properties of surfactant aggregates. These results strongly suggest that ion hydration free energy can provide information about the ion specific effects in aqueous solution. However, one should note that the properties of substrate (the gemini in our case) should be taken into account not less carefully in order to fully predict Hofmeister effects.

Keywords: ion specific effects, self-assembly, gemini surfactants, micellization, interfacial properties, chemical trapping, molecular dynamic simulations, rheology, wormlike micelles, crystal structure.

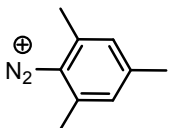
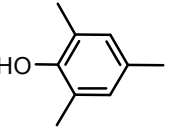
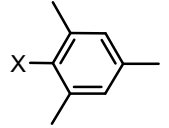
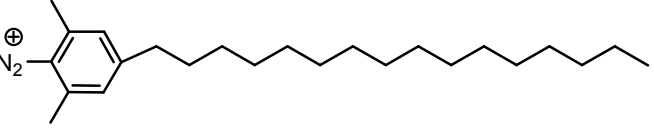
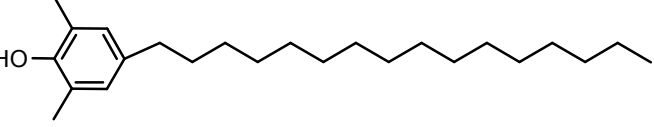
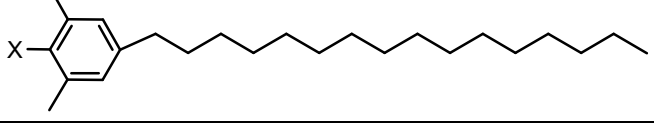
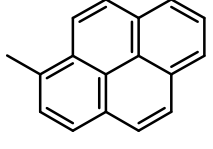
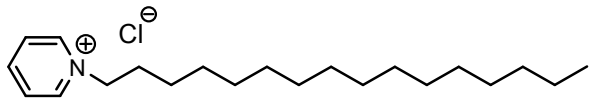
- Glossary -

Table I-1. Abbreviations and molecular structures of cationic gemini and counterions used in this work.

Gemini surfactant	
10-2-10 X (quaternary ammonium)	
10-2-10 ter X (tertiary ammonium)	
10-2-10 amine	
Inorganic counterions	
Γ^- (iodide)	Γ^-
Br^- (bromide)	Br^-
Cl^- (chloride)	Cl^-
F^- (fluoride)	F^-
NO_3^- (nitrate)	
PH (H_2PO_4^- , dihydrophosphate)	
MeSO_3^- (methyl sulphonate)	

Organic counterions	
TFA (trifluoroacetate)	
C1 (HCOO ⁻ , formate)	
C2 (CH ₃ COO ⁻ , acetate)	
C3 (CH ₃ CH ₂ COO ⁻ , propionate)	
C4 (CH ₃ (CH ₂) ₂ COO ⁻ , butyrate)	
C5 (CH ₃ (CH ₂) ₃ COO ⁻ , pentanoate)	
C6 (CH ₃ (CH ₂) ₄ COO ⁻ , hexanoate)	
C8 (CH ₃ (CH ₂) ₆ COO ⁻ , octanoate)	
C10 (CH ₃ (CH ₂) ₈ COO ⁻ , decanoate)	

Table I-2. Abbreviations and structures of arenediazonium probe and the products obtained during chemical trapping experiment. 1-methylpyrene probe and cetylpyridinium chloride used for fluorescence quenching experiment.

Chemical trapping	
1-ArN ₂ ⁺ (2,4,6-trimethylbenzenediazonium)	
1-ArOH (2,4,6-trimethylphenol)	
1-ArX (X = counterions)	
16-ArN ₂ ⁺ (4-n-hexadecyl-2,6-dimethylbenzenediazonium)	
16-ArOH (4-n-hexadecyl-2,6-dimethylphenol)	
16-ArX (X = counterions)	
Fluorescence quenching	
1-methylpyrene (probe)	
cetylpyridinium chloride (quencher)	

- List of used abbreviations -

cmc – critical micelle concentration in mol of alkyl chain (single chain surfactant) per liter

CMC – critical micelle concentration in mol of gemini surfactant per liter

COM – center of mass

CT – chemical trapping

CTAB – cetyltrimethylammonium bromide

DFT – density functional theory

DIPEA – N,N-diisopropylethylamine (Hünig's base)

DLVO – Derjaguin and Landau, Verwey and Overbeek

DMEDA – N,N'-dimethylethylenediamine

EDL – electrostatic double layer

FQ – fluorescence quenching

GB⁻ – general base

HPLC – high-performance liquid chromatography

MD – molecular dynamic

NMR – nuclear magnetic resonance

RDF – radial distribution function

r.t. – room temperature

SASA – solvent accessible surface area

SDS – sodium dodecyl sulfate

SSFQ – steady state fluorescence quenching

- List of used abbreviations -

TMEDA – N,N,N',N'- tetramethylethylenediamine

TRFQ – time resolved fluorescence quenching

XPS – X-ray photoelectron spectroscopy

- Table of Contents -

– General introduction –	23
Chapter I. Amphiphiles. Bibliographic study	25
1. Amphiphilic molecules. Types and properties.....	27
2. Micellization	30
2.1. Ionic surfactant self-assembly.....	30
2.2. Ionic gemini surfactant self-assembly	32
3. Ion specific effects	34
3.1. Hofmeister series.....	34
3.2. First attempts to explain ion specificity.....	35
3.3. Overview of the classical theories.....	37
3.4. What is missing in classical theories? Important interactions	42
3.5. The latest attempts to shed light on Hofmeister effects	44
3.6. The latest studies	47
Chapter II. Synthesis and characterization of cationic gemini surfactants.....	51
Introduction.....	53
1. Synthesis and characterization of 10-2-10 gemini	55
1.1. General synthetic procedure for quaternary 10-2-10 gemini compounds with different counterions	55
1.2. Synthesis of tertiary ammonium 10-2-10 gemini surfactants.....	66
2. Experimental section	72
2.1. Materials.....	72
2.2. Synthetic procedures for quaternary 10-2-10 gemini surfactants.....	72
2.3. Synthetic procedures for tertiary 10-2-10 gemini surfactants	76
Chapter III. Contribution of ion specific effects to the physical properties of micellar aggregates at the bulk solution level.....	79
Introduction.....	81
1. Conductivity measurements.....	83
1.1. Surfactant properties estimated by conductivity measurements.....	83
1.2. Results and discussions	87
2. Aggregation number. Fluorescence quenching technique.....	103

2.1. Theoretical aspects of fluorescence quenching techniques as a method to determine aggregation number	104
2.2. Results and discussions	108
3. Conclusions	116
4. Experimental section.....	118
4.1. Conductivity measurements	118
4.2. Spectrofluorometric measurements	120
Chapter IV. Interfacial properties of micellar aggregates <i>via</i> the chemical trapping experimental method	123
Introduction	125
1. Chemical trapping. Principle and main assumptions.....	126
1.1. Arenediazonium ion chemistry.....	126
1.2. Arenediazonium ion as a probe of the interfacial region of the micelles	127
1.3. Main assumption of the chemical trapping	128
2. Results and discussions	131
2.1. Inorganic counterions.....	131
2.2. Carboxylate counterions.....	135
2.3. Complications.....	136
3. Conclusions	139
4. Experimental section.....	140
4.1. Materials.....	140
4.2. Dediazonation reaction	140
4.3. HPLC analysis	141
Chapter V. Structural and interfacial properties of micellar aggregates <i>via</i> computer simulations	143
Introduction	145
1. Results and discussions	147
1.1. Contribution of ion specific effects to the micelle structure	147
1.2. Interfacial concentrations	157
1.3. Position of arenediazoniom probe (16-ArN ₂ ⁺) used for chemical trapping study within the micelle	162
2. Conclusions	164
3. Experimental section.....	166

3.1. Materials	166
3.2. Methods	166
Chapter VI. Rheological study of the Hofmeister effects at semi-dilute regime	169
Introduction.....	171
1. Wormlike micelles	172
2. Results and discussions	175
3. Conclusions.....	179
4. Experimental section	180
4.1. Material and methods	180
4.2. Data analysis	180
Chapter VII. Impact of counterion nature on the crystal structure of cationic gemini surfactants..	183
Introduction.....	185
1. Results and discussions	186
1.1. Packing of gemini surfactants in the crystalline structure.....	186
1.2. Distances between counterion and nitrogen of the headgroups for gemini n-2-n X, where X = Γ^- , Br^- and Cl^-	191
2. Conclusions.....	194
3. Experimental section	195
3.1. Preparation of the single crystals	195
3.2. X-ray single-crystal diffraction.....	195
– <i>General conclusions</i> –	197
– <i>Perspectives</i> –	201
– <i>References</i> –	203

- General introduction -

It has been a long time now that surfactant molecules have played an important role in many fields of scientific research such as biomaterials, colloid chemistry, polymer chemistry, matter science and nanomaterials. This is due to their particular capacity to self-assemble in solution forming a variety of aggregates with different properties based on their amphiphilic nature. Surfactants contain both hydrophilic and hydrophobic moieties in one molecule. The self-assembling features, such as stability or critical micelle concentration as well as morphology of the aggregates can be controlled by the molecular structure of surfactants or the physical-chemical conditions such as solvent, temperature, added salts, etc. For the ionic surfactants, one of the crucial parameters that determine their self-assembling behavior is the nature of counterions.

Understanding the influence of ion specific effects on the properties and structure of aggregates still remains one of the challenging problems in the chemistry of proteins, biomembranes and associated colloids such as micelles, emulsions and vesicles. Franz Hofmeister was the first who reported in 1888 that different salts have different ability to precipitate proteins from aqueous solution. Based on these observations, Hofmeister proposed the order of cations and anions that reflects their effect on the proteins. Later on, it was shown that many properties of proteins and colloids in aqueous solution correlate with Hofmeister series. Many studies have been done in order to explain these phenomena theoretically and experimentally. However, there is still no consensus on how different forces play the roles in cooperative manner. Thus, the prediction of morphologies and properties of aggregates for a particular ion molecule in a given condition remains a major barrier for routine applications.

In this work, we combine experimental and computational approaches in order to rationalize ion specific effects of ionic surfactant based on the balance of forces which controls their self-organization process and aggregate morphology.

In the first Chapter, we present an overview of the literature dealing with the self-assembly of surfactants. Structure of the main classes of amphiphiles and their self-organization features are discussed. The thermodynamic description of micellization process for single chain and gemini amphiphiles with particular emphasis on ionic surfactants is given. This is followed by the introduction of the Hofmeister effects and main classical theories that were created in order to

describe these phenomena based on all the forces that contribute to ion specific effects. At the end, we give some examples of very recent studies of Hofmeister effects.

The main goal of the present work is to compare the effects of different anions on the self-assembly of cationic surfactants. We mainly focused on the gemini surfactants with the same headgroups, however, some comparison was performed in order to investigate the impact of the headgroups nature on the ion specific effects. The Chapter II contains the introduction of the systems chosen for this study, as well as the synthetic procedure for the surfactant molecules.

The micellization of gemini surfactants with different counterions was first characterized in the bulk solution as discussed in the Chapter III. To obtain better understanding of the properties of aggregates, the interfacial properties of the formed micelles were characterized using experimental and computational approaches. This gave us access to the information about direct interactions of ions with macromolecule. Chapter IV describes the experimental study using chemical trapping technique that allowed us to estimate the ion and water concentrations within the micellar interface. To complete and support these results computer modeling discussed in Chapter V was used. There we show how applying the molecular dynamic simulations to our micellar systems allows us to characterize the effect of anion nature on the structural properties of the micelle including its morphology and counterion density within the interface.

In the Chapter VI the ion specific effects in the system of higher complexity was studied. The impact of the counterions nature on the large worm like micelles was investigated by rheology.

In the last Chapter, we focused on the effect of counter ions on the packing of gemini amphiphile molecules in the crystals. Comparison of the results obtained for the same system in aqueous solution and in solid state showed the importance of ion-water interactions in the ion specific effects.

This comprehensive study allowed us to shed light on the relations between ion type and the hydration, hydrogen bonding, electrostatic, ion pairing, and polarization interactions that balance the hydrophobic effect and control the physical properties of solutions of ionic amphiphiles.

Chapter I. Amphiphiles. Bibliographic study

1. Amphiphilic molecules. Types and properties.

Amphiphilic molecules are largely studied and used for different fields of science and technology due to their unique self-assembling behavior.

Amphiphiles are called surfactants when they exhibit an interfacial activity by lowering the surface tension of the liquid or interfacial tension between two liquids assembling at the interface. Numerous variations are possible in the types of head groups and tail groups of surfactants. For example, the head group can be anionic, cationic, zwitterionic, or nonionic[1]. Its size can also vary changing the properties of the surfactant molecule. The hydrophobic moiety can have different lengths as well as various substitutes[2]. Besides, among others the linkages between the hydrophilic and hydrophobic parts provides a large variety of amphiphiles (Figure I-1). Hydrophilic head group can be covalently linked to single, double or triple hydrophobic alkyl chains. Two hydrophilic head groups covalently linked by one hydrophobic alkyl tail result in so-called bolaform amphiphiles. Two surfactant molecules covalently linked at their charged head groups are termed a gemini (dimeric) amphiphile[2, 3].

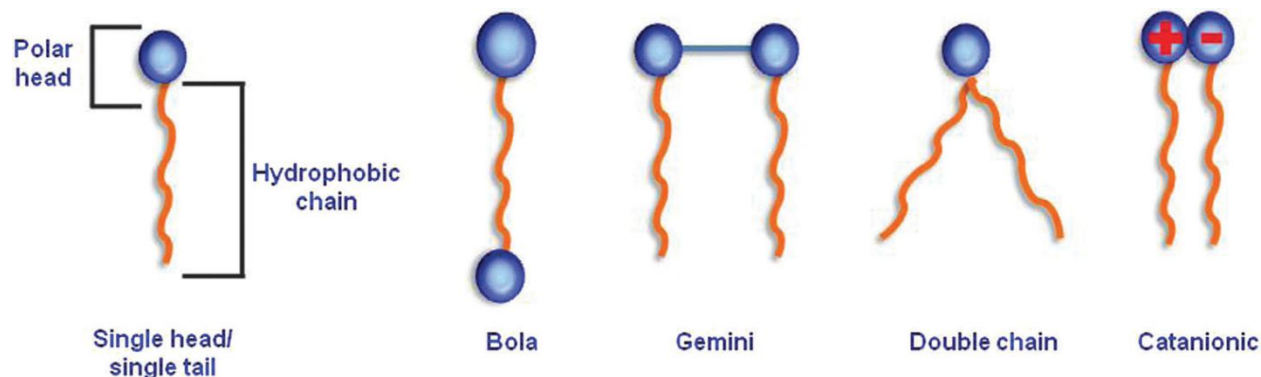


Figure I-1. Types of amphiphilic molecules[3].

Due to the presence of two ambivalent moieties in the surfactant molecules, they associate spontaneously in solution, forming the supramolecular structures. Tanford proposed two main antagonistic forces that drive the self-assemble process[4, 5]. One is *hydrophobic* interactions between the aliphatic chains. This energy represents a favorable process of bringing the surfactant's tail from contact with water to contact with other tails, thus providing the stimulus for self-organization. At the same time, *repulsive* forces between polar headgroups such as electrostatic interactions, hydration and steric effects, prevent the formation of large aggregates.

A variety of factors affect the self-assembly process of amphiphiles. Apart from experimental conditions (concentration, temperature, pH, ionic strength, etc) aggregate formation to

a large extent depends on the structural properties of the molecules resulting in different aggregate morphologies. Based on the free energy model proposed by Tansford, Israelachvili *et al.*[6, 7] developed a geometry-based approach to predict the shape of formed aggregates. The dependence between the surfactant molecules and associated aggregates was described by critical packing parameter (*cpp*), $p = v/a_0l$, where v and l are volume and extended length of the hydrophobic part respectively, and a_0 is a surface area occupied by the surfactant headgroup. Critical packing shape is determined by the balance between the hydrophobic effects for assembly of the amphiphile tails (which causes the organization of amphiphilic molecules and, hence, reduces a_0) and the tendency of hydrophilic headgroups to maximize their contact with water (and increases a_0). The balance between these two main forces leads to an optimal area per amphiphilic headgroup, for which the interaction energy is minimum[8]. Thus, due to difference in p , a variety of structures such as spherical micelles, rodlike micelles, vesicles, bilayers can be formed, for clarity see the Figure I-2.

Although this description remains largely conceptual and not to be taken literally, or “visually”, the global behavior of the amphiphilic molecules can be well described, *i.e.* big head amphiphiles tend to form spherical micelles whereas upon decreasing the size of the headgroup (either sterically or by decreasing the repulsion [screening the apparent charge]) they tend to form less curved aggregates, cylindrical micelles, towards bilayers, then inversed micelles, etc.

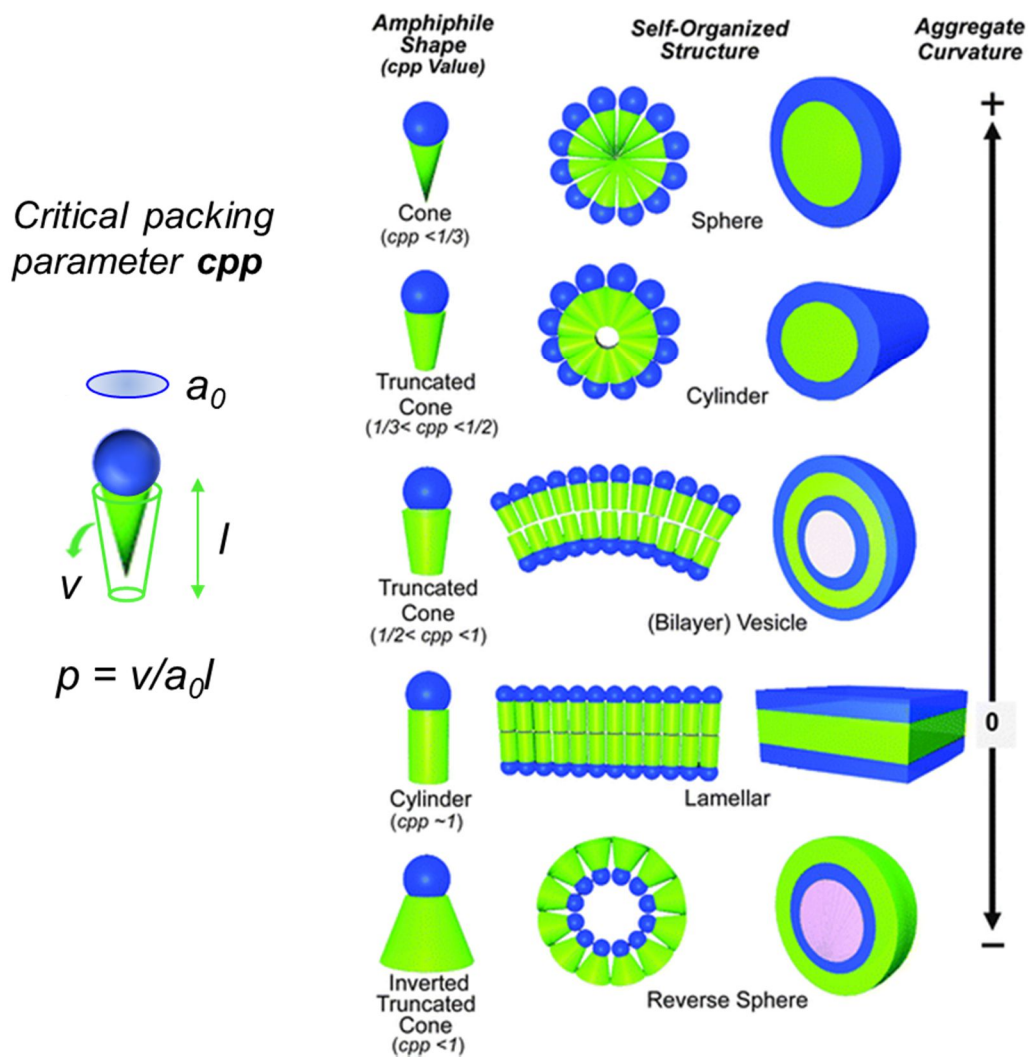


Figure I-2. Relationship between structure of the amphiphilic molecule, that determines critical packing parameter (cpp), and morphology of the aggregates formed in the solution (adapted from ref.[8]).

2. Micellization

2.1. Ionic surfactant self-assembly

The behavior of ionic surfactants at low concentrations is very similar to the one of classical electrolyte (salt). However, with increasing surfactant concentration, a heterogeneous system occurs due to the formation of self-assembled aggregates called micelles. This concentration is called critical micelle concentration, *cmc* (Figure I-3). The aggregation properties of amphiphiles have been studied since the 1950s. In 1948 Debye proposed the theory that micellization is driven by two antagonistic forces: repulsive Coulomb forces between headgroups and attractive van der Waals forces between hydrophobic tails[9, 10]. After that, numerous theoretical studies[5, 11-15] were developed in order to improve the model proposed by Debye. The overview of all these studies was done by L. Romsted[2].

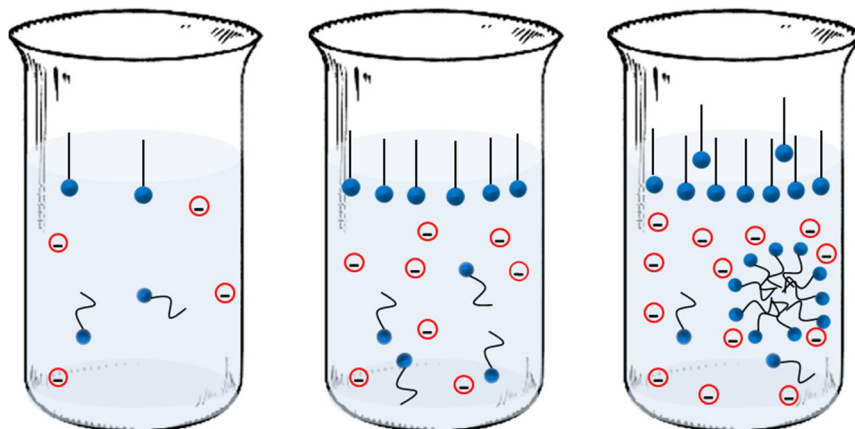


Figure I-3. Schematic representation of micellization in water upon addition of small quantities of the single chained cationic surfactant.

Another model was proposed by Nagarajan and Ruckenstein[16] in order to give a thermodynamic description of the process of micelle formation. According to this theory there are five main contributions to the aggregation free energy per surfactant molecule of size N and shape S well described by Zana[17]:

$$g_N^{(S)} = g_{hc} + g_{int}(a) + g_{el}(R) + g_{st}(a) + g_{es}(a, R) \quad (\text{I-1})$$

where a is the area per molecule on the aggregate surface and R is the aggregate size that is related to N and a by aggregate geometry (for spherical micelles, $Na = 4\pi R^2$). These five main thermodynamic terms are as follows:

- (1) The first force that provides the micellization is the hydrophobic effect. It can be characterized as the free energy per surfactant molecule g_{hc} gained by isolating hydrocarbon

chains from water. This free energy is negative and is approximately independent of aggregate geometry S , its contribution favors the increase in aggregate size and has linear dependence in N with a reduction of roughly $k_B T$ per hydrocarbon chain[17].

- (2) The formation of surfactant aggregates generates an interface between the hydrophobic core region consisting of the surfactant tails and the surrounding water medium. This contribution g_{int} is unfavorable for the aggregate and can be described as follows:

$$g_{int}(a) = \gamma_1(a - a_{min}) \quad (\text{I-2})$$

where γ_1 is the interfacial tension of the core-water interface (\sim hydrocarbon-water interfacial tension) and a_{min} is the minimum area per molecule (*i.e.*, the interfacial area occupied by a headgroup).

- (3) The third contribution of the free energy is attributed to the packing of the non-polar chains into the hydrophobic core g_{el} , namely the difference in the chain length regarding relaxed length l_0 (typical for liquid hydrocarbons).

$$g_{el}(R) = \frac{1}{2}k'(R - l_0)^2 \quad (\text{I-3})$$

The elastic constant k' depends on the chain statistics, as well as the packing parameter.

- (4) The contribution to the $g_N^{(S)}$ from the presence of polar headgroups includes steric repulsion between the headgroups. From the entropy of mixing per molecule for steric free energy g_{st} we obtain:

$$g_{st}(a) = k_B T \left[\ln\left(\frac{a_{min}}{a}\right) + \left(\frac{a}{a_{min}} - 1\right) \ln\left(1 - \frac{a_{min}}{a}\right) \right] \quad (\text{I-4})$$

- (5) For the ionic surfactants there is one more term that makes a significant impact on the free energy of aggregates formation: electrostatic repulsion between the headgroups g_{es} . Oppositely to g_{int} , it acts to increase the area per molecule. The free energy of the electrostatic repulsion based on Poisson-Boltzmann theory is given by:

$$g_{es} = \frac{2k_B T}{\beta} \left\{ \beta \ln[\beta + (1 + \beta^2)^{1/2}] - (1 + \beta^2)^{1/2} + 1 - 2c\lambda_D \ln \left[\frac{1}{2} + \frac{1}{2}(1 + \beta^2)^{1/2} \right] \right\} \quad (\text{I-5})$$

where $\beta = 4\pi l_B \lambda_D / a$ is a dimensionless charging parameter depending on two length: Debye screening length λ_D and the Bjerrum length l_B . The Debye screening length in the solution depends on added salt (here monovalent) concentration C_{salt} , $\lambda_D = (8\pi l_B C_{salt})^{-1/2}$;

and $l_B = e^2/\epsilon k_B T$ is about 7 Å for aqueous solution with dielectric constant $\epsilon = 80$ at room temperature. Finally, c is the mean curvature of the aggregate (e.g., $1/R$ for spherical micelles).

For the surfactant of the shape S and chemical potential μ , the aggregation number N and area per molecule a (as well as aggregate size R) can be determined as follows:

$$g_N^{(S)}(a) = \mu, \quad \frac{dg_N^{(S)}(a)}{da} = 0 \quad (\text{I-6})$$

By increasing the chemical potential ($\mu > k_B T \ln \Phi_{cmc}$, where k_B is Boltzmann constant and Φ_{cmc} is volume fraction of the surfactant at the *cmc*), micellization takes place:

$$\Phi_{cmc} = \exp[g_{N^*}/(k_B T)], \quad k_B T_m = \frac{g_{N^*}}{\ln \Phi} \quad (\text{I-7})$$

where T_m is temperature at the micellization point and average aggregate size at the *cmc*, N^* , can be calculated now from the expression of $g_N^{(S)}$ at its minimum.

2.2. Ionic gemini surfactant self-assembly

In the present work our interest is focused on the cationic gemini surfactants: two alkyl chains bound with two monovalent cationic headgroups that are linked by a spacer. The self-assembly properties for such kind of amphiphiles significantly differ from their single chain length analogs. The CMC for gemini surfactants is typically several orders of magnitude lower than that of corresponding monochain analogs. It strongly depends on the chain length of the hydrophobic part, nature of the headgroup, spacer length and type of counterions[17, 18].

The presence of two tails, polar headgroups and spacer should be considered for the estimation of the thermodynamics of aggregate formation, Equation (I-1). Here we would like to give a short overview of how the dimeric nature of the surfactant contributes to each thermodynamic term described above.

- (1) The hydrophobic term per g_{hc} surfactant molecule now should include the contribution of the two tails plus spacer. However, only the spacer moiety, that integrates the micellar hydrophobic core (s_{core}) should be taken into account. This penetrating moiety is taken as difference between the total spacer length (s) and the mean head-head distance, $s_{core} = s - a^{1/2}/b$, where b is the segment length of the spacer model proposed by Gaussian[17].

The co-localization of the hydrophobic chains and spacer in one molecule from the beginning favor the micellization, hence the gain in hydrophobic energy per aliphatic group is smaller than for monomeric surfactants.

- (2) The interfacial contribution g_{int} in the case of gemini surfactants should be modified regarding the presence of the spacer. The spacer chain length that occupies the core-water interface and participates in shielding is proportional to $a^{1/2}$. Thus, this contribution can be given by:

$$dg_{int} \simeq (\gamma_2 - \gamma_1) a^{1/2} w \quad (\text{I-8})$$

where γ_2 is the interfacial tension of the spacer-water interface and w is a spacer width. However, this correction takes place just when spacer does not consist of hydrocarbons, otherwise $\gamma_2 = \gamma_1$ and g_{int} term is the same as for the single chain analogs.

- (3) As we already mentioned, the presence of short spacer would keep the two hydrophobic chains at closer distance than they would stay in single chain surfactants. This feature of gemini structure reduces the entropy of the tail chain. In comparison with a single chain surfactant, where the area of the tail that interacts with water equals approximately $a_{tail} \sim v/R$, for gemini the presence of the spacer reduces the accessible area per tail to $a_{sp} \sim (sb)^2$, where s is the number of segments of a Gaussian model for the spacer. Taking this into account thermodynamic contribution can be presented as:

$$g_{tail} \simeq k_B T \ln \left(\frac{a_{tail}}{a_{sp}} \right) \simeq k_B T \ln \left(\frac{v}{Rb^2 s^2} \right) \quad (\text{I-9})$$

- (4) The last contribution that has to be modified is electrostatic repulsion of the headgroups. Similar to the impact of the spacer on the chains, short linker decrease the distance between the headgroups in respect to single chain analogues. This results in a nonuniform charge distribution of ion pairs over the micellar interface. The solution to this challenge is well described by Camesano and Nagarajan in their work[19]. They recommend a semi-empirical correction factor to g_{es} contribution, which disappears when the spacer is longer than the mean interhead distance and the charges are uniformly distributed on the micellar surface.

In addition, besides all the thermodynamic terms that were discussed above, for the ionic surfactants, the impact of counterions on the aggregate formation is very strong.

3. Ion specific effects

3.1. Hofmeister series

The most important contribution to the discovery of ion specific effects was done by Franz Hofmeister in 1888. He published a series of papers[20] where he described the different ability of a variety of salts to precipitate proteins. This work was later translated in English[21]. Based on his observations, Hofmeister organized cations and anions according to their ability to precipitate the proteins. Now this ordering is known as *Hofmeister series*, Figure I-4. However it would be fair to note that the first investigations of salt effects on the viscosity of aqueous solutions were done by Poiseuille in 1847[22], who observed that some salts increase the viscosity of water, whereas others decrease it.

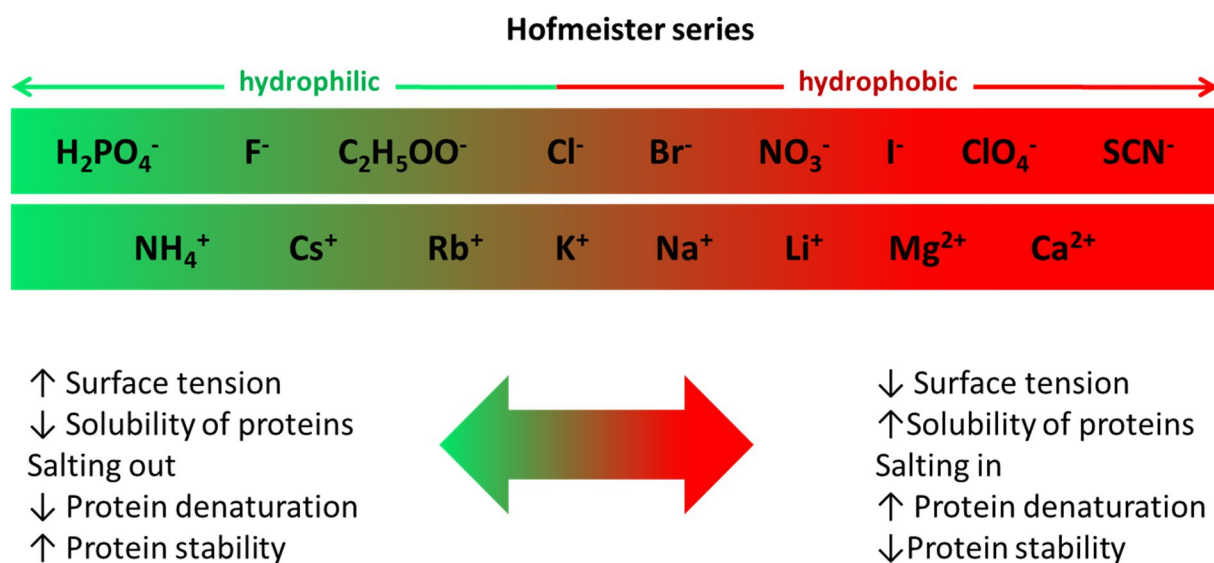


Figure I-4. Typical ordering of anions and cations in Hofmeister series (adapted from ref.[23])

It was not easy to understand observed phenomena in the 19th century due to the limited available analysis techniques. However, this did not stop Hofmeister from performing seminal experiments and he was able to draw non trivial conclusions from this work about specific ion effects that allowed him to order salts according to their “water withdrawing capability”: “... the colloid precipitating effect of a salt is dependent on its water absorbing capability, one can expect that this activity against the various colloid substances should be constant in relation to other salts. It also can be expected, that the precipitating capability of salts is parallel to other physical and chemical properties, if it has been proved or it is most likely, that these properties are dependent on the water absorbing capability of the salts”[24]. This was on his opinion the most important effect of

salts on the colloid system. Nevertheless, his observations also seemed to be related with what we would call specific ion adsorption, hydration–dehydration, ion exchange effects that occur at colloidal surfaces.

There are countless phenomena related to ionic effects in physical chemistry and biochemistry. A number of reports can be found on the ion dependence of the surface tension of aqueous solutions[25, 26]. Bubble interactions and coalescence are also known to be influenced by salt effects; colloidal particles in solution are strongly influenced by background salt. A lot of biological systems are linked with ionic effects. They participate in the osmotic regulation of the cells, enzymes activities, bacteria growth and other vital processes.

Nonetheless, a unifying theory is still missing and the Hofmeister series yet represents an appealing challenge in colloid and interface science. Still today there is a debate about the relative importance of direct ion–ion interactions and of ion–water interactions to explain or even to predict these effects. Some scientists are convinced that the proper description of the dispersion forces will finally solve the problem, others think that the proper geometry of ions or charged headgroups and of water is decisive.

3.2. First attempts to explain ion specificity

After Hofmeister published his works on ion specificity in 1880s, a number of studies were done to elucidate the discovered phenomena. For example, Robertson in 1911[27] found that the influence of added salts on the precipitation of proteins depends on the concentration of the salt employed. At low and at high concentrations the salts can act as precipitants and as coagulants respectively. In 1920 Loeb[28] showed that pH of the solution of proteins has an important influence on the salt effects.

First attempts to explain ion specificity were essentially related to the specific interactions between ions and water. Such kind of interactions would make a strong influence on the physicochemical properties of salt solutions, particularly on conductivity and viscosity.

Kohlraush has performed a large number of experiments to study the conductivity properties of the electrolyte solutions, establishing that they obey Ohm's law[29]. He described that the mechanism for conductivity was based on the “independent migration” of ions through the aqueous solution due to the presence of an electric field. The current which goes through the solution is given by the product of the velocity of the ion and its charge. The electrochemical mobility, μ_i ($\text{cm}^2\text{V}^{-1}\text{s}^{-1}$), is given by the ratio between the velocity and the applied electric field.

The conductivity measurements showed that the mobility of the ions in water has a non-linear dependence on the ion size and follows the order: $\text{Cs}^+ > \text{Rb}^+ > \text{K}^+ > \text{Na}^+ > \text{Li}^+$ for alkali metal cations, and $\text{Br}^- > \text{I}^- > \text{Cl}^- > \text{F}^-$ for halide anions (Figure I-5). The observations do not correlate with expectations: the more mobile anions are the ones with smaller radii. This could be explained by the fact that the actual effective size of ions in water is very different from that in a crystal. Small ions (*e.g.* Li^+ , F^-) are strongly hydrated and move bearing several water molecules with them and so they move slowly compared with bigger, poorly hydrated ions (*e.g.* Cs^+ , Br^-).

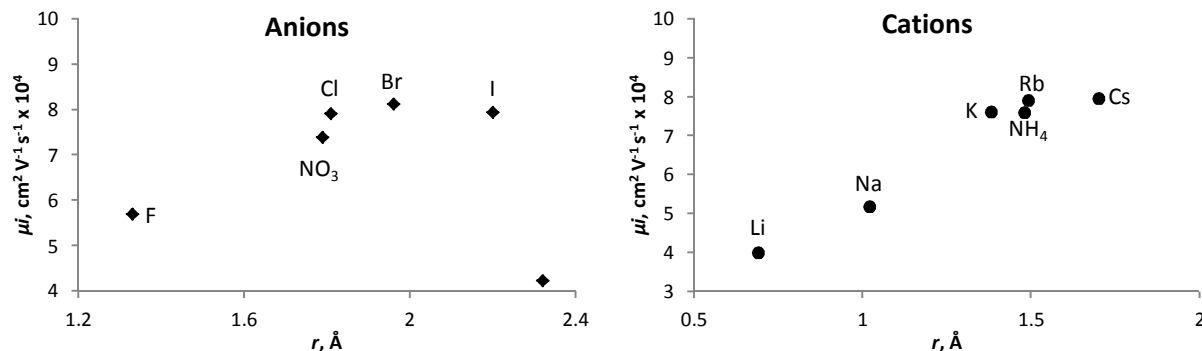


Figure I-5. Ion mobility, μ_i , as a function of ion radius, r , for some anions (left) and cations (right). Values for μ_i and r were taken from ref.[29] and [30] respectively.

As we already mentioned the first study on electrolyte viscosities was done by Poiseuille in 1847. Jones and Dole in 1929[31], Cox and Wolfenden in 1934[32], and several other groups further refined the specific ion effect on water viscosity. It was noted that some aqueous electrolytes enhance the viscosity relative to pure water, whereas, some others decrease it.

As was discussed by Marcus[33, 34], the effect of ions on the structure of water can be described by B coefficient of the dynamic viscosity of an electrolyte solution, η , which derives from the Jones-Dole[31] expression (originally expressed in terms of the fluidity $1/\eta$):

$$[(\eta/\eta^*) - 1] = Ac^{1/2} + Bc + \dots \quad (\text{I-10})$$

where η^* is the viscosity of the solvent (water), A is a coefficient that can be calculated from the conductivity of the electrolyte and B is an “ion specific parameter” known as Jones–Dole viscosity B coefficient. Usually Equation (I-10) holds well for $c < 0.1$ M, and for more concentrated salt solutions further terms are needed (*e. g.* an extra term Dc^2 is added)[34].

According to Gurney[35], ions having positive value of viscosity coefficient, $B > 0$, increased the viscosity of aqueous solutions, were deemed to be “structure making”. Ions having negative value of viscosity coefficient, $B < 0$, decreasing the viscosity of water, were called as “structure breaking”. It was supposed that a “water structure” (which can be thought as a dynamic

fluctuating hydrogen bond network) existed, and that this was specifically affected by electrolytes. Ions dedicated to be “water-structure makers” were called “kosmotropes”, whereas, “water-structure breakers” were called “chaotropes”.

The term structure-making and structure-breaking was used for many years. However, it is somewhat misleading. According to recent studies, it was shown that at least monovalent ions do not influence the structure of water beyond the first hydration shell[36-39]. Therefore, there is no significant long-range structuring of water due to the presence of ions.

3.3. Overview of the classical theories

Extensive work devoted to the study of electrolyte bulk solutions, colloidal systems within bulk or on the interface has allowed the development of theories that try to explain the behavior of the solutions containing anions. Here we will discuss the different theories which describe the intermolecular interactions present in salt solutions (from electrolyte to colloid systems). These simplified models or “classical theories”, consider the solvent as a continuum characterized by dielectric constant[40].

First we will briefly overview the *electrolyte (salt) solutions*. The **electrostatic Coulomb forces** are considered to be the main interactions between ions in water. In this context electrostatic self energy will be introduced.

Next we will discuss theories developed for the more complex *colloid solutions*. First one is called electric double layer (EDL) theory. It describes the electrostatic forces between two interacting colloidal particles separated by the electrolyte medium. Later, the modified version of this model, DLVO theory, was proposed. In this theory, the new term, **attractive** van der Waals forces are introduced on top of the repulsive electrostatic contribution. We will then introduce the Lifshitz theory, which also takes into account other non-electrostatic forces such as Keesom and Debye potentials.

All these well-known theories and concepts can be easily traced in physical chemistry textbooks, as, for example, ref.[41, 42].

3.3.1. *Electrostatic forces in the electrolytes*

3.3.1.a Coulomb forces

In classical theory of electrolyte solutions the first assumption is that ionic interactions between the colloid particles could be described by Coulomb electrostatic interactions only:

$$V(\mathbf{r}) = \pm \frac{z_1 z_2 e^2}{4\pi\epsilon_0\epsilon_r r} \quad (\text{I-11})$$

where $z_1 e$ and $z_2 e$ are the charges of the ions, r is the interionic distance, ϵ_0 is the permittivity in vacuum and ϵ_r is the static dielectric constant of solvent. The ions are considered as point charges and r is assumed to be far beyond larger than their actual physical size.

In the electrolyte solution, the Coulomb forces are screened by cooperative effects of neighboring ions. Thus, the potential of mean force between two ions in an electrolyte solution can be approximated as:

$$V(\mathbf{r})_{eff} \propto V(\mathbf{r}) e^{-\kappa_D r} \quad (\text{I-12})$$

where κ_D is inverse of the Debye screening length:

$$\kappa_D = \left[\frac{e^2 \rho (v_1 z_1^2 + v_2 z_2^2)}{\epsilon_0 \epsilon_r k_B T} \right]^{1/2} \quad (\text{I-13})$$

T , k_B , e , and ρ are the absolute temperature, Boltzmann constant, unit charge, and number density of ions, while v_1 and v_2 are the stoichiometric coefficients for the specific electrolyte $M_{v_1}^{z_1} X_{v_2}^{z_2}$ respectively.

3.3.1.b Self energy

The self energy is the energy required to bring in an ion from “infinity” (no interaction) to a spatial location r in the surrounded medium (*i.e.* dielectric medium)[43, 44]. The self-energy consists of two terms electrostatic and nonelectrostatic contributions.

Here an electrostatic term is introduced, known also as Born self energy, in order to present the electrostatic forces in the solution of electrolytes. Assuming that the charge e_v located on the surface of a sphere of radius a , the electrostatic self energy can be described as[42]:

$$E_v = \frac{e_v^2}{4\epsilon_r \kappa_D a^2} (1 - e^{-2\kappa_D a}) \quad (\text{I-14})$$

For the dilute electrolyte ($\kappa_D a \ll 1$) this equation can be simplified as follows:

$$E_v = \frac{e_v^2}{2\epsilon_r a} \quad (\text{I-15})$$

The Equation (I-15) gives Born self energy of an ion immersed in a dielectric medium.

However, one should keep in mind that in addition to the electrostatic Born self free energy, there is the nonelectrostatic contribution, the dispersion self free energy, which has a significant contribution to the self energy of an ion[45, 46].

Self energy can be used to estimate solubility by comparing the free energies of a solid ionic crystal with the free energies of transfer of ions to the solute[46, 47].

3.3.2. The balance of forces in associated colloids

3.3.2.a The electrostatic double layer (EDL)

The force between two colloidal particles can be considered using the double-layer model. It is the basis for the later developed DLVO theory (see subchapter 3.3.2.b), which still remains the core of colloid science.

The spontaneous charging of the particle surface in a liquid medium results in the formation of a double layer. The EDL can be defined as follows: “An electrical double layer is a non-homogeneous region of finite thickness containing significant variations in charge density across its thickness which consequently produces a potential drop across this dimension; the non-homogeneity invariably arises as a consequence of the competition between entropy and energy effects in the system’s attempt to minimize its free energy”[48]. There are several theories that tried to describe the EDL of colloids. First, Helmholtz proposed that two layers of opposite charge formed at the electrode/electrolyte interface and were separated by a small distance, H , where the electrical potential (Ψ_s) decreases linearly away from the surface of the bulk, see the Figure I-6 (a). Later this model was modified by Gouy in 1910 and Chapman in 1913. They took into account the fact that ions in the electrolyte solution are mobile and introduced the diffuse layer model, where ions of opposite sign to that of the electrode are distributed in a region of thickness much larger than H , as describes the Figure I-6 (b). Differently from Helmholtz’s model, the electric potential within the diffuse layer decreases exponentially. In 1924 Stern proposed to combine Helmholtz and Gouy-Chapman models that describe two different regions for the charge density called Stern layer and the diffuse layer, Figure I-6 (c). The last model is consider to be the basis of the EDLs, even though different modifications were performed in order to improve it[49, 50].

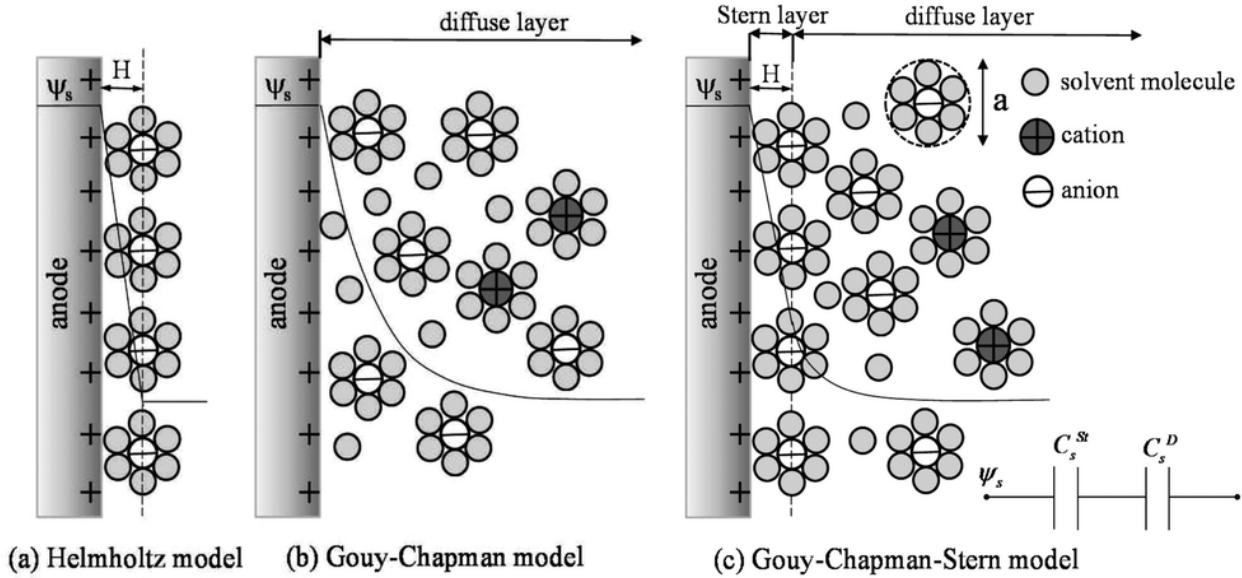


Figure I-6. Schematic representations of EDL structures according to the Helmholtz model (a), the Gouy–Chapman model (b), and the Gouy–Chapman–Stern model (c). H is the double layer distance described by the Helmholtz model. ψ_s is the potential across the EDL[51].

Solving the Poisson-Boltzmann equation that is used to describe the interaction energy between the ions within the electric field, and accounting the induced osmotic pressure due to different ionic densities within the EDL and bulk, the force per unit area ($\kappa_D l > 1$) can be described as follows[42]:

$$F(l) = f(\sigma) e^{-\kappa_D l} \quad (\text{I-16})$$

The prefactor depends on the assumption of the constant charge or potential on the surface.

More details about EDL theories can be found in following references[49, 52, 53]

3.3.2.b The DLVO theory

In the light of what has been discussed above, it is clear that, electrostatic potential does not reflect any specific electronic property of the molecules/ions but only their net charges and stoichiometric coefficients (*i.e.*, monovalent salts such as KBr and LiAc should behave identically).

Therefore, the theory that would include the contribution which accounts for the stability of colloid suspensions *via* van der Waals attractive interactions was introduced in 1941 by Derjaguin and Landau[54]. Independently, Verwey and Overbeek obtained the same results in 1948[55]. In the DLVO theory two types of forces were considered to act between two like-charged colloidal particles (Figure I-7):

- (i) *repulsive*: electrostatic (long-range interactions),

(ii) *attractive*: van der Waals (short-range interactions).

Attractive interactions between two individual molecules in DLVO theory are attributed to the dispersion potential (also called London or van der Waals forces). They have a quantum mechanical nature and describe the interaction between two instantaneous dipoles and depend on the polarizability and ionization potential of the molecule. Van der Waals interactions are inherent to the ions, neutral molecules and solvents. Hamaker obtained attractive forces by pairwise summation of London forces between atoms. For the two particles modeled as planar interfaces at the distance l , potential of interaction per unit area is[42]:

$$V(l) = -\frac{A}{12\pi l^2} \quad (\text{I-17})$$

where A is the Hamaker constant.

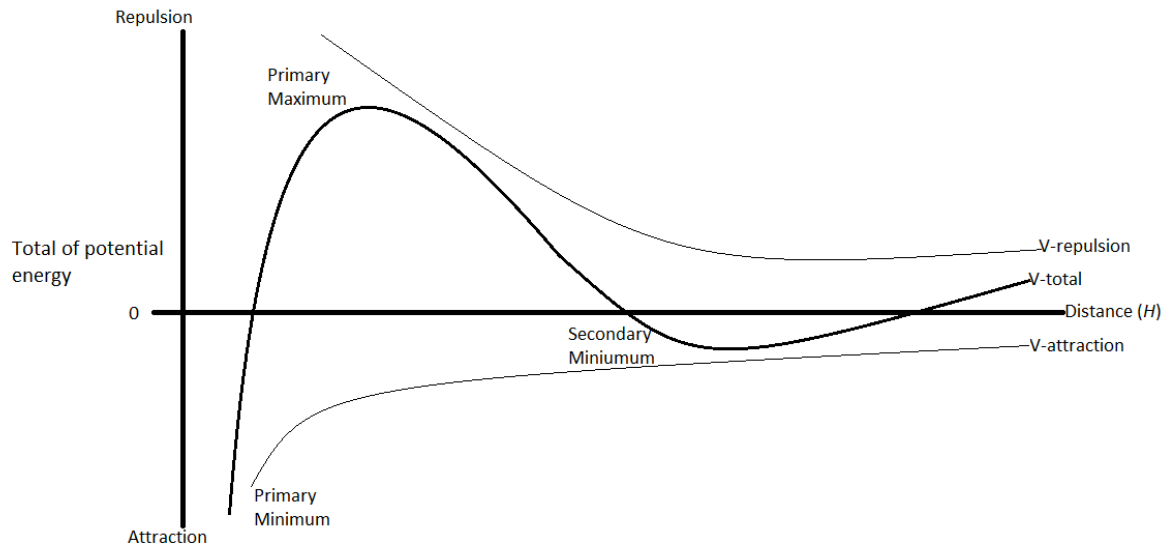


Figure I-7. Schematic representation of the free energy profile of interaction between two particles according to the DLVO theory.

However DLVO theory still could not account for ion specificity. Measured forces between cationic bilayers[56] or osmotic forces in lamellar phases[57] for bromide and acetate containing systems, showed that forces at the same salt concentration differ by a factor of 50. This can be due to[58-60]:

- (1) The DLVO theory does not take into account the other forces of nonelectrostatic nature (many body forces) such as permanent dipole–dipole (Keesom) and induced dipole–permanent dipole (Debye)

- (2) Attractive forces were treated assuming that an intervening liquid behaves the same way as bulk liquid, exhibiting the same properties up to the surface
- (3) Surfaces considered to be molecularly smooth
- (4) The number of fitting parameters attributed to the EDL theory increases the number of assumptions necessary to treat the data
- (5) The electrostatic and quantum mechanical forces can be treated separately
- (6) The medium is considered as continuum

These are the reasons why the DLVO failed at the concentration higher than 0.1 M.

3.3.2.c Lifshitz theory

In order to fix it, the next model called Lifshitz theory took into account all many body forces. This theory, developed in 1955, is based on DLVO theory and retains its assumptions: electrical and quantum mechanical forces can be treated independently, surfaces of the interacting particles are molecularly smooth, an intervening liquid has bulk liquid properties up to the surface. However, in this theory, the calculation of the attractive forces is done using quantum field theory. This theory accounts for all nonelectrostatic forces. They are many body dipole-dipole, dipole-induced dipole and induced dipole-induced dipole forces. They are temperature dependent and cannot be derived from summation of two-body molecular potentials.

The extension of Lifshitz theory, developed by Dzyaloshinski, Lifshitz and Pitaevski[61] including the interactions of the particles in the intervening liquid medium, invokes the complex mathematical analysis of quantum field theory. The attempts to simplify this model resulted in the collapse of the whole theory to a semiclassical theory[42, 62].

Even though this theory failed to comprehensively describe the contribution of all forces involved in stabilizing colloidal systems (note that it is still based on main assumptions of DLVO theory), it provides the first insight into the understanding of the long-range forces responsible for the molecular recognition, where many body potentials seem to play the main role.

3.4. What is missing in classical theories? Important interactions

We recall that standard classical theories of colloidal and physical chemistry do not involve ion specificity and fail to predict the behavior of the system for salt concentrations higher than 0.1 M. The first attempts to include specific ion effects by accounting dispersion many body forces were done introducing the Lifshitz theory. Nevertheless, the calculated difference in forces for various salts was still very weak. Hereupon modifications of Lifshitz theory[63] as well as the later

studies[64-66] have been focused on describing the Hofmeister effects with refined calculations on many body forces.

Hydration of the ion also plays an important role suggesting that hydration forces are important. Moreover, as it was shown later[67], the water structure around the ion should be considered in order to give better estimation of the ion specificity.

Another approach widely used for a last decades to study the molecular systems is computational simulations. The most famous is molecular dynamic (MD) simulations. It gives the opportunity to follow the mechanisms and dynamics of the molecular assembly systems at an atomistic level. The first MD simulations also emphasized the importance of ion polarizability[68]. Nevertheless, some recent studies[69-71] showed that MDs can provide ion specificity without inclusion of polarizability, using nonpolarizable force field. However, in these cases Lennard-Jones parameters that describe system accounting repulsive and attractive forces should be chosen carefully.

The theory that would describe ion specific effects has to account the following features:

- (1) The charge density of the ion, defined as the electric charge per unit volume, *i.e.* ion size, is the most important parameter that affects its properties[36]. The main challenge in this case is to define the proper ion radius. It can be treated as radius delivered from the crystal structure or effective radius, which includes the first hydration shell. This is not a trivial question and there is no final consensus on this issue. Besides, when the ion is polyatomic the charge density is no longer homogeneously distributed, this introduces a higher level of system complexity.
- (2) Considering the water-solid interface, an intriguing result was reported by Lund *et al.*[69, 72] where they showed that hydrophobic anions interact to the higher extent with hydrophobic surface of the macromolecule through hydrophobic attraction, whereas hydrophilic anions interact more favorably *via* electrostatic forces with cationic surfaces. Hence electrostatic effects may not always be dominant, the chemical structure and geometry of the whole system can even overcome electrostatic repulsions.
- (3) Ion specific effects cannot be characterized just by well-defined ion specific parameters that would describe properties in solution. The properties of the ions is strongly influenced by their environment, *i.e.* headgroups[73] or counterions[70] in their vicinity. This fact can also explain why the order in the Hofmeister series slightly differs between various sources. For example, Yang[74] in his review noticed that depending on the

enzymes, their activity in salt solution can change following or not following Hofmeister series, depending on the nature of enzymes. The order of the Hofmeister series can be reversed by slight variation of peptide properties by capping one of the functional group[75].

- (4) It follows from the foregoing that the structure and chemical composition of the macromolecules should be known in order to be able to estimate any Hofmeister effects. A number of recent works[72, 75, 76], especially in MD simulations, emphasize that ion-protein interactions cannot be described by simplified models of a uniformly charged protein “surface”. The surface of the protein accessible for the ions and water should be estimated in order to predict the specific interactions and therefore analyze the Hofmeister effects.
- (5) Finally, ion specific effects are salt concentrations and pH dependent (especially for biomolecules such as proteins and enzymes)[24]. As we discussed previously at a salt concentration lower than 0.1 M, electrostatic forces dominate, whereas for higher concentrations due to the screening of the electrostatic interactions, ion specificity is much more pronounced.

Accounting all these features that should be taken into account to characterize the ion specific effects, it seems that all simplified theories would be rather helpless. However the opposite was proven by Collins and his “concept of matching affinities”[36, 77].

3.5. The latest attempts to shed light on Hofmeister effects

Relatively recently, Collins proposed a simple theory that provides a better understanding of a multitude of experimental results in biology and colloidal science. For the ion classification, Collins uses terms kosmotropes and chaotropes depending on the sign of Jones-Dole viscosity B coefficient (see subchapter 3.2). Note that here, the used terms describe the affinity of water for the ion and not the water-structuring around it. Rather kosmotropes and chaotropes are understood as a characterization of the “degree of hydration”. Small ions of high charge density (kosmotropes, shown above the line) bind nearby water molecules tightly, thus immobilizing them, whereas large monovalent ions of low charge density (chaotropes, shown below the line) actually “free up” nearby water molecules, allowing more rapid motion than in bulk solution, see Figure I-8.

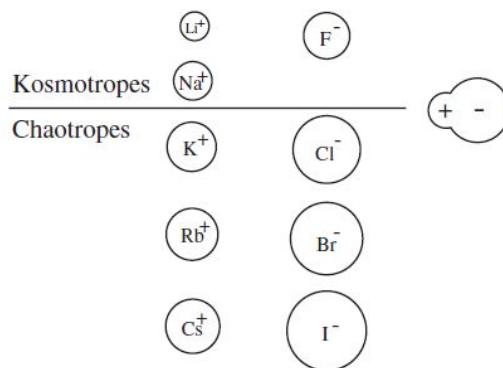


Figure I-8. Division of the group IA cations and the VIIA halide anions into strongly hydrated kosmotropes and weakly hydrated chaotropes. The ions are drawn approximately to scale. A virtual water molecule is represented by a zwitterion of radius 1.78 Å for the anionic portion and 1.06 Å for the cationic portion. In aqueous solution, Li⁺ has 0.6 tightly attached water molecules, Na⁺ has 0.25 tightly attached water molecules, F⁻ has 5.0 tightly attached water molecules, and the remaining ions have no tightly attached water[77].

The law of matching affinities is based on the observation that, for single valence ions, the oppositely charged ions with alike size tend to come together in solution to form contact ion pairs whereas oppositely charged ions with differing size tend to stay apart[36, 77]. Collins deduced his rules of cation-anion pairing by the observation of the “volcano plot” (Figure I-9 (A)). The “volcano plot” is a relationship between the standard enthalpy of solution of a crystalline alkali halide (at infinite dilution) ΔH_{sol}° , and the difference between the absolute enthalpies of hydration of the corresponding gaseous anion $\Delta H_{hyd}^{\circ}(anion)$ and cation $\Delta H_{hyd}^{\circ}(cation)$.

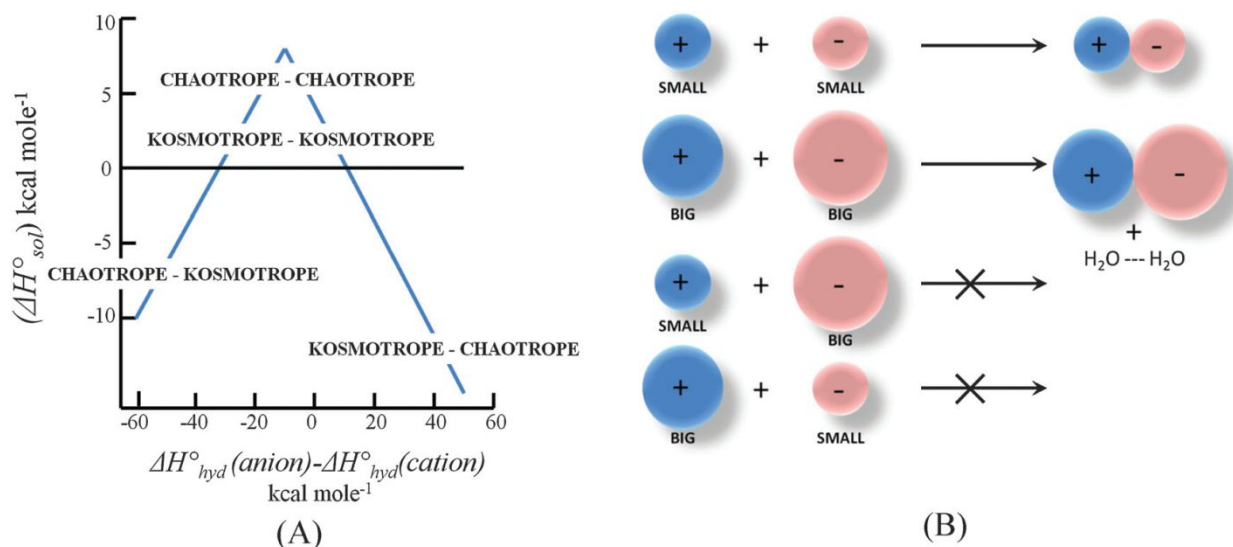


Figure I-9. The law of matching water affinities. (A) Volcano plot. (B) Schematics of law of matching affinities: a kosmotropic (chaotropic) cation would form a contact ion pair with a kosmotropic (chaotropic) anion, whereas a kosmotropic (chaotropic) cation would not form a contact ion pair with a chaotropic (kosmotropic) anion[23].

The concept of matching water affinities explains the different types of interactions that: “Cations and anions form direct stable ion pairs if their hydration enthalpies (considered to be a measure of “water affinities”) match”[23]. Two hard ions of high charge density being strongly hydrated of opposite charge have a strong reciprocal attraction. Coming close, they form direct ion pairs liberating the hydration spheres between them in the bulk solution. For the soft ions of low charge density the association of opposite charged ions is favorable due to the decrease of ion-water contact. Hence, the weakly hydrated chaotropic ions can also form direct ion pairs expelling also the hydration water between them. The interaction of one hard and one oppositely charged soft ion is then straightforward: here, the attraction by the soft ion is not strong enough so that the hard ion loses its hydration shell. As a consequence, a soft/hard ion pair is always separated by water and cannot form strong ion pairs, see Figure I-9 (B).

This concept can be applicable to explain many phenomena in Hofmeister effects[24], *i.e.* why hard anions are usually considered as salting-out and soft anions as salting-in, whereas for cations it is just the other way around. Soft cations are salting-out and “hard cations” salting-in. Besides, MD simulations, done in the group of Jungwirth, confirm Collins’ law of matching water affinity[78, 79]. Encouraging results were obtained by Vlachy *et al.*[24, 73]. Using a computational approach they succeeded in classifying the headgroups in a Hofmeister-like series in order to estimate the contribution of the nature of the headgroups on the ion specific effects. It was shown

that according to the law of matching water affinity, hard headgroups tend to form contact ion pairs with hard counterions, whereas for the soft headgroups ion pairing with poorly hydrated soft counterions is preferable, Figure I-10.

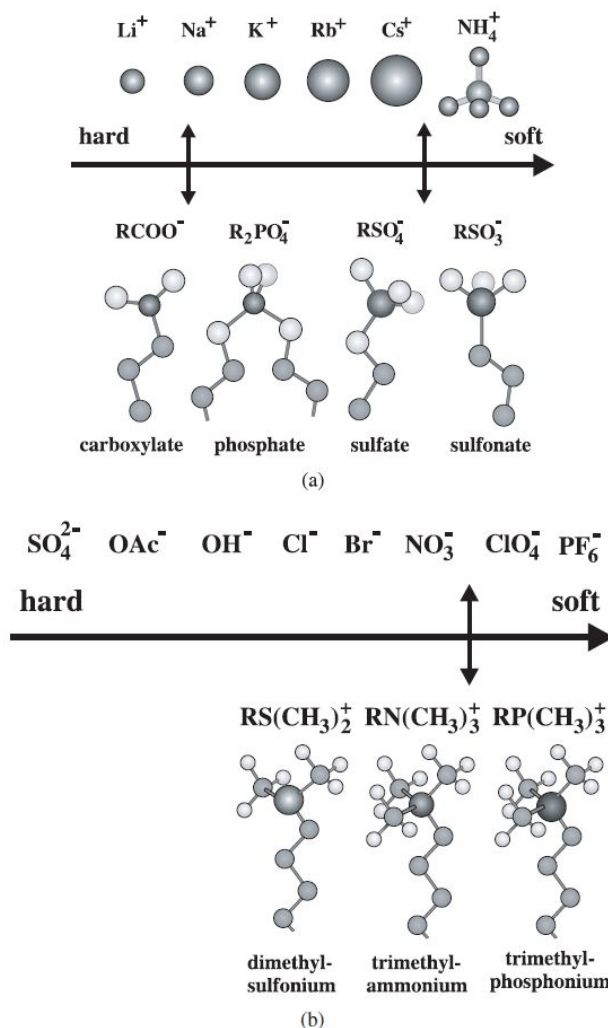


Figure I-10. “Like seeks like”: hard headgroups preferentially interact with hard counterions; soft headgroups preferentially interact with soft counterions. (a) Cations with negatively charged headgroups, and (b) anions with positively charged headgroups[24].

However, one should remember that this concept of matching water affinities is a very simplified one that should only be taken as a rule of thumb. In real systems the additional effects, implementing more complex interactions need to be considered[80].

3.6. The latest studies

In this last part of our introduction we would like to discuss some of the latest studies on Hofmeister effects including theoretical, computational and experimental approaches.

For example, Ruckenstein and Huang[81] in their study discovered how does the nature of an electrolyte influence to the strength of repulsion between two charged plates. Conversely to the classical DLVO theory, their theory considers the hydration of the ions and reflects the specificity for the ions of opposite signs to that of the surface charge. As was reported, the strength of the repulsive force between two charged plates for different anions present in the solution follows the order $\text{OH}^- < \text{Ac}^- < \text{F}^- \sim \text{Cl}^- < \text{Br}^- < \text{H}_2\text{PO}_4^- < \text{I}^- < \text{NO}_3^- < \text{ClO}_4^-$. And for the cations follows the order $\text{NH}_4^+ > \text{Cs}^+ > \text{Na}^+ > \text{K}^+ > \text{Li}^+ > \text{H}_3\text{O}^+$, see Figure I-11.

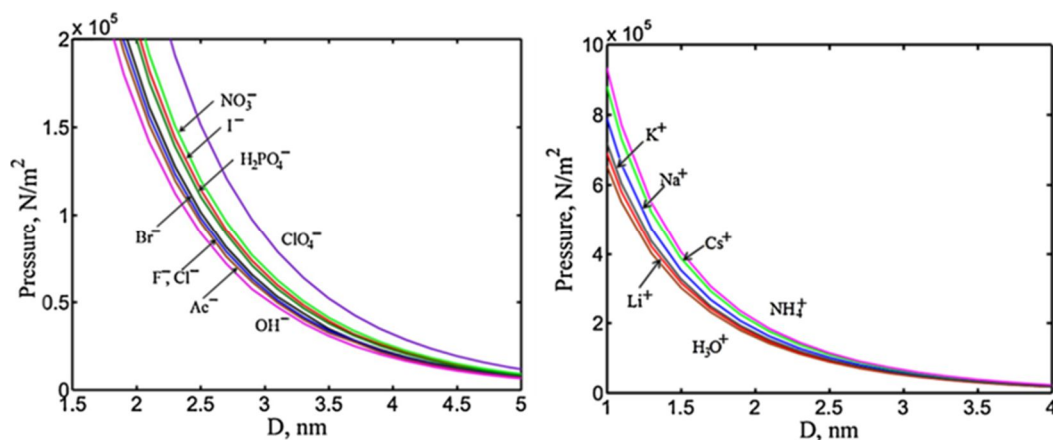


Figure I-11. Repulsive force between two plates at various surface charge densities for various anions and a cations. Salt concentration $c = 0.1$ M. Surface charge density 0.02 C/m^2 [81].

Another work by Song and co-workers[82] which demonstrates how complex ion–ion interactions, originating from electrostatic interactions, and ion–water interactions manifest themselves in the Hofmeister effects. It was shown that analyzed water diffusion constant changing (at least partially) due to electrostatic interactions between the ion and water. It also was found that energy attributed to the perturbation of the hydrogen bonds of water is important for the charge density at water-air interface. It will be directly influenced by ion nature.

In addition to the theoretical studies, Hofmeister effects also were investigated by experimental and computational approaches.

Willott *et al.*[83] investigated the ion specific effects on the polymer brushes¹ with different hydrophobicity. First, it was shown that the behavior of these polymer brushes in the aqueous solution is strongly dependent on the salts concentration. Second, these systems as well are ion dependent. The strongly kosmotropic acetate anions display low affinity for the hydrophobic polymers, and largely unscreened electrosteric repulsions allow the brushes to remain highly

¹ **Polymer brushes** are surface coatings of densely packed flexible polymer chains anchored by one end to an interface

solvated at higher acetate concentrations. The mildly chaotropic nitrate and strongly chaotropic thiocyanate anions exhibit a polymer hydrophobicity-dependent affinity for the brushes.

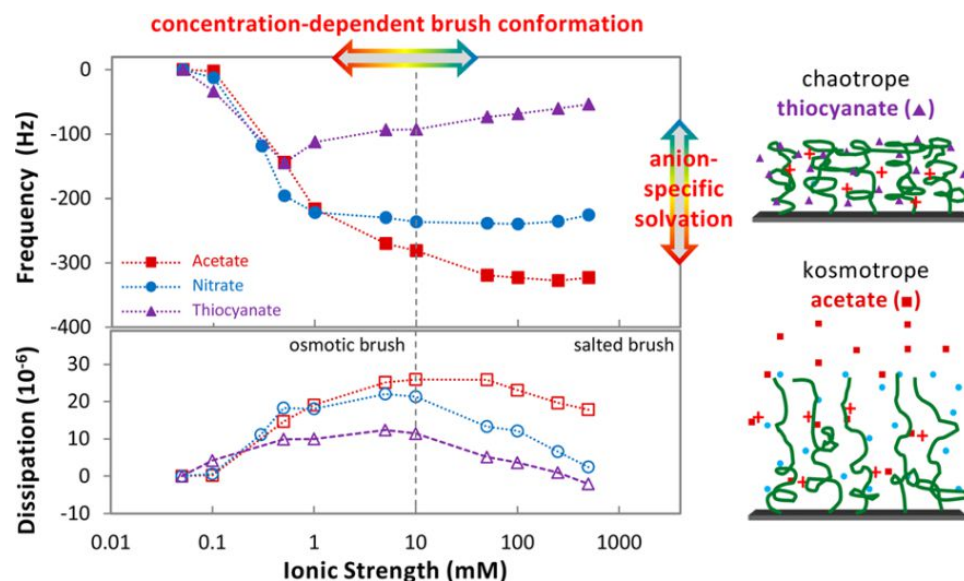


Figure I-12. Equilibrium QCM-D frequency response and dissipation changes of poly(DEA) brush as a function of the solution concentration of potassium acetate (■), nitrate (●), and thiocyanate (▲). The pH was controlled at 5.5 ± 0.1 . On the right there is a schematic illustration of the ionic-strength-dependent conformational brush behavior[83].

Recently the group of Chaimovich[84] published a work where they discussed the impact of counterions on the dodecyltrimethylammonium micelles focusing on the properties of triflate (Tf^-). Combining experimental and computational results they showed that in comparison to other micelle types, the DTATf micelles have a higher average number of monomers per aggregate, an uncommon disk-like shape, smaller interfacial hydration, and restricted monomer chain mobility. These results demonstrate that the $-\text{CF}_3$ group in Tf^- was directly responsible for the observed shape changes by decreasing interfacial hydration and increasing the degree of order of the surfactant chains in the DTATf micelles.

Concerning the systems of higher level of complexity such as rod-like micelles, the effect of different anions on the rheological behavior of cetyltrimethylammonium-salicylate wormlike micelles was investigated by Alkschbirs *et al.*[85]. Such wormlike micelles, being a dynamic system, exhibit interesting viscoelastic properties due to their ability to break and reform within a characteristic lifetime. Hence the each system can be described in terms of time required for breaking or reptation. This time for each process calls relaxation time. In the work of Alkschbirs *et al.* it was shown, that the systems in the presence of salts present shorter relaxation times due to the

charge neutralization associated with the adsorption of the anions on the micelles surface. The magnitude of the effect depends on the nature of the anions, which follows the Hofmeister series.

In our work we elucidate the interactions contributing to ion specific effects at molecular and bulk solution levels by carrying out complementary experiments and simulations to determine the effect of systematic changes of amphiphile structure, with a particular focus on headgroup structure and counterion type, on their aggregate properties. The goal of this comprehensive analysis is to get insight into the effect of interfacial ionic and molecular interactions on aggregate properties (*via* physical characterization) based on determination of interfacial water, headgroup, and counterion concentrations by experiment (chemical trapping) and by simulation (molecular dynamics and density functional theory, MD/DFT). The analysis of the relationship between the properties of the ions such as hydration, hydrogen bonding, electrostatic, ion pairing, and polarization interactions and the behavior of amphiphile aggregates in the solution gave us better understanding of the interactions contributing to the balance of forces that control the physical properties of solutions of ionic amphiphiles.

As was discussed above, such ion property as ion size and polarizability are directly related to the dispersion forces that seem to play an important role in the stabilization of the colloids. Moreover, the size and morphology of the ion can have some specific steric effect on the structure of aggregates. Hydration free energy, estimated from Born self energy, gives an information about interactions between ions and water molecules. Ions with higher negative values of free hydration energy (hydrophilic) interact with water more favorably forming the hydrated ion spheres, whereas ions having lower negative hydration energy are weakly hydrated and are called hydrophobic. The hydration number is another measure of ion hydration. The electron density of the ion, that is one of the most important characteristic of the ion specificity, can be correlated with pKa values of the conjugated acid. Finally, as would be discussed later, lyotropic number is directly related to the Hofmeister series. Correlation between these anions properties and the properties of self-assembly of the cationic gemini surfactants would be discussed in this work.

Chapter II. Synthesis and characterization of cationic gemini surfactants

Introduction

As was described in Chapter I, the influence of ion specific effects on the self-assembly process of amphiphile molecules has remained unsolved challenge for a long time. Even though many experimental and computational studies were performed in order to understand the contribution of ion properties to the Hofmeister effects, the unifying theory is still missing and thus the Hofmeister series yet represent an appealing challenge in colloid and interface science. Simplifying the macromolecular system under investigation, we decreased the number of factors that can influence its colloidal properties, focusing on ion effects. In our work, cationic gemini surfactant with different counterions were studied. Keeping the same cationic part (amphiphile molecule) we changed only the counterion in order to analyze the ion effects on the self-assembly process of this surfactant.

Gemini surfactants are very interesting for several reasons[86]. They have significantly lower CMCs compared to their monomeric analogs, while retaining high solubility. This feature results in large variations in morphologies of self-assembled systems. In the present study we focus on cationic gemini surfactant $C_2H_4-1,2-((CH_3)_2N^+C_{10}H_{21})_2$ denoted as 10-2-10, associated with variety of counterions X. Then length of the hydrophobic chains, C10 was chosen by the requirement of the method used (see below) to study and characterize micellar solutions. Each ammonium headgroup is neutralized by a monovalent counterion. Due to the relatively short alkyl chain length, 10-2-10 gemini surfactants can form spherical micelles up to relatively high concentrations above their CMCs. This feature is important for the investigation of these compounds by chemical trapping and fluorescence quenching experiments. Indeed, for these probing techniques, the required amphiphile/probe ratio should be fixed in order to analyze data precisely. Thus, CMCs of the gemini amphiphile should be greater than 1mM.

As summarized in Glossary, we focused on the anions that provide significant variation in hydrophilicity ($X = \text{halide ions, } H_2PO_4^-, NO_3^-, HCOO^-, CH_3COO^-, CF_3COO^-$). It was interesting to compare counterions with similar hydrophilicity ($H_2PO_4^-, CH_3COO^-$ and F^-) or hydrophobicity (Br^- , NO_3^-) and with somewhat different characteristic trends such as ionization degree and CMC in solution. We have also studied organic anions from formate to octanoate ($HCOO^-$ to $CH_3(CH_2)_6COO^-$) because they show distinct changes in their interfacial properties when the chain length of the alkyl group increases. For example, for the short hydrocarbon chains carboxylate: e.g. C1–C3, normal surfactant behaviors were observed whereas when tail lengths are about 6 carbons or

longer, they behave like cationic amphiphile[87, 88] or mixed micelle[89]; in the later case, counterion tail contributes to the hydrophobic effect.

Another type of cationic surfactant that was investigated is tertiary 10-2-10 X gemini ($X = \Gamma^-$, Br^- , Cl^-). For these gemini, one of the two methyl groups from a quaternary gemini surfactant headgroups have been replaced by a proton as shown in Figure II-1. These gemini were compared with the quaternary one since the variation of the hardness/softness of the headgroups could change the balance of forces that control the self-assembly. Weakly hydrated ions should form ion pairs with quaternary ammonium headgroups more easily than strongly hydrated ions and the interactions should follow a Hofmeister series, as is generally observed with ionic surfactants. However, the headgroups with tertiary ammonium may be more hydrated and may interact with the counterions by hydrogen bonds, which would be strongest for the small anion, *e.g.*, F^- , and the Hofmeister series might be reversed.

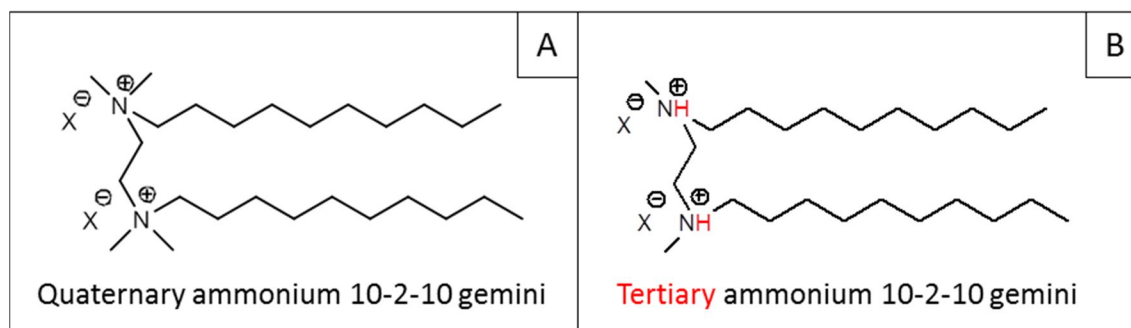


Figure II-1. Structure of quaternary (A) and tertiary (B) ammonium 10-2-10 gemini surfactants.

1. Synthesis and characterization of 10-2-10 gemini

In this paragraph we focus on the synthesis and characterization of cationic 10-2-10 gemini surfactants with various counterions. The details of the synthetic procedures will be described in the experimental section.

1.1. General synthetic procedure for quaternary 10-2-10 gemini compounds with different counterions

Quaternary ammonium 10-2-10 gemini surfactant with different counterions were synthesized according to the procedure reported for 14-2-14 X salts by Manet *et al.*[90] with modification, due to the high solubility of 10-2-10 amphiphile molecules compared to their 14-2-14 analogue.

First of all 10-2-10 Br was synthesized by a dialkylation reaction of N,N,N',N'-tetramethylethylenediamine (TMEDA) with decylbromide. This compound was then used for the counterion exchange reactions. The procedure of salt metathesis reactions is closely related to the affinity of the anion to the headgroup, as well as the acidity of the acid. Thus, we have used three approaches for anion exchange, depending on the pKa of the acid as summarized in Figure II-2. When the pKa of the acid (HX) is above 3, bromide counterions of amphiphiles are exchanged by mixing the corresponding HX and gemini bromide, in the presence of Ag₂CO₃ (Figure II-2, synthetic route A). In this case, the silver salt of the acid and the 10-2-10 with the carbonate anion (CO₃²⁻) surfactant were formed before the complete ion exchange. In the case of acetate and fluoride anions their silver salts are commercially available, thus the ion exchange can take place directly leading to the formation of the corresponding 10-2-10 X (Figure II-2, synthetic route B). Thus, for route A and B, ion exchange takes place, and a precipitate of AgBr is observed. After AgBr was removed, amphiphiles having X counterions were isolated and purified.

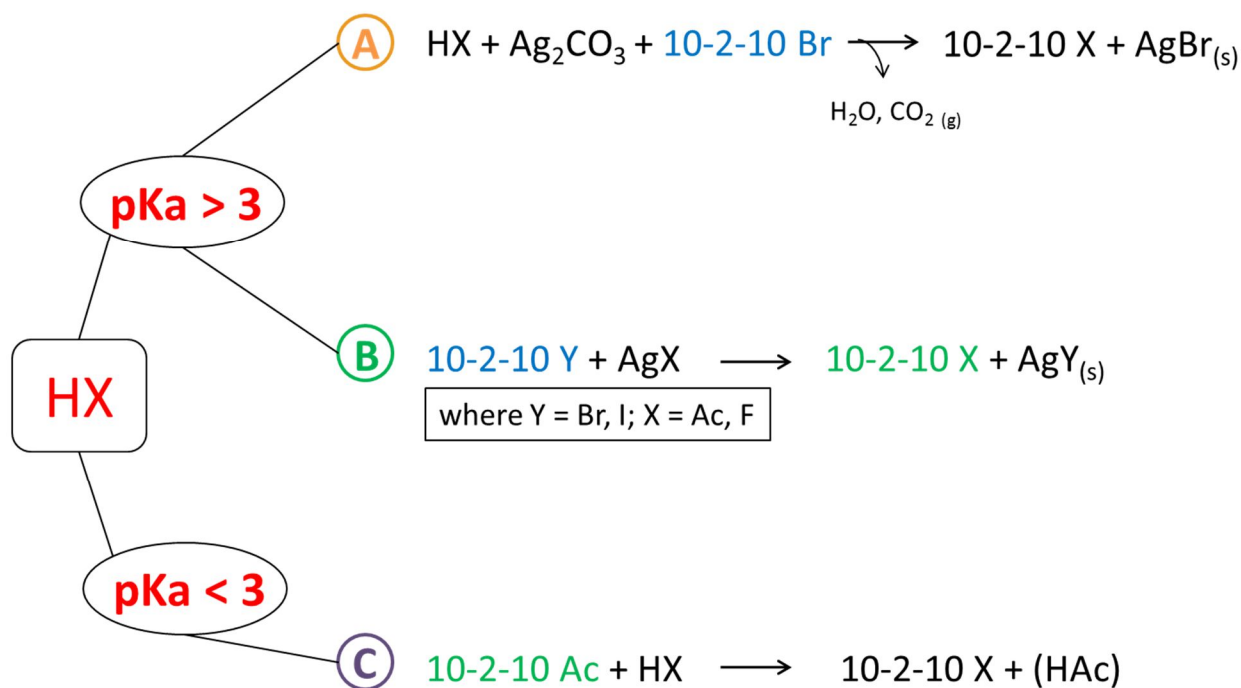
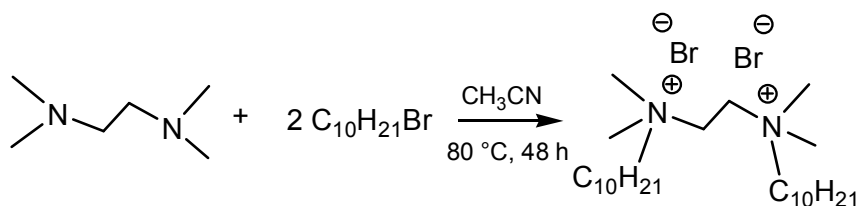


Figure II-2. Scheme of the synthetic routes for counterion exchange for 10-2-10 X gemini.

When the pKa of the acid is below 3 (Figure II-2, synthetic route C), gemini acetate is used for anion exchange with the corresponding acid, leading to the formation of amphiphiles with various counterions. For all these ion exchange reactions, methanol was used as solvent. The obtained salts were purified by washing the solid with adequate solvent or by crystallization.

1.1.1. Synthesis of 10-2-10 Br

10-2-10 Br was synthesized by dialkylation of TMEDA with 1-bromodecane in acetonitrile at 80 °C, over 2 days (Scheme II-1). This compound was obtained as a white powder in good yields (80-85%).



Scheme II-1. Synthesis of 10-2-10 Br

The purity of this compound was checked by NMR analysis. The typical ^1H NMR spectrum for 10-2-10 Br in MeOD is presented in Figure II-3. Since the molecule of 10-2-10 gemini is

symmetric, NMR peaks overlap and only one set of signals is observed for both monocationic chains. The singlet at 4.06 ppm and multiplet at 3.51 ppm are attributed to the four protons of the spacer and the four protons of the α -CH₂ for both chains respectively. Twelve hydrogen atoms from the methyl groups of ammonium heads appear as a singlet at 3.28 ppm. The other three signals, two multiplets and one triplet are assigned to the protons of the alkyl chains. Four protons for β -CH₂ groups, twenty eight protons for the other CH₂ groups and terminal methyl groups appear at 1.85, 1.42-1.31 and 0.90 ppm respectively.

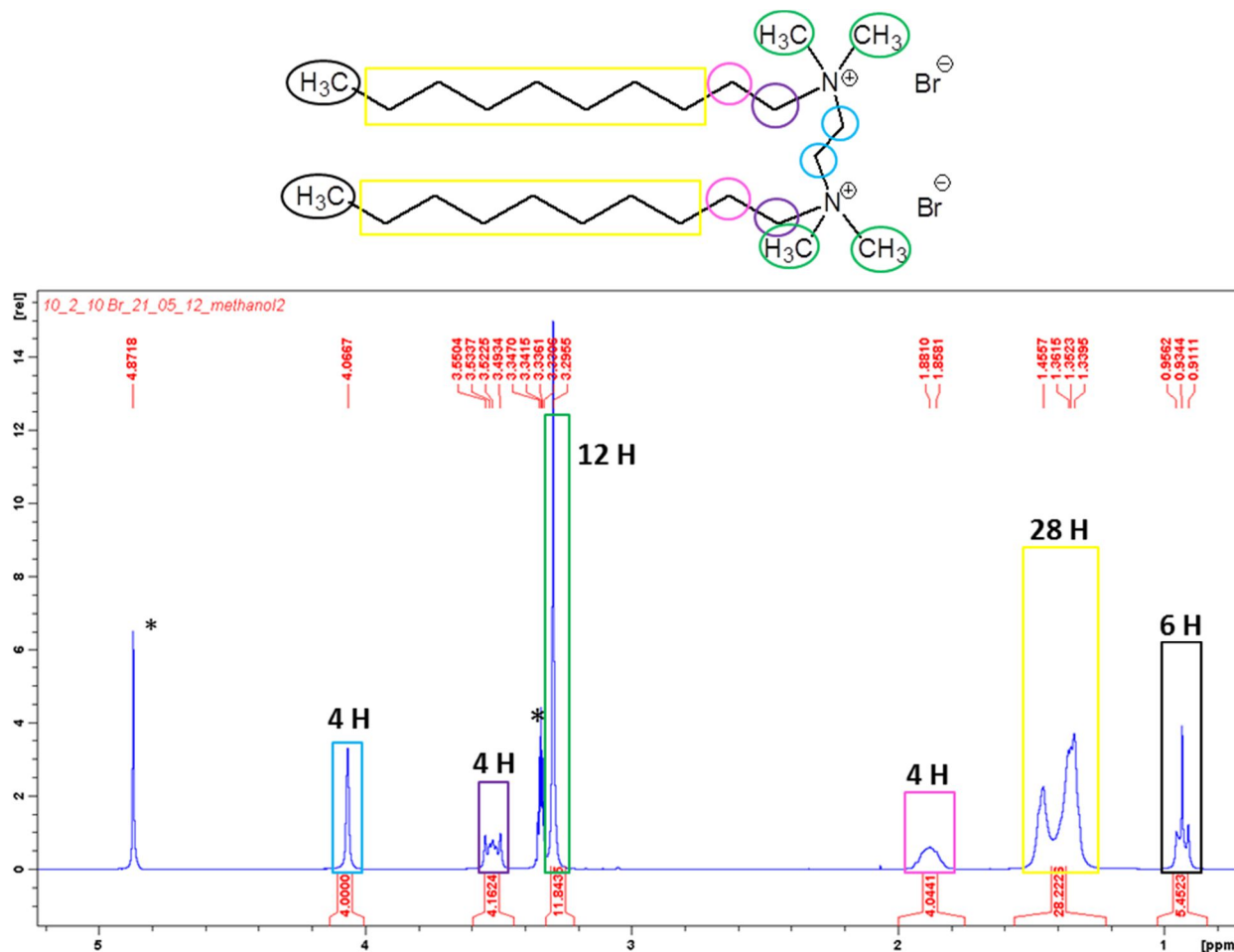


Figure II-3. ¹H NMR spectrum of 10-2-10 Br in MeOD. The colors indicate different protons detected by ¹H NMR in the molecule. The peaks with the star are attributed to the solvent.

As NMR is not able to provide information about the stoichiometry between the bromide anion and the nitrogen, XPS analysis was also used to characterize the 10-2-10 Br powder. Indeed, it is important to have a pure 10-2-10 Br salt, since this compound is a starting material for counterion exchange. Theoretically one molecule of 10-2-10 Br has 2 nitrogen atoms, 26 carbon atoms and 2 bromide anions. According to the results obtained by XPS, we found a ratio of 2, 27.1 and 2.1 for nitrogen, carbon and bromine atoms respectively (Table II-1). Considering a standard error due to

the deconvolution of the peak and the sensitivity of the machine, these results show that the experimental stoichiometry of Br^- is in good agreement with the theoretical one. The excess of carbon typically comes from atmospheric contamination. Furthermore, the position of the N1s peak (around 402 eV) strongly suggests that all nitrogen atoms in this compound are in their ammonium form[91] (Figure II-4).

Table II-1. Quantification of N, C and Br for 10-2-10 Br molecule via XPS.

Element	N1s (300 eV)	C1s (285 eV)	Br3d (68 eV)
Theoretical	2	26	2
Experimental	2	27.1	2.1

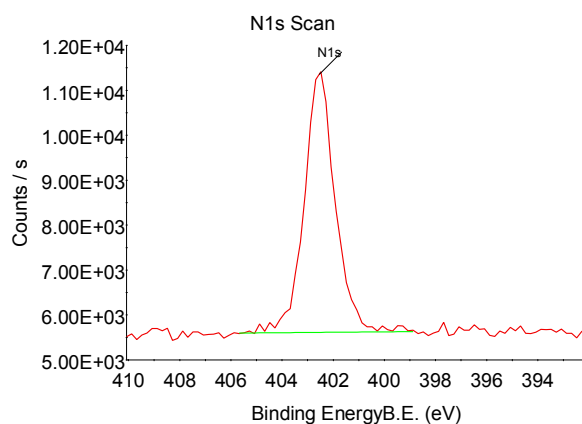


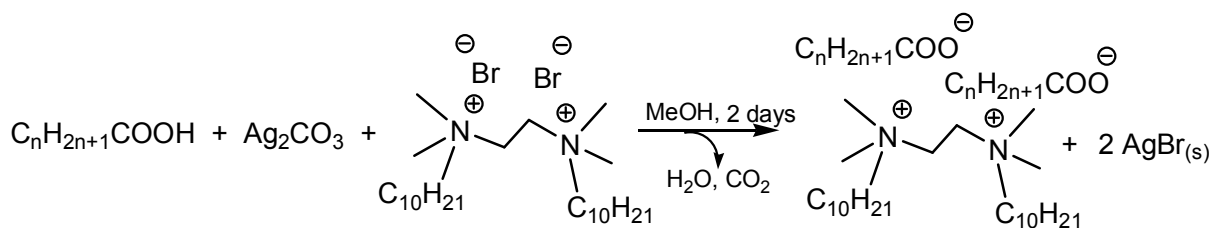
Figure II-4. XPS high resolution spectrum of the N1s region for 10-2-10 Br.

1.1.2. Synthesis of 10-2-10 I

10-2-10 I was synthesized according to the same procedure used for the synthesis of 10-2-10 Br. TMEDA was dialkylated with 1-iododecane in acetonitrile. The compound was obtained with product yield ~80%. Its purity was checked by ^1H NMR analysis.

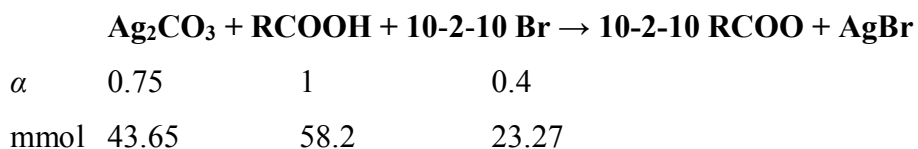
1.1.3. Counterion exchange for the ions of weak acids ($\text{pK}_a > 3$), using the synthetic route A

The synthetic approach used for anion exchange with weak acids is summarized in Scheme II-2.



Scheme II-2: Synthesis of 10-2-10 gemini with carboxylate counterions.

As mentioned before, for counterion exchange in the case of weak acids (HX, $pK_a > 3$), a one-pot reaction was carried out, where Ag_2CO_3 was used as a reagent providing the counterion exchange between HX and 10-2-10 Br. Intermediate products were not isolated. To obtain desired 10-2-10 carboxylate, Ag_2CO_3 (0.75 eq.) and acid (1 eq.) were mixed in MeOH (75 mL) under continuous stirring at 40 °C during 30 min. After 10-2-10 Br (0.4 eq.) solubilized in MeOH (75 mL) was added. The reaction mixture was stirred at the 40 °C for 2 days. Aluminum foil was used to protect the reaction mixture from light in order to prevent photoreaction. The advantage of this method is that there is no need to isolate the silver salt before the exchange reaction with gemini salt.



After completion, the solvent was concentrated under vacuum and the silver salts were removed by filtration through celite. This step was performed 2 to 3 times. Note that a minimum amount of MeOH was used to avoid the solubilization of silver salts. After filtration, the methanol was evaporated under vacuum. The residue in the case of acids with three and four carbon atoms (C3-C4) was dissolved in hot (60 °C) CH_3CN (~ 10 mL) and cooled to room temperature to give crystals of 10-2-10 C3/10-2-10 C4. For the compound bearing counterions of five carbon atoms (C5), a mixture of $CH_3CN/MeOH$ (200/0.5mL, v/v) was used. Gemini with C6-C8 counterions were solubilized in hot methanol (60 °C) and precipitated with acetone due to their much higher hydrophobicity. All obtained products (crystals or powder) had a grey color due to the impurity of silver salts. These compounds were again solubilized in hot CH_3CN for C3-C4 and $CH_3CN/MeOH$ for C5 and these hot mixtures were filtered through celite. After cooling down the solvent, a white precipitate was formed. It was collected and dried under vacuum. The compounds with counterions

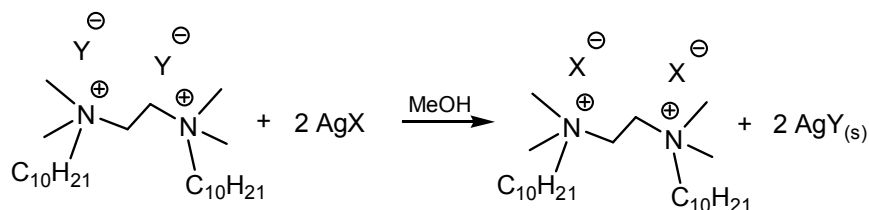
of C6-C8 chain length were filtered through Celite from MeOH (r.t.). The MeOH was evaporated under vacuum, until the residue on the bottom becomes totally dry, otherwise the traces of water will influence the solubility of the compound during precipitation. The residue was dissolved with a minimal amount of MeOH at 60 °C and precipitated by adding acetone.

The purity of the obtained compounds (C3-C8) was verified by ¹H NMR in MeOD with increased recycling delay (D₁): C3 – 20s, C4-C5 – 15s, C6 – 10s instead of 2s, usually used. Recycling delay was increased to obtain good integration of the peaks corresponding to the carboxylate moieties. It is during this delay that the excited sample returns to its equilibrium state and the optimum delay is sample dependent. Compared with the gemini moiety, the carboxylate counterions are small molecules and their relaxation time is higher due to their fast motion. One can see that with increasing the size of the anion (increasing the length of the hydrophobic chain), less time for the recycling delay is required.

The completion of the reaction was checked using a method that is based on the photoreduction of AgBr to silver metal and molecular bromide as follow: 25 mg of obtained powder for C1-C6 and 10 mg for C8 was dissolved in 0.5 mL of MeOH and 20 mg of AgAc was added in this solution, and the mixture was irradiated with the natural light for 1 day. If the ion exchange is not complete, mixture will become black due to the reduction of AgBr (formed by ion exchange between 10-2-10 Br and silver acetate) to black silver metal and molecular bromide. If the exchange reaction was complete, the test will be negative, as no black silver metal can be obtained due to the absence of AgBr in the mixture.

1.1.4. Counterion exchange for the ions of weak acids (pK_a > 3), using the synthetic route B

The synthetic procedure for the counterion exchange of week acid ions, made with synthetic route B Figure II-2 is shown on the Scheme II-3, where Y = Br and I for synthesis of 10-2-10 Ac and 10-2-10 F respectively.



Scheme II-3: Synthesis of 10-2-10 Ac.

Since silver acetate and silver fluoride are commercially available we can directly perform the exchange reaction with the gemini amphiphile (see Scheme II-3). Although the synthesis of

10-2-10 Ac and 10-2-10 F lead to AgY formation, their synthetic methods are different, and will be discussed separately.

Synthesis of 10-2-10 Ac

To obtain 10-2-10 Ac, a counterion exchange was performed by the reaction between 10-2-10 Br and silver acetate. Formation of AgBr precipitate drives the reaction and provides the formation of 10-2-10 gemini salt of Ac, in about 70%.

Synthesis of 10-2-10 F

To prepare 10-2-10 F we used 10-2-10 I instead of 10-2-10 Br for the exchange reaction, since for the iodide salt reaction completion can be easily assessed, by adding hydrogen peroxide to the mixture. If the reaction is incomplete, the colorless solution of 10-2-10 I becomes yellow due to the oxidation of iodide to molecular iodine, indicating that there is still 10-2-10 I present in the reaction mixture.

In this case the photoreduction experiment was inappropriate to follow the reaction, since it will oxidize both the 10-2-10 Br and AgF, consequently the disappearance of 10-2-10 Br cannot be quantified precisely. To check if the reaction is complete, the test experiment has been done as follow: we stopped the stirring and took an aliquot of the transparent solution and then add H₂O₂ to this solution. If the solution turns yellow, there is still 10-2-10 I and the exchange reaction is not finished.

The purification of 10-2-10 F was performed by filtering the reaction mixture through celite and evaporation of methanol solution under vacuum. This step was repeated several times until the residue of 10-2-10 F will become white. Crystals of 10-2-10 F were obtained by crystallization the compound from acetone, filtered and dried under vacuum. It is important to note that, this compound cannot be dried by lyophilization, due to its decomposition under strong vacuum.

Stability of 10-2-10 F

10-2-10 F is stable for a few days at room temperature, and after it starts to decompose slowly. The use of strong vacuum facilitates its decomposition. The compound changes its color from white to brownish and acquires unpleasant odor. The decomposition of 10-2-10 F can be followed by proton NMR as shown on the Figure II-5. This figure presents the ¹H NMR spectra of 10-2-10 F just after the synthesis (A) and after several days at room temperature (C).

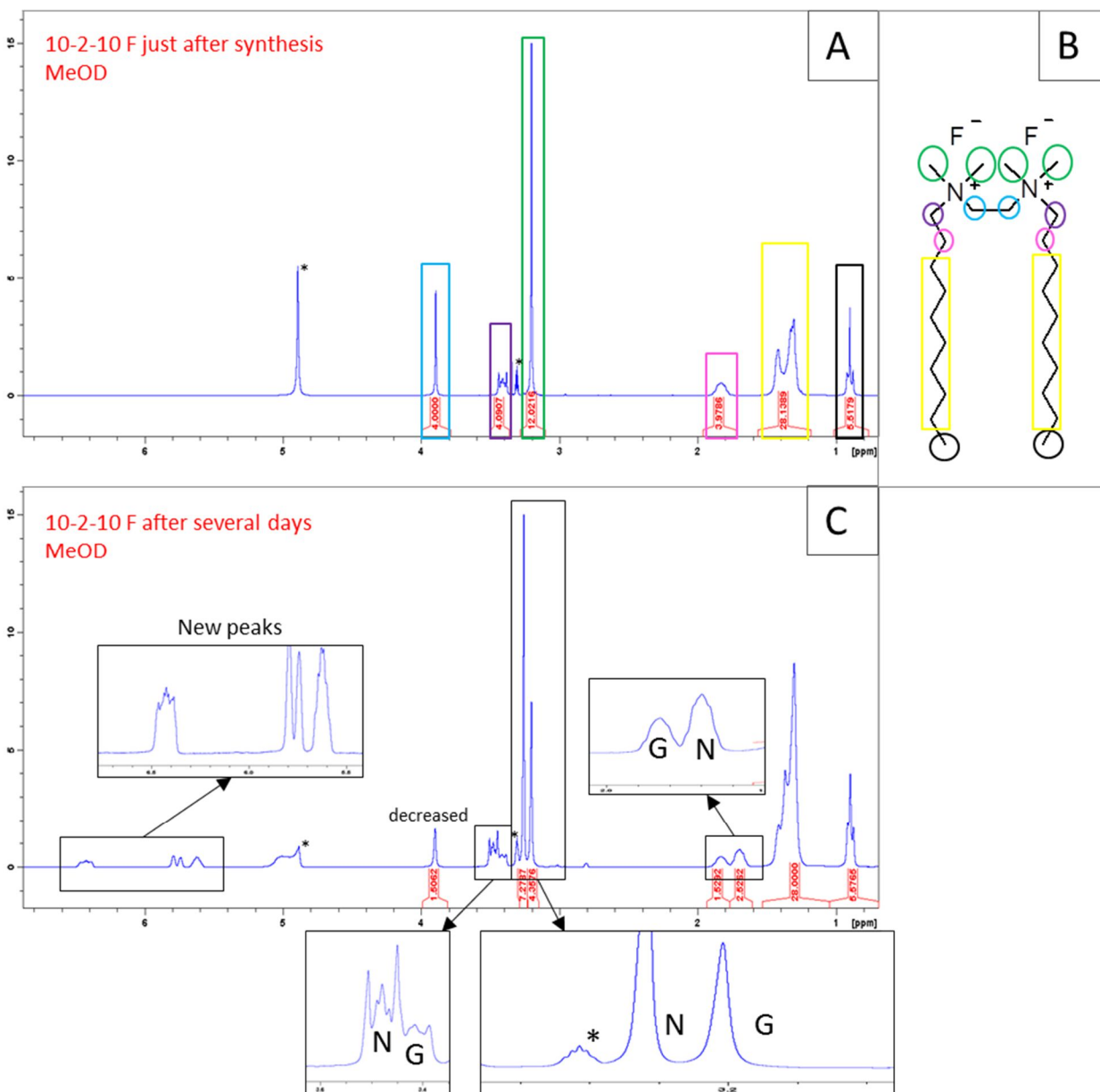
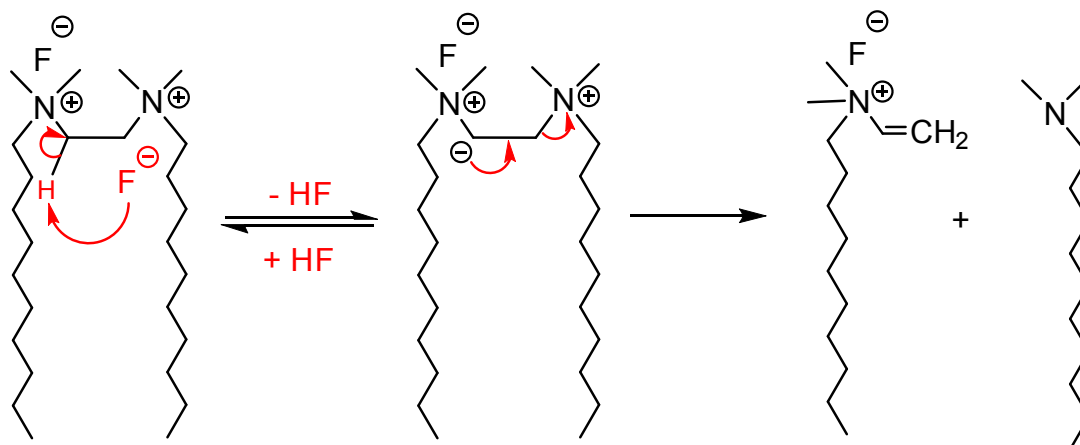


Figure II-5. ¹H NMR spectra of 10-2-10 F just after synthesis (A) and ¹H NMR of 10-2-10 F after the decomposition (C). Each signal at ¹H NMR spectrum (A) represents a group of protons in the structure of gemini (B). On the Figure (C), label N represents new peaks that appeared during decomposition, whereas label G represents the remaining peaks of 10-2-10 F. Peaks for solvent are noted with the star.

The decomposition of 10-2-10 F is confirmed by the appearance of new peaks in the range of 5-7 ppm, indicating the formation of unsaturated bonds. The integration of the peak attributed to the spacer decrease from 4 to 1.5. The intensity of the signals attributed to methyl groups in α and β position to the nitrogen atom decreases, when the new peaks appear (Figure II-5 C), indicating the transformation of 10-2-10 F gemini molecule to decyl(dimethyl)amine and decyl(dimethyl)vinylammonium fluoride as shown in Scheme II-4. Due to the low stability of the

fluoride ions and the high acidity of protons in α position to the nitrogen atom, the fluoride reacts with the spacer by deprotonation generating hydrogen fluoride, decyl(dimethyl)amine and the vinyl ammonium compound.



Scheme II-4. Decomposition of 10-2-10 F.

The XPS analysis of 10-2-10 F was not possible due to the high vacuum (10^{-7} Pa) used with this technique. In this case, 10-2-10 F decomposes during the experiment and two peaks are obtained for N1s as shown in the XPS spectra below (Figure II-6). The first peak at 399 eV (A) probably corresponds to the decyl(dimethyl)amine and the second one at 403 eV (B) to the ammonium decyl(dimethyl)vinylammonium fluoride. This XPS result confirms the dissociation of the 10-2-10 F gemini compound into two nitrogen-based molecules: amine and ammonium.

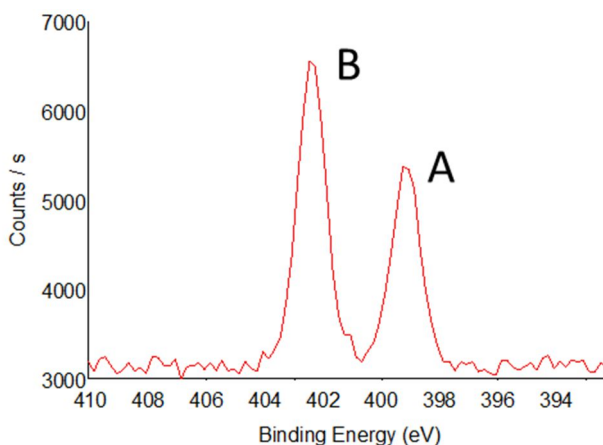
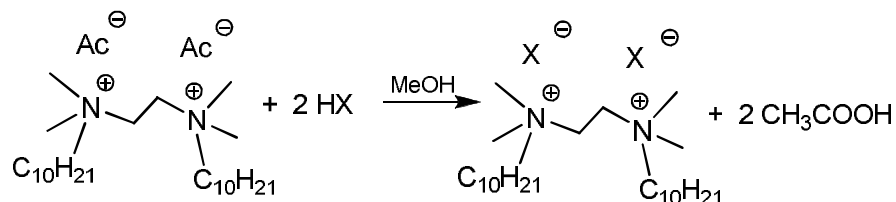


Figure II-6. XPS high resolution spectrum of the N1s region for 10-2-10 F. Peaks A and B correspond to amine (~ 399 eV) and ammonium (~ 403 eV) respectively.

1.1.5. Counterion exchange for the ions of strong acids ($pK_a > 3$), using the synthetic route C

For exchange reactions with strong acids 10-2-10 Ac was used instead of 10-2-10 Br as shown in Scheme II-5. Since acetic acid is a weak acid, it is easy to replace the acetate anion with an

anion from a strong acid (HNO₃, H₃PO₄, HCl, TFA, MeSO₃H and even HCOOH). The general procedure for all the anions, with exception of H₂PO₄⁻ and HCOO⁻, is described below.



Scheme II-5. Synthesis of 10-2-10 gemini with counterions originated from a strong acids.

To a methanol solution of 10-2-10 Ac, 2 or 3 equivalents of HX were added, and the mixture was stirred at 40 °C for 2 h. The reaction was monitored by ¹H NMR by the disappearance of the signal attributed to acetate at 1.90 ppm. The final product was precipitated by adding less polar solvent in the methanol solution (Table II-5) and dried under vacuum.

The purity of compounds was checked by ¹H NMR. No significant change was observed by ¹H NMR after the ion exchange. The anion cannot be observed by ¹H NMR, and the signals attributed to the gemini amphiphile are similar to those of the corresponding bromide salt (Figure II-3). Thus, the ¹H NMR spectra of these are not shown here.

Synthesis of 10-2-10 H₂PO₄.

Since 10-2-10 H₂PO₄ was poorly soluble in MeOH the procedure described above was modified. Thus, a methanol solution of H₃PO₄ 85% wt was added dropwise to a methanol solution of 10-2-10 Ac under continuous stirring at room temperature. A white precipitate of 10-2-10 H₂PO₄ was formed immediately. The reaction mixture was stirred overnight to complete the reaction. The completion of the reaction was checked by ¹H NMR using D₂O as a solvent. The disappearance of the signal attributed to acetate anion peak at 1.90 ppm indicated that reaction was complete. The precipitate was filtered and dried under vacuum line and by lyophilization.

The compound was characterized by ¹H, ¹³C and ³¹P NMR. By phosphorous NMR it could be determined if the phosphate was mono or dianionic. For this experiment we took monosodium and disodium phosphate salts which give a signal at 3.1 and 5.7 ppm in ³¹P NMR (D₂O) respectively as reference. The signal of 10-2-10 H₂PO₄ in ³¹P NMR appears at 3.2 ppm, indicating that the phosphate was monoanionic, see Figure II-7.

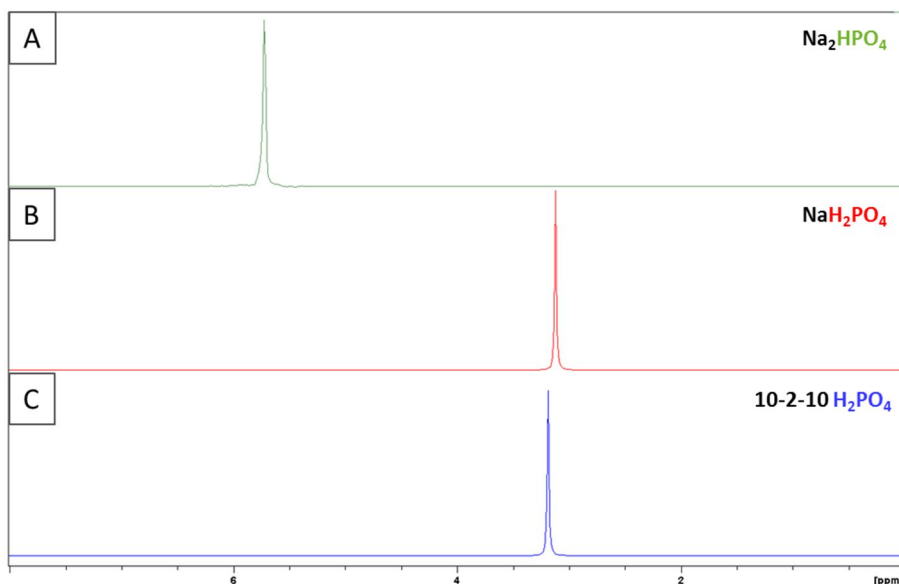


Figure II-7. ^{31}P NMR spectrum of Na_2HPO_4 (A), NaH_2PO_4 (B) and 10-2-10 H_2PO_4 (C) in D_2O .

Synthesis 10-2-10 C1 (formate)

The pKa of formic acid is 3.75. It is a weak acid, but stronger than acetic acid (pKa = 4.75). Hence method C can be used for an anion exchange with some modifications of the typical synthesis.

To the methanol solution of 10-2-10 Ac was added formic acid in molar ratio 1:20; this large excess of formic acid was deliberately used to carry out the complete exchange of Ac. The reaction mixture was stirred at 40 °C during 24 hours, and monitored by ^1H NMR. The disappearance of the acetate peak at 1.90 ppm indicated that exchange reaction was complete. The solvent was removed under vacuum and the excess of formic acid was removed by heating the mixture at 55 °C under high vacuum over 5 days. The precipitate was solubilized in a small amount of acetone at 60 °C and kept at -20 °C for 1 day. The obtained crystals were filtered and dried under vacuum. The yield was 87%.

The stoichiometric ratio and purity of the compound was checked by proton NMR. It is important to notice that the recycling delay (D_1) was increased up to 25 s in order to obtain the correct integration of the peaks. The need to increase the recycling delay suggests that the relaxation time is higher for formate anion than for gemini amphiphile molecule. It can be explained by the small size of the anion that makes it quite mobile and request more time for nuclei to return from excited to ground state.

1.2. Synthesis of tertiary ammonium 10-2-10 gemini surfactants

In the tertiary 10-2-10 gemini surfactants, one methyl group of the headgroup was substituted by a proton as shown in Figure II-8.

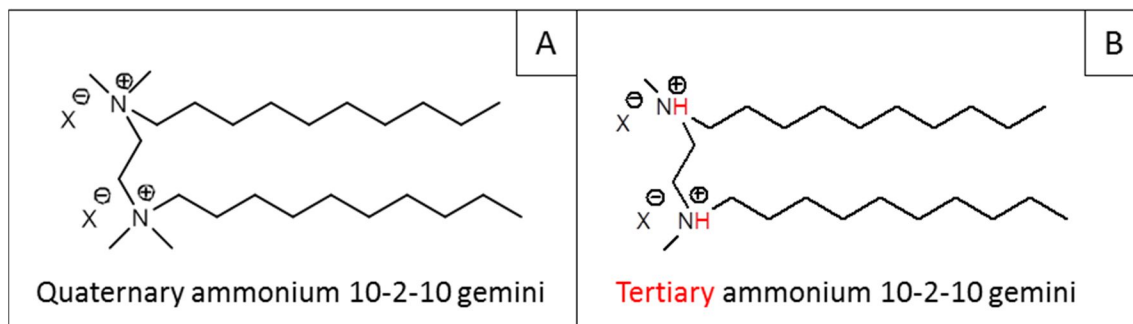
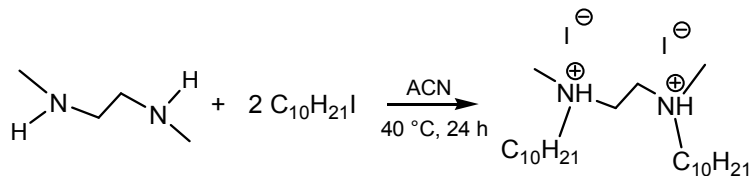


Figure II-8. Structure of quaternary (A) and tertiary (B) ammonium 10-2-10 gemini surfactants.

We have investigated tertiary ammonium gemini surfactants with iodide, bromide and chloride as counterions. The synthesis of these three compounds was performed using different procedures. Tertiary 10-2-10 I was synthesized in a similar manner to its quaternary ammonium counterpart. N,N'-dimethylethylenediamine (DMEDA) was used instead of TMEDA, and dialkylated with 1-iododecane. The synthesis of 10-2-10 ter Br and 10-2-10 ter Cl proceeded through the tertiary amine formed in the first step with 1-bromodecane, which was then protonated with the corresponding acid in a second step.

1.2.1. Synthesis of 10-2-10 ter I

Since the iodide ion is a good leaving group, the synthesis of 10-2-10 ter I could be performed by dialkylation of DMEDA with 1-iododecane in acetonitrile at 40 °C as shown in Scheme II-6.



Scheme II-6. Synthesis of 10-2-10 ter I.

Figure II-9 shows the ^1H NMR spectrum of tertiary (A) and quaternary (B) 10-2-10 I in MeOD. The integration for the signals attributed to the methyls of headgroups (in green) changed from 12 (Figure II-9 B) to 6 protons (Figure II-9 A). Moreover the singlet, multiplet and singlet that

correspond to the spacer, α -CH₂ and methyl groups of the headgroups respectively shifted significantly for 10-2-10 ter I in comparison to 10-2-10 I (for clarity see the Figure II-9).

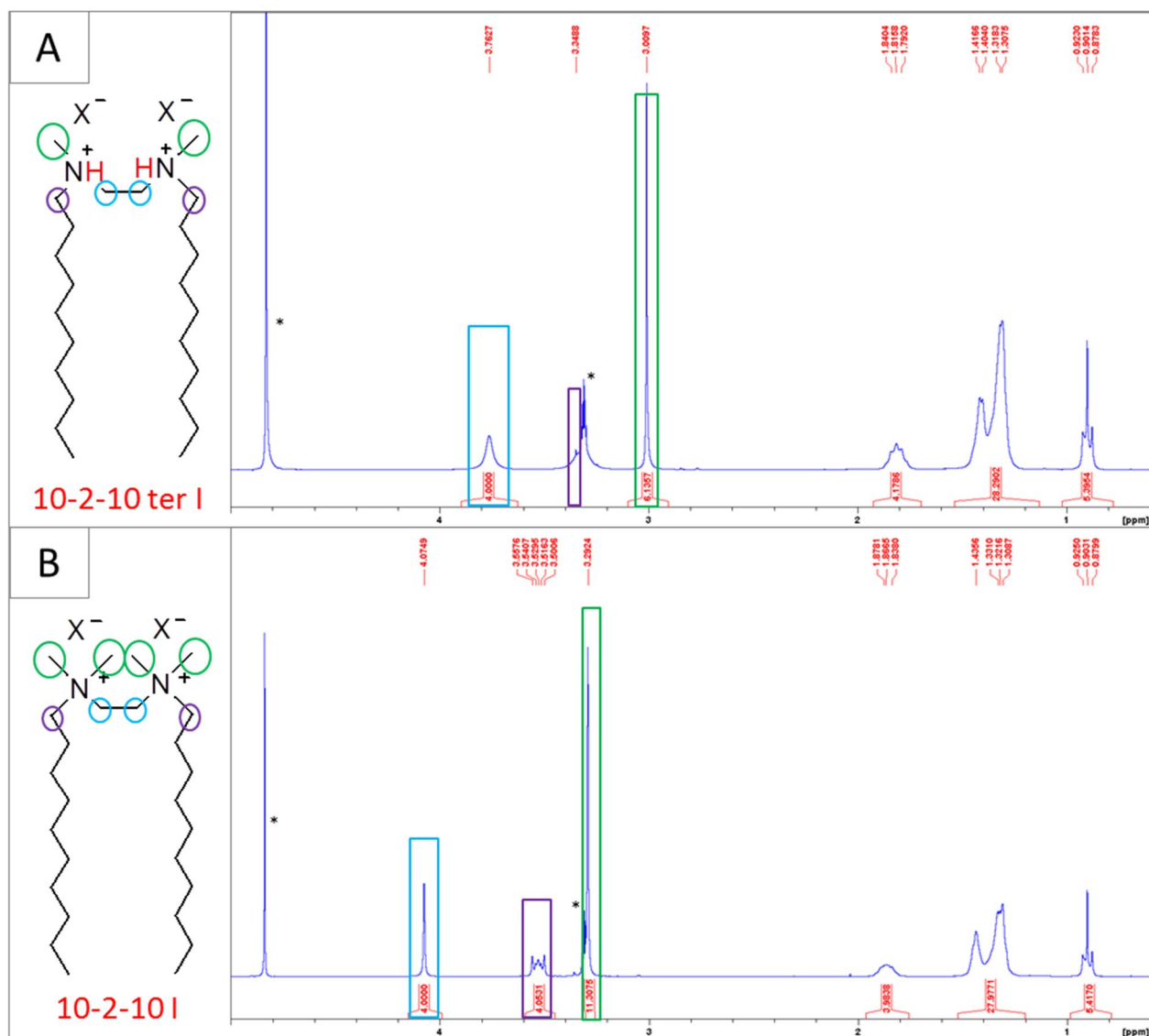


Figure II-9. ¹H NMR spectrum of tertiary (A) and quaternary (B) ammonium 10-2-10 I in MeOD. Color labeling of certain proton groups on the molecular structure and NMR spectrum highlight the shift of the peaks corresponding to the protons in α position regardless ammonium for tertiary gemini in comparison with quaternary ammonium. Peaks for solvent were noted with the star.

10-2-10 ter I was also characterised by XPS. Taking into account a standard error due to the fitting and the sensitivity of the machine, obtained stoichiometry of iodide correlates well with theoretical values (Table II-2). On the Figure II-10 we can see that position of N1s peak (\sim 401 eV) strongly indicates that most of nitrogen is in ammonium form, the small peak around 399 eV indicates that there is also some unprotonated form that could be a result of incomplete alkylation

with DMEDA, or from diprotonation of the tertiary gemini. However this compound could not be determined by proton NMR, hence its ammount is less than 3%.

Table II-2. Quantification of N, C, I and O for tertiary ammonium 10-2-10 I molecule via XPS.

Element	N1s (300 eV)	C1s (285 eV)	I3d5 (621 eV)	O1s (68eV)
Theoretical	2	24	2	0
Experimental	2	22.3	1.8	0.1

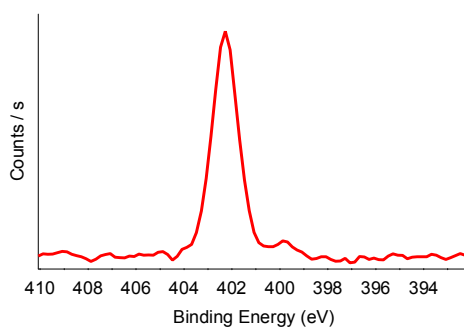


Figure II-10. XPS high resolution spectrum of the N1s region for 10-2-10 ter I.

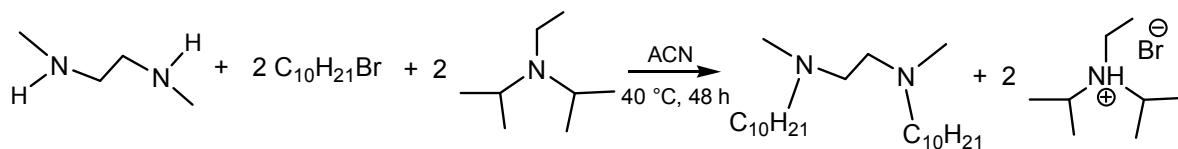
1.2.2. Synthesis of 10-2-10 ter Br

For the initial synthesis of 10-2-10 ter Br we applied the same method as was used for 10-2-10 ter I, consisting of the dialkylation of DMEDA by 1-bromodecane. Unfortunately, the ^1H NMR indicated that the product contained an impurity with signals at 3.42 and 2.81 ppm. The compound was finally purified by repetitive recrystallization from $\text{CH}_3\text{CN}/\text{MeOH}$, however the yield of the pure 10-2-10 ter Br was low (about 30%). Low yields of pure product and time-consuming repeated recrystallizations convinced us to modify this synthetic procedure.

In a new procedure, the 10-2-10 amine compound was first prepared, and protonated with HBr.

Synthesis of 10-2-10 amine

10-2-10 amine was prepared by dialkylation of DMEDA with 1-bromodecane in the presence of Hünig's base N,N-diisopropylethylamine (DIPEA) in acetonitrile, at 40 °C (Scheme II-7).

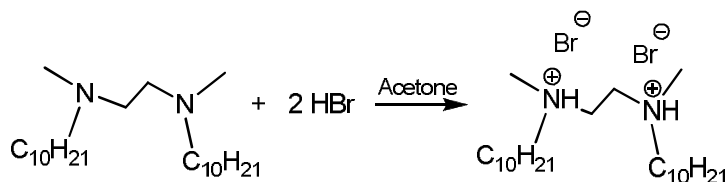


Scheme II-7. Synthesis of 10-2-10 amine.

After the reaction was complete, the solvent was evaporated and the resulting residue solubilized in CHCl_3 . Hünig's base was extracted with H_2O and organic phase containing 10-2-10 amine was collected and dried over MgSO_4 . The solvent was removed under vacuum and crude amine compound was obtained. ^1H NMR signals for protons in α -position regardless nitrogen atom indicate that 10-2-10 gemini is in the amine form. In comparison with 10-2-10 ter I (Figure II-9 A), the peaks of the 10-2-10 amine (spacer protons, α - CH_2 and α -N methyl groups) appeared at 2.82, 2.65 and 2.46 ppm instead of 3.76, \sim 3.32 and 3.01 ppm in the case of 10-2-10 ter I.

Synthesis of 10-2-10 ter Br

This compound was obtained by protonation of the 10-2-10 gemini amine with bromic acid (Scheme II-8).



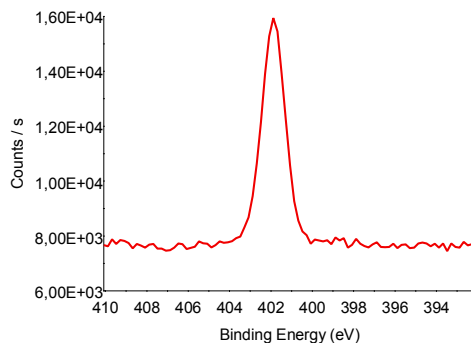
Scheme II-8. Synthesis of 10-2-10 ter Br.

A white precipitate was formed by adding HBr to a solution of 10-2-10 amine in acetone under stirring. Obtained 10-2-10 ter Br was collected and purified by crystallization from $\text{MeOH}/\text{CH}_3\text{CN}$.

The characterization of 10-2-10 ter Br by ^1H NMR and XPS indicated that all the 10-2-10 amine was transformed to the ammonium form giving desired tertiary 10-2-10 Br. Considering a standard error of the technique, the XPS results show a good agreement between experimental and theoretical values as shown in the Table II-3. The excess of C and O seen in this spectrum comes from atmospheric contamination. Furthermore, the position of the N1s peak (around 402 eV) strongly suggests that nitrogen species in the compound are in ammonium form[91] (Figure II-11).

Table II-3. Quantification of N, C, Br and O for tertiary ammonium 10-2-10 ter Br molecule via XPS.

Element	N1s (300 eV)	C1s (285 eV)	Br3d (68 eV)	O1s (68eV)
Theoretical	2	24	2	0
Experimental	2	26.6	2.1	0.2

**Figure II-11. XPS high resolution spectrum of the N1s region for 10-2-10 ter Br.****1.2.3. Synthesis of 10-2-10 ter Cl**

10-2-10 ter Cl was synthesized in a similar way to 10-2-10 ter Br by protonation of 10-2-10 amine with HCl. However, we considered that the starting material could contain traces of Br⁻ ion from the initial synthetic reaction (Scheme II-7). Since HBr is a stronger acid than HCl and thus Br⁻ ions cannot be easily replaced by Cl⁻ anion, an additional method was used for purification. To remove all traces of bromide, AgAc was used to precipitate any residual Br⁻ ions. Formed AgBr was removed by filtration through celite. Being derived from a weak acid, the acetate anion will not react with 10-2-10 amine, as easily shown with proton NMR. The position of the proton peaks α to the nitrogen atom corresponds to those of the 10-2-10 amine: 2.82, 2.65 and 2.46 ppm for the spacer, α -CH₂ and α -CH₃ respectively. This in addition to the absence of acetate peak, allows us to conclude that the surfactant molecule stays in amine form.

The synthesis of 10-2-10 ter Cl was performed by adding HCl 37 wt% to a solution of 10-2-10 amine in acetone under stirring. The obtained powder was purified from silver salts by filtration over celite in MeOH and then crystallized from MeOH.

Proton NMR and XPS were used to check the structure and purity of the compound. Obtained XPS results are compatible with theoretical values within experimental error (Table II-4).

Silica and oxygen were the result of surface and atmospheric contamination and not from the compound. We can see that the amount of Br in the system is insignificant. On the Figure II-12 XPS spectra for N1s region is presented. One can see that the large peak at 402 eV corresponds to the ammonium in the gemini molecules indicating that 10-2-10 amine was protonated. However, similar to 10-2-10 ter I there is small peak at 399 eV indicating that small amount of the compound was left in amine form. Even so this compound cannot be detected by NMR that means that its amount is less than 3%.

Table II-4. Quantification of N, C, Cl, O, Si and Br for tertiary ammonium 10-2-10 ter Cl molecule via XPS.

Element	N1s (300 eV)	C1s (285 eV)	Cl2p (198 eV)	O1s (68eV)	Si2p (99 eV)	Br3d (68 eV)
Theoretical	2	24	2	0	0	0
Experimental	2	22.4	1.9	0.6	0.3	0.04

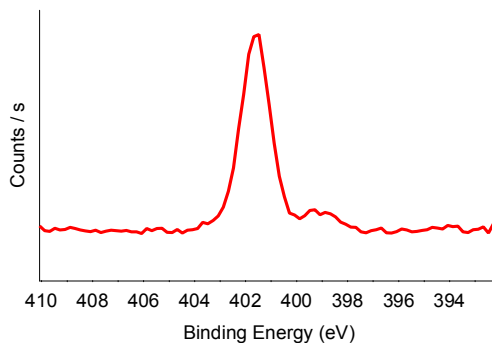


Figure II-12. XPS high resolution spectrum of the N1s region for 10-2-10 ter Cl.

2. Experimental section

2.1. Materials

Reagent grade solvents for syntheses were used as received. All chemicals were of analytical grade and used as received. Methanol ($\geq 99.6\%$), acetonitrile ($\geq 99.9\%$), acetone ($\geq 99.5\%$) and diethyl ether ($\geq 99.5\%$) were purchased from Sigma-Aldrich, deuterium oxide (99.96%) and methanol-D₄ ($\geq 99.8\%$) purchased from Euriso-top. All other compounds were purchased from Sigma-Aldrich and used without further purification.

The ¹H and ¹³C NMR spectra were recorded at 25 °C on a Bruker AC 300 FT at 300 MHz (¹H) and 75 MHz (¹³C). Chemical shifts (δ) are reported in parts per million against referenced solvent signals.

X-ray photoelectron spectroscopy (XPS) was carried out on a ThermoFisher Scientific K-ALPHA spectrometer. Surface analysis was done with a monochromatized AlK α source ($h\nu = 1486.6$ eV) and a 200 micron spot size. A pressure of 10^{-7} Pa was maintained in the chamber during analysis. The full spectra (0-1350 eV) were obtained with constant pass energy of 200 eV and high resolution spectra at constant pass energy of 40 eV. Charge neutralization was activated even for those conductive samples. High resolution spectra were fitted and quantified using the AVANTAGE software provided by ThermoFisher Scientific. Since XPS is only a semi-quantitative analysis the error of the experiment can be count as 5 to 10% depending on the sensitivity factors which were used to reach quantification.

2.2. Synthetic procedures for quaternary 10-2-10 gemini surfactants

10-2-10 Br. To an acetonitrile solution (120 mL) of TMEDA (15 mL, 99.4 mmol) was added 1-bromodecane in molar ratio 1:3 (62.2 mL, 298 mmol). The reaction mixture was stirred at 80 °C under reflux for 48 h. After completion, the reaction mixture was cooled to 4 °C and the obtained precipitate of 10-2-10 Br was washed with acetone (1x500 mL), recrystallized from CH₃CN and dried under vacuum and lyophilized. 10-2-10 Br was obtained as a white solid in 85% yield.

¹H NMR (300 MHz, MeOD, 25 °C):

$\delta = 4.06$ (s, 4H, (CH₃)₂N⁺-(CH₂)₂-N⁺(CH₃)₂), 3.51 (m, 4H, CH₃-(CH₂)₇-CH₂-CH₂-N⁺), 3.28 (s, 12H, (CH₃)₂N⁺-(CH₂)₂-N⁺(CH₃)₂), 1.85 (m, 4H, CH₃-(CH₂)₇-CH₂-CH₂-N⁺), 1.42-1.31 (m, 28H, CH₃-(CH₂)₇-CH₂-CH₂-N⁺), 0.90 (t, 6H, CH₃-(CH₂)₉-N⁺).

¹³C NMR (300 MHz, MeOD, 25 °C): 65.6 (⁺NCH₂), 55.8 (⁺NCH₂), 50.5 (⁺NCH₃), 31.7 (CH₂), 29.3 (CH₂), 29.2 (CH₂), 29.1 (CH₂), 28.9 (CH₂), 25.9 (CH₂), 22.4 (CH₂), 22.3 (CH₂), 13.1 (CH₃).

10-2-10 I. 3 mL (19.87 mmol) of TMEDA was mixed with 9.33 mL (43.7 mmol) of 1-iododecane in acetonitrile (50 mL) in molar ratio 1:2.2. The reaction mixture was stirred at 80 °C under reflux for 48 h. The reaction mixture was cooled to 4 °C and the obtained powder was washed with diethyl ether and recrystallized from acetonitrile as follows: the compound was dissolved in 10 mL of CH₃CN at 60 °C and cooled to room temperature, providing crystals. These crystals were filtered and dried under vacuum. The purity of 10-2-10 I was checked by ¹H NMR analysis.

¹H NMR (300 MHz, MeOD, 25 °C):

δ = 4.08 (s, 4H, (CH₃)₂N⁺-(CH₂)₂-N⁺(CH₃)₂), 3.53 (m, 4H, CH₃-(CH₂)₇-CH₂-CH₂-N⁺), 3.30 (s, 12H, (CH₃)₂N⁺-(CH₂)₂-N⁺(CH₃)₂), 1.86 (m, 4H, CH₃-(CH₂)₇-CH₂-CH₂-N⁺), 1.43-1.31 (m, 28H, CH₃-(CH₂)₇-CH₂-CH₂-N⁺), 0.90 (t, 6H, CH₃-(CH₂)₉-N⁺).

10-2-10 with carboxylate counterions. Here we present NMR spectrum for 10-2-10 with counterions: C3-C8.

10-2-10 C3: ¹H NMR (300 MHz, MeOD, 25 °C, D₂=20 s):

δ = 3.93 (s, 4H, (CH₃)₂N⁺-(CH₂)₂-N⁺(CH₃)₂), 3.43 (m, 4H, CH₃-(CH₂)₇-CH₂-CH₂-N⁺), 3.21 (s, 12H, (CH₃)₂N⁺-(CH₂)₂-N⁺(CH₃)₂), **2.16 (q, 4H, CH₃-CH₂-COO⁻)**, 1.83 (m, 4H, CH₃-(CH₂)₇-CH₂-CH₂-N⁺), 1.41-1.31 (m, 28H, CH₃-(CH₂)₇-CH₂-CH₂-N⁺), **1.10 (t, 6H, CH₃-CH₂-COO⁻)**, 0.90 (t, 6H, CH₃-(CH₂)₉-N⁺).

10-2-10 C4: ¹H NMR (300 MHz, MeOD, 25 °C, D₂=15 s):

δ = 3.94 (s, 4H, (CH₃)₂N⁺-(CH₂)₂-N⁺(CH₃)₂), 3.42 (m, 4H, CH₃-(CH₂)₇-CH₂-CH₂-N⁺), 3.21 (s, 12H, (CH₃)₂N⁺-(CH₂)₂-N⁺(CH₃)₂), **2.14 (t, 4H, CH₃-CH₂-CH₂-COO⁻)**, 1.83 (m, 4H, CH₃-(CH₂)₇-CH₂-CH₂-N⁺), **1.68-1.56 (m, 4H, CH₃-CH₂-CH₂-COO⁻)**, 1.41-1.31 (m, 28H, CH₃-(CH₂)₇-CH₂-CH₂-N⁺), 0.92 (m, 6H, CH₃-(CH₂)₉-N⁺ and **6H, CH₃-(CH₂)₂-COO⁻**).

10-2-10 C5: ¹H NMR (300 MHz, MeOD, 25 °C, D₂=15 s):

δ = 3.94 (s, 4H, (CH₃)₂N⁺-(CH₂)₂-N⁺(CH₃)₂), 3.43 (m, 4H, CH₃-(CH₂)₇-CH₂-CH₂-N⁺), 3.21 (s, 12H, (CH₃)₂N⁺-(CH₂)₂-N⁺(CH₃)₂), **2.15 (t, 4H, CH₃-(CH₂)₂-CH₂-COO⁻)**, 1.83 (m, 4H, CH₃-(CH₂)₇-CH₂-CH₂-N⁺), **1.63-1.55 (m, 4H, CH₃-CH₂-CH₂-COO⁻)**, 1.41-1.31 (m, 28H, CH₃-(CH₂)₇-CH₂-CH₂-N⁺ and **4H, CH₃-CH₂-(CH₂)₂-COO⁻**), 0.92 (m, 6H, CH₃-(CH₂)₉-N⁺ and **6H, CH₃-(CH₂)₃-COO⁻**).

10-2-10 C6: ¹H NMR (300 MHz, MeOD, 25°C, D₂=15 s):

$\delta = 3.93$ (s, 4H, (CH₃)₂N⁺-(CH₂)₂-N⁺(CH₃)₂), 3.43 (m, 4H, CH₃-(CH₂)₇-CH₂-CH₂-N⁺-), 3.21 (s, 12H, (CH₃)₂N⁺-(CH₂)₂-N⁺(CH₃)₂), **2.14** (t, 4H, CH₃-(CH₂)₃-CH₂-COO⁻), 1.82 (m, 4H, CH₃-(CH₂)₇-CH₂-CH₂-N⁺), **1.65-1.55** (m, 4H, CH₃-(CH₂)₂-CH₂-CH₂-COO⁻), 1.41-1.31 (m, 28H, CH₃-(CH₂)₇-CH₂-CH₂-N⁺ and **8H**, CH₃-(CH₂)₂-(CH₂)₂-COO⁻), 0.90 (m, 6H, CH₃-(CH₂)₉-N⁺ and **6H**, CH₃-(CH₂)₄-COO⁻).

10-2-10 C8: ¹H NMR (300 MHz, MeOD, 25°C):

$\delta = 3.95$ (s, 4H, (CH₃)₂N⁺-(CH₂)₂-N⁺(CH₃)₂), 3.42 (m, 4H, CH₃-(CH₂)₇-CH₂-CH₂-N⁺-), 3.21 (s, 12H, (CH₃)₂N⁺-(CH₂)₂-N⁺(CH₃)₂), **2.15** (t, 4H, CH₃-(CH₂)₅-CH₂-COO⁻), 1.82 (m, 4H, CH₃-(CH₂)₇-CH₂-CH₂-N⁺), **1.60** (m, 4H, CH₃-(CH₂)₄-CH₂-CH₂-COO⁻), 1.41-1.31 (m, 28H, CH₃-(CH₂)₇-CH₂-CH₂-N⁺ and **16H**, CH₃-(CH₂)₄-(CH₂)₂-COO⁻), 0.90 (m, 6H, CH₃-(CH₂)₉-N⁺ and **6H**, CH₃-(CH₂)₆-COO⁻).

10-2-10 Ac. To a solution of 10-2-10 Br (30g, 53.7 mmol) in 200 mL MeOH was added silver acetate (22.41 g, 134.3 mmol) in molar ratio 1:2.5. The reaction mixture was protected from light with aluminum foil, and stirred at 40 °C until the completion of ion exchange. Reaction was followed by ¹H NMR, by the appearance of a signal at 1.90 ppm (integration 6H), assigned to the methyl groups of the acetate anion. Reaction completion was assessed by photoreduction of the obtained AgBr to silver metal and molecular bromide, as described in section 1.1.3. After completion, silver bromide and excess of silver acetate were removed by filtration through celite. After evaporation of the solvent under vacuum, the residue was dissolved in MeOH and filtered through celite, and the solvent was evaporated under vacuum until the dry residue was formed (to avoid the concentration of water from the solvent). The residue was dissolved in MeOH (5 mL) at 60 °C and the product was crystallized by adding 700 mL of acetone. 10-2-10 Ac was obtained as white crystals in 70% yield.

¹H NMR (300 MHz, MeOD, 25°C):

$\delta = 3.94$ (s, 4H, (CH₃)₂N⁺-(CH₂)₂-N⁺-(CH₃)₂), 3.42 (m, 4H, CH₃-(CH₂)₇-CH₂-CH₂-N⁺-), 3.20 (s, 12H, (CH₃)₂N⁺-(CH₂)₂-N⁺-(CH₃)₂), **1.90** (s, 6H, CH₃-COO⁻), 1.82 (m, 4H, CH₃-(CH₂)₇-CH₂-CH₂-N⁺-), 1.41-1.30 (m, 28H, CH₃-(CH₂)₇-CH₂-CH₂-N⁺-), 0.90 (t, 6H, CH₃-(CH₂)₉-N⁺-).

¹³C NMR (300 MHz, MeOD, 25°C): 178.7 (C=O), 65.6 (⁺NCH₂), 55.7 (⁺NCH₂), 50.3 (⁺NCH₃), 31.7 (CH₂), 29.3 (CH₂), 29.2 (CH₂), 29.0 (CH₂), 28.9 (CH₂), 25.9 (CH₂), 23.2 (CH₃CO₂), 22.4 (CH₂), 22.3 (CH₂), 13.1 (CH₃).

10-2-10 F. For 10-2-10 F synthesis 1 eq. of 10-2-10 I (2 g, 3.06 mmol) was mixed with 2.05 eq. of AgF (0.78 mg, 6.13 mmol) in MeOH (40 ml) and stirred at 40 °C for 2 hours. Proton NMR spectroscopy was used to check the purity of obtained compound.

The purification of 10-2-10 F was performed by filtering the reaction mixture through celite and evaporation of methanol solution under vacuum. This step was repeated several times until the residue of 10-2-10 F will become white. This white precipitate was dissolved in 3 mL of acetone at 50 °C and cooled to 4 °C. Crystals were formed, filtered and dried under vacuum. It is important to note that, this compound cannot be dried by lyophilization, due to its decomposition under strong vacuum.

¹H NMR (300 MHz, MeOD, 25°C):

$\delta = 3.90$ (s, 4H, $(\text{CH}_3)_2\text{N}^+(\underline{\text{CH}_2})_2\text{-N}^+(\text{CH}_3)_2$), 3.41 (m, 4H, $\text{CH}_3\text{-(CH}_2)_7\text{-CH}_2\text{-}\underline{\text{CH}_2}\text{-N}^+$), 3.20 (s, 12H, $(\underline{\text{CH}_3})_2\text{N}^+(\text{CH}_2)_2\text{-N}^+(\underline{\text{CH}_3})_2$), 1.83 (m, 4H, $\text{CH}_3\text{-(CH}_2)_7\text{-}\underline{\text{CH}_2}\text{-CH}_2\text{-N}^+$), $1.42\text{-}1.31$ (m, 28H, $\text{CH}_3\text{-(CH}_2)_7\text{-CH}_2\text{-CH}_2\text{-N}^+$), 0.90 (t, 6H, $\underline{\text{CH}_3}\text{-(CH}_2)_9\text{-N}^+$).

10-2-10 with ions of strong acids. 10-2-10 gemini with counterions of strong acids was synthesized by reaction of 10-2-10 Ac with HX in molar ratio 1:2 (1:3 in case of HCl). The reaction mixture was stirred at 40 °C in MeOH for 2 h. The reaction was monitored using ¹H NMR by the disappearance of the signal of Ac peak at 1.90 ppm. The resulting mixture was evaporated under vacuum and dry residue was dissolved in a minimal volume of MeOH (Table II-5). The product was precipitated by adding a low polarity solvent as described in Table II-5. The solid was washed (3 times) with the same solvent used to precipitate the product and dried under vacuum and by lyophilization. 10-2-10 X was obtained as white powder.

Table II-5. Detailed information for the synthetic procedure for 10-2-10 X (X = NO₃⁻, Cl⁻, TFA, MeSO₃⁻).

10-2-10 gemini	mmol of 10-2-10 Ac	mmol of HX (per 100 wt%)	V of MeOH for solubilization (mL)	Solvent for precipitation and washing
NO ₃	11.42	22.83	12	Diethyl ether (was added dropwisely under continuous stirring)
Cl	29.02	87.07	15	Diethyl ether (was added dropwisely under continuous stirring)
TFA	25.15	50.31	4	Diethyl ether
MeSO ₃	11.61	23.22	1	Acetone

10-2-10 H₂PO₄. The solution of 10-2-10 Ac (7 g, 13.54 mmol) in MeOH (80 mL) was prepared and added dropwise to the solution of H₃PO₄ 85 wt% (1.82 mL, 31.87 mmol) in MeOH (80 mL) under continuous stirring at room temperature. The obtained white precipitate was filtered and dried under vacuum and by lyophilization. The yield was 68%.

¹H NMR (300 MHz, D₂O, 25°C):

δ = 3.90 (s, 4H, (CH₃)₂-N⁺-(CH₂)₂-N⁺-(CH₃)₂), 3.44 (m, 4H, CH₃-(CH₂)₇-CH₂-CH₂-N⁺-), 3.25 (s, 12H, (CH₃)₂-N⁺-(CH₂)₂-N⁺-(CH₃)₂), 1.76 (m, 4H, CH₃-(CH₂)₇-CH₂-CH₂-N⁺-), 1.38-1.30 (m, 28H, CH₃-(CH₂)₇-CH₂-CH₂-N⁺-), 0.88 (t, 6H, CH₃-(CH₂)₉-N⁺-)

¹³C NMR (300 MHz, D₂O, 25°C): 63.6 (⁺NCH₂), 53.9 (⁺NCH₂), 52.5 (⁺NCH₃), 31.7 (CH₂), 29.3 (CH₂), 29.2 (CH₂), 29.1 (CH₂), 28.9 (CH₂), 25.6 (CH₂), 22.5 (CH₂), 13.8 (CH₃).

³¹P NMR (300 MHz, D₂O, 25°C): 3.2.

10-2-10 Cl. To a MeOH solution (150 mL) of 10-2-10 Ac (13 g, 25.15 mmol) was added HCOOH (17.75 mL, 503.06 mmol) in molar ratio 1:20. The yield was 87%.

¹H NMR (300 MHz, MeOD, 25°C, D₂=25 s):

δ = 8.57 (s, 2H, H-COO), 3.93 (s, 4H, (CH₃)₂-N⁺-(CH₂)₂-N⁺-(CH₃)₂), 3.42 (m, 4H, CH₃-(CH₂)₇-CH₂-CH₂-N⁺-), 3.21 (s, 12H, (CH₃)₂-N⁺-(CH₂)₂-N⁺-(CH₃)₂), 1.83 (m, 4H, CH₃-(CH₂)₇-CH₂-CH₂-N⁺-), 1.42-1.31 (m, 28H, CH₃-(CH₂)₇-CH₂-CH₂-N⁺-), 0.91 (t, 6H, CH₃-(CH₂)₉-N⁺-).

2.3. Synthetic procedures for tertiary 10-2-10 gemini surfactants

10-2-10 ter I. To a solution of DMEDA (2 mL, 18.58 mmol) in CH₃CN (40mL), 1-iododecane (8.72 mL, 40.88 mmol) was added and the reaction mixture was stirred for 24 hours at 40 °C. After completion, the solvent was removed under vacuum and obtained compound was purified by crystallization from MeOH (10 mL). White crystals were collected and dried under vacuum.

¹H NMR (300 MHz, D₂O, 25°C):

δ = 3.65 (s, 4H, CH₃-NH⁺-(CH₂)₂-NH⁺-CH₃), 3.24 (m, 4H, CH₃-(CH₂)₇-CH₂-CH₂-NH⁺-), 2.96 (s, 6H, CH₃-N-(CH₂)₂-NH⁺-CH₃), 1.78 (m, 4H, CH₃-(CH₂)₇-CH₂-CH₂-NH⁺-), 1.36-1.30 (m, 28H, CH₃-(CH₂)₇-CH₂-CH₂-NH⁺-), 0.88 (t, 6H, CH₃-(CH₂)₉-NH⁺-).

10-2-10 amine. 1-bromodecane (8.29 mL, 39.95 mmol) was mixed with DMEDA (2 mL, 18.58 mmol) and DIPEA (6.95 mL, 39.95 mmol) in acetonitrile (30 mL). The reaction mixture was stirred at 40 °C for 2 days. The completion of the reaction was monitored with ¹H NMR (MeOD), the absence of peaks of DMEDA at 2.67 and 2.38 ppm indicated that the dialkylation was complete.

After reaction the solvent was evaporated and extraction was used for separation of amine and Hünig's base. For the extraction water was used to extract the base, whereas amine compound remained in CHCl₃. The organic phase containing 10-2-10 amine was collected and dried over MgSO₄, filtered and evaporated to give the 10-2-10 amine compound.

¹H NMR (300 MHz, MeOD, 25 °C):

δ = 2.82 (s, 4H, CH₃-N-(CH₂)₂-N-CH₃), 2.65 (m, 4H, CH₃-(CH₂)₇-CH₂-CH₂-N-), 2.46 (s, 6H, CH₃-N-(CH₂)₂-N-CH₃), 1.57 (m, 4H, CH₃-(CH₂)₇-CH₂-CH₂-N-), 1.34-1.30 (m, 28H, CH₃-(CH₂)₇-CH₂-CH₂-N-), 0.90 (t, 6H, CH₃-(CH₂)₉-N-).

10-2-10 ter Br. To an acetone solution (15 mL) of 1 eq. of 10-2-10 amine (2 g, 5.23 mmol) under stirring was added 2.2 eq. of HBr 48 wt% (1.35 mL, 24.86 mmol). A white precipitate was formed, collected and purified by crystallization from a hot mixture (60 °C) of MeOH/CH₃CN 22 mL (1:10 ratio). The mixture was cooled down to room temperature and crystals were collected and dried under vacuum.

¹H NMR (300 MHz, D₂O, 25 °C):

δ = 3.65 (s, 4H, CH₃-NH⁺-(CH₂)₂-NH⁺-CH₃), 3.26 (m, 4H, CH₃-(CH₂)₇-CH₂-CH₂-NH⁺-), 2.96 (s, 6H, CH₃-N-(CH₂)₂-NH⁺-CH₃), 1.74 (m, 4H, CH₃-(CH₂)₇-CH₂-CH₂-NH⁺-), 1.36-1.30 (m, 28H, CH₃-(CH₂)₇-CH₂-CH₂-NH⁺-), 0.88 (t, 6H, CH₃-(CH₂)₉-NH⁺-).

10-2-10 ter Cl. Purification: 1 eq. of 10-2-10 amine (1.9 g, 5.15 mmol) was mixed with 2 eq. AgAc (1.72 g, 10.31 mmol) in 30 mL of MeOH. The reaction was stirred for 24 h at 40 °C. Then the suspension was filtered over celite to remove precipitate of AgBr and unreacted AgAc. Solvent was removed under vacuum. Black color of the compound indicates that additional purification of the compound was needed (filtration on the celite from acetone). After all the trace of Br was removed 10-2-10 ter Cl can be synthesized.

10-2-10 amine was solubilized in 5 mL of acetone and an excess of HCl 37 wt% (1.06 mL, 34.8 mmol) was added under the stirring. The obtained powder was purified by filtration on celite from methanol, crystallized in MeOH, crystals were collected and dried under vacuum.

¹H NMR (300 MHz, D₂O, 25° C):

$\delta = 3.63$ (s, 4H, CH₃-NH⁺-(CH₂)₂-NH⁺-CH₃), 3.24 (m, 4H, CH₃-(CH₂)₇-CH₂-CH₂-NH⁺-), 2.95 (s, 6H, CH₃-N-(CH₂)₂-NH⁺-CH₃), 1.76 (m, 4H, CH₃-(CH₂)₇-CH₂-CH₂-NH⁺-), $1.36-1.30$ (m, 28H, CH₃-(CH₂)₇-CH₂-CH₂-NH⁺-), 0.88 (t, 6H, CH₃-(CH₂)₉-NH⁺-).

**Chapter III. Contribution of ion specific effects to the
physical properties of micellar aggregates at the bulk
solution level**

Introduction

In the previous Chapters we overviewed the studies on the Hofmeister effects of the different colloidal systems. Here, we describe the impact of the nature of counterions to the self-assembly of the cationic gemini surfactant molecules in aqueous solutions. Even though a similar study was done previously on the 14-2-14 gemini systems[90], the determination of the physical properties for 10-2-10 gemini systems was necessary in order to provide the information that is important for further investigation of the systems by other techniques (chemical trapping, Chapter IV; molecular modeling, Chapter V). Two types of counterions: inorganic counterions and alkyl carboxylates, along with two types of 10-2-10 gemini: quaternary ammonium gemini (10-2-10 X) and tertiary ammonium gemini with the same chain length (10-2-10 ter X, in which one of the methyl at the headgroup is replaced by a proton) were studied in order to investigate both the ion specific effects and the contribution of the structural properties of the headgroup to the self-assembly behavior. Indeed, we expect that in addition to the properties of the counterions, the properties of the cation of gemini headgroup would influence the balance of the forces that determines the association between the ions (Figure III-1). More precisely, exchanging the methyl group by a proton would have an important effect on the delocalization of cationic charge of the headgroups and thus affect the interaction between the headgroups and the counterions.

To characterize the micellization process as well as micellar structure we used conductivity measurements to determine critical micelle concentration (CMC), ionization degree (α), and the free energy of micellization (ΔG_M°). The aggregation number of the surfactant molecules (N) indicates how many monomers (gemini molecules) form a micelle on average and is measured using a fluorescence quenching technique in collaboration with Dr. Dario Bassani. In order to study the properties of 10-2-10 ter X we also used NMR and pH measurements.

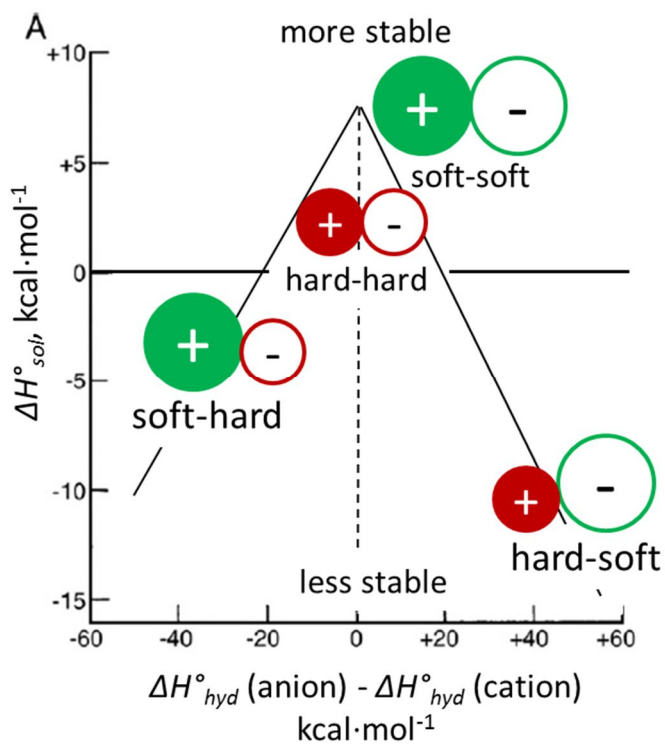


Figure III-1. Relationship between salt heat of dissolution and difference in enthalpies of hydration for cation and anion for salts composed from soft/hard ions[36]

1. Conductivity measurements

In this section we present the determination of the micellisation parameters such as CMC, ionization degree and free energy of micellization from the conductivity measurements.

Below the CMC, surfactants in solution are solubilized without forming persistent aggregates. Contribution to the conductivity comes from the mobility of cations and anions and increase linearly with surfactant concentration. Above the CMC, conductivity changes due to the increase of the concentration of charged micellar aggregates that have much lower mobility compared to non-cooperative ions. Thus, we obtain two different slopes in the plot of conductivity versus surfactant concentration that reflect the binary behavior of the system (before and after CMC). This allows us to estimate the ion mobility which decreases when micellar aggregates form.

1.1. Surfactant properties estimated by conductivity measurements

1.1.1. Critical micelle concentration

The determination of the CMC was performed by two methods. First one is the Williams and Phillips method[92], that is individuating the intersection of two straight lines in the graph of conductivity (κ) versus concentration (C) values. The first line (with slope S_1) and second line (with slope S_2) correspond to the conductivity set of values below and beyond the CMC respectively. This commonly used approach gives easy access to the CMC when the break between the two slopes of the pre-micellar and micellar transition is abrupt (Figure III-2 left). However in the case when micellar aggregates are formed very gradually it becomes more difficult to define the break in the slopes (Figure III-2 right). Among other methods to estimate the CMC[93-96], we chose the method proposed by Carpena *et. al*[97], based on fitting the conductivity data to a nonlinear function obtained by direct integration of a Boltzmann type sigmoidal function. It was shown that this approach is more adequate for the analysis of conductivity data than conventional and differential conductivity methods[97-99].

The fitting equation that was used to estimate experimental conductivity data is presented below:

$$F(x) = F(0) + A_1 x + \Delta x (A_2 - A_1) \ln \left(\frac{1 + e^{\frac{x-x_0}{\Delta x}}}{1 + e^{-\frac{x_0}{\Delta x}}} \right) \quad (\text{III-1})$$

where x is the concentration of the compound, and $F(0)$ is the conductivity at $x = 0$, A_1 and A_2 are the slopes of the pre and post-CMC regions of conductivity versus concentration (x) respectively, x_0 is a central point of the transition and Δx is a width of this transition.

Fitting was done using Origin 9.1. For each individual set of experimental data, parameters $F(0)$, A_1 , A_2 and x_0 were chosen as follows: $F(0) = \kappa$ for water, $A_1 = S_1$, $A_2 = S_2$, $x_0 = \text{CMC}$ and Δx was chosen from the type of the transition in the slope. The low (high) values means an abrupt (gradual) transition. In our case Δx was chosen as around $0.1x_0$ in the fitting parameters[97, 98].

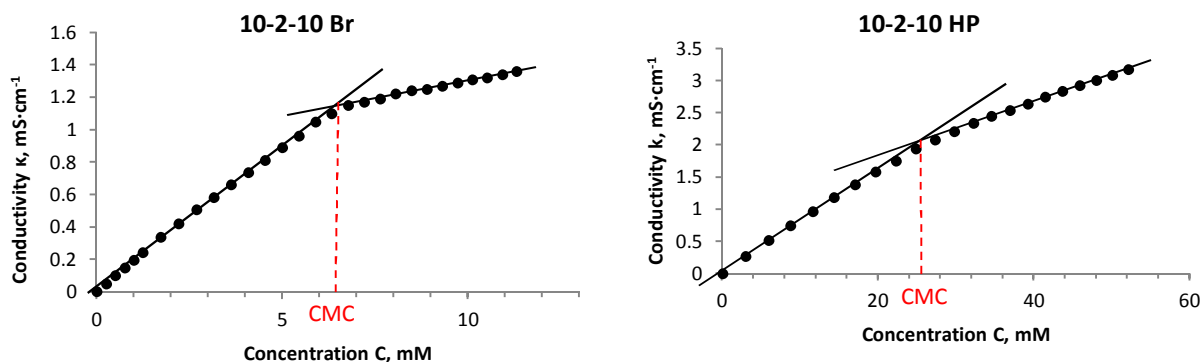


Figure III-2. Example of conductivity dependence versus surfactant concentration for 10-2-10 Br (left) and 10-2-10 HP (right)

1.1.2. Ionization degree

In this work, we used two approaches to estimate the degree of counterions dissociation, or ionization (α). The most common way to determine ionization degree was initially proposed by Zana[17], α is a ratio in the slopes of the plot of κ versus C above and before the CMC:

$$\alpha_z = S_2/S_1 \quad \text{(III-2)}$$

However, it was shown in literature that this method overestimates the real values due to the approximation that a micellized surfactant ion, whose electrical charge is not compensated by a bound counterion, contributes to the conductivity of the solution to the same extent as if it were free[17, 100].

In 1956 Evans proposed a more correct method to estimate the ionization degree, which elucidates the contribution of the micelles to the conductivity of the solution by taking into account the screening of the micellar charge by the counterions[101]. To describe this screening, parameters need to be adjusted. The molecule of the 10-2-10 X gemini, composed of amphiphilic cation with

charge +2 (A^{2+}) and 2 counterions of the charge -1 ($2X^-$), is written as A_2X for simplification.

Before CMC the concentration of cations and anions equals:

$$[A^{2+}] = C \quad (\text{III-3})$$

$$[X^-] = 2C \quad (\text{III-4})$$

where C is the surfactant concentration.

Beyond the CMC the concentration of free amphiphilic cations in solution remains constant:

$$[A^{2+}] = CMC \quad (\text{III-5})$$

the concentration of the micelles equals:

$$[\text{micelle}^A] = \frac{C-CMC}{N} \quad (\text{III-6})$$

where N is the number of monomers that form a micelle.

The concentration of counterions is thus given by:

$$[X^-] = 2(CMC + (C - CMC)\alpha) = 2(\alpha C + (1 - \alpha)CMC) \quad (\text{III-7})$$

The conductivity of the solution of the amphiphilic salt A_2X at the concentration C before the CMC consists of the sum of the conductivity from cations and anions at this concentration:

$$\kappa = \lambda_A C_A + \lambda_X C_X \quad (\text{III-8})$$

where λ_A and λ_X are the equivalent conductivities of the amphiphile ions and counterions and

$$C_A = [A^{2+}], C_X = [X^-] \quad (\text{III-9})$$

Hence, it follows that:

$$\kappa_{C < CMC} = (\lambda_A + 2\lambda_X)C \quad (\text{III-10})$$

$$S_1 = (\lambda_A + 2\lambda_X) \quad (\text{III-11})$$

where S_j is the slope of the specific conductivity-concentration curve below the CMC.

Above the CMC specific conductivity can be presented as a sum of three components: conductivity due to the single amphiphilic ions at the CMC, micellar ions and free counterions:

$$\kappa = \lambda_A C_A + \lambda_X C_X + \lambda_M C_M \quad (\text{III-12})$$

where $C_M = [\text{micelle}^A]$

Substituting Equations (III-5), (III-6) and (III-7) into Equation (III-12) we get $\kappa_{C > CMC}$:

$$\kappa_{C > CMC} = \lambda_A CMC + \lambda_X 2(\alpha C + (1 - \alpha)CMC) + \lambda_M \left(\frac{C-CMC}{N} \right) \quad (\text{III-13})$$

Evans proposed the way to estimate the conductivity of micellar ions that gives the most

adequate results for the determination of ionization degree [101, 102]:

$$\lambda_M = N^{5/3} \alpha^2 \lambda_A \quad (\text{III-14})$$

Substitution of the Evans model of micellar conductivity, Equation (III-14), in Equation (III-12) and expression of λ_A from Equation (III-11) will give us the conductivity of the surfactant solution above the CMC:

$$\kappa_{c>CMC} = \left(S_1 (1 - N^{2/3} \alpha^2) + \lambda_X 2\alpha (\alpha N^{2/3} - 1) \right) CMC + \left(\alpha^2 N^{2/3} (S_1 - 2\lambda_X) + \alpha 2\lambda_X \right) C \quad (\text{III-15})$$

Since N was independently determined from fluorescence quenching (for more details see subsection 2), λ_X is a literature value and S_1 and S_2 - slope of the specific conductivity-concentration curve below and above the CMC respectively, S_2 can be defined as:

$$S_2 = \alpha^2 N^{2/3} (S_1 - 2\lambda_X) + \alpha 2\lambda_X \quad (\text{III-16})$$

Although α is usually defined as a value at the CMC, in reality, the aggregates are not well formed just at the CMC, and it is difficult to measure N at this concentration. That is why in our study we measured α at $2 \times CMC$.

Hereafter, we present ionization degrees calculated using Zana's (α_Z) and Evans' method (α_E) using Equations (III-2) and (III-16).

1.1.3. Free energy of micellization

To study a colloidal system, it is important to have information about its thermodynamic properties, in particular the Gibbs energy of micellization ΔG_M° as it is one of the key factors in micelle formation.

Free energy of micellization for ionic surfactants (one chain connected to one monovalent head that has monovalent counterion) is usually described by the equation [17, 103]:

$$\Delta G_M^\circ = RT(1 + \beta) \ln c_{mc} \quad (\text{III-17})$$

However, for ionic surfactants some molecular factors should be taken into account, such as number of hydrophobic and hydrophilic moieties per molecule, valence of counterions as well as headgroups, added salts, etc. Hence it is important to use the proper relationship between ΔG_M° and the CMC for a correct analysis of the results. R. Zana in his paper ref. [103] described ΔG_M° for the different types of ionic surfactants. For gemini amphiphiles with two polar head groups (monovalent) linked to two tails and two counterions (monovalent), the free energy of micellization per mole of alkyl chain is:

$$\Delta G_M^\circ = RT(0.5 + \beta) \ln cmc - RT/2 \ln 2 \quad \text{(III-18)}$$

In this equation, β is the degree of counterion binding ($\beta = I - \alpha$) and the cmc is expressed in mol of alkyl chain/L. In this study we are using CMC that is critical micelle concentration in mol of gemini surfactant per liter. Thus, $cmc = 1/2 \cdot CMC$.

To calculate the free energy of micellization, we used ionization degree that was estimated using Evans' method (Equation (III-16)).

1.2. Results and discussions

In this section, the results obtained by conductivity measurements for quaternary 10-2-10 gemini with two groups of counterions: inorganic and alkyl carboxylates as well as for 10-2-10 ter gemini with some halides as counterions are presented.

1.2.1. Quaternary 10-2-10 with inorganic counterions

Table III-1 reports the results obtained by conductivity measurements for quaternary ammonium gemini (10-2-10 X) with inorganic counterions, X = halides, NO_3^- , MeSO_3^- , PH, C2 and TFA. As mentioned in paragraph 1.1.1, the CMC values were calculated by two different methods: CMC^a was obtained by intersection of two straight lines (S_1 and S_2) in the graph of conductivity (κ) versus concentration (C)[92] and CMC^b was obtained by fitting the experimental conductivity data based on integration of a Boltzmann type sigmoidal function[97]. From the Table III-1 we can see that discrepancy between two values is negligible. For the rest of the chapter, we will use CMC values estimated by the method established by Caprena *et al.* For all other characteristics of gemini surfactant such as α , ΔG_M° and N , we used conductivity data obtained employing the fitting approach described above.

Table III-1. CMC^a, CMC^b, α_Z , α_E and $-\Delta G_M^\circ$ for quaternary 10-2-10 gemini with inorganic counterions.

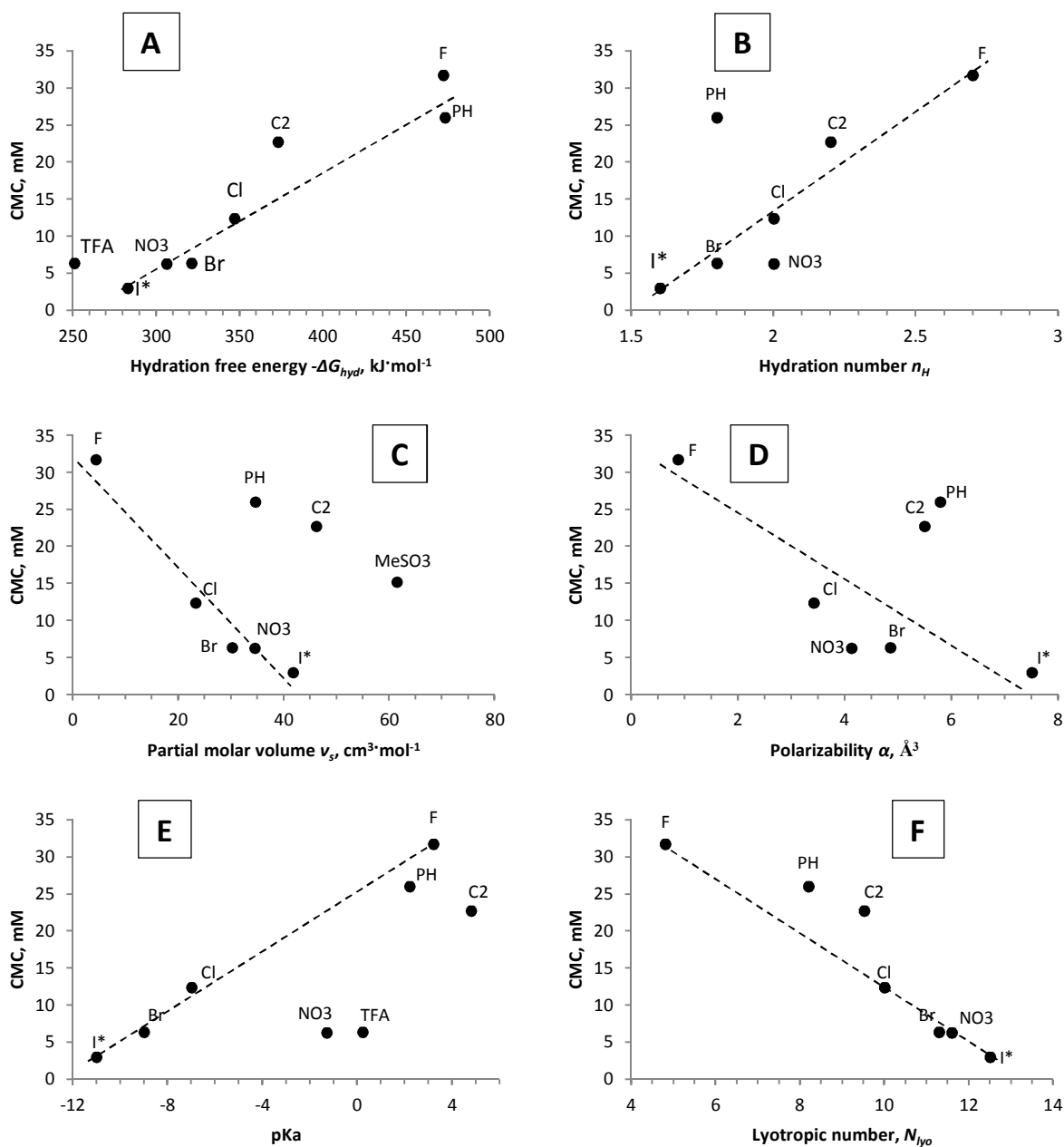
Counterion	Temperature, °C	CMC ^a , mM	CMC ^b , mM	α_Z	α_E	$-\Delta G_M^\circ$, kJ·mol ⁻¹
Br	30	6.5	6.4	0.21	0.15	15.69
Cl	30	12.8	12.4	0.43	0.21	12.88
F	30	34.9	31.7	0.68	0.29	9.28
NO ₃	30	6.4	6.3	0.24	0.15	15.69
MeSO ₃	30	15.3	15.2	0.44	0.23	12.04
PH	30	26.4	26.0	0.49	0.25	10.18
C2	30	23.3	22.7	0.52	0.26	10.53
TFA	30	6.4	6.4	0.17		
I	50	3.0	3.0	0.12		

a - CMC was calculated by intersection point of two straight lines before and after the CMC, S_1 and S_2 respectively

b - CMC by fitting based on the integration of a Boltzmann function[97]. All other parameters were calculated accounting these values of CMC.

Analyzing the CMCs for 10-2-10 gemini, we can see that the micellization of the amphiphiles follows the Hofmeister series: $\Gamma^- < \text{TFA} \sim \text{NO}_3^- \sim \text{Br}^- < \text{Cl}^- < \text{MeSO}_3^- < \text{C2} < \text{F}^- < \text{PH}$, except F^- anion. A similar trend was found for the 14-2-14 gemini with different counterions performed by S. Manet previously in the group[90].

In order to characterize the contribution of counterions to the self-assembly of 10-2-10 gemini, we plotted values of the CMC as a function of different ion properties. In Figure III-3 the CMC as a function of counterion properties is reported. We examined various ion properties such as hydration free energy $-\Delta G_{hyd}$, hydration number n_H , partial molar volume v_s , polarizability α , pKa and lyotropic number N_{lyo} , see Figure III-3 A, B, C, D, E and F respectively.



* - experiment was done at 50°C

Figure III-3. CMC values of 10-2-10 X (at 30 °C and 50 °C in the case of 10-2-10 I) as a function of ion properties. (A) Hydration free energy $-\Delta G_{hyd}$, $\text{kJ}\cdot\text{mol}^{-1}$; (B) hydration number n_H ; (C) partial molar volume v_s , $\text{cm}^3\cdot\text{mol}^{-1}$; (D) polarizability α , \AA^3 [30]; (E) pKa [common values]; (F) lyotropic number N_{lyo} [104, 105].

Considering halide counterions only, it is clear that CMCs versus all ion properties exhibit a quasi-linear dependence, despite the fact that CMC for 10-2-10 I was measured at a higher temperature, due to its low solubility. The CMC values increase with increasing $-\Delta G_{hyd}$, n_H , and pKa, (A, B, and E), and decreasing counterion size, polarizability, and N_{lyo} (C, D and F). The good

correlation of micellization process with physical properties for these anions can be due to two main reasons: these are monoatomic chemically related elements (halogens) and they have the same number of electrons of the external electron orbitals, thus ion size (density) is the main parameter that changes significantly from F to I. Since these properties of the ions vary monotonously from F to I, it is indeed expected that their aggregation behavior and CMC also vary monotonously.

For the polyatomic counterions, their non-spherical shape and inhomogeneous distribution of electron density make a significant contribution to the ion and aggregation behavior. Figure III-3 (A) shows the trend of the CMC values as a function of $-\Delta G_{hyd}$. For more hydrophobic ions (lower $-\Delta G_{hyd}$) the CMC is lower, whereas for more hydrophilic (higher $-\Delta G_{hyd}$) the CMC is higher. However, for some of the ions, this trend is not as simple, indicating that the CMC does not depend on one parameter only, but is presumably a result of cooperative effects of several parameters.

It is interesting to compare counterions such as monoatomic Br^- and polyatomic NO_3^- , as their CMC (for 10-2-10 Br and 10-2-10 NO_3^-) are almost the same (6.4 and 6.3 mM respectively), but, the properties of the anions differ slightly. The free energy of hydration $-\Delta G_{hyd}$ and the partial molar volume v_s (Figure III-3 (A) and (B) respectively) suggest that the aggregate formation for the surfactant with NO_3^- counterions is expected to be at lower concentration (lower CMC) than for Br^- . However, the hydration number n_H , polarizability and pKa (Figure III-3 B, D and E respectively) suggest that CMC for NO_3^- to be higher than for Br^- . Moreover, the planar morphology of the NO_3^- anion could affect the self-assembly process. Being planar, NO_3^- can intercalate between the polar headgroups and dehydrate the micellar surface in comparison with spherical Br^- . All these parameters influence the balance of forces that drives the micellization resulting in similar CMC values for gemini with Br^- and NO_3^- . How much each property contributes to the micellization is difficult to estimate at this point.

Although PH and F^- have almost the same high hydration free energy, $-\Delta G_{hyd}$, (473 and 472 $\text{kJ}\cdot\text{mol}^{-1}$ correspondingly, Figure III-3 A) there is a strong difference in their hydration number, n_H : 1.8 for PH, compared to 2.7 for F^- , (Figure III-3 B) which may have some effect on the CMC. In a previous study[90] on 14-2-14 gemini, comparing PH and F^- counterions, a higher CMC was observed for PH and attributed to entropic effects. High n_H of F^- would induce entropy of the system due to the liberation of water during micellization. Whereas, polarizability and low hydration number of PH would not favor micellization. However, in the present case, the opposite tendency

was observed for the related 10-2-10 gemini. The CMC obtained for PH (26.0 mM) is lower than that for F⁻ (31.7 mM). These results are puzzling and additional investigation of these systems is required in order to understand the mechanism that drives their aggregation.

Comparing the three large polyatomic anions, PH, C2 and MeSO₃⁻ (v_s is 34.6, 46.2 and 61.3 cm³·mol⁻¹) with monoatomic iodide (v_s is 41.7 cm³·mol⁻¹), we can see that even though they are highly polarizable, their CMCs are much higher than that of I⁻ (Figure III-3 C and D). These results suggest that hydrophilic properties of PH, C2 and MeSO₃⁻ have a higher contribution than their size and polarizability.

For halides, the electronic nature of the ions, reflected by their pKa, correlates very well with the values of the CMC. This is not the case for the polyatomic PH, C2, NO₃⁻ and TFA, which do not have a homogeneous electron density (Figure III-3 E).

Finally, we observed that obtained CMC values correlate well with the lyotropic number of the anions (Figure III-3 F). This number gives information on the ability of salts to induce the flocculation of colloidal systems[106]. Furthermore, there is a linear dependence between the lyotropic number and the electric field strength of the ion[105, 106]. Since we observe a direct impact of the lyotropic number on the assembly behavior of micelles in solution, we can conclude that there is a close correlation between the electric field strength and micellar assembly.

The correlation coefficient R² for different graphics (Figure III-3) was determined. When R² equals 1, the dependence of Y on X is linear. In our case, all values of R² are small, indicating that the CMCs have no linear dependence on ion properties. However, analyzing obtained values of R² we can see which property of the ion can better describe the CMC. Obtained results are presented in Table III-2.

Table III-2. The correlation coefficient R² of the dependence CMC on the different ion properties.

Ion property	$-\Delta G_{hyd}$	n_H	v_s	α	pKa	N_{lyo}
R ²	0.876	0.526	0.204	0.261	0.555	0.883

ΔG_{hyd} -free energy of hydration (kJ·mol⁻¹), n_H - hydration number, v_s - partial molar volume (cm³·mol⁻¹), α - polarizability (Å³), N_{lyo} - lyotropic number

Analyzing correlation coefficients, it seems that the free energy of hydration and lyotropic number (originally correlates well with Hofmeister series) are the two parameters which correlate better with the CMC and consequently the self-assembly of surfactant with corresponding

counterion. However, although obtained CMC values also have a good correlation with the hydration number, n_H , (Figure III-3 B), except that PH significantly go out from the trend, R^2 gives just 0.526.

The ionization degree, or fraction of free counterions, characterizes the association strength between counterions and headgroups. On Figure III-4, α_E versus CMC shows that as the CMC increases, so does the ionization degree. This implies that more hydrophilic ions are more dissociated, and that micellization is less favorable, than for ions that make strong ion pairs with the headgroups due to their hydrophobicity. Surprisingly, PH has a lower ionization degree than C2, which may be due to its low hydration number (1.8) with respect to C2 (2.2), or due to its slightly higher polarizability (5.79 \AA^3) compared to C2 (5.50 \AA^3).

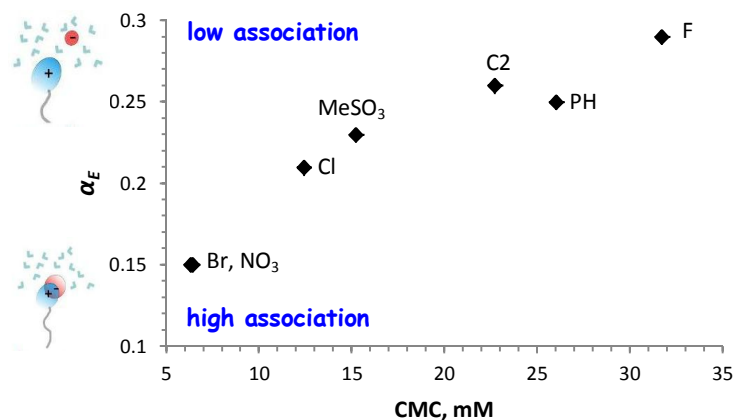


Figure III-4. Ionization degree α_E , as a function of CMC for 10-2-10 X.

The free energy of micellization (Table III-1) follows the same trend as the CMC. $-\Delta G_M^\circ$ is higher for more hydrophobic counterions ($15.69 \text{ kJ}\cdot\text{mol}^{-1}$ for 10-2-10 Br) and decreasing in order $\text{Br}^- \sim \text{NO}_3^- > \text{Cl}^- > \text{MeSO}_3^- > \text{C2} > \text{PH} > \text{F}^-$ ($9.28 \text{ kJ}\cdot\text{mol}^{-1}$), see Figure III-5.

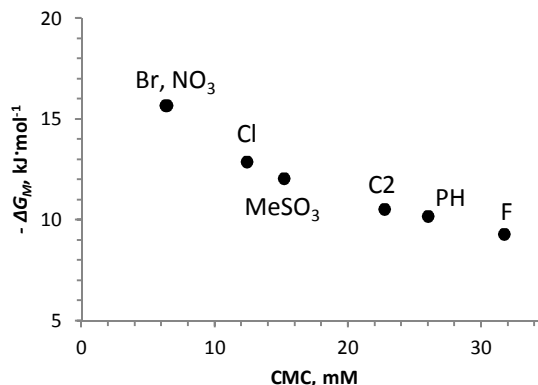


Figure III-5. Free energy of micellization $-\Delta G_M^\circ$, as a function of CMC.

1.2.2. Quaternary 10-2-10 gemini with carboxylate counterions

The results obtained for 10-2-10 gemini with carboxylate counterions *via* conductivity measurements are presented in Table III-3: CMC, α_Z , α_E and $-\Delta G_M^\circ$. Figure III-6 shows the CMC (A) and α (B) as a function of counterion chain length. We can see that the CMC and α decrease with increasing chain length of the counterions. This trend is expected as hydrophilicity decreases for the counterions of longer chain lengths. However, an exception is observed for C1. In spite of its higher hydrophilicity ($-\Delta G_{hyd} = 403 \text{ kJ}\cdot\text{mol}^{-1}$) in comparison to C2 ($-\Delta G_{hyd} = 373 \text{ kJ}\cdot\text{mol}^{-1}$), its CMC is slightly lower. Hence, other properties of the ion also contribute to the self-assembly process. This was already observed with 14-2-14 gemini[90], although C1 is more hydrophilic than C2, it is less hydrated ($n_H = 2.1$) than C2 ($n_H = 2.2$). Moreover, C1 is the only counterion of the series that does not have an alkyl group attached to the carbonyl moiety, which has a strong impact on electron density. This is reflected by the pKa value (3.75) which is more than one unit lower than that of other *n*-alkyl carboxylates (around 4.8).

Table III-3. CMC, α_Z , α_E and $-\Delta G_M^\circ$ for quaternary 10-2-10 gemini with carboxylate counterions.

Counterion	Temperature, °C	CMC, mM	α_Z	α_E	$-\Delta G_M^\circ, \text{kJ}\cdot\text{mol}^{-1}$
C1	30	21.7	0.49	0.23	10.88
C2	30	22.7	0.52	0.26	10.25
C3	30	20.0	0.38	0.22	11.30
C4	30	14.3	0.33	0.21	12.09
C5	30	9.4	0.28		
C6	30	5.7	0.22		
C8	30	1.0	0.10		

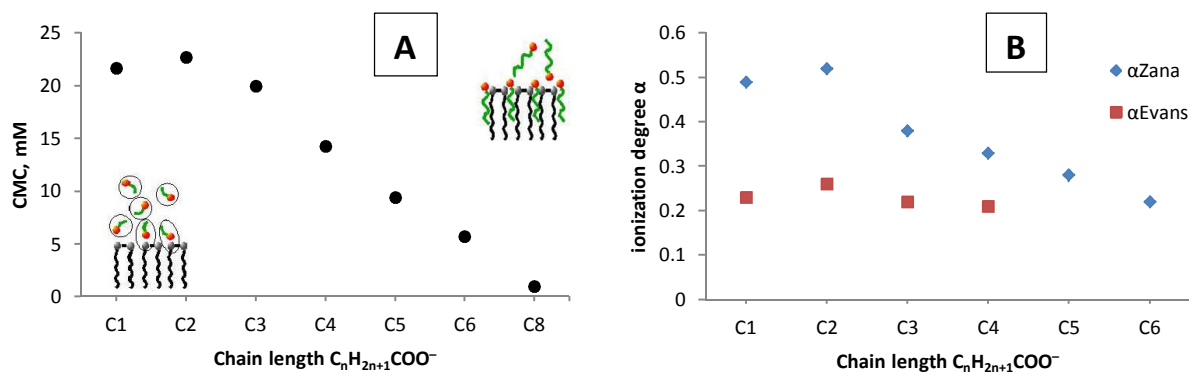


Figure III-6. CMC (A) and ionization degree α (B) as a function of counterion chain length.

The free energy of micellization has the same trend as the CMC and α . With increasing chain length, $-\Delta G_M^\circ$ increases in the following order C2 < C1 < C3 < C4. For the counterions with longer chain lengths we would expect a further increase in $-\Delta G_M^\circ$ that would indicate their favorable contribution to the self-assembly process.

In this system therefore, the variation of just one parameter of the system (hydrophilicity of the counterion) has a predictable effect on the micellization properties. An increase in hydrophobicity (increase in of the chain length) favors micelle formation by decreasing CMC, α and increasing $-\Delta G_M^\circ$, C1 being the exception in this tendency.

1.2.3. Tertiary 10-2-10 gemini with halide counterions

In order to estimate the impact of the nature of cation-anion interactions on the Hofmeister series, we changed the properties of the headgroup of the gemini surfactant by substituting the quaternary ammonium group with a tertiary one, see Figure III-7. We denote tertiary ammonium gemini as 10-2-10 ter X. The objective is to investigate the effect of the cation nature on the counterion effect.

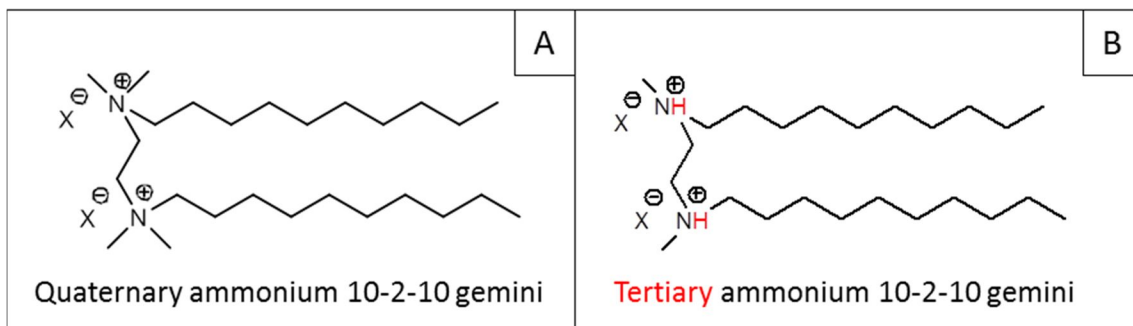


Figure III-7. Structure of quaternary (A) and tertiary (B) ammonium 10-2-10 gemini surfactants.

To obtain CMC values for 10-2-10 ter X conductivity measurements were performed. Two types of counterions: Br^- and Cl^- were analyzed. The results are presented in the Table III-4 along with the quaternary analogs.

In the ammonium headgroups, replacing a methyl by a proton induced a significant change in the properties of the gemini and it was observed that the CMC values for 10-2-10 ter X are an order of magnitude lower than for 10-2-10 X. A much stronger propensity of the 10-2-10 ter X to form micelles in comparison to 10-2-10 X is clearly observed.

Table III-4. CMC^a and CMC^b for tertiary and quaternary 10-2-10 gemini with Br^- and Cl^- as counterions.

Counterion	Temperature, °C	CMC ^a , mM	CMC ^b , mM
<i>tertiary ammonium 10-2-10 gemini (10-2-10 ter X)</i>			
Br	30	0.54	0.40
Cl	30	0.34	0.33
<i>quaternary ammonium 10-2-10 gemini (10-2-10 X)</i>			
Br	30	6.5	6.4
Cl	30	12.8	12.4

The conductivity slopes for tertiary and quaternary gemini were then compared. While the transition of the conductivity slope is abrupt at the CMC for 10-2-10 Br (Figure III-8 right), the break in the slope for 10-2-10 ter Br is very subtle (Figure III-8 left) and it is difficult to define the CMC from the conductivity measurements only.

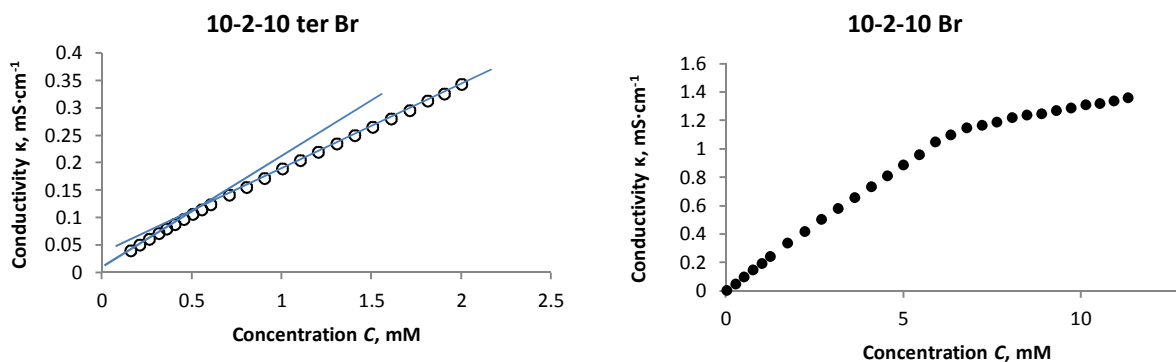


Figure III-8. Conductivity as a function of the surfactant concentration for 10-2-10 ter Br (right) and 10-2-10 Br (left).

Considering the issue cited in the previous paragraph, we therefore used a complementary technique, ^1H NMR[107] in order to confirm the CMC values. Figure III-9 presents the NMR spectrum for 10-2-10 ter Br in D_2O over the concentration range 0.3 - 2 mM. Chemical shifts for the signals of the singlet at 3.61 ppm and the multiplets at 3.22 ppm and 2.78 ppm at a surfactant concentration of 0.5 mM indicate the aggregation formation and the appearance of the micelles. The most efficient method to monitor micelle formation by NMR is to follow the shift in the resonance attributed to the spacer protons that are expected at 3.61 ppm in the dissociated form. As a result, values of the CMC for 10-2-10 ter Br obtained by proton NMR (~ 0.5 mM) correlate with values obtained by conductivity measurements within experimental error.

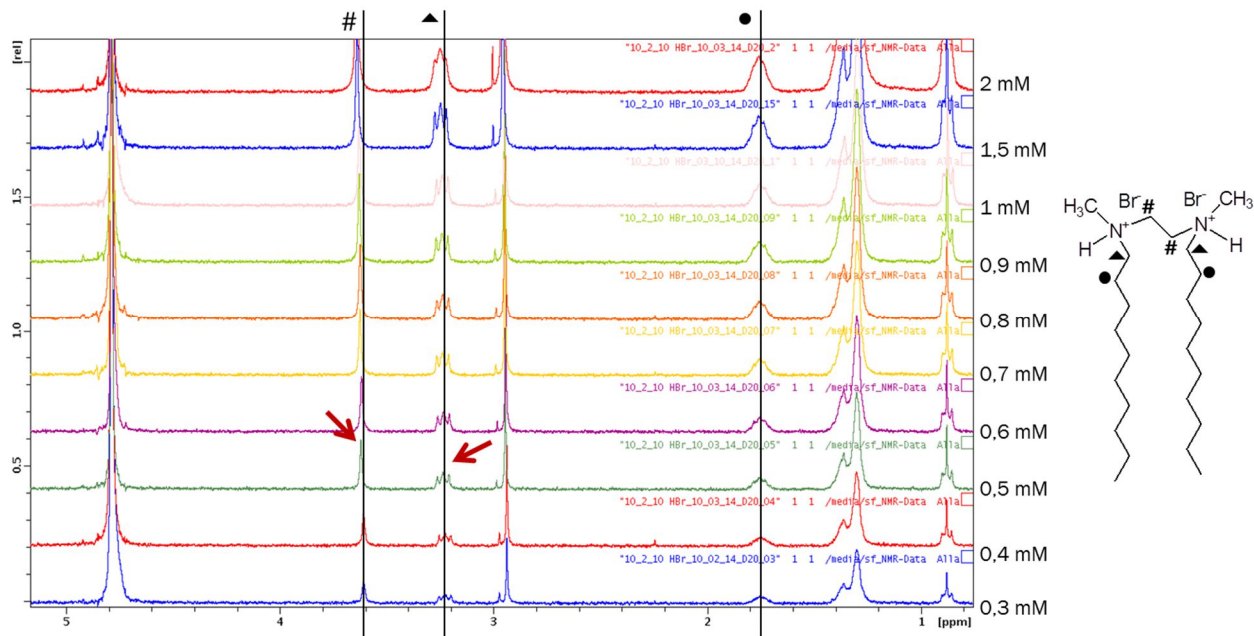
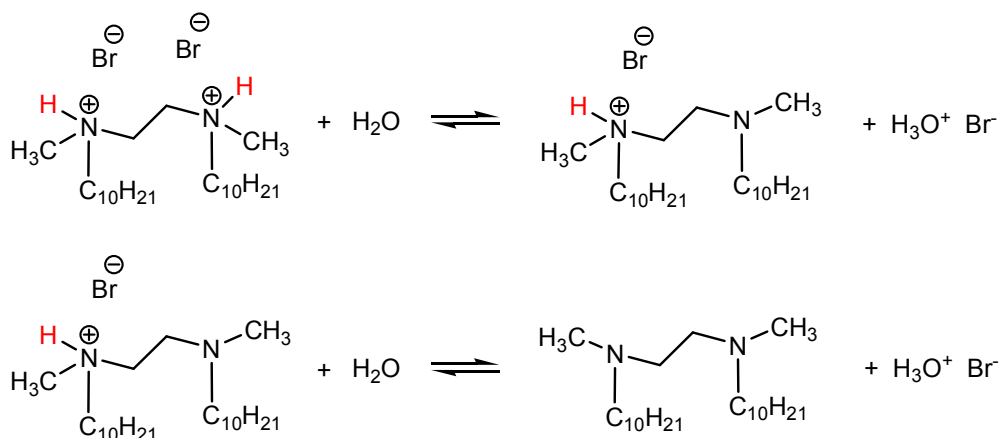


Figure III-9. CMC determination of 10-2-10 ter Br by ^1H NMR. Comparison of the spectrum of 10-2-10 ter Br in D_2O at different concentrations: 0.3 mM, 0.4 mM, 0.5 mM, 0.6 mM, 0.7 mM, 0.8 mM, 0.9 mM, 1 mM, 1.5 mM and 2 mM. Red arrows indicate the shift of the peaks at 0.5 mM.

The decrease in CMC values as observed for 10-2-10 ter Br compared to 10-2-10 Br could, at the first sight, be explained by the deprotonation of the headgroup(s) in the aqueous solution (Scheme III-1). The pH of 10-2-10 ter Br at 1.5 mM equals around 4 much lower than that for 10-2-10 Br (~ 8). The solution is acidic due to the dissociation of the protonated headgroups.



Scheme III-1. Dissociation of tertiary gemini on the example of 10-2-10 ter Br. After first dissociation reaction monocationic gemini is forming (determined by K_{a1}). After second dissociation reaction neutral amine is forming (determined by K_{a2}).

In order to estimate the pKa for both protons we did a titration of 10-2-10 ter Br with added HBr by a 25 mM solution of NaOH. On Figure III-10 one observe three equivalence points indicated by dash lines. The first (1.24 mL), second (1.76 mL) and third (2.47 mL) equivalence points correspond to the volume of NaOH required for the titration of HBr, the deprotonation of one headgroup and of the second headgroup of the gemini respectively. The pKa₁ and pKa₂ for the gemini are defined as the pH at the half-way of each titration and are equal to 4.40 and 5.35 respectively, see Figure III-10.

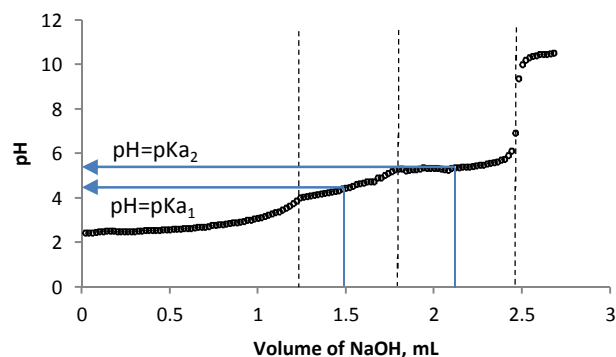
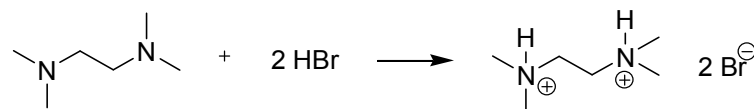


Figure III-10. Titration curve for 10-2-10 ter Br at a concentration 1.5 mM in presence of 3 mM HBr with NaOH (25mM). Dash lines indicate the equivalence points, blue solid lines correspond to pKa.

The HBr solution was added progressively (the variation of pH 4 down to 2) to the 1.5 mM aqueous solution of 10-2-10 ter Br (pH ~ 4) and followed by ¹H NMR. No change in the chemical shifts was observed. This indicates that no change in protonation occurs over this range of pH, that is, 10-2-10 ter Br is dicationic in the studied concentration range. This result was further confirmed by the titration done on tetramethylethylenediamine (TMEDA) with HBr, Scheme III-2 (performed by our collaborator Changyao Liu).



Scheme III-2. Protonation of TMEDA by HBr.

Titration was performed by adding different amounts of HBr (from 0 to 0.4 M) to a 0.1 M solution of TMEDA. The change in the protonation state of the compound was followed by ¹H NMR. Figure III-11 shows that positions of the peaks corresponding to the -CH₃ and CH₂-groups

shift from 2.09 ppm and 2.36 ppm for TMEDA to 2.90 ppm and 3.56 ppm respectively at a concentration of 0.2 M HBr (pH = 5) and stay constant with further increasing the acid concentration. These results indicate that after full protonation of the amine, the positions of the peaks attributed to the α -CH₃ and spacer CH₂ groups for the 10-2-10 gemini also would not change with excess of HBr.

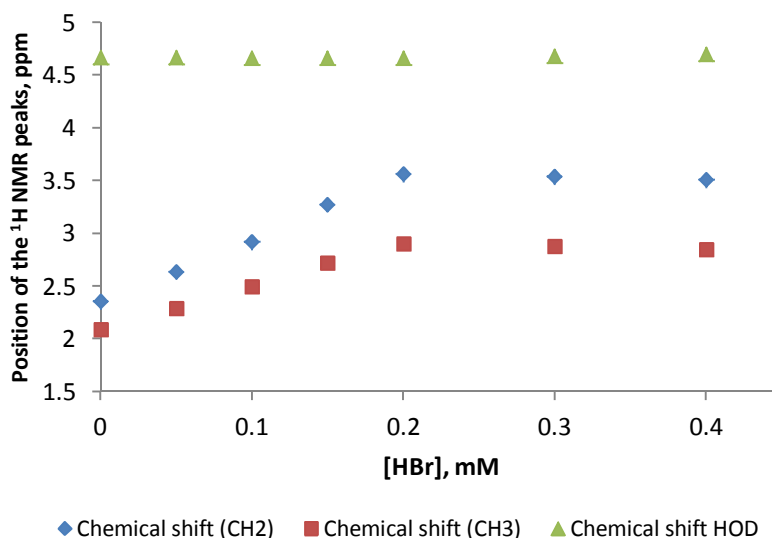


Figure III-11. Position of the ¹H NMR peaks for the TMEDA as a function of added HBr.

Since pH and NMR measurements do not show evidence of the monocationic gemini molecules, we can suppose that the stronger tendency for 10-2-10 ter Br to form aggregates should result from other reasons. In order to investigate the nature of cation-anion interactions, density functional theory (DFT) calculations were performed to probe the binding energies in continuum water for 1,2-bis-trimethylammonium (1-2-1) and 1,2-bis-dimethylammonium (1-2-1 ter) complexes with Cl⁻, Br⁻ and I⁻ anions. 1-2-1 and 1-2-1 ter were used as analogs of the headgroups of quaternary and tertiary 10-2-10 to simplify the system. In Table III-5 the free energies of binding (ΔG_B) between counterion and headgroup are presented. In order to analyze this data, the notion of binding energy is defined as follows: it is the free energy released when the complexes are formed. For example, the free energy of the complex between chloride ion and 1-2-1 is 3.17 kcal/mol lower in free energy than the sum of the components (Figure III-12). Therefore, the binding energy for the 1-2-1 Cl system is 3.17 kcal/mol.

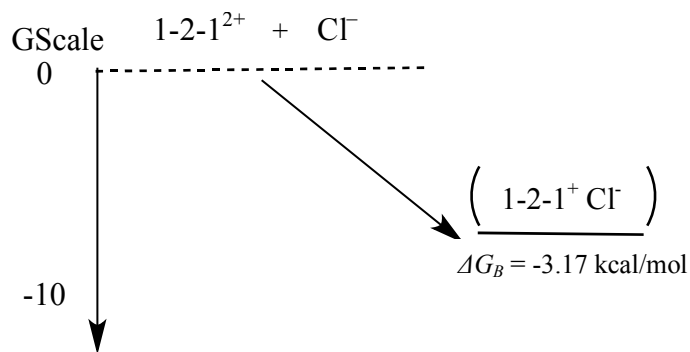


Figure III-12. Schematic representation of the free energy of binding on the example of 1-2-1 Cl complex formation.

We first observe that ΔG_B is significantly lower for the 1-2-1 ter X than for its quaternary analog. A more negative value of binding energy implies that the complex is strongly bound. These results show therefore that association between anion and headgroup is much stronger for the 1-2-1 ter analog, which has a proton instead of methyl group per each ammonium. Second, regardless of tertiary or quaternary 1-2-1 cations, the DFT results suggest that ΔG_B is lowest for Cl^- (the strongest association with the headgroup) and highest for I^- (the weakest interactions with the headgroup). Whereas, experimentally we observe the opposite behavior for the quaternary 10-2-10 X complexes. Such a discrepancy can be due to the cooperative effect that the 10-2-10 X surfactants exhibit by self-assembling into micellar aggregates.

Table III-5. The binding energies ΔG_B between positively charged cationic 1-2-1/1-2-1 ter and counterion.

Compound	Binding energy ΔG_B , kcal/mol		
	Cl	Br	I
1-2-1	-3.17	0.006	0.83
1-2-1 ter	-16.0	-11.6	-8.21

The much stronger association between halides and cations for the tertiary 1-2-1 in comparison to the quaternary ones can be attributed to the formation of hydrogen bonds between counterions and the proton of the gemini headgroups as shown in Figure III-13. Hydrogen bonding is clearly a major factor in stabilizing each of the complexes with the halogen series. Formation of hydrogen bonds between X^- and ammonium proton was shown as well by crystallography and

discussed in Chapter VII. Although in solution the strength of this hydrogen bond is weaker than in the crystal structure, the contribution to the properties of the surfactant in solution is clearly observable experimentally, as seen by the low solubility and computationally by noting the lengthened N-H bonds and the shortened X-H bonds.

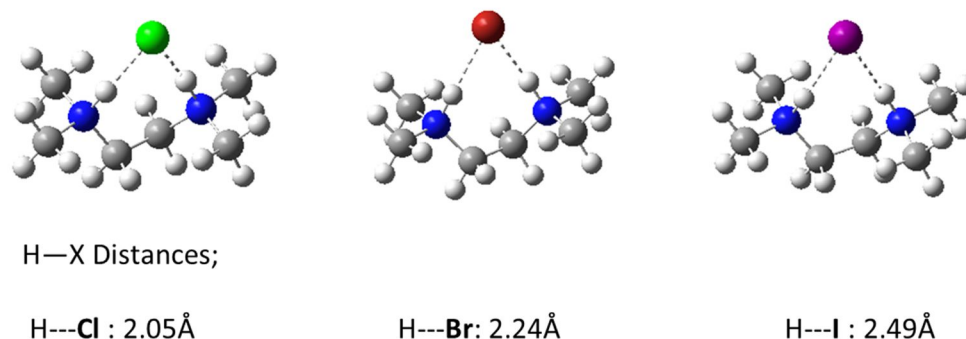


Figure III-13. Representation of the hydrogen bonds between protons of the 1-2-1 ter and halides. Color code: grey, white, blue, green, red and purple corresponds to carbon, hydrogen, nitrogen, chloride, bromide and iodide respectively.

It is interesting to discuss the counterion effect on the CMC values of tertiary gemini by comparing Br^- and Cl^- counterions. In contrast to the quaternary analogs where the CMC for Cl^- is twice higher than for Br^- (12.4 and 6.4 mM respectively), in the case of tertiary gemini the CMC for Cl^- is slightly lower than for Br^- (0.33 and 0.40 mM respectively). These results suggest that the variation of the headgroup properties has an important effect on the counterion-surfactant interactions and consequently on their aggregation behavior. Decreasing softness (increasing hardness) of the cation by replacement one methyl to proton changes the interaction between cations and anions. As it was discussed by Collins and coworkers[36], and is schematically shown in Figure III-1, the highest association are expected for soft-soft ions due to their high polarizability and hydrophobicity. The next more stable ion pairs are formed by hard-hard ions. Hard ions are often highly hydrated, and ion pair formation is favored due to the liberation of the water to the bulk, and hence the increase in the entropy of the system. Ion pairing between soft-hard or hard-soft ions is less preferable. For example, quaternary ammonium gemini have fully methylated headgroups and can be considered to be soft cations. They tend to form strong ion pairs with soft anions such as Γ^- . Hard counterions such as F^- do not form tight ion pairs with soft quaternary headgroups, as was shown previously. Full protonation of the headgroup (for secondary ammonium ions) would in theory convert these to harder cations, and the interactions between secondary ammonium

headgroups and hard counterions such as F^- or in lesser extent, Cl^- should be stronger than for the softer anions such as Br^- or I^- . Thus, gemini with tertiary ammoniums in a headgroup are expected to have intermediate properties. This is exactly what is observed for 10-2-10 ter Br and Cl. Their CMCs are very close and change the order in the Hofmeister series. Br^- and Cl^- now exhibit similar properties. Meanwhile, the strong decrease of CMC for tertiary gemini compared to quaternary gemini was not expected, since the fact that the tertiary ammonium headgroups are harder cations than the quaternary ammonium ones should lead to the decrease the strength of the interaction (increase the CMCs) with the soft anion. As it was discussed, the possible decrease in the ionic interactions is compensated by the formation of hydrogen bonds as suggested by the DFT calculations.

2. Aggregation number. Fluorescence quenching technique

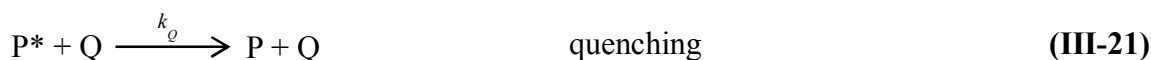
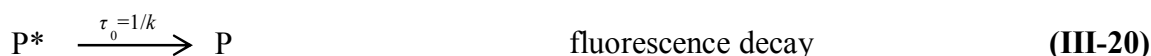
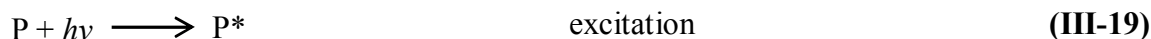
The aggregation number of a surfactant gives the number of surfactant molecules making up an aggregate at a given concentration and temperature. This is related to the size of the aggregate, and this information is required for α_E determination and computer modeling that were applied in this work. There are several methods that can be used to estimate the aggregation number[86, 108]. They are generally based on determining the size of aggregates using techniques such as light-scattering[109, 110], fluorescence correlation spectroscopy[111], small-angle neutron scattering[112], NMR self-diffusion coefficient[113], electron-paramagnetic resonance[114], etc. However most of these techniques have restrictions to the properties of colloid systems or depend on the intermicellar interactions, or are not easily accessible because of the necessary facilities to house such experimental setups[115, 116]. Fluorescence quenching (FQ) techniques are amongst the most widespread methods for investigating the structure of microheterogeneous media. In contrast to the techniques mentioned previously, fluorescence probing methods allow to determine the aggregation number independently of intermicellar interactions and micelle shape, by measuring the concentration of aggregates[86, 115].

Fluorescence quenching techniques are generally based on using a luminescent hydrophobic chromophore to probe the interior of micelles. Moreover, this technique can also provide information about the probe's microenvironment[117] and polydispersity of the micelles[118]. However probe (P) and quencher (Q), applied for the system, have to be chosen very carefully and their concentration must be kept low to prevent the significant influence on the micelle size. Addition of a quencher to the system will result in a decrease of the probe's emission intensity due to the distribution of the quencher inside the micelles. The decrease in intensity is related to the probability of a micelle containing the probe and the quencher, the lifetime of the excited probe, and the quenching rate of the probe by the quencher. There are two methods of fluorescence quenching (FQ): steady-state fluorescence quenching (SSFQ) and time-resolved fluorescence quenching (TRFQ), which are compared below.

2.1. Theoretical aspects of fluorescence quenching techniques as a method to determine aggregation number

2.1.1. Fluorescence quenching in homogeneous media

If the reaction under investigation occurs in homogeneous solution and contains the hydrophobic fluorescent probe (P) and a solute that quenches the probe excitation (Q), dynamic quenching can be described by the following reactions[115]:



where $\tau_0 = 1/k$ is a probe fluorescence lifetime in the absence of added quencher, k is the sum of the unimolecular decay constants and k_Q is the second-ordered quenching rate constant. In the presence of Q at concentration [Q] the probe lifetime τ equals:

$$\frac{1}{\tau} = \frac{1}{\tau_0} + k_Q[Q] \quad \text{(III-22)}$$

Equation III-22, known as the Stern-Volmer equation and is widely used to determine bimolecular rate constants for excited-state reactions involving an emissive species:

$$\frac{\tau_0}{\tau} = 1 + \tau_0 k_Q[Q] \quad \text{(III-23)}$$

For a dynamic quenching process, the ratio τ_0/τ equals to the ratio I_0/I_Q of the fluorescence intensities measured in the absence and presence of quencher, I_0 and I_Q , respectively, giving:

$$\frac{I_0}{I_Q} = 1 + \tau_0 k_Q[Q] \quad \text{(III-24)}$$

If the fluorophore forms a stable complex with Q that is non-fluorescent, then the quenching process is termed static quenching and the slope of the Stern-Volmer equation gives the association constant:



where K_s is an association constant for the quencher-fluorophore complex that depends from the nature of probe/quencher pair and on its microenvironment.

In the cases where both static and dynamic quenching are operational, the Stern-Volmer equation becomes:

$$\frac{I_0}{I_Q} = (1 + \tau_0 k_Q [Q])(1 + K_S [Q]) \quad (\text{III-26})$$

2.1.2. Steady-state fluorescence quenching (SSFQ) in micelles

In the case of micellar solutions, the system becomes heterogeneous and requires an appropriate kinetic model that is based on a set of assumptions. We consider a system that includes only dynamic quenching and for simplification assume that P and Q do not exchange with the bulk during the photochemical process (immobile P and Q)[119]. This implies that P and Q stay in the same micelle significantly longer than the probe's excited-state lifetime, which is on the order of tens of nanoseconds. The model also assumes that the distribution of the probes and quenchers in the micelles follows Poisson's statistics. One important consideration is that the concentration of P has to be much lower than the micelle concentration, [M], to avoid placing two probes within the same micelle. This could lead to collisional quenching of the probe's emission, or to the formation of an excimer possessing different emission properties.

If all these assumptions are satisfied, with increasing the quencher concentration, [Q], as [Q]/[M], the ratio of the fluorescence emission intensities in the absence and in the presence of Q is given by[115, 119]:

$$\frac{I_0}{I_Q} = \exp\left(\frac{[Q]}{[M]}\right) \quad (\text{III-27})$$

Since the P and Q are immobile during the photochemical reaction we can compare this system with quenching in homogeneous solutions. The difference between Equation (III-24) and Equation (III-27) comes from the compartmentalization of the P and Q in the micellar microenvironment.

The main assumption of the model used to obtain Equation (III-27) is that the ratio $k_Q/k \gg 1$, that means that $\tau \ll \tau_0$ and indicates that the quenching of P* is much faster than the other decay processes.

In practice, SSFQ involves measurements of the fluorescence emission intensity with increasing ratio of [Q]/[M] using a spectrofluorometer. However, this only gives the difference between I_0 and I_Q and does not provide information concerning the fluorescence decay. As a consequence, it is impossible to distinguish micelles that have one or more molecules of quencher. When $\tau \ll \tau_0$ this difference between micelles with one or more Qs is negligible.

Obtaining $[M]$ from the semi-logarithmical dependence of I_0/I_Q against $[Q]$ one can determine N :

$$N = \frac{C - CMC}{[M]} \quad (\text{III-28})$$

where the difference in total surfactant concentration, C , and CMC will give concentration of the amphiphile molecules that form micelles. It was shown by Zana and others[86] that when k_Q is not much higher than k , the values of N became underestimated.

2.1.3. *Time-resolved fluorescence quenching (TRFQ) in micelles*

The main benefit of TRFQ lies in the use of fluorescence decay rates to determine the proportion of micelles containing both probe and quencher[120]. The basic experiment is the same as for SSFQ, but the decay curves of the probe's emission rather than its intensity are recorded in the absence and presence of increasing concentrations of Q. Emission decay rates can be recorded using a single photon counting setup, a high-speed streak camera, or a phase-shift technique.

Assumptions used in the TRFQ analyses are as follows:

- (i) The system includes dynamic quenching and P remains confined to the aggregate during the photochemical process. However, it is not required that Q remains immobile in the micelle during the process.
- (ii) The distribution of the probes and quenchers follows Poisson's statistics.
- (iii) The probe concentration should remain low to avoid excimer formation.
- (iv) Quencher molecules do not interact with each other, and the quenching rate of the excited probe in a micelle containing more than one quencher is equal to the sum of the quenching rates of the individual quenchers.

The probe's lifetime in micelles without Q gives a monoexponential decay ($k_0 = 1/\tau_0$). It should be noted that in cases where the excited probe is quenched by oxygen, the lifetime of the probe inside a micelle is often comparable to that of the probe in de-oxygenated solution due to the lower oxygen concentration inside the micelles. Upon addition of Q, the emission decay is no longer monoexponential due to the quenching of some of the probes. The time dependence of the fluorescence intensity is described using the Infelta-Tachiya model[118, 119, 121, 122]:

$$I(t) = A_1 \exp[-A_2 t - A_3 \{1 - \exp(-A_4 t)\}] \quad (\text{III-29})$$

where A_1 is the fluorescence intensity at time equals zero (I_0); A_2 is the fluorescence decay constant in the absence of Q ($A_2 = k_0 = 1/\tau_0$); A_3 is the average occupation number of quenchers per micelle ($\langle n \rangle = [Q]/[M]$); and A_4 is the quenching rate constant (k_Q) of P* by Q inside a micelle.

The fluorescence decay curves are fitted to Equation (III-29) using a non-linear least-squares algorithm contained in the commercial software from the instrument or the Decan 1.0 software[123], so that $\langle n \rangle$ can be determined. Subsequently, the aggregation number (N) at each $[Q]$ can be calculated as:

$$N = \frac{C-CMC}{[M]} = \langle n \rangle \frac{C-CMC}{[Q]} \quad \text{(III-30)}$$

For a Gaussian micelle size distribution, the quencher averaged aggregation number N_{av} , for any particular $[Q]$ derived by a fit of the decay to the Equation (III-29), is written as a series in the quencher concentration. This N_{av} can be presented as weight averaged aggregation number N_W with some deviation[124]:

$$N_{av} = N_W - \frac{\sigma^2}{2} \frac{[Q]}{C-CMC} \quad \text{(III-31)}$$

where σ is the standard deviation in the aggregation number.

Weighted averaged aggregation number N_W is defined as:

$$N_W = \frac{\sum_n n^2 X_n}{\sum_n X_n} = \frac{\sum_n n^2 X_n}{C-CMC} \quad \text{(III-32)}$$

where n is the aggregation number and X_n is the distribution function. The intercept of N_{av} vs $(1/2)([Q]/(C - CMC))$ yields the true or weight averaged aggregation number, N_W , and the slope yields the variance of the aggregation number distribution[124]. Note, that at very low quencher concentrations, the fits to the decay curves are subject to a higher error and have been found to overestimate the aggregation numbers, sometimes by as much as 15%. Recommended values of $\langle n \rangle$ for single chain amphiphiles are around 1[124].

It is important to highlight that in comparison with SSFQ, TRFQ does not rest on the assumption that $k_Q/k \gg 1$ and that this technique can account for molecules of Q that are exchanged between the micelle and the environment during the excited state lifetime of P*. Furthermore, as it was mentioned in paragraph 2, additional information can be obtained from the decay constant of

the probe and k_Q , which decreases with increasing size of micelles or when the viscosity of the probe/micellar microenvironment increases[115].

In the present work 1-methylpyrene and cetylpyridinium chloride were used as fluorescent probe (P) and quencher (Q), respectively (Figure III-14). The excitation wavelength was 310 nm, and the emission was monitored at 370 nm. The decay of emission was recorded in the absence of quencher, giving a lifetime of τ_0 (P*) of around 110 ns (in the case of bromide counterions, a shorter lifetime of ca. 70 ns was obtained, presumably due to the external heavy atom effect), and in the presence of quencher. More details about the experimental conditions can be found in experimental section.

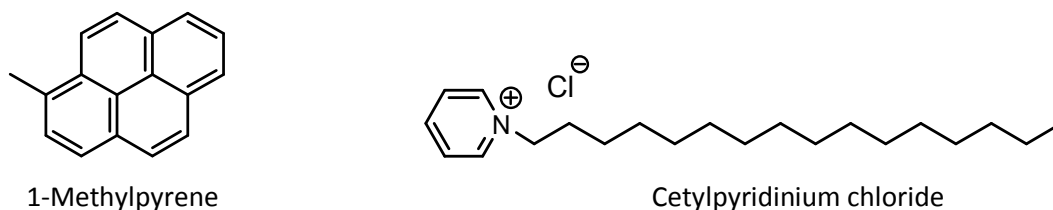


Figure III-14. Molecular structure of probe, 1-methylpyrene, and quencher, cetylpyridinium chloride.

2.2. Results and discussions

In this paragraph we focus on the contribution of counterion properties to the aggregation number (N) of the micelles determined by TRFQ. The investigated systems included quaternary ammonium 10-2-10 X gemini with inorganic counterions ($X = \text{Br}^-$, Cl^- , I^- , NO_3^- , MeSO_3^- , PH, C2 and TFA) and carboxylate counterions (C1-C6). N was also determined for tertiary ammonium 10-2-10 ter Br. As TRFQ provides information on micellar aggregates properties. Analyzing it, the impact of counterion nature, as well as contribution of the headgroups properties (for 10-2-10 ter Br) on the morphology of aggregates can be estimated.

2.2.1. Quaternary ammonium 10-2-10 with inorganic counterions and tertiary ammonium 10-2-10 ter Br

Time-resolved fluorescence quenching experiments were done for 10-2-10 X gemini, where $X = \text{Br}^-$, Cl^- , F^- , NO_3^- , MeSO_3^- , PH, C2 and TFA at concentrations $2x\text{CMC}$ and $3x\text{CMC}$ as well as for 10-2-10 ter Br at $2x\text{CMC}$. Averaged aggregation number, N_{av} , as well as the weight averaged aggregation numbers, N_w , (determined from the intercept of a linear fit to N_{av} vs $[\text{Q}]/(\text{C} - \text{CMC})$)

and the standard deviation in micelle aggregation numbers σ (from Equation (III-31)) are given in Table III-6.

Table III-6. CMC and N for 2xCMC and 3xCMC for the 10-2-10 X and 10-2-10 ter X surfactants obtained from TRFQ using 1-methylpyrene as a probe and CPC as a quencher.

Counterion	CMC, mM	2xCMC			3xCMC		
		N_{av}	N_w	σ	N_{av}	N_w	σ
<i>quaternary ammonium 10-2-10 gemini (10-2-10 X)</i>							
F	31.7	27	28	8.3	37	57	59
PH	26	25	28	13.6	38	75	78
C2	22.7	23	24	7	25	35	49
MeSO₃	15.2	28	30	18.4	31	37	33
Cl^a	12.4	34	35	10	40	40	17
Br^b	6.4	35	35	9	35	36	13
TFA	6.4	33	33	5.4	39	38	9.5
NO₃	6.3	33	34	4.5	35	36	6.3
<i>tertiary ammonium 10-2-10 gemini (10-2-10 ter X)</i>							
Br	0.4	16	23				

N_{av} - averaged aggregation number, N_w - weight averaged aggregation number, **a** - average of two independent measurements, **b** - average of three independent measurements

Comparing N_{av} and N_w we can see that for a concentration of 2xCMC, the difference in values for the different counterions is small. However, at 3xCMC for the hydrophilic F⁻, PH and C2 the N_w has larger values than N_{av} . We attribute this to the presence of polydispersity in the system, as estimated from the standard deviation in the N_w aggregation number, σ .

At 2xCMC, most of the investigated surfactant systems show low polydispersity, with values of σ lower than 20. However, at higher surfactant concentrations (3xCMC), the situation is different. The most polydispersed micellar system is the one with the PH counterion ($\sigma = 78$) as we can see from Figure III-15, where N varies from 33 to 66. A relatively high polydispersity is also observed for F⁻ and C2, where σ are 59 and 49, respectively. In contrast, micelles formed by 10-2-10 gemini associated with Cl⁻, Br⁻, TFA and NO₃⁻ are monodisperse at this concentration. Interestingly, polydispersity is pronounced for the gemini amphiphiles with hydrophilic counterions. We can assume that more hydrophobic counterions, when they are small and do not integrate the micellar core (like alkyl carboxylates), will better stabilize the micelles and thus aggregates of similar numbers are built.

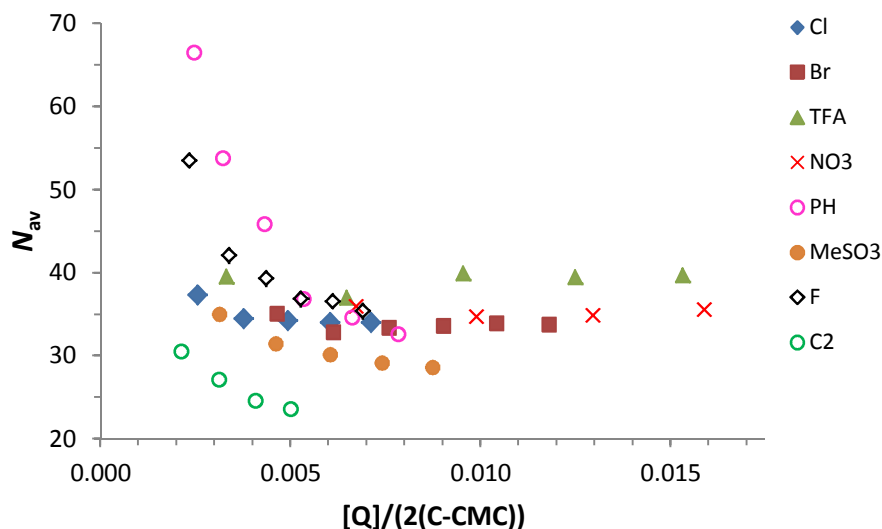


Figure III-15. N_{av} as a function of $[Q]/(2(C-CMC))$ for 10-2-10 X at 3xCMC, where X= F^- , Br^- , Cl^- , NO_3^- , PH, TFA, C2 and $MeSO_3^-$.

A diagram presenting N_{av} for 2xCMC and 3xCMC is shown in Figure III-16. For all cases, the N_{av} for 3xCMC is larger than that for 2xCMC, and the difference is more significant for the most hydrophilic ions such as F^- and PH. Interestingly, an N_{av} for 10-2-10 ter Br (16) at 2xCMC is ca. half that of its quaternary analog 10-2-10 Br (35). This may be because of its smaller headgroup size compared to 10-2-10 Br, which allows it to form stable smaller aggregates.

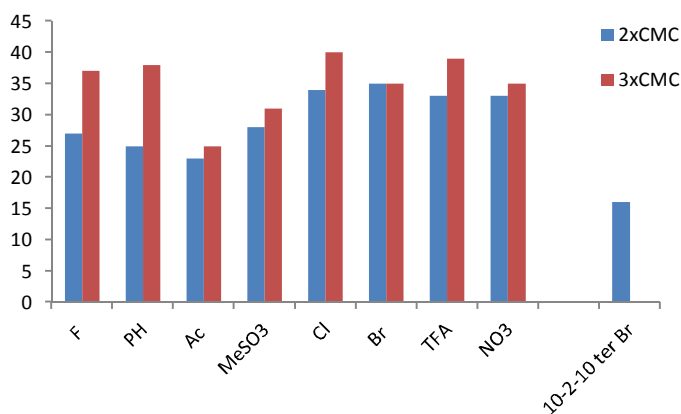


Figure III-16. Diagram presenting N_{av} for 10-2-10 X, where X = F^- , PH, C2, $MeSO_3^-$, Cl^- , Br^- , TFA at twice and thrice the CMC and for 10-2-10 ter Br at twice the CMC.

It is interesting to compare the N of 10-2-10 gemini with that of the monomeric analogs, decyltrimethylammonium bromide (DeTAB). Different values of the aggregation number are reported for the latter, depending on the technique that was used: 36[125], 39[126], 48[127] at the

CMC. The aggregation number for DeTAB is only slightly higher than 10-2-10 Br, although one could have expected that the N of gemini is the half of that of monomeric surfactant given that it has two hydrocarbon chains.

Surprisingly, there is only a small variation in the values of aggregation numbers at twice the CMC for all counterions despite the important variation in the values of their CMC (between 6.3 mM for NO_3^- and 31.7 mM for F^- counterions). There is a slight tendency for the more hydrophilic counterions (F^- , PH, C2, MeSO_3^-) to have a lower aggregation number at 2xCMC than more hydrophobic ones (Figure III-16). For example, the N_{av} of 10-2-10 PH and 10-2-10 Br at 2xCMC are 25 and 35, respectively. Such aggregation behavior can be explained by the electrostatic repulsion of the positively charged headgroups due to the low ionization degree (α) for hydrophilic counterions. Conversely, for hydrophobic counterions where the charge of the micellar headgroups is better screened by the anions due to the higher α of the micelle, integration of new monomers to the aggregate is more favorable (Figure III-17).

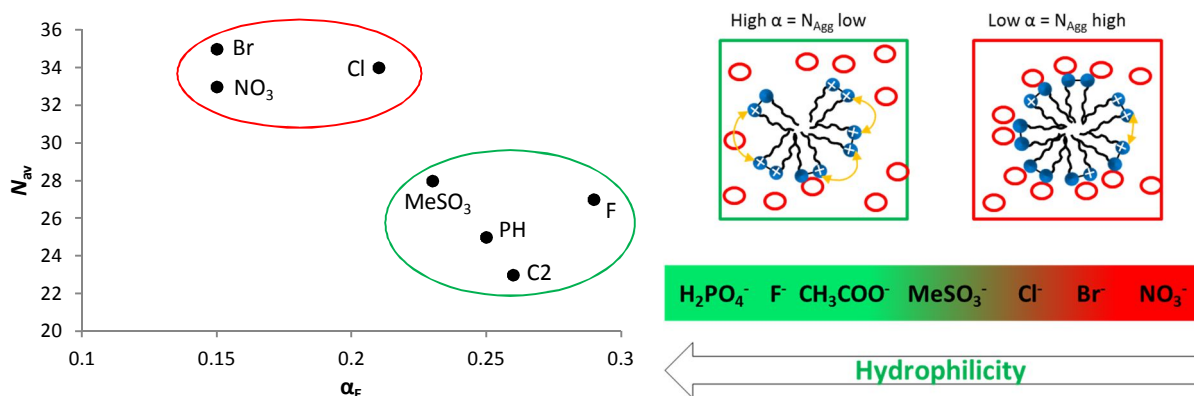


Figure III-17. N_{av} as a function of α_E for 10-2-10 X gemini, where X = F^- , PH, C2, MeSO_3^- , Cl^- , NO_3^- , Br^- . Red color indicates hydrophobic counterions and green corresponds to the hydrophilic counterions. On the right there is the schematic representation of aggregation behavior according to Hofmeister series.

2.2.2. Quaternary ammonium 10-2-10 with carboxylate counterions

Aggregation number for the quaternary 10-2-10 with carboxylate counterions (from C1 to C6) were obtained by TRFQ at 2xCMC and 3xCMC to investigate the contribution of hydrophobicity of the counterions to the aggregation behavior of micellar solution. The same approach to estimate averaged aggregation number, N_{av} , weight averaged aggregation numbers, N_{w} ,

and the standard deviation in micelle aggregation numbers, σ , as for inorganic counterions was used. The results are presented in Table III-7.

Table III-7. CMC and N for 2xCMC and 3xCMC for the 10-2-10 X surfactants obtained from TRFQ using 1-methylpyrene as a probe and CPC as a quencher.

Counterion	CMC, mM	2xCMC			3xCMC		
		N_{av}	N_w	σ	N_{av}	N_w	σ
C1	21.7	28	31	19	37	47	42
C2	22.7	23	24	7	25	35	49
C3	20.0	24	25	6	26	31	25
C4	14.3	23	27	21	27	37	37
C5	9.4	25	26	7	30	34	21
C6	5.7	26	27	10	28	32	21

N_{av} - averaged aggregation number, N_w - weight averaged aggregation number

Similarly to the inorganic counterions at 2xCMC, the difference in values between N_{av} and N_w is insignificant. However, with increasing concentration, the change becomes more visible. At 3xCMC the estimated N_w values are higher than those of N_{av} . This difference comes from the polydispersity of the systems. In Figure III-18, the dependence of N_{av} versus $[Q]/(2(C-CMC))$ is presented. From this we can see that the highest variation of N_{av} is for C1 and C2 counterions, as also confirmed from the dispersion coefficient, σ , determined to be 42 and 49, respectively. For the counterions with longer chains σ decreases indicating that the polydispersity decreases. Similar results were obtained for inorganic counterions, where larger polydispersities were observed for more hydrophilic counterions (F^- , PH, Figure III-15). However, it is noteworthy that for alkyl carboxylates and inorganic counterions having similar CMCs and hence hydrophobicity (*i.e.* C6 and Br^- or C4 and Cl^-), the organic anions exhibit a higher polydispersity than the inorganic ones.

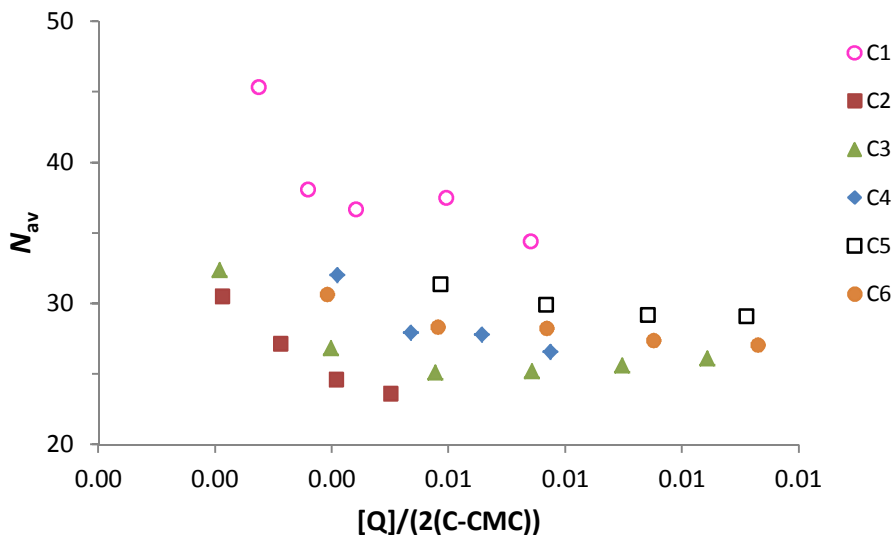


Figure III-18. N_{av} as a function of $[Q]/(2(C-CMC))$ for 10-2-10 X at 3xCMC, where X = C1, C2, C3, C4, C5 and C6.

It is expected that the aggregation number for gemini would be larger at 3xCMC than at 2xCMC due to the growth of the aggregates with surfactant concentrations. The difference in N_{av} between 2xCMC and 3xCMC for 10-2-10 gemini with carboxylates is relatively small, except for C1, the most hydrophilic counterion (Figure III-19).

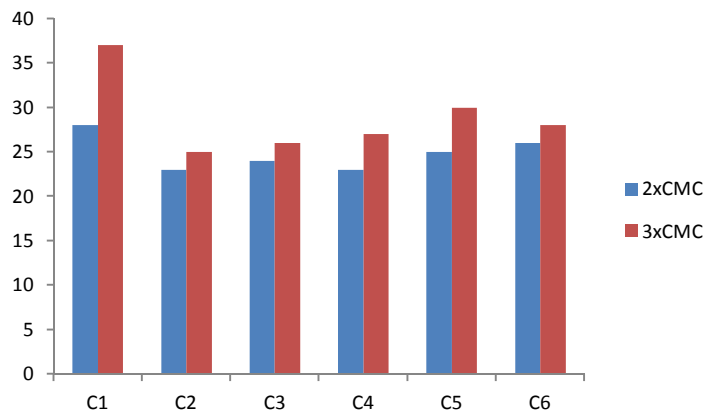


Figure III-19. Diagram presenting N_{av} for 10-2-10 X, where X = C1-C6 at twice and trice the CMC.

In the same way as for the 10-2-10 gemini with inorganic counterions, the values of N_{av} at twice the CMC are very similar for all carboxylate counterions despite that their values of CMC vary from 22.7 to 5.7 mM for C2 to C6. Taking into account the polydispersity, we can say that for

all carboxylates (except just C1) N_{av} does not vary much and equals ~ 24 independently from the ionization degree (Figure III-20, note we use α_Z in order to estimate the ionization degree for all counterions) due to the presence of ordered counterion layer. For C1, the aggregation number is slightly higher even though its α_Z is lower than for C2.

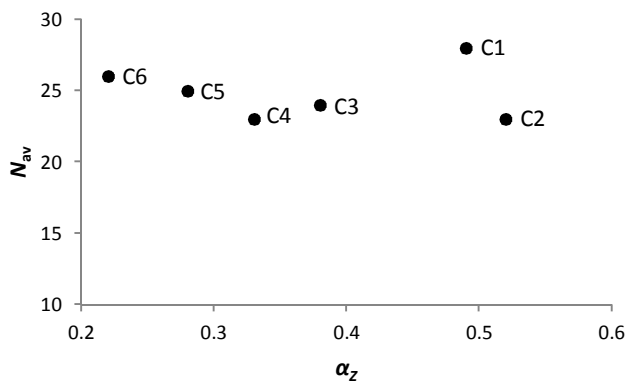


Figure III-20. N_{av} as a function of α_Z for 10-2-10 X gemini at 2xCMC, where X = from C1 to C6.

In comparison with inorganic counterions, almost no increase in N_{av} for the more hydrophobic counterions C4, C5 and C6 was observed. We propose that this is due to the fact that the longer hydrophobic chains may influence the packing parameter of the micellar aggregates by penetrating into the micellar hydrophobic core, thus limiting the increase of their N_{av} . In order to estimate how the hydrophobicity of the counterion influences the N_{av} , we estimated the carbon content of the micelles. Knowing the aggregation number and ionization degree of the micelle we can recalculate how many carbons contain the micellar core according to the equations:

$$Carb_M = Carb_S + Carb_C \quad (\text{III-33})$$

Where $Carb_S$ and $Carb_C$ are respectively:

$$Carb_S = 20N_{av} \quad (\text{III-34})$$

$$Carb_C = 2(1 - \alpha)N_{av}L \quad (\text{III-35})$$

where L is the number of carbons in the counterion chain.

Figure III-21 compares the number of carbons in the liquid hydrocarbon core of the micelle without the contribution of counterions (black rounds, $Carb_S$) and counting the contribution of the

aliphatic chains of the counterions (red squares $Carb_C$), assuming that the C4 counterion has already started to penetrate the micellar core.

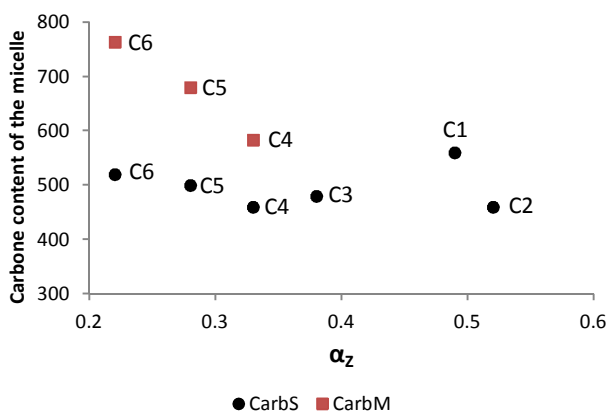


Figure III-21. Carbone content of the micelle as a function of α_z for 10-2-10 X gemini, where X = from C1 to C6. Black solid rounds represent the carbon content of the micelle without accounting the counterions ($Carb_S$), and the red squares represent carbon content of the micelle accounting the counterions ($Carb_M$).

Indeed, it is clear that the carbon content of the micelle increases for the more hydrophobic counterions. Therefore, penetration of the micellar core by the hydrophobic chain of longer alkyl carboxylates prevents an increase in the number of aggregates, in other words, the integration of extra gemini molecules, and simultaneously augments the micellar volume.

3. Conclusions

In this Chapter we described our study of ion specific effects of counterions on the 10-2-10 X gemini surfactant self-assembly process. The physical properties in bulk solution for quaternary ammonium gemini surfactant salts with different counterions and tertiary ammonium gemini with halides were investigated. Conductivity measurements were used to study the properties of ionic solutions to estimate the CMC, ionization degree (determined by two methods: Zana's (α_Z) and Evans' (α_E)) and free energy of micellization ($-\Delta G_M^\circ$). Time-resolved fluorescence quenching was used to investigate the aggregation number of the micelles (N).

In summary, the CMC values for 10-2-10 X follow the Hofmeister series $\Gamma^- < \text{TFA} \sim \text{NO}_3^- \sim \text{Br}^- < \text{Cl}^- < \text{MeSO}_3^- < \text{C}_2 < \text{F}^- < \text{PH}$. Self-assembly of quaternary gemini surfactants depends on the hydrophilic/hydrophobic properties of the counterion ($-\Delta G_{hyd}$). For 10-2-10 X with monoatomic counterions ($X = \text{halides}$), the CMC depends monotonously on all examined ion properties. In the case of polyatomic counterions, however, it is difficult to correlate the behavior of the surfactant to just one ion property. Various properties determine cooperatively the forces that drive micelle formation. Meanwhile, as was mentioned before, free energy of hydration best predicts the behavior of the surfactant molecules in solution. To follow the contribution of just hydrophobic component to the micellization, aliphatic carboxylates were chosen as counterions that have the same chemical nature. The main trend indeed suggests that increase of the chain length (hydrophobicity) of the counterion promotes micellization of the surfactant.

Ionization degree determines the fraction of free ions. Gemini with more hydrophilic/hydrated counterions have higher ionization degrees, indicating that they have lower interactions with headgroups of the gemini surfactants. Instead, amphiphiles with poorly hydrated hydrophobic counterions have lower ionization degrees and tend to associate strongly to form ion pairs. The same behavior is observed for 10-2-10 with carboxylate counterions: the more hydrophobic the counterion, the lower ionization degree α is. Free energy of micellization ΔG_M° is a characterization of the thermodynamic properties of the system. It increases with increasing hydrophobicity of the ion which favors micelle formation.

The aggregation numbers of the micelles were not found to depend significantly on the counterion properties, and are around 30. However there is still a small dependence of the N values on the ionization degree of the system. Micellar systems with counterions which are characterized

by higher ionization degree tend to have smaller values of the aggregation number. Whereas larger aggregation numbers are observed for the micellar systems with counterions having lower α . This tendency may be due to the electrostatic repulsion of the gemini headgroups in the case of high α that is disfavors the integration of the new monomers to the micelle. For the surfactants with low α , this effect is screened by counterions.

In order to understand better the balance of forces that drives the self-assembly of cationic gemini surfactants, we employed other techniques such as chemical trapping, molecular dynamics (interfacial properties), rheology and crystallography described in the following chapters.

In addition, we showed that the changes in the properties of the headgroup (substrate) would affect the order of anions in Hofmeister series. Increasing the hardness of the cationic headgroup for gemini by replacement one methyl by a proton, we could reverse the Hofmeister effects. For 10-2-10 ter X, we observed that Cl^- , having slightly smaller CMC (0.33 mM), can be considered to be more associated with the headgroup than Br^- (CMC is 0.40 mM).

4. Experimental section

4.1. Conductivity measurements

Methodology. Conductivity measurements were performed using benchtop meter CONSORT C860 (Belgium) with platinum electrode SK10T (Belgium). The temperature was maintained at 30 ± 0.1 °C using a thermostat Huber Ministat CC. All solutions were prepared with milliQ water ($18.2 \text{ M}\Omega\cdot\text{cm}$). The technique is very sensitive to the presence of ions, so the electrode as well as glassware should be rinsed several times with ultrapure water before usage.

For quaternary 10-2-10 X gemini the conductivity measurements were performed through the increase of the concentration of amphiphile molecules in the pure water. The stock solution of the surfactant was prepared at concentration much higher CMC (if the solubility of surfactant molecule allows). And after, the aliquots of this stock solution were added to the same sample of pure water increasing the concentration of amphiphiles. For tertiary 10-2-10 ter X gemini conductivity measurements were carried out by dilution the concentrated surfactant solution (usually ~ 4 times higher than CMC) with extra pure water. The solution was continuously stirred to keep the equilibrium in the system. Indicated conductivity values were collected at each concentration after stabilization of the system (5-10 min).

Treatment of the results. As it was already mentioned in subchapter 1.1. of this chapter, we used two methods for the data treatment to determine CMC's and α_z values: (a) intersection point of two straight lines before and after CMC, S_1 and S_2 respectively; (b) fitting based on the integration of Boltzmann function. The data for the both methods are given in the Table III-8.

Table III-8. Summary table for the results obtained with conductivity measurements.

Gemini	T (C°)	CMC ^a mM	S_1^a	S_2^a	CMC ^b mM	S_1^b	S_2^b	λ_x^c (25°C)	λ_x (T)	α_z^a	α_z^b
			$S \cdot \text{cm}^2 \cdot \text{mol}^{-1}$			$S \cdot \text{cm}^2 \cdot \text{mol}^{-1}$					
10-2-10 Br	30	6.5	168.6	37.3	6.4	173.3	36.8	78.1	85.9	0.22	0.21
10-2-10 Cl	30	12.8	185.1	82.8	12.4	190.8	82.1	76.3	83.9	0.45	0.43
10-2-10 F*	30	34.0	92.7	69.8	31.7	98.6	67.3	55.4	60.9	0.75	0.68
10-2-10 NO3	30	6.4	157.4	40.8	6.3	164.9	39.0	71.4	78.6	0.26	0.24
10-2-10 PH	30	26.4	78.4	40.1	26.0	80.5	39.6	36	39.6	0.51	0.49
10-2-10 TFA	30	6.4	87.1	15.7	6.4	88.1	15.2	-	-	0.18	0.17
10-2-10 MeSO3	30	15.3	91.1	43.4	15.2	93.2	41.3	45.9 ^d	50.5	0.48	0.44
10-2-10 I	50	3.0	172.8	22.6	3.0	177.5	21.5	76.8	115.2	0.13	0.12
10-2-10 C1	30	22.1	132.7	67.9	21.7	136.4	66.7	54.6	60.1	0.51	0.49
10-2-10 C2	30	23.3	103.0	68.0	22.7	111.2	58.3	40.9	45.0	0.66	0.52
10-2-10 C3	30	19.9	93.1	48.1	20.0	101.7	39.1	35.8	39.4	0.52	0.38
10-2-10 C4	30	14.8	80.2	33.4	14.3	87.3	29.1	32.6	35.9	0.42	0.33
10-2-10 C5	30	10.0	79.1	31.5	9.4	87.3	24.3	-	-	0.40	0.28
10-2-10 C6	30	5.8	84.8	19.3	5.7	87.7	19.2	-	-	0.23	0.22
10-2-10 C8	30	1.0	92.5	11.2	1.0	95.4	9.8	-	-	0.12	0.10
<i>Tertiary</i>											
10-2-10 ter Br	30	0.54	216.3	160.2	0.4	218.8	152.3	78.1	85.9	0.74	0.70
10-2-10 ter Cl	30	0.34	218.0	178.5	0.33	219.9	176.2	76.3	83.9	-	-

a - data from conductivity measurement estimated by intersection of two lines (S_1 and S_2)

b - data from conductivity measurement estimated by fitting based on the integration of Boltzmann function

c - data taken from ref.[128]

d - data taken from ref.[30]

Note that values for the CMC calculated using fitting model are slightly smaller (or almost equal) the ones calculated using the intersection point. As it was already discussed before in this chapter (section 1.1.1) the method proposed by Carpena *et al.* consider to be more accurate for the CMC determination. In our particular case discrepancy between results obtained from two methods is negligible.

For 10-2-10 Br, as the compound with better purity due to the simpler way of synthesis, the conductivity measurements were done 10 times to see the discrepancy between the measurements. From the obtained data: $\text{CMC}^a = 6.54 \pm 0.24$ and $\text{CMC}^b = 6.43 \pm 0.27$ we can say that both methods give statistically coherent results. An error of the experiment with 10-2-10 Br is less than 5%.

However it is possible that it can slightly increase for the other systems due to more complex synthesis (see the Chapter II) and possible impurities that can influence to the real concentrations and conductivity values.

Molar ionic conductivity was taken from the CRC Handbook of Chemistry and Physics (85th edition)[128] and Marcus Yizhak, Ion properties[30] for MeSO_3^- . The calculation of the ionic conductivity at given temperature were done according to the equation[129]:

$$\lambda_{i,T}^{\circ} = \lambda_{i,25^{\circ}\text{C}}^{\circ} [1 + 0.02(T - 25^{\circ}\text{C})] \quad \text{(III-36)}$$

where $\lambda_{i,T}^{\circ}$ is a molar ionic conductivity at given temperature T and $\lambda_{i,25^{\circ}\text{C}}^{\circ}$ is a molar ionic conductivity at 25 °C.

Theoretical S_I values consist of twice ionic molar conductivity of the counterion (2 anions per one gemini) plus conductivity from the amphiphilic cation. In our study S_I values correspond to the expected ones within error that could come from the experiment due to manual performance of the measurements. The exception is F^- and I^- where S_I is lower than $2\lambda_x(T)$. The conductivity was measured just after synthesis though we have $S_I = 99 \text{ S}\cdot\text{cm}^2\cdot\text{mol}^{-1}$ instead of $\sim 140 \text{ S}\cdot\text{cm}^2\cdot\text{mol}^{-1}$ that means there are less mobile species. This may be because 10-2-10 F is known to decompose quite fast, therefore there are less 10-2-10 in solution than expected.

As for 10-2-10 I the error comes from the measurements at high temperature. Machine was calibrated at the room temperature and experiment was carried out at 50 °C that caused some error in the slope.

4.2. Spectrofluorometric measurements

Methodology. Stock solutions: amphiphile at 2xCMC and 3xCMC in ultrapure water (18.2 $\text{M}\Omega\cdot\text{cm}$), probe at concentration $\sim 5\cdot 10^{-4}$ M (absolute ethanol) and quencher ($\sim 4\cdot 10^{-3}$) in MilliQ water were prepared the day before to make the systems stabilize. To a solution of gemini (2.5 mL) in quartz cell (10 mm) was added 15 μL (10 μL or less for surfactants with low CMC) of 1-methylpyrene. Final probe concentration in the cell is $\sim 3\cdot 10^{-6}$ M. The decay of emission was first recorded in the absence of the quencher, which gave us a lifetime of 1-methylpyrene equal to $\sim 110\text{ns}$. For the determination of N we added quencher aliquots such that the average number of quencher molecules per micelle varied from 0.2 to 2. The fluorescence decay curves were recorded using a FL3-22 SPEX spectrofluorometer (Figure III-22). The excitation wavelength was 310 nm, and the emission was monitored at 370 nm. All measurements were performed at room temperature.

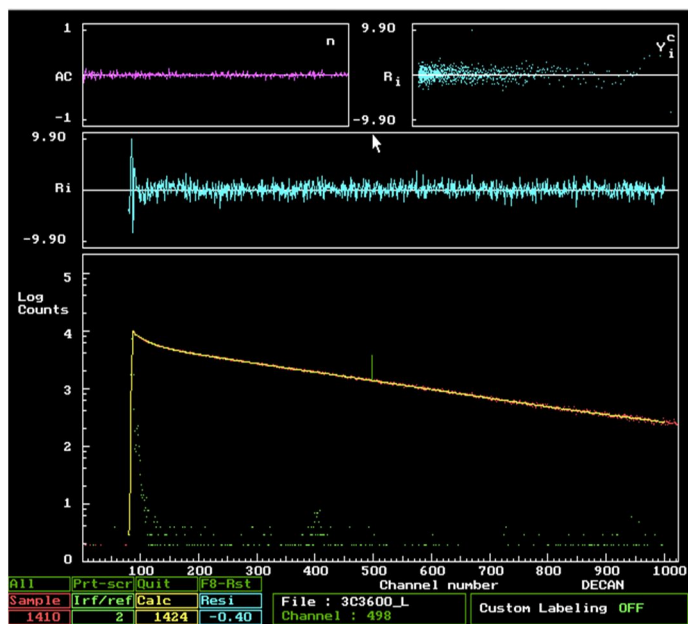


Figure III-22. Time-resolved fluorescence emission of 1-methylpyrene in presence of 10-2-10 C3 (60 mM 3xCMC) and cetylpyridinium chloride (0.6 mM)

Data analysis. Data processing was done by fitting the fluorescence decay curves to Equation (III-29) using a non-linear least-squares fitting program provided with the instrument or with the program developed by Boens *et al.*[123].

**Chapter IV. Interfacial properties of micellar aggregates
via the chemical trapping experimental method**

Work described in this chapter was performed by our collaborators from Rutgers University, New Jersey, USA. The experiments were carried out by PhD students Changyao Liu and Xiang Gao under supervision of Prof. Larry Romsted.

Introduction

Many experimental techniques have been used to investigate the behavior of colloid solutions (conductivity, NMR, UV/visible, fluorescence spectroscopies, light scattering). However most of them give information about the bulk properties or monitor just one component at a time. Quantitative analysis of micellar composition, especially their interfacial composition is extremely difficult. The Chemical Trapping (CT) method, established by L. Romsted, is a novel method to estimate the interface composition of amphiphile assemblies. CT is based on the heterolytic dediazonation of an arenediazonium probe located within the interfacial region of surfactant aggregates. Because of its amphiphilic structure (a charged headgroup with a long hydrophobic chain), the product distributions provide information on the molecular population within the interface. Dediazonation proceeds by spontaneous loss of N_2 and the rate constant for the reaction is extremely insensitive to the nature of nucleophile and solvent polarity. These properties make it an excellent probe of the interfacial region of micelles because the reaction is insensitive to the interfacial composition. The method reports on changes in interfacial molarities of the nucleophiles (*e.g.*, counterions, water, alcohols, etc.) that can be related to changes in aggregate structure and/or morphological transition[130, 131].

In our work we used chemical trapping to estimate interfacial concentrations of different counterions for cationic gemini surfactant 10-2-10 X with different counterions ($X = I^-$, Br^- , Cl^- , $MeSO_3^-$, C2, C3, C4) and compare the influence of the counterion type on the aggregates' composition, morphology and interfacial properties to shed light on the balance of forces that control amphiphile self-assembly. Chemical trapping was previously successfully applied to dimeric surfactants[132, 133].

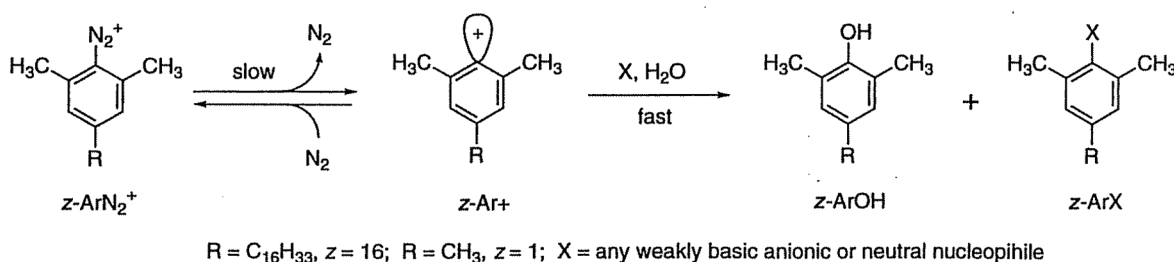
This chapter begins with a brief overview of selected arenediazonium chemistry. The principle of the method is described in part 1 and part 2, and will be dedicated to the results and discussions.

1. Chemical trapping. Principle and main assumptions

1.1. Arenediazonium ion chemistry

Depending upon arenediazonium ion structure, reactant and solvent properties, the reaction can yield various products (Scheme 3, Chapter 10 in ref.[134]) that characterized its rich and complex chemistry. The nature of the products is strongly influenced by a seemingly minor change in substituent on the arene ring, the nucleophilicity of solvent, the nucleophile type or the reducing capability of the reactant[135-137]. Here, we will focus on the heterolytic dediazonation reaction, which is accompanied by the loss of molecular nitrogen and formation of highly reactive intermediate. There are two types of such reactions: *heterolytic* release of N_2 in the presence of weakly base nucleophiles with the generation of aryl cation as intermediate and the *homolytic* loss of molecular nitrogen that requires an electron transfer from a reductive agent. The other type of reaction that we should mention in this chapter is the *diazonium coupling* that is general base (GB^-) catalyzed reaction. Products of this mechanism are competing with CT reaction, however in certain cases it is difficult to avoid them. This will be discussed in more detail below.

CT is based on heterolytic dediazonation of an arenediazonium ion in the presence of nucleophiles. As a probe, 4-alkyl-2,6-dimethylbenzenediazonium ion ($z\text{-ArN}_2^+$) (molecular structure is in Glossary) was chosen[134], based on the reaction described below (Scheme IV-1). The rich chemistry of $z\text{-ArN}_2^+$ puts some limitation on the experimental conditions that can be used. For example, sometimes reducing the concentrations of reactive components and lowering the pH helps avoiding the side products.



Scheme IV-1. Heterolytic dediazonation by release of N_2 in the presence of weakly basic nucleophiles for 4-alkyl-2,6-dimethylbenzenediazonium ions[134].

Compared to other spontaneous reactions, dediazonation of arenediazonium ion has several advantages that make it suitable for CT. The rate constant for heterolytic dediazonation is almost totally insensitive to the solvent polarity[138, 139] and hence changes in the reaction medium have

little effect on the measured rate constant. The loss of N₂ generates a highly reactive intermediate. Therefore, for an arenediazonium ion whose reactive group is located within the micellar interface, the final product yields primarily depend on the interfacial nucleophile concentration and only modestly on the selectivity of the reaction towards the different nucleophiles[134]. Finally, many of the reaction products are stable and can be analyzed quantitatively by HPLC.

Indeed, as shown in Scheme IV-1, the rate-determining step is the loss of N₂ with formation of a highly reactive aryl cation that reacts almost immediately with the nucleophiles in its vicinity. This stepwise mechanism[140] combined with a low selectivity toward weakly basic nucleophiles, makes arenediazonium a good probe for examining the interface composition of amphiphile assemblies.

1.2. Arenediazonium ion as a probe of the interfacial region of the micelles

The CT method uses an arenediazonium ion as a probe that is assumed to be located in the interfacial region of the surfactant aggregates where it reacts with nucleophiles to give products that provide information about their concentrations within the interfacial region. Due to its amphiphilic nature and because ions and molecules are moving at near diffusion controlled rates, low concentrations of 16-ArN₂⁺ easily integrate into the micelles without significantly affecting the structures and with the reactive diazonium group positioned within the interface of the surfactant aggregate (Figure IV-1). We will present evidence supporting this assumption from molecular dynamic simulations described in Chapter V.

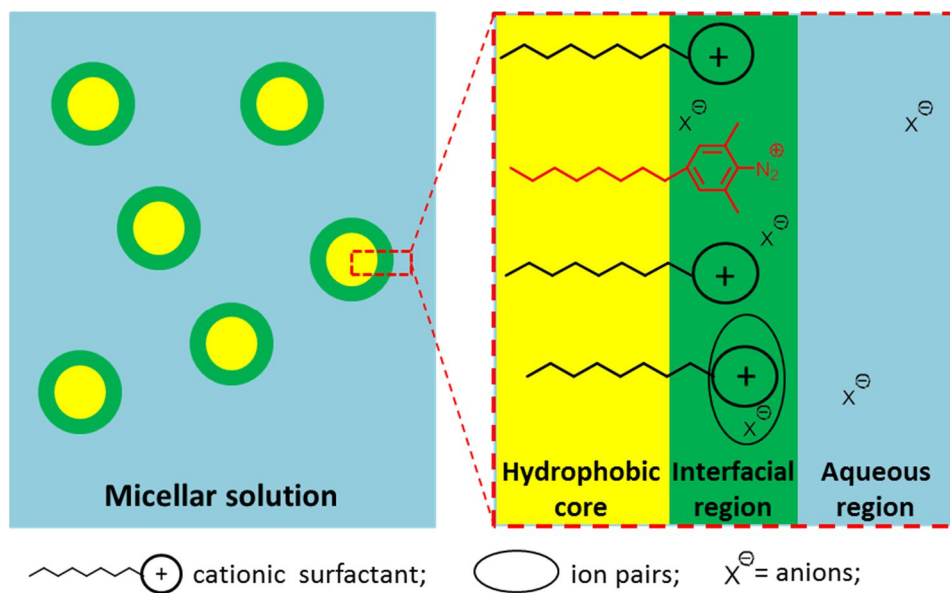


Figure IV-1. Representation of cationic micellar solution where arene-diazonium ion traps H_2O (not shown) and counterions in the interfacial region of the aggregates (adapted from image by C. Liu and ref[141]).

The surfactant solution is assumed to be in dynamic equilibrium, the distribution of its components is described by pseudophase model in which the association colloidal solution is treated as two pseudophases: aqueous phase and the totality of aggregated surfactant as the second phase[142, 143]. As it was discussed by Larry Romsted in the ref.[134], transfer rates for the elements of the system, including probe, between pseudophases are much higher than dediazonation reaction rate. We can therefore assume that the reaction yield after dediazonation of the probe comes from sampling the entire interfacial region of the aggregated surfactant (16-ArN_2^+) or aqueous region in case of short-chain analog (1-ArN_2^+).

Thus, 16-ArN_2^+ is well-suited for quantifying the molecular populations at interfacial region of colloidal systems[131-133, 141, 144].

1.3. Main assumption of the chemical trapping

The CT method assumes that *the selectivity of the dediazonation reaction, S_W^X , is the same in surfactant aggregates' interface and in aqueous solution*[132, 139, 141, 145] (Equation (IV-1)). This assumption is supported by the particularly small selectivity for the type of nucleophile and insensitivity to the solvent polarity,

$$S_W^X = \frac{(\%1\text{-ArX})[\text{H}_2\text{O}]}{(\%1\text{-ArOH})[\text{X}]} = \frac{(\%16\text{-ArX})\text{H}_2\text{O}_m}{(\%16\text{-ArOH})X_m} \quad (\text{IV-1})$$

where square brackets refer to total (stoichiometric) concentration in solution in moles per liter; the subscript m to interfacial molarity of interfacial volume in moles per liter; % indicates percent yield of a product determined by HPLC; and parentheses refer to product yields.

In micellar solutions the resulting product yields are proportional to the concentrations of ions or water within the interfacial layer and not to their stoichiometric concentrations in solution[141]. To estimate the concentration at the interface, the model arenediazonium reaction in water is used as shown in Figure IV-2, where on the left, the reaction at the interfacial region of aggregates is presented, and on the right the reaction in aqueous solution for short chain analogs is shown. When the product yields for the short chain dediazonation reaction, 1-ArX and 1-ArOH, in the reference aqueous solution (Figure IV-2 right) are the same as product yields for the long chain dediazonation products, 16-ArX and 16-ArOH, in the interfacial region (Figure IV-2 left), *i.e.*, when the selectivity of the arenediazonium ion is the same in both cases, the concentration of the reactive components in the water and interface are the same. *When the yield is the same, the concentration is the same.*

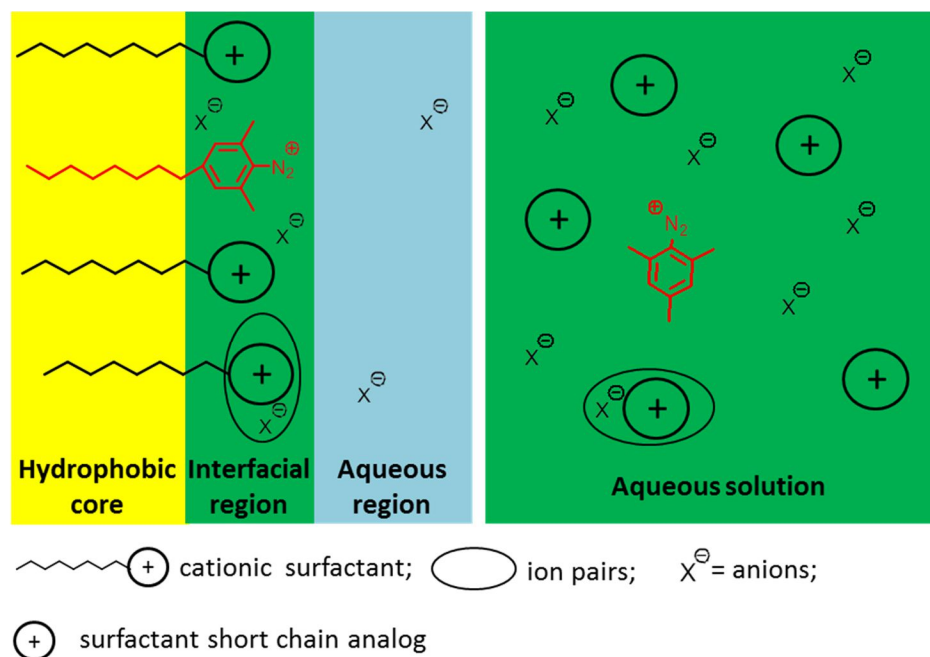


Figure IV-2. Left picture represents dediazonation reaction of the probe 16-ArN_2^+ within the interface of an amphiphile aggregates with subsequent formation of products 16-ArX and 16-ArOH (H_2O molecules not shown). Right picture represents the same dediazonation reaction of the short chain analog of the probe - 1-ArN_2^+ in aqueous solution with formation of 1-ArX and 1-ArOH (H_2O molecules not shown), (adapted from image by C. Liu and ref[141]).

Put differently, the product yields from the reference reaction of the short chain analog (1-ArN_2^+) are proportional to the stoichiometric concentration of reactants (water and nucleophiles) in the same way as product yields for probe (16-ArN_2^+) reaction are proportional to the

concentrations within the interfacial layer.

Using this assumption, we can easily estimate and quantify the interface concentrations by referring to the dediazonation yields in the aqueous solution, where concentration of surfactant and nucleophiles are known.

2. Results and discussions

In this part, we present the results obtained from chemical trapping for 10-2-10 gemini with some of Hofmeister anions, such as Br^- , Cl^- , I^- , MeSO_3^- , C2 and carboxylate counterions: propionate (C3) and butyrate (C4). Observed interfacial concentrations of counterions as well as water molarity allow us to estimate the interfacial components of the micellar aggregates and correlate them to the nature of the counterions and to the surfactant self-assembling process. We will also summarize briefly the limitations and problems we faced with applying this technique to different anions.

2.1. Inorganic counterions

The CT experiments were done for 10-2-10 X gemini with counterions such as: $\text{X} = \text{I}^-$, Br^- , Cl^- , C2 and MeSO_3^- , in the concentration range from around $2x\text{CMC}$ to 250 mM, except 10-2-10 I due to its low solubility (25 mM). The concentration range was chosen to follow the relationship between the interfacial counterion and water concentrations as well as the change in aggregate morphology[131, 141].

In the Table V-1 we report the results obtained by HPLC measurements for dediazotiation reaction of 16-ArN_2^+ in 10-2-10 Br micellar solutions (was chosen as an example) at 25 °C in the concentration range from 10 to 250 mM (1 mM HBr was added in each sample to lower the pH to about 3). Calibration curves for each observed compound were used to transform the peak areas to product concentrations and then to the observed yields, that were normalized to 100% by counting 16-ArH in a total yield[132]. Results for all others counterions were produced but not shown here.

Table IV-1. HPLC average peak areas, observed and normalized yields for reaction of 16-ArN₂⁺ in 10-2-10 Br micelles from 10 mM to 250 mM at 25 °C. [HBr] = 1 mM^d

[10-2-10 Br] mM	Average Peak Areas (10 ⁶ μV•s) ^a			Observed Yields (%)				Normalized Yields (%) ^c	
	16-ArOH	16-ArH	16-ArBr	16-ArOH	16-ArH	16-ArBr	Total ^b	16-ArOH _N	16-ArBr _N
10	7.832	0.1482	4.269	69.1	1.2	26.8	98.3	72.4	27.6
20	8.143	0.1083	4.553	71.8	0.8	28.6	102	71.7	28.3
30	7.807	0.1035	4.549	68.9	0.8	28.6	99.0	70.9	29.1
50	8.484	0.1132	5.230	74.8	0.9	32.9	109	69.7	30.3
100	6.936	0.4618	4.674	56.7	3.7	27.2	91.3	68.9	31.1
150	3.224	0.3003	2.228	53.0	4.7	25.9	88.3	69.0	31.0
250	3.137	0.4578	2.348	51.6	7.3	27.3	93.5	68.3	31.7

a. 100 μL sample injections. Peak areas are average of triplicate injections. Eluting solvents: 65%MeOH/35%*i*-PrOH; Flow rate: 0.4 ml/min; Detector wavelength: 220 nm. **b.** % Total = %16-ArOH + %16-ArBr + 2 %16-ArH **c.** % 16-ArBr_N = 100 (%16-ArBr)/(%16-ArOH + %16-ArH + %16-ArBr); % 16-ArOH_N = 100 (%16-ArOH + %16-ArH)/(%16-ArOH + %16-ArH + %16-ArBr). **d.** Reaction time ca. 48 h to ensure the complete dediazonium reaction. The concentrations of 16-ArN₂BF₄ were around 10⁻⁴ M but vary in each experiments.

Total yields of the desired products vary between 83 and 100%. Variation of this yield is caused by side products produced because of the rich chemistry of arenediazonium ion. One of them, for example, is reaction between z-ArN₂⁺ and CH₃CN, solvent in which stock solution was prepared[134, 146]. Meanwhile, the formation of the side products generally does not affect the relative yields of 16-ArX and 16-ArOH significantly[145].

Normalized product yields for 1-ArX (left) and 1-ArOH (right) from the reference dediazonium reaction in aqueous solution are on the Figure IV-3. We can see that values of 1-ArX(%) as a function of the counterion concentration ($[X_t] = 2[1-2-1 X]$) are the highest for Γ⁻, the most hydrophobic counterion, and lowest for the most hydrophilic acetate. The opposite trend is observed for 1-ArOH(%), that is, the more hydrophobic counterion, the lower the product yield of 1-ArOH(%). Using this data, selectivities of arenediazonium ion towards counterions compared to H₂O, S_W^X , were estimated (Equation (IV-1)).

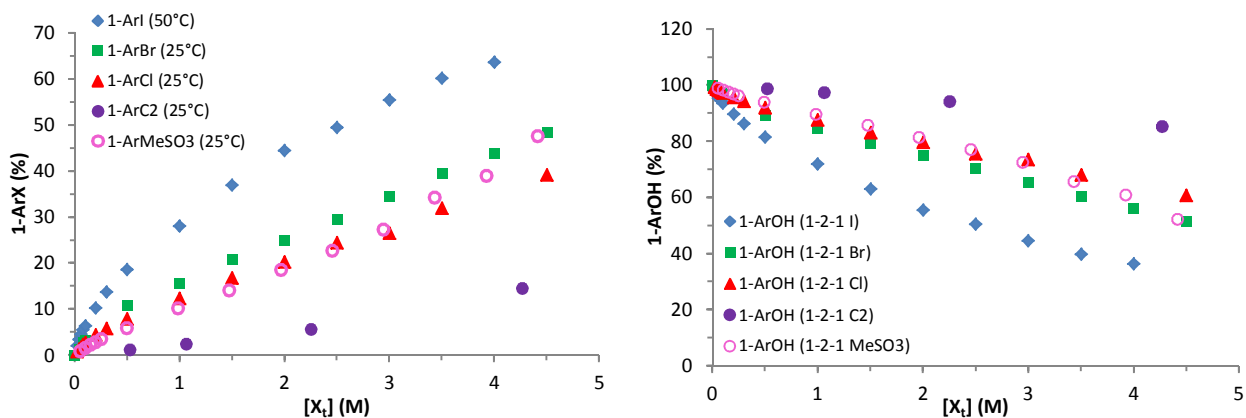


Figure IV-3. Normalized product yields (%) for 1-ArX and 1-ArOH as a function from counterion concentration $[X_t] = 2[1-2-1 X]$.

The same tendency as for normalized product yields was observed for S_W^X : dediazonation reaction is more selective towards hydrophobic counterions (I^- , $\Delta G_{hyd} = -283 \text{ kJ}\cdot\text{mol}^{-1}$) and least selective towards the anions with high hydrophilicity (C2, $\Delta G_{hyd} = -373 \text{ kJ}\cdot\text{mol}^{-1}$)[30]. It is noteworthy that the arenediazonium ions are much more selective towards ions than water at low counterion concentrations, however with increasing $[X_t]$ the selectivity decreases (Figure IV-4).

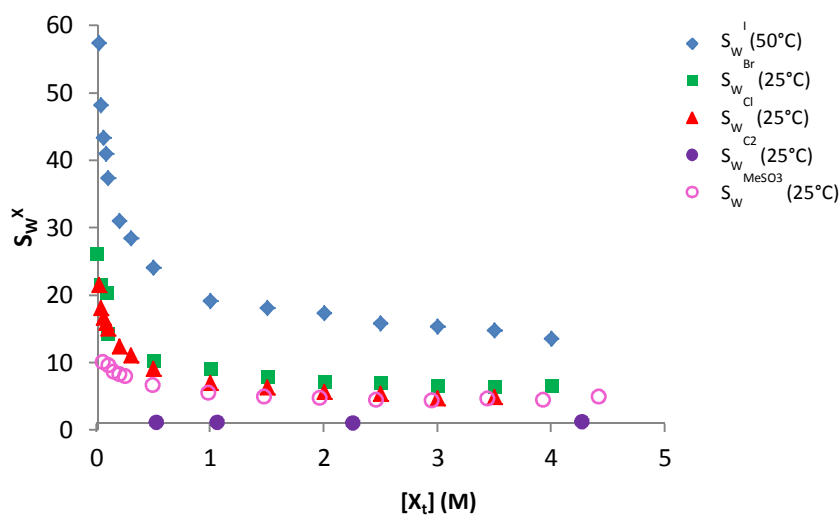


Figure IV-4. Selectivities, S_W^X , from the reaction of 1-ArN_2^+ with X^- in 1-2-1 X aqueous solution. $[X_t] = 2[1-2-1 X]$

As mentioned in subchapter 1.3, CT uses the assumption that the selectivity of 1-ArN_2^+ in the aqueous solution and selectivity of 16-ArN_2^+ in the micellar solution are the same: if concentration is the same, the product yield is the same. Using the yields of the reaction with the short chain analog as a function of $[X_t]$ in which the stoichiometric solution concentrations were known, we can transfer normalized product yield of 16-ArX to the interfacial concentrations (X_m ,

mol/L) using graphs on Figure IV-3. At the same time estimation of H_2O_m within the interfacial layer of micelles can be done using the second part of Equation (IV-1):

$$H_2O_m = [(\%16-ArOH) \cdot S_w^X \cdot X_m] / [100 - (\%16-ArOH)].$$

On the Figure IV-5 we represent estimated interfacial molarities of counterions, X_m , (left) and interfacial water molarities, H_2O_m , (right) for the micellar solution of 10-2-10 gemini with I^- , Br^- , Cl^- , C2 and $MeSO_3^-$ as a function of stoichiometric surfactant concentration in solution. Note that even though stoichiometric surfactant concentration is in mmol/L, the interfacial molarities of counterions are 100 to 1000 fold higher.

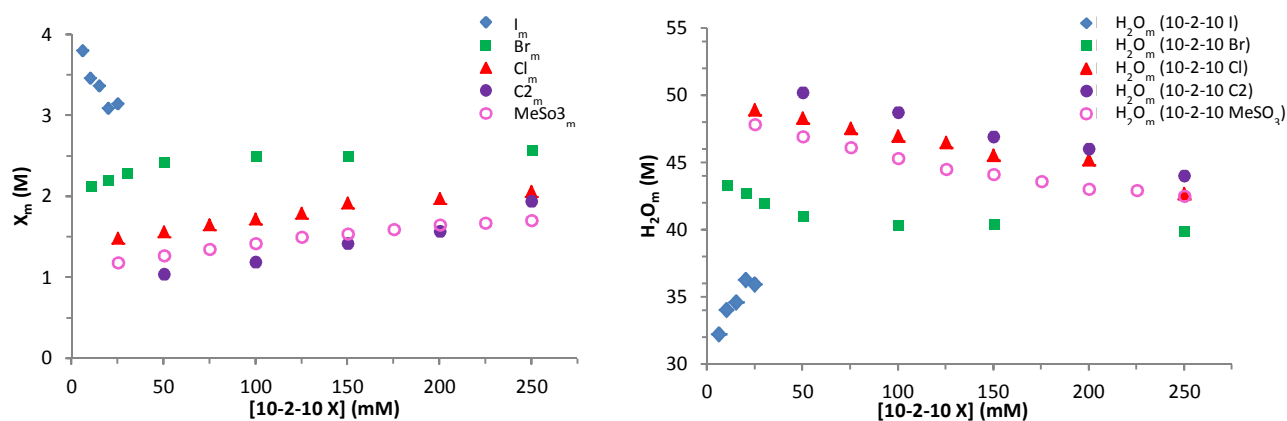


Figure IV-5. Interfacial counterion (X_m) and water (H_2O_m) molarities in 10-2-10 X micellar solution at 25 and 50 °C in case of 10-2-10 I.

The interfacial molarities are higher for hydrophobic I^- and Br^- , e.g., at $\sim 2 \times$ CMC they are 3.8 and 2.1 respectively. They decrease with respect to the anion hydrophobicity: 1.5, 1.2 and 1.0 for Cl^- , $MeSO_3^-$ and C2 respectively. Note that for 10-2-10 C2, the solution contains a significant amount of acetic acid that was added to hold the pH constant, however, C2_m still has one of the lowest interfacial molarities. The H_2O_m has an opposite trend: the more hydrophilic counterion is, the higher the interfacial water molarity is.

With increasing surfactant concentration, the interfacial concentrations of the X_m increases and H_2O_m decreases, more or less monotonously for hydrophilic counterions, but the slope for Br^- shows a break at about 50 mM. The reasons for the break in the values for Br_m and the downward slope for I_m are currently unknown and must await future research. These results correlate well with physical properties of the surfactants, such as solubility, CMC and ionization degree, which significantly depend on the ions and reflect their hydrophobic/hydrophilic properties. For example,

values of CMC for 10-2-10 gemini follows the trend $\Gamma^- < \text{Br}^- < \text{Cl}^- < \text{MeSO}_3^- < \text{C2}$ and their ionization degree (α_z) is respectively 0.12; 0.21; 0.43; 0.44 and 0.52. These results describe the interactions between counterions and headgroups, low ionization degree typical for the ionic micelles in the case when anion and cation are strongly bound and prone to ion pairs formation. High degree of ionization is a result of weak screening of the micelle. Counterions are highly hydrated and interact with polar headgroups weakly (*e.g.*, F^- , PH)[21, 147].

The results obtained by the different methods (conductivity and CT) correlate very well in that both show that the behavior of the amphiphile self-assembly depends on ion specificity and tends to follow the Hofmeister series.

2.2. Carboxylate counterions

To investigate the influence of counter anion hydrophobicity on the interfacial micellar composition, chemical trapping was carried out for 10-2-10 gemini with alkyl carboxylate counterions: C2, C3 and C4. The selectivity of arenediazonium ion towards carboxylate counterions comparing to water, S_w^X , was assumed to be the same as for acetate (paragraph 2.1.), because of the low selectivity of this ion and because of the presence of the same carboxylate reactive group.

Interfacial counterion (X_m) and water (H_2O_m) molarities for micellar solutions of 10-2-10 gemini with carboxylate counterions are shown in Figure IV-6 (left and right respectively). Although X_m and H_2O_m values for all three counterions are different, C2, being the smallest carboxylate anion has the lowest X_m (at 2xCMC 1.0 M) and higher for C3 and C4 (at 2xCMC 1.3 and 1.5 M respectively) respecting the hydrophobicity order. Interfacial water concentrations for C2, C3 and C4 show the opposite trends as the anions, but there is a smaller spread in the H_2O_m values, especially for C2 and C3 (Figure IV-6 right).

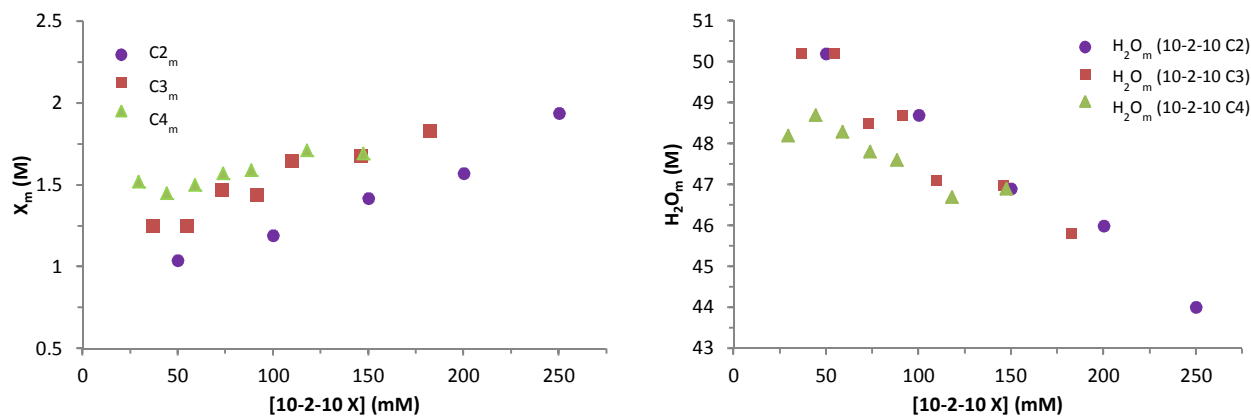


Figure IV-6. Interfacial counterion (X_m) and water (H_2O_m) molarities in 10-2-10 X micellar solution at 25 °C.

CT results fit the expected tendency, the interfacial concentration of the counterions in micellar solution increase for more hydrophobic ions and correlate with measured ionization degree (α_z) that is 0.52, 0.38 and 0.33 for C2, C3 and C4 respectively (Chapter III), demonstrating a correlation between the counterion hydrophobicity and association degree in gemini interfaces.

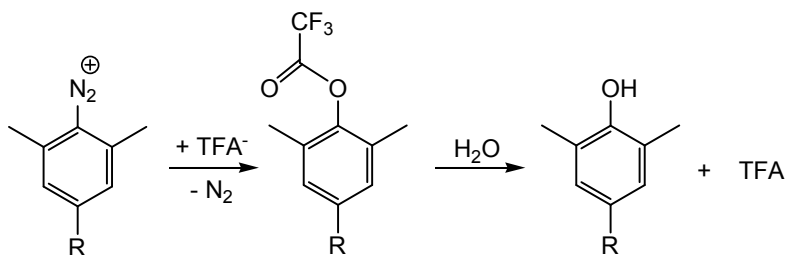
2.3. Complications

The chemical trapping method has certain previously described limitations[134]. Strongly basic nucleophiles cannot be used in chemical trapping due to their extremely rapid reaction with the terminal nitrogen resulting in undesired side products that make quantification of counterions very difficult. The mechanism of this type of reaction are well described by Hegarty[148]. Other competing reactions include formation of an indazole side product at high pH[149] and reduction of the arenediazonium ion by the phenol product. Finally, unfavorable physical properties, such as high solution viscosity may cause complete mixing problems.

Here, we will briefly overview some other problems and limitations that were observed during chemical trapping experiments for some of the anions, such as NO_3^- , TFA, PH ($H_2PO_4^-$) and carboxylates which made the determination of the interfacial concentration much more difficult.

1. Instability of the reaction product *e.g.*, by fast hydrolysis. Dediazoniation with NO_3^- in 10-2-10 NO_3 micelles by the HPLC revealed only a phenol product (*z*-ArOH). This indicates that the expected phenol nitrate ester (very good leaving group) hydrolyzes in the time frame of these experiments and requires a faster method for following the reaction.

2. **TFA** is also a good leaving group, however not as good as nitrate. The z-ArTFA product was observed, however it hydrolyzed rapidly during the HPLC analysis (Scheme IV-2) and estimation of the product yield was difficult.



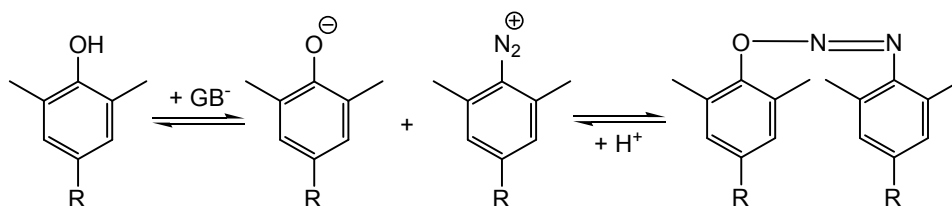
Scheme IV-2. Reaction product of heterolytic dediazonation of arenediazonium ion in presence of trifluoroacetate and its hydrolysis.

One possible solution to such problems is to run these reactions in isotopically labeled water. In this case phenol formed from the reaction between the probe and H_2O^{18} (z-ArO¹⁸H) can be distinguished from the phenol which is the secondary product from phenyl nitrate ester or from z-ArTFA after hydrolysis (z-ArO¹⁶H). Analyzing products using mass spectrometry, the product yield for both product (z-ArO¹⁸H and z-ArO¹⁶H) should be estimated.

3. Another counterion that requires adjustment of the conditions for HPLC product analyzes is H_2PO_4^- . It gives the stable phosphate ester as a product of dediazonium ion reaction. However, z-ArH₂PO₄ has two protons and the phosphate ester will dissociate into its monoanion form, which will require the development of new HPLC conditions to quantitate the ester and other products. The work still in progress to find the proper conditions for the separation of charged molecules.

4. A new big challenge appeared during the CT experiments on gemini micelles with **carboxylate** counterions. An unidentified peak with a long retention time and therefore hydrophobic nature was observed on the HPLC chromatograms of the long chain products formed in micelles, but not in the reaction with short chain analog. The probable site of the formation of the “mystery” peak is within the micellar interface because of the high concentrations of reactants. No dependence on the chain length of the carboxylate counterion was observed. Attempts to isolate the unknown compound and analyze it by NMR and HPLC failed due to its instability. The size of the “mystery” peak decreases with increasing pH indicating that the formation and breakdown of the product is acid catalyzed.

After long characterization process of this undefined compound by one of our collaborators, Xiang Gao, Larry Romsted and his students decided that the mystery peak is a diazoether formed in a reaction between the arenediazonium ion, the phenolic product that is general base catalyzed by carboxylate groups. The very reactive phenolate reacts with arenediazonium ions concentrated in the interfacial region of the micelles giving a uncharged very hydrophobic diazoether (two 16 carbon tails attached to two aromatic rings (44 total carbons), Scheme IV-3. Although stable in neutral solution, the ether decomposes in acid and is sensitive to temperature increases. The compound representing the “mystery” peak has not been isolated yet, its expected properties are consistent with the above observations.



Scheme IV-3. Formation of diazoether as a reaction between phenate and diazonium ion in presence of general base, in our case - carboxylates.

3. Conclusions

For the first time, the CT method was applied to micellar solution of 10-2-10 gemini amphiphiles with variety of counterions to study ion specific effects through quantification of interfacial counterion, X_m , and water, H_2O_m , molarities. The results show that X_m strongly depends on ion nature and follows the trend $I^- > Br^- > Cl^- > MeSO_3^- > C2$ for the small anions, and $C4 > C3 > C2$ for carboxylate counterions. Poorly hydrated and strongly associated counterions with the polar headgroup are located primarily in the interfacial region of the micelle and hence give high X_m monitored by arenediazonium ion. Contrary, interfacial concentration of highly hydrated ions is low and indicates low degree of counterion-headgroup binding. The CT results are consistent with investigated physical properties of the 10-2-10 surfactant in bulk solution such as the CMC and ionization degree, and all correlate with the Hofmeister series. We demonstrated quantitatively that hydrophobicity/hydrophilicity of the anion plays a crucial role in determining interfacial properties of micellar aggregates.

4. Experimental section

4.1. Materials

10-2-10 gemini with different counterions were synthesized as described in Chapter II. Values of CMCs were measured by conductivity (Chapter III). The arenediazonium salt 4-*n*-hexadecyl-2,6-dimethylbenzenediazonium tetrafluoroborate (16-ArN₂BF₄) and its short chain analog 2,4,6-trimethylbenzenediazonium tetrafluoroborate (1-ArN₂BF₄) were prepared by C. Liu as previously reported[139]. The products of dediazonation reaction that were used as HPLC standards in reference aqueous solution such as 1-ArOH, 1-ArBr, 1-ArCl, 1-ArI were purchased from Sigma-Aldrich, and others (1-ArC₂, 1-ArO₃SMe) were synthesized by C. Liu (publication is in preparation). For dediazonation products of the probe (HPLC reference for long chain compounds), such as 16-ArOH, 16-ArH, 16-ArBr and 16-ArCl, the synthesis procedure was established previously[139, 146]. Other long chain stable products were synthesized using a protocol created by C. Liu and X. Gao. The short chain analogs of gemini 1-2-1 X were prepared by C. Liu following the same procedure as the one was used for gemini 10-2-10 X (Chapter II). All solutions were prepared with distilled deionized water.

4.2. Dediazonation reaction

Dediazoniation reactions in reference aqueous solution and in gemini micellar solutions were carried out by adding stock acetonitrile solutions (ice cold) of 1-ArN₂BF₄ or 16-ArN₂BF₄ (final concentration was 10⁻⁴ M) to 1-2 mL volumetric flasks containing short chain analog 1-2-1 X or gemini surfactant 10-2-10 X respectively and thermostated at 25 °C. Note, the reaction with iodide counterion was performed at 50 °C due to its low solubility. Because the arenediazonium ion, due to its high reactivity, reacts with MeCN in the stock solutions, it must be prepared fresh and used fast. Since dediazonation is the 1st order reaction, after around 10 half-lives (48 h) the reaction can be assumed to be complete and the products can be separated and analyzed. In each reaction with 1-ArN₂⁺ cyclohexane (50 μL) was layered on top of each solution to minimize loss of 1-ArOH, and 1-ArX by evaporation. In order to minimize the formation of the reduced product 1-ArH[132], diazoether and indazole[134, 136], the pH was kept below 5 by adding corresponding acid, 1 mM in case of strong acids such as HCl, and a concentration close or equal to the surfactant concentration in solution in case of weak acids, such as acetic acid.

4.3. HPLC analysis

Product yields were determined on a Perkin-Elmer Series 200 equipped with a UV/Vis detector, a Varian Microsorb MV C₁₈ columns (length, 25 cm; particle size, 5 μm), and a computer-controlled Perkin-Elmer 600 Series Interface. Calibration curves for calculating product yield from peak areas for all the products are prepared from independently synthesized compounds at concentration range that correspond to the expected one from chemical trapping experiment. Products of the dediazonation reactions were separated and analyzed by the HPLC under conditions summarized in Table IV-2.

Table IV-2. Conditions for product separation on the HPLC for 10-2-10 gemini and its short chain analog 1-2-1 X.^a

Counter-ions	1-2-1 gemini				10-2-10 gemini			
	Eluent (v/v)	Detector wavelength (nm)	Flow rate (ml/min)	Injection volume (μl)	Eluent (v/v)	Detector wavelength (nm)	Flow rate (ml/min)	Injection volume (μl)
Cl, Br, I C2, C3, C4	80% MeOH / 20% H ₂ O	230	0.6	50	65% MeOH / 35% i-PrOH	220	0.4	100
MeSO ₃	55%CH ₃ C / 45%H ₂ O	230	0.4	50	80% MeOH / 20% i-PrOH	220	0.4	100

a. Each product yield was analyzed thrice by HPLC.

**Chapter V. Structural and interfacial properties of
micellar aggregates *via* computer simulations**

The computational work described in this chapter was performed by our collaborators from the Institut Européen de Chimie et Biologie, Pessac, France. Specifically, the molecular dynamics simulations were carried out by Dr. Massimiliano Porrini, formerly postdoc researcher in the team of Dr. Michel Laguerre.

Introduction

In previous chapters we described the investigated systems of cationic 10-2-10 gemini with inorganic and alkyl carboxylate counterions using different experimental techniques: conductivity, ^1H NMR, fluorescence quenching, chemical trapping. In this chapter, we present the results obtained by molecular dynamics (MD) simulations on the same systems, which give the opportunity to follow the mechanisms and dynamics of the molecular assembly systems at an atomistic level. MD simulation technique is a powerful tool to investigate the structure and dynamics of supra- and macro-molecules and nanoobjects[150-153]. In few words, during an MD run, the phase space of the system under investigation is sampled within the framework of classical mechanics. By integrating the equations of motions of Newton of each present atom, trajectories of the system evolving in time can be obtained. Assuming that the convergence has been reached and that the ergodic hypothesis is valid, physical properties of the system can then be evaluated which can explain, either complement or support experimental observations. The forces acting on the atoms are derived from a so-called force field, a collection of functional forms and parameters that is supposed to best represent the (electronic) potential energy surface, within which the nuclei move. Therefore, accuracy of the calculations strongly relies on how the chosen force field correctly describes the interaction forces. The other type of MD simulations that gives more accurate results due to the accounting the quantum effects of the electrons is *ab-initio* approach. However it can be applied just for small systems due to the time required for the calculations.

On the other hand, if the size of the system is relatively small and the effect of the electrons on the structure is sought, one among all the *ab-initio* methods can be implemented, in which the quantum effects of the electrons are taken into account.

Being a suitable tool for simulating the structures and dynamics of molecular assemblies, MD simulations have already been widely applied for the study of the Hofmeister effects[69, 76, 154, 155] as well as for the investigation of micellar solutions[156-158]. In particular, it has been

used to investigate the Hofmeister effects on the air/water interface[64], surfaces[154, 159] and biological macromolecules or their models[69, 76, 155].

Concerning simulations on surfactants systems, it is worth mentioning the work of C. Bruse *et al.*[157], where MD was used to characterize sodium dodecyl sulfate (SDS) micelle built from 60 units and solvated in water. They focused on shape, roughness of the micelle and interfacial sodium distribution. S. Storm *et al.* in their paper[158] studied the aggregation of SDS and cetyltrimethylammonium bromide (CTAB) in micellar structures, in particular, their size, shape and density profile were analyzed. Our group has already investigated gemini cationic surfactants with MD[156], specifically we studied the orientation of the amphiphile molecules in cylindrical micelles that was driven by the balance of electrostatic interaction between headgroups, as well as headgroups and counterions, van der Waals interaction and steric repulsion between hydrophobic tails.

In the present work we used MD simulations to characterize the interactions and concentration of headgroups, halides, polyatomic and carboxylate counterions and water within the interfacial region of ionic micelles (cationic gemini surfactant) and to study their aggregates morphology (sphericity, roughness and counterions' orientation). The main difficulty is to choose the parameters for the system which mimic best the interactions between surfactants, counterions and water molecules. The choice of parameters for monoatomic ions, *i.e.* the Lennard-Jones parameters describing the van der Waals forces, is even larger if one considers the wealth of different experimental and theoretical data available in literature[71, 160, 161]. In this work we implemented CHARMM force field (as it is considered to be the best all-atom force field for surfactant molecules). However, since it lacks a consistent set of parameters for all the halides, we opted to use those recently developed by Jorgensen and co-workers in the framework of OPLS force field[161] for the halides and acetate, whereas the parameters for all other counterions were used from CHARMM force field.

1. Results and discussions

In the present paragraph we will overview the results from the computational modeling focusing on the aggregate morphology and interfacial concentrations for 10-2-10 micelle with the following counterions: halides, PH, NO_3^- , TFA and a series of carboxylates. As it was described in Chapter III, the aggregation number of micelles at twice the CMC was relatively similar 30 ± 5 . For the MD simulations, we chose the same aggregation numbers for all the gemini systems (27 monomers), so that differences in the calculated properties will be only due to the ion properties and not to the morphological effects. We then compared nucleophiles interfacial concentrations computed from simulations with those measured with chemical trapping technique using the arenediazonium probe (Chapter IV).

1.1. Contribution of ion specific effects to the micelle structure

As it was discussed previously, ion specific effects have a significant influence on the micellar systems, and in this paragraph we sought to estimate how properties of an ion such as its hydrophobicity, size and morphology influence the size and shape of the modeled micelle and its ion distribution. Structural parameters such as radius of gyration (R_g), solvent accessible surface area (SASA) of the hydrophobic tails and eccentricity (ϵ) were calculated with different counterions in order to estimate the compactness, the roughness and the sphericity of the micelles respectively. The ion association between polar heads of the micelles and counterions was analysed with the evaluation of the radial distribution function (RDF) of each counterion with respect to the nitrogen atoms of the micellar headgroups.

- (i) The radius of gyration is the mass weighted scalar length of each atom from the center-of-mass (COM). The equation is as follows :

$$R_g = \sqrt{\frac{\sum r^2 m}{\sum m}} \quad (\text{V-1})$$

where r is the radius and m is the mass of the atom. R_g was analyzed using AmberTools13[162].

- (ii) Solvent accessible surface area is the surface area of a macromolecule that is accessible to a solvent molecule. It can be schematically presented as shown on Figure V-1. SASA was estimated using VMD software[163].

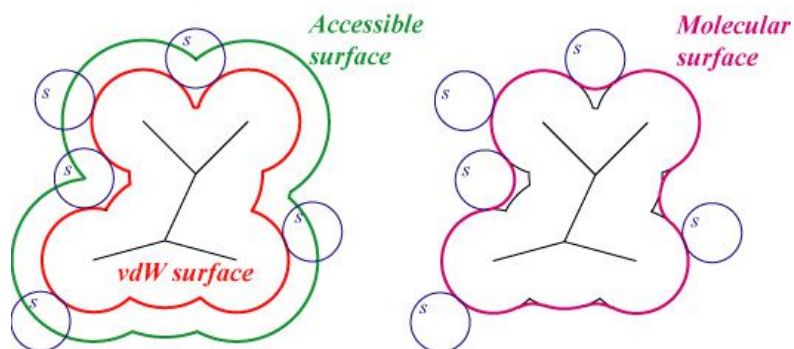


Figure V-1. Representation of SASA. Color code: in red is VdW surface of a molecule, in green is the accessible surface of the same molecule, in magenta is molecular surface[164].

(iii) Radial distribution function describes how density varies as a function of distance from a reference particle (r), see Figure V-2. RDF can be described by equation:

$$g(r) = 4\pi r^2 \rho dr \quad (\text{V-2})$$

where ρ is a number of particles per unit volume. RDF was analyzed using GROMACS analysis tools[165].

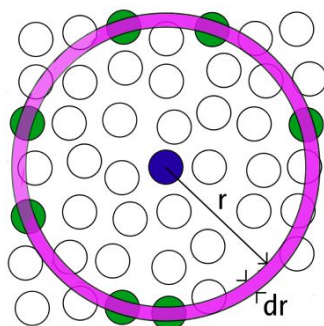


Figure V-2. Schematic representation for the evaluation of the radial distribution function[166].

(iv) Eccentricity is a measure of sphericity and can be defined as:

$$\varepsilon = 1 - \frac{I_{max}}{I_{ave}} \quad (\text{V-3})$$

where I_{min} is the moment of inertia along the x , y , or z axis with the smallest magnitude and I_{ave} is the average of all three moments of inertia. For the perfect sphere $\varepsilon = 0$ and for the ellipse $0 < \varepsilon < 1$.

1.1.1. Halides

Halides are monoatomic ions and their impact on the amphiphile self-assembly process can be explained by ion properties such as hydration free energy, size, acidity and polarizability. Note,

that the last one was not accounted in the MD simulations. It is well known that for the halide series hydrophobicity and atom size decrease from iodide to fluoride, $\Gamma^- > \text{Br}^- > \text{Cl}^- > \text{F}^-$; physical properties (like solubility, CMC and ionization degree) of bulk surfactant solutions reflect this nature very well, see Chapter III for more details on this matter.

Simulations clearly show that the various ions affect differently the micelle structure. In Figure V-3 A, B and C we report the distribution of the three structural parameters that were measured *via* MDs: R_g , SASA and ε for the 10-2-10 gemini micelle with Γ^- , Br^- , Cl^- and F^- as counterions.

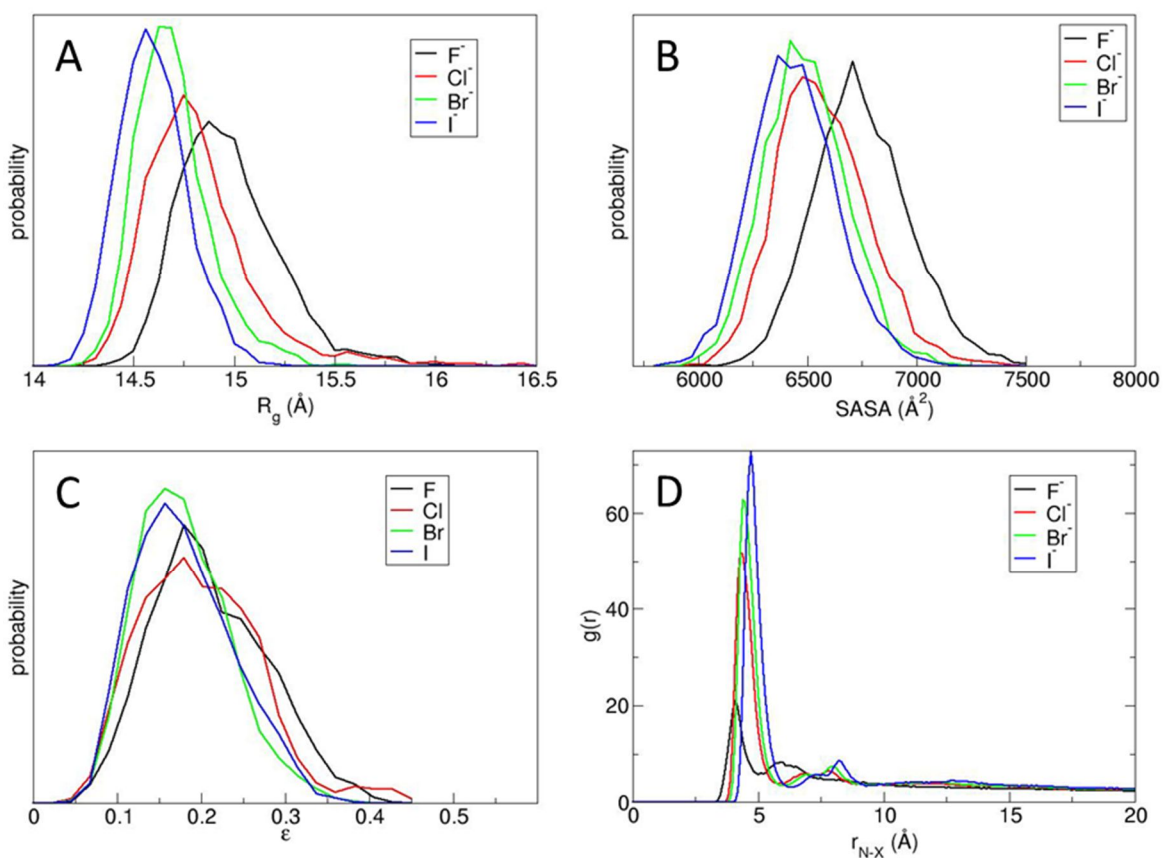


Figure V-3. Distributions of the (A) R_g , (B) hydrophobic tails SASA, (C) ε and (D) RDF of counterions with respect to nitrogen atoms of the micelle. Black, red, green and blue refer to the solution with fluoride, chloride, bromide and iodide ions respectively.

Figure V-3 A demonstrates that the lowest R_g , that indicates the compactness of the micelle (*i.e.* the lower the R_g , the more compact the micelle), corresponds to 10-2-10 I micellar system, and the average R_g increases for 10-2-10 micelle along with Br^- , Cl^- and F^- . 10-2-10 X micellar systems are referred to by their respective counterions (X) throughout this chapter. Figure V-3 B shows the

roughness of the micelle, measured in terms of SASA of the hydrophobic chains. This property follows the same trend, being that the micelle with Γ^- is the least rough. Analyzing the data, we can see that ion specific effects have a direct influence on the stability of the micelle, with iodide ion being the most stabilized and fluoride the least. These two structural properties correlate well with Hofmeister series: the strong interaction of Γ^- anions with the polar heads of the micelle, by substantially screening the electrostatic repulsion among positively charged groups (ionization degree equals 0.12), creates a tighter packing of the whole micelle, subsequently lowering the mean value of the R_g . This effect is also shown by the mean value of SASA of the hydrocarbon tails: a tighter packing of the micellar surface is responsible for better sheltering the hydrocarbon core of the micelle from the solvent molecules.

The mean values of eccentricity for all four counterions vary in from 0.15 to 0.19. ε shows that the micelles are virtually spherical, see Figure V-3 C. In fact, micelles with a mean value of $\varepsilon < 0.5$ can be considered spherical[158]. In this case the ion specific effects play a less evident role: the micelles with iodide or bromide counterions are slightly more spherical than those with fluoride and chloride counterions. Intriguingly, ε for F^- anion has second shoulder at approximately 0.25. It may indicate that there are two populations of aggregates for 10-2-10 F. It is in a good agreement with experimental results obtained by fluorescence quenching, where it was shown that F^- has the highest polydispersity among the halides.

The RDFs presented on Figure V-3 D describe counterion density with respect to the nitrogen atoms of the headgroups: interestingly, the highest value was found for Γ^- and the lowest for F^- . The first RDFs peaks for the counterions is around 4.5 Å and represents the so-called *contact* ion pair; from the height of the peaks we can see that the cationic heads of the 10-2-10 micelle are capable of attracting around three times more Γ^- or Br^- than F^- . The second peaks, corresponding to *solvent-shared* ion pairs, are located at around 7.5 Å for Cl^- , Br^- , Γ^- respectively and at 6 Å for F^- . Finally, the third peak at around 12 Å, which represents the *fully-solvated* ion pairs, is very weak.

1.1.1. Polyatomic counterions

Polyatomic ions have a complex morphology and cannot be described simply by one parameter, as was discussed in Chapter III. To analyze the micellar properties of the 10-2-10 gemini with polyatomic counterions (TFA, NO_3^- , C2 and PH) by MD, we investigated their R_g , SASA, ε and RDF, see Figure V-4 A, B, C and D respectively.

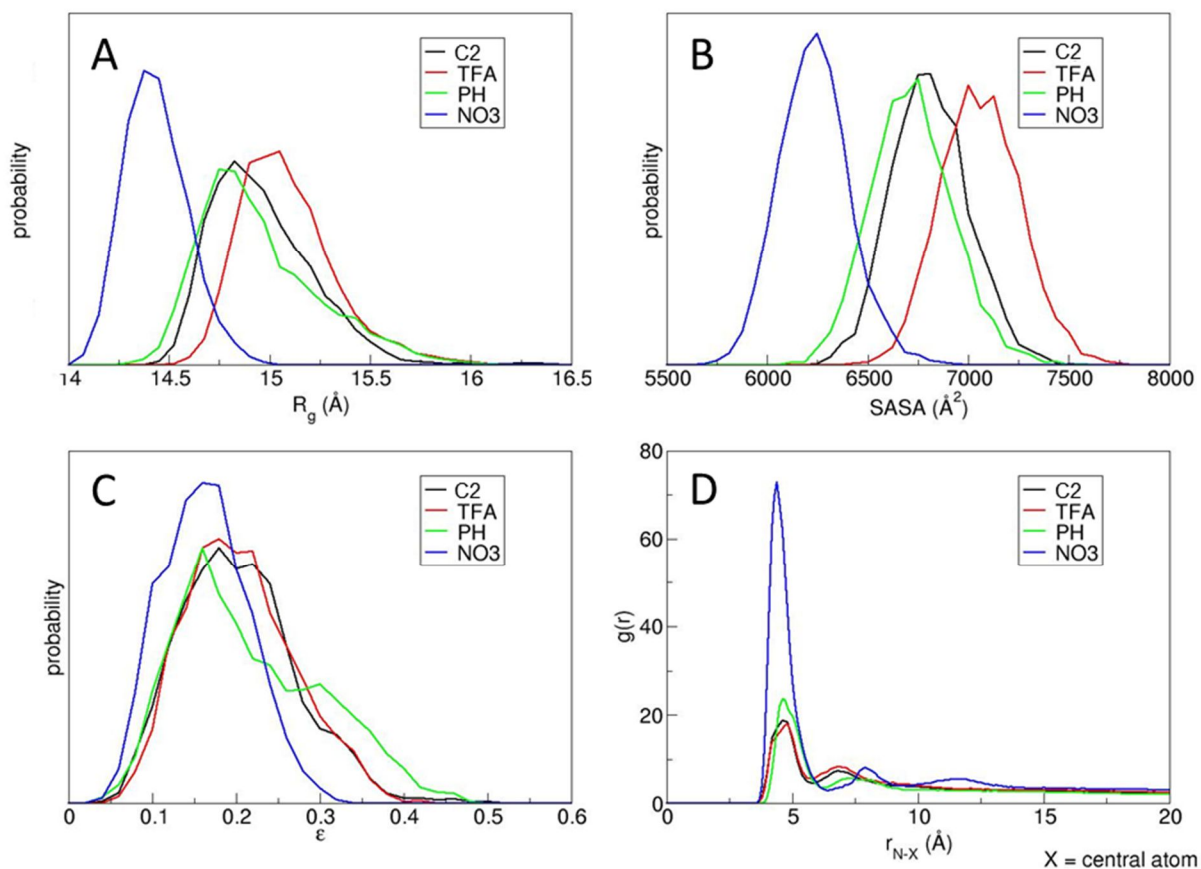


Figure V-4. Distributions of the (A) R_g , (B) hydrophobic tails SASA, (C) ϵ and (D) RDF of counterions with respect to nitrogen atoms of the micelle. Central atom for each anion chosen as X. Black, red, green and blue refer to the solution with acetate, trifluoroacetate, phosphate and nitrate ions respectively.

Figure V-4 A shows that NO_3^- leads to the lowest R_g by far (~ 14.4 Å). Compared to the micelles with 10-2-10 Br (~ 14.7 Å), which has the similar CMC (6.4 mM (Br^-) and 6.3 mM (NO_3^-)), the micelles of 10-2-10 NO_3^- are slightly more compact. Such behavior could be explained by the flat morphology of NO_3^- anion that allows it to embed itself between the headgroups and shrinks the micelle due to the electrostatic interactions. Hydrophilic PH and C2 have R_g values similar to that of F^- , where the micelles are characterized by a lower compactness. On the other hand, TFA, being the most hydrophobic counterion, with properties close to the Br^- and NO_3^- , exhibits the highest R_g (~ 15 Å). The same trend was observed for the roughness of the micelles characterized by SASA (see Figure V-4 B). The packing of the micellar surface is the tightest for the NO_3^- anion and lowest for the TFA. PH and C2 take the intermediate positions. The observed behavior for TFA does not correlate with our expectations in view of the experimental data. We

have shown that Br^- , NO_3^- and TFA share very close values for the properties of the surfactant solution, such as CMC, ionization degree and aggregation number (Chapter III).

Figure V-4 C represents the eccentricity for the micelles with different counterions. One can see that micelles with NO_3^- are more spherical (~ 0.15) than with PH, C2 and TFA (~ 0.2), and close in value to the monoatomic Γ^- and Br^- . Whereas, there is no significant difference between the hydrophilic PH, C2 and TFA. Similarly to ϵ for F^- , we found two populations of micellar shape for PH (first and second peaks are at 0.15 and 0.3 respectively). These results again reflect very well the polydispersity for 10-2-10 PH micelles, obtained experimentally by fluorescence quenching technique.

RDFs for polyatomic counterions were calculated as a distance from the nitrogen atom of the headgroup to the central atom of the anion (nitrogen for NO_3^- , phosphorus for PH, carboxyl carbon for C2 and TFA). Figure V-4 D shows that similarly to monoatomic counterions, RDF is characterized by three peaks that correspond to *contact*, *solvent-shared* and *fully-solvated* ion pairs. The first peak (*contact* ion pairs) appears at around 4.5 Å for all the counterions and corresponds to that of halides. The NO_3^- peak is almost 4 times higher when compared to PH, C2 and TFA and has $g(r)$ close to the ones of Γ^- and Br^- . It indicates that NO_3^- has much stronger interactions with positive headgroups than others. This fits well with the behavior observed experimentally (CMC, α). However, the TFA shows RDF $g(r)$ very close to that of C2, whereas from the experimental data, we would expect $g(r)$ close to NO_3^- . Such discrepancy between experimental observation and obtained calculations can be explained by the choice of parameters for the counterion. TFA parameters are missing in CHARMM36 force field and to derive them we used CGenFF program[167]. However, the penalty scores² were large (some of them were ~ 80) and unfortunately we did not reoptimize them due to the lack of time. This can be the reason why the properties of the simulated 10-2-10 TFA do not reflect the experimental observation. Second peaks attributed to the *solvent-shared* ion pairs is around 7 Å for C2 and TFA, 7.5 Å for PH and 8 Å for NO_3^- . The third peaks, indicating *fully-solvated* ion pairs, are very weak for all counterions except NO_3^- (12 Å) which shows very distinctive three peaks. For C2, TFA and PH, the distribution around the polar heads is less structured, and the third peaks are not observable.

² "penalty scores" give the information about the validity of the parameters. Penalties between 10 and 50 indicate that some basic validation is recommended; penalties higher than 50 usually are usually associated with parameters or charges that need additional optimization, see ref.168. Vanommeslaeghe, K., E.P. Raman, and A.D. MacKerell, *Automation of the CHARMM General Force Field (CGenFF) II: Assignment of Bonded Parameters and Partial Atomic Charges*. Journal of Chemical Information and Modeling, 2012. **52**(12): p. 3155-3168.

1.1.1. Carboxylate counterions

MD simulations were also performed for the 10-2-10 gemini with carboxylate counterions in order to investigate the effect of hydrophobicity on the micellar properties such as compactness, roughness, sphericity and counterions density described by R_g , SASA, ε and RDF respectively (Figure V-6).

Surfactants with carboxylate counterions are of interest because increasing the chain length of carboxylates, and thus increasing their hydrophobicity, induces a change in their behavior regardless of the micelle. Short chain carboxylates show “ordinary” counterion like properties, form “classical” micelles. Whereas, alkyl carboxylates with chain length ≥ 6 make more complex structures: catanionic (mixed) micelles. On Figure V-5, snapshots of the 10-2-10 micelles with the C1, C2, C3 and C6 counterions are represented. One can see that the small anions C1, C2 and C3 are located at the interface of the micelle. In sharp contrast, for the C6 molecule, all the counterions are integrated with their chains residing into the aliphatic micellar core.

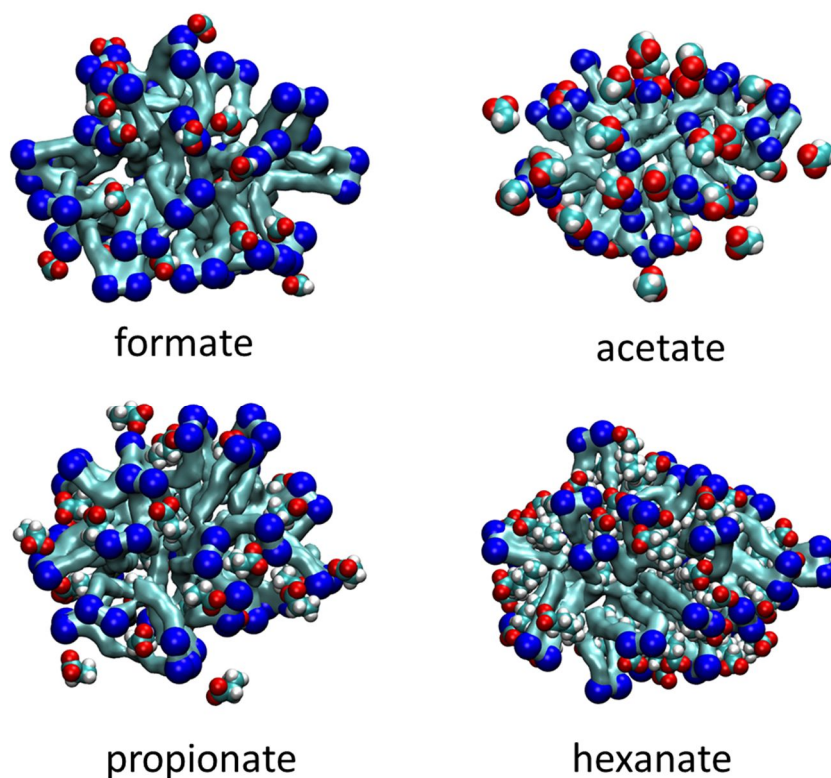


Figure V-5. Images from MD simulations of 10-2-10 micelle with formate (C1), acetate (C2), propionate (C3) and hexanoate (C6) as counterions.

Analyzing the structural properties of the micelles (Figure V-6), we can see that R_g , SASA and ε strongly depend on chain length and follow the following trend: $C1 \sim C2 < C3 < C4 < C5 < C6$. Compactness and roughness of the micelles decrease (R_g and SASA increase) with increasing hydrophobicity of the anion. This behavior is opposite to the one observed for inorganic halides and polyatomic counterions. However, this can be explained by the fact that carboxylates orient their aliphatic moieties towards the hydrophobic core of the micelle and that penetration into the micelle is a function of increasing chain length (Figure V-7). Therefore, the compactness of the micelle would decrease for the more penetrating counterions (Figure V-6 A). At the same time, roughness would increase due to the less tight packing of the surfactant molecules within the micellar aggregate (Figure V-6 B).

The effect of chain length is less obvious for the eccentricity of the micelle (Figure V-6 C). The mean value of ε is very close for C1, C2 and C3, around 0.2. This value slightly increases for the more hydrophobic C5 and C6 (~ 0.28).

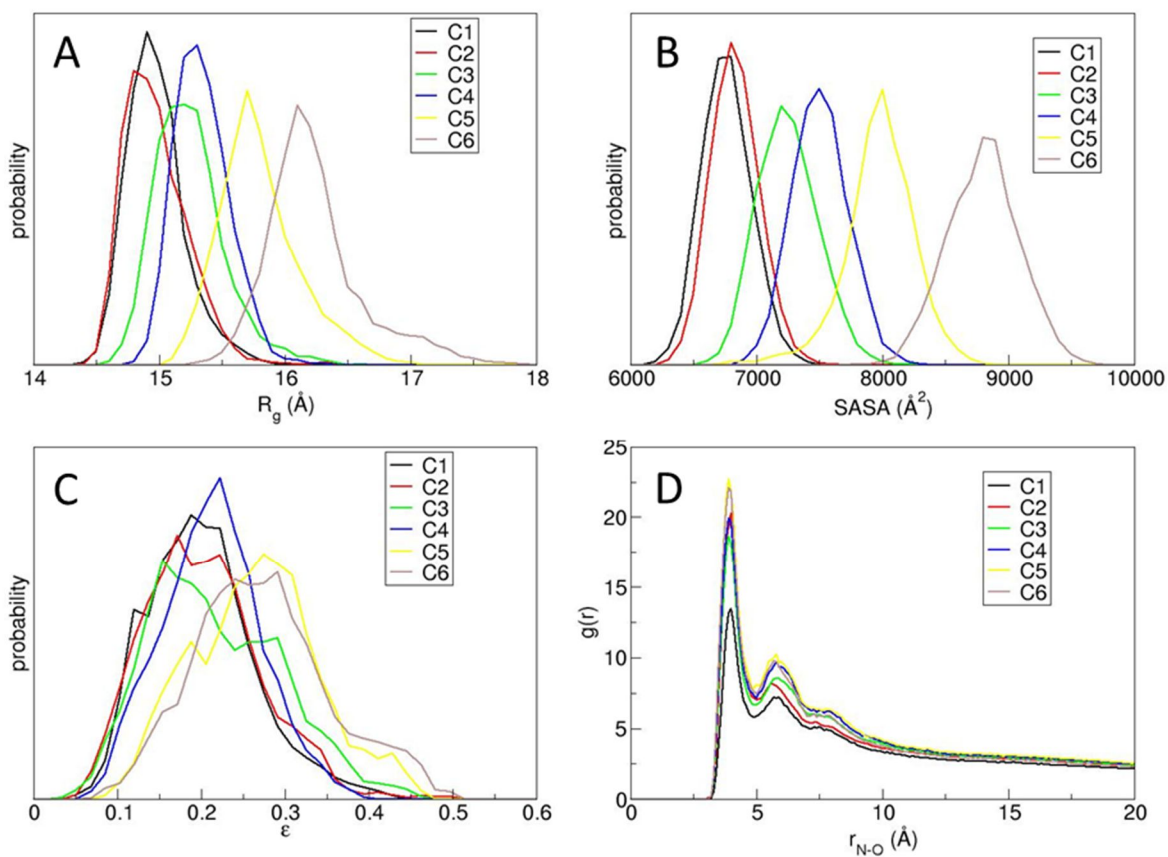


Figure V-6. Distributions of the (A) R_g , (B) hydrophobic tails SASA, (C) ϵ and (D) RDF of counterions (oxygen) with respect to nitrogen atoms of the micelle. Black, red, green, blue, yellow and brown refer to the solution with C1, C2, C3, C4, C5 and C6 ions respectively.

RDF of each counterion with respect to the nitrogen atoms of the micelle was estimated as the distance from the gemini nitrogen to the oxygen of the carboxylate group. Figure V-6 D shows that three peaks corresponding to the *contact*, *solvent-shared* and *fully-solvated* ion pairs have the same position for all carboxylate counterions. The increase in the peak height from C1 to C6 indicates that increasing the length of the hydrophobic chain of the counterions results in an increase of the association between the nitrogen atom of the headgroup and its counterion and thus, in an increase in the density of the ion pair.

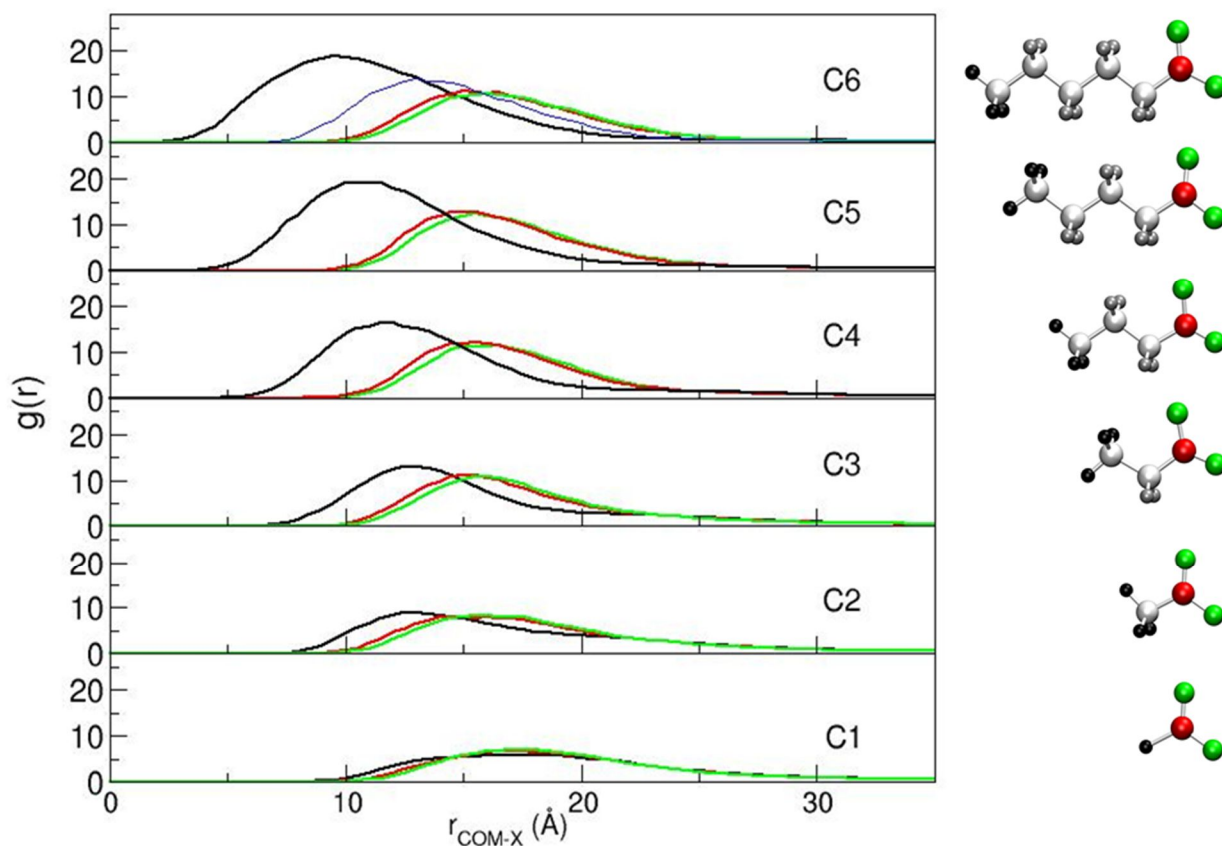


Figure V-7. Radial distribution function $g(r)$ as a function of the distance from the center of mass (COM) of the micelle for 10-2-10 gemini with carboxylate counterions. Color code: green, red, white, silver and black refer to carbonyl oxygen, carbonyl carbon, alkyl carbon, CH_2 hydrogen and terminal methyl hydrogen atoms respectively.

The Figure V-8 summarizes the parameters of the micelle for all types of counterions (halides, polyatomic and carboxylates) obtained by MD simulations as a function of CMCs. The radius of gyration R_g (Å) for the halides increases for the halides and polyatomic counterions going from more hydrophobic I^- , Br^- and NO_3^- , having lower CMCs, towards hydrophilic F^- and PH , having relatively high CMCs. In contrast, the micelles associated with carboxylate counterions have the opposite behavior. The R_g of more hydrophobic counterions such as C6, C5, which CMC values are close of those for I^- , Br^- and NO_3^- , is much higher than for hydrophilic C1 and C2. The similar tendency was obtained for SASA (B) and ϵ (C). The dependence of the roughness of the micelle on the type of counterion is less pronounced for halides and polyatomic ions, whereas for carboxylate counterions it increases significantly from C1 to C6 (B). Eccentricity of the micelle does not vary much with counterions, from 0.16 for the most spherical micelle with iodide to 0.26 for C6 counterion. Nevertheless, the tendency to form more spherical micelles for hydrophobic “ordinary” counterions and hydrophilic counterions is observed.

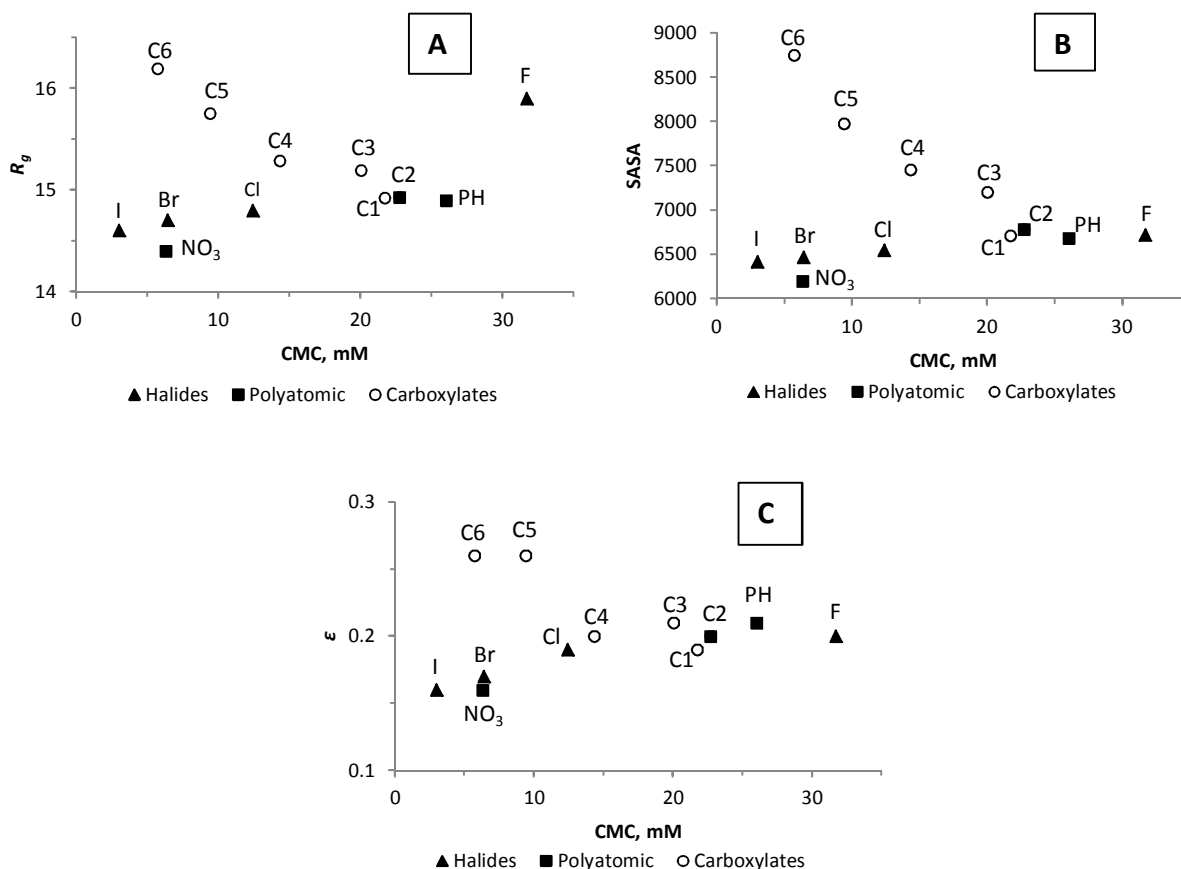


Figure V-8. Structural parameters of the micelle: R_g (A), SASA (B) and ϵ (C) as a function of CMC for 10-2-10 gemini with different counterions.

These results strongly suggest that hydrophobic alkyl carboxylates, penetrating the micelle, change its micellar structure, making it more swollen and rough, and less spherical. Whereas, halides and polyatomic counterions of similar hydrophobicity, favor the compression of the micelle, making it less rough and more spherical.

1.2. Interfacial concentrations

In order to give a better estimation of the interfacial counterions and water molarities of the micelles, we compared the results deriving from two completely different approaches: chemical trapping technique (described in Chapter IV) and MD simulations of 10-2-10 with three different counterions: Br^- , Cl^- , and C2. This is the first work in which experimental and computed interface ion concentrations are compared quantitatively. We will show that the two approaches agree remarkably well one with another.

The interfacial molarities obtained from chemical trapping experiments for the micellar solutions of 10-2-10 gemini in the following millimolar concentration ranges $50 < [10-2-10 \text{ C2}] < 250$, $25 < [10-2-10 \text{ Cl}] < 250$ and $10 < [10-2-10 \text{ Br}] < 250$ are presented in Chapter IV.

The concentrations distributions of counterions and water along the radial distance from the micelle centre of mass (COM) were analyzed. Starting from the COM of the micelle, we considered concentric spherical layers of 1.0 Å in width and then evaluated the cumulative number of counterions and water molecules therein. In the case of acetate, we considered in the calculation the two oxygen atoms, which represent the reactive (nucleophilic) moiety of the molecule.

Note that for the 10-2-10 gemini surfactant, micelles were formed with the aggregation number measured at $2x\text{CMC}$, where the stoichiometric concentration was much lower than those of the simulated systems (ca. 82 mM). At the concentration 82 mM, which means ~ 4 , ~ 6 and ~ 14 times the critical micelle concentration (CMC) of the surfactant in presence of C2, Cl⁻ and Br⁻ respectively, there might occur a sphere-to-rod transition[133, 145], however such a transformation cannot occur in the simulation box.

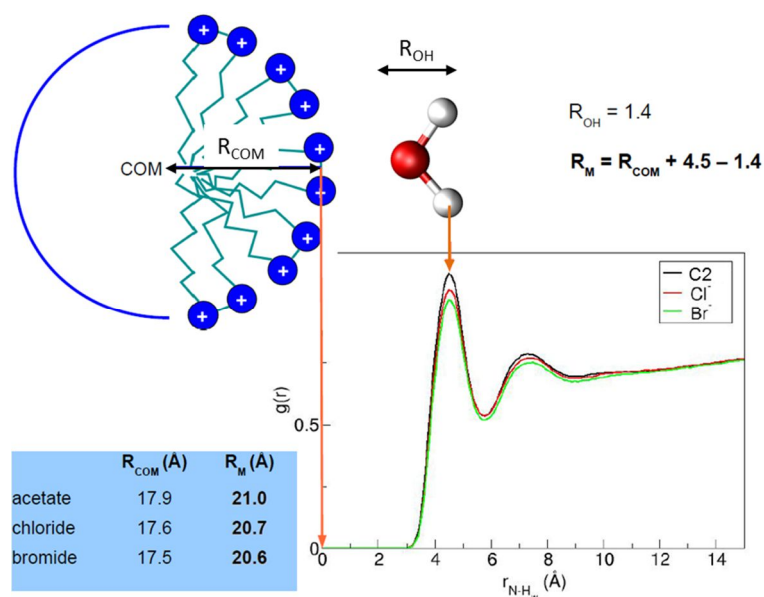


Figure V-9. Dimension of the micelle R_{M} was considered as being the distance from the center of mass of the micelle until the first hydration layer (methyl groups were included). The RDF of the water hydrogen atom with respect to the nitrogen of the headgroup shows the distance 4.5 Å. R_{M} is calculated by adding the distance of the nitrogen atoms from the centre of mass (R_{COM}) to this Nitrogen-Hydrogen distance and subtracting the radius of water (1.4 Å) which determined the dimension of the micelle[157].

The Figure V-10 presents the local concentrations of water $[\text{H}_2\text{O}]_{\text{L}}$ and counterions $[\text{X}]_{\text{L}}$ as a

function of the radial distance of the spherical layer (1 Å thick) from the COM. The vertical dotted lines mark off the dimension of the micelle, derived with the approach of Forbes and co-workers[157], in which we used the time averaged distances of nitrogen atoms from the micelle COM (for the 10-2-10 gemini micelles ca. 17.5, 17.6 and 17.9 Å with Br⁻, Cl⁻ and C2 anion respectively) and the first peak of the RDF of water hydrogen atoms with respect to nitrogen atoms, a detailed explanation of the calculation is described in the caption of Figure V-9. The vertical dash-dot lines (Figure V-10) correspond to the highest computed value of interfacial concentrations of counterion.

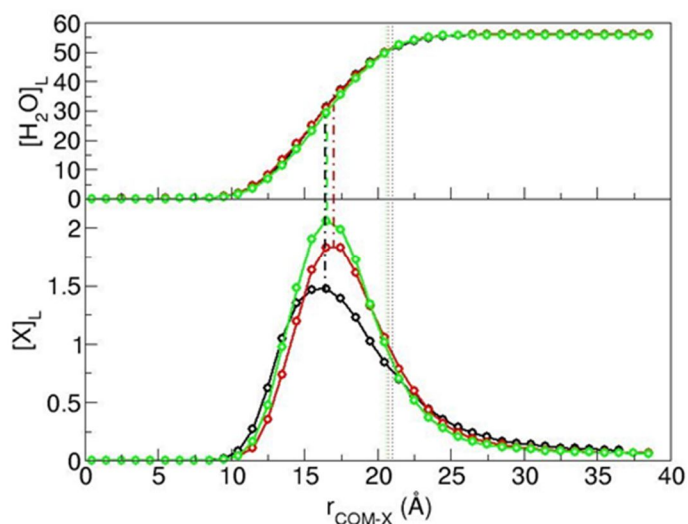


Figure V-10. The x axis defines the radial distance of the spherical layers from the micelle COM. The y axis of the top and bottom graphs shows the local concentrations (within each layer of 1 Å) molarities of water and counterions, respectively. Black, red and green lines refer to C2, Cl⁻ and Br⁻ respectively. Vertical dotted lines delimit the average radius of the micelle and vertical dash-dotted lines are placed at the location of the maximum of counterions concentrations.

In Table V-1 the comparison of interfacial concentrations (in M) between chemical trapping measurements and MD calculations is made. Only the molarity at the peak of distributions of the counterion are reported (see Figure V-10), the electrophilic moiety of the arenediazonium probe samples the region around peak of the counterion distribution in chemical trapping experiments (this assumption was validated from the MD runs in the presence of the probe, see below). The notable agreement between measured and computed interface molarities of counterions validate mutually the MD simulation approach (the choice of the force field, *i.e.* the use of the set of mixed parameters within CHARMM force field) and chemical trapping technique to characterize quantitatively the interfacial properties of cationic association colloids.

Table V-1. Experimental and calculated interfacial concentrations (in M) for ions and water. The calculated ion interfacial concentrations refer to the peaks of their distributions, whereas the calculated water concentrations are those resulting from the projection of the location of these peaks onto the respective water concentration gradients (see graph in Figure V-10 for clarity). The experimental values are those corresponding at the salt stoichiometric concentrations of 2xCMC.

	acetate	chloride	bromide
X_m (exp.)	1.2 (1.3)	1.5	2.2
X_m (calc.)	1.5	1.8	2.1
H_2O_m (exp.)	50	48	43
H_2O_m (calc.)	31	34	29

The calculated interface concentrations of water are overall lower than the experimental values. This might be an overestimation due to the assumptions used for the chemical trapping results analysis. The chemical trapping treats the interfacial region and bulk aqueous solution as the same when the product yields in both regions are the same (see Chapter IV). However, this is not necessarily true because the interfacial region has an adjacent hydrocarbon core that the bulk solution does not. Moreover, the headgroups in the interfacial region have a radial orientation that is not present in bulk solution. At the same time the underestimation can come from the MD simulations. For example, the interfacial water concentration was estimated at a distance from the COM that correlated with the maximum of the peaks for the counterions. However, we cannot be absolutely sure that chemical trapping reaction took place exactly at the same distance from COM.

According to the Hofmeister series, the counterion association with cationic micelle is the highest for the Br^- and lowest for the C2, this correlates well with the experimental measurement: CMC and ionization degree α (Chapter III). Deriving an absolute value for α from atomistic simulations, on the other hand, is not trivial. One has to define the boundary, beyond which the counterions are considered dissociated with the micelle. Indeed the distinction between “bound” and “free” ions is somewhat arbitrary[169] and the experimental measurements of this factor strongly depend on the technique used[170].

In Figure V-11 we show the curves for the fraction of the number of counterions (left axis) as a function of r_{COM-x} . Beyond the interfacial region as defined above 18 Å (Figure V-11), the tendency of counterions dissociation is consistent with the experimental values from conductivity measurements: bromide ions are the most associated and acetate ions are the most dissociated. At

the same time to make a more quantitative analysis from MD results, RDFs profiles of the counterions with respect to nitrogen atoms of surfactants polar heads, r_{n-x} were shifted along the x axis by (added to) a length equal to the average distances of nitrogen atoms from the micelles COM, (r_{COM}) and then superposed to the trends of the ion dissociation[84] $r_{n-x} + r_{COM} = r_{COM-x}$. The resulting graph is displayed in Figure V-11.

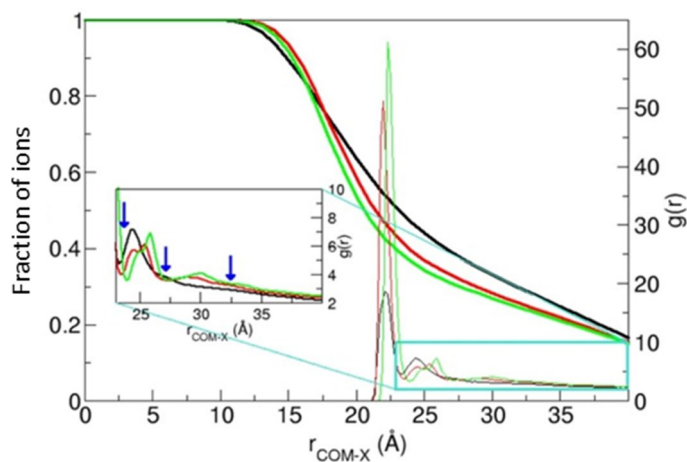


Figure V-11. The fraction of the number of counterions (*left y axis*) as a function of r_{COM-x} with the steps of 1.0 Å and N-X RDFs profiles (*right y axis*) for 10-2-10 micelles. Black, red and green lines refer to C2, Cl⁻ and Br⁻ respectively. The RDF profiles have been translated along the x axis by the average distance of the nitrogen atoms from the micelle COM (17.5, 17.6 and 17.9 Å for C2, Cl⁻ and Br⁻ respectively). The inset shows a magnification of the RDF profiles within the range $23 \text{ \AA} \leq r \leq 40 \text{ \AA}$.

The RDFs show that the counterion density around the surfactants' headgroups is the highest for Br⁻ and the lowest for C2. The first peak in the RDFs of the 10-2-10 gemini is ca. 21Å, which represent the *contact* ion pair distance. The second peak, the *water-shared* or *water-separated* ion pairs, is at ca. 25 Å. The third peak at ca. 30 Å, represents the *fully-hydrated* ion pair. This signal is very weak and only observed with gemini micelles with Cl⁻ and Br⁻ counterions. In order to estimate the ionization degree *via* MDs, we delivered the fraction of ions at the distance from the COM corresponding to the three troughs on the RDFs profiles, considering that counterions in these regions are not associated with thr micelles Table V-2.

Table V-2. Comparison of calculated and experimental (α_E) ionization degrees. The three sets of calculated values are obtained from the first, second and third (when applicable) peaks of the RDF of the counterion with respect to nitrogen atoms of the micelle polar heads. The values between brackets refer to the points just beyond the “last” peak. For clarity see Figure V-11 and their insets.

Counterions	$g(r_{N-X})$ 1 st min.	$g(r_{N-X})$ 2 nd min.	$g(r_{N-X})$ 3 rd min.	α_E
C2	0.51	(0.39)	-	0.29
Cl ⁻	0.41	0.33	(0.26)	0.21
Br ⁻	0.37	0.31	0.23	0.16

In all cases, the computed ionization degrees from MD are very close to the experimental values with all three peaks included.

The largest boundaries located just beyond the third peak of the RDFs, *i.e.* at ~ 32 Å (10-2-10) from the micelles COMs are quite broad. They can be regarded as the delimitation of the so called *double layer* (that is *Stern layer* plus *diffuse layer*) defined in the field of electrochemistry[171, 172]. Beyond the diffuse layer there is the bulk solution, where the counterions are completely dissociated from the micelle. The charge layer thickness of the micelles (that is the surface delimited by the average distance of the nitrogen atoms from the micelle COM ~ 17.7 Å) is ≥ 13 Å. These results are in good agreement with the theoretical value of the *Debye length*, $\kappa^{-1} = 3.04/I^{1/2}$, where I is the ionic strength of the solution in mol/L. For the gemini 10-2-10 micelles $I \approx 0.082$ M, which give a *Debye length* of about 11 Å.

It is worth noting that the *Debye length* in the Debye-Hückel theory quantifies the length range of the decay of the micelle electrostatic interactions. In conductivity measurements of this type of cationic gemini surfactants solutions, the ions residing within the diffuse layer can be considered associated with the micelle and the micelle itself is able to drag them to the electrode.

1.3. Position of arenediazonium probe (16-ArN₂⁺) used for chemical trapping study within the micelle

In order to evaluate the position of the arenediazonium probe within the micelle interface we simulated a micelle (27 gemini) in the presence of the 16-ArN₂⁺ probe. Originally in the chemical trapping experiments the probe concentration is kept 100 times lower than surfactant concentration, so that in the average only one probe molecule is incorporated per micelle. In Figure V-12 A we show the RDFs calculated from the micelle’s COM of headgroups nitrogen atoms, counterions (Cl⁻), nitrogen atoms bound to the benzyl ring and aromatic carbon from which molecular nitrogen

dissociates and to which the competing nucleophiles eventually bind. These results show that although the aliphatic 16-carbon tail of the probe is longer than the 10-carbon tail of the 10-2-10 surfactants, the arenediazonium ion can accommodate totally within the micelle, with its reactive moiety exactly at the interface: the position of the probe nitrogen atoms overlap both with the nitrogen atoms of the aggregate polar heads and the counterions (Figure V-12 (A)). These results also demonstrate well the “liquid” nature of both micelles and probe, as it is well visualized from a simulation snapshot shown in Figure V-12 (B).

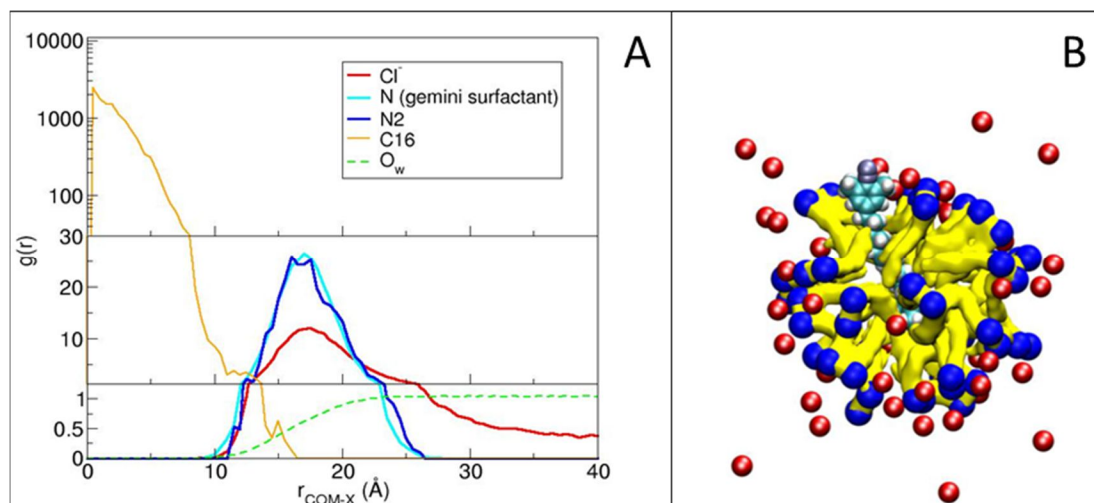


Figure V-12. (A) RDFs evaluated from the micelle COM. In blue, ice-blue, orange, red and green are RDFs for arenediazonium nitrogen (N_2), nitrogen correspondent to gemini (N gemini surfactant), carbon from the last methyl group of the probe’s tail (C16), chloride counterions (Cl^-) and water respectively. (B) Depiction of the 10-2-10 micelle (yellow surface for the aliphatic tails and blue beads for the polar heads), together with the probe 16-ArN₂⁺ (shown with VDW representation: white, cyan and ice-blue balls for hydrogen, carbon and nitrogen atoms respectively) and with Cl^- anions (red balls).

2. Conclusions

Ion specific effects were studied using MD simulations. We investigated aggregates organization of the micelles of 10-2-10 gemini with different counterions. We investigated the interfacial properties of the micellar assemblies as well as structure of the micellar aggregate as a function of the type of monoatomic or polyatomic counterions.

Analyzing the R_g , SASA, ε and RDF, we showed that, due to their strong association and ion pair formation with quaternary ammonium headgroups of the amphiphilic molecule, the more hydrophobic counterions (Γ^- , Br^- and NO_3^-) produce more compact and stable micelles, where tight packing of the micellar surface protect the hydrocarbon core of the micelle from the solvent molecules. Conversely, hydrated and hydrophilic ions (F^- , PH, C1, C2), interact in a weaker fashion with positively charged headgroups, have a lesser degree of contact ion pairing and compress the micelle to a lower extent, thus increasing roughness. The exception being TFA. This counterion is considered hydrophobic, with $-\Delta G_{hyd} = 251 \text{ kJ}\cdot\text{mol}^{-1}$, and in solution it affects the surfactant properties in the same way that Br^- or NO_3^- do. However, MD calculations showed that its properties were closer to that of C2. Such discrepancy can be explained by use of not optimized parameters for this counterion.

The ion specific effects of the mono- and polyatomic anions, with the exception of TFA, calculated by MD simulations exhibit the same trend as was observed experimentally (see Chapter III). This trend follows the Hofmeister series where the lyotropic properties decrease according to the following order: $\Gamma^- > \text{NO}_3^- \sim \text{Br}^- > \text{Cl}^- > \text{C2} > \text{F}^- \sim \text{PH}$.

Simulations for the gemini associated with carboxylate counterions showed that the chain length of the anion has a strong impact on the micellar properties. We found that the longer the counterion chain length, the more R_g , SASA, ε and $g(r)$ increased. This is due to the orientation of their aliphatic moieties pointing towards the hydrophobic core of the micelle and hence penetrating into the micelle for the longer chain lengths. In this context the micelle of 10-2-10 with C6 as counterion is behaving as 16-2-16 gemini.

By deriving the boundaries of interfacial region and diffuse layer of the aggregate, we could calculate by MD simulations the interfacial concentrations of counterions and water molecules, which showed a remarkable agreement with the chemical trapping values. Surprisingly, in comparison with Cl^- and Br^- , we found that due to its highly “diffuse” trend of concentration

distribution, the C2 counterions is simultaneously the most penetrating anion into the hydrophobic core of the micelle and the one with the highest ionization degree. Within the acetate molecule, the methyl moieties have a relatively hydrophobic nature while the carboxyl group displays a more hydrophilic one. We envisage that this ambivalent nature of acetate could explain for its observed behavior within the micelle. The different degree of hydrophobicity between Cl^- and Br^- is also shown: Br^- , less hydrophilic, is more concentrated at the interfacial region than Cl^- .

Moreover, it was shown that the arenediazonium probe, used for the chemical trapping measurements, is well accommodated within the micelle and its reactive part colocalized with gemini headgroups and counterions at the interfacial region.

In addition, it is noteworthy that, even though polarizability of the anions was not counted in MD simulations, the obtained results that are in good agreement with experimental data. This therefore strongly suggests that the parameters used for the molecular dynamic simulations were chosen correctly.

3. Experimental section

3.1. Materials

3.1.1. Parameters validation

Given that monoatomic cations and anions parameters differ considerably among all the published force fields and a consistent set of parameters is missing for the halides series in CHARMM36 force field, we implemented the set of parameters from OPLS force field[161] For consistency, OPLS parameters were also used for the acetate anion[173] where the chemical trapping results were compared with Cl^- and Br^- .

There are different case studies in which OPLS parameters were used within CHARMM force field giving good results[174] and moreover some CHARMM22 non-bonded parameters were originally taken from OPLS force field[175]. In the present work we implemented OPLS parameters for the halide counterions and CHARMM36[176] parameters for the gemini surfactants that compose the micelle and all the other polyatomic counterions (together with the CHARMM modified TIP3P model for the water molecules).

We validated these simulation settings against two structural properties of Cl^- and Br^- immersed in water: 1) the position of the first peak of the radial distribution function (RDF) of water oxygen atoms with respect to the anion and 2) the interaction energy of the counterion with one water molecule. The first structural data was confronted with the related experimental value taken from Marcus work[160] (which is a review that contains ions data generally used as target in computational works); while the second one with *ab-initio* results taken from ref.[177]. Our finding shows that using OPLS parameters for counterions within CHARMM force field give results in good accordance with experimental data.

3.2. Methods

A micelle made up of 27 gemini surfactants 10-2-10 was build using Packmol software[178] and immersed in the box of water with a volume of $\sim 83 \times 80 \times 82 \text{ \AA}^3$ and ~ 17900 water molecules (Figure V-13). The system was then neutralized with 54 counterions randomly placed in the box; the resulting concentration of the counterion in the box is ca. 164 mM (stoichiometric concentration of the salt equal to ca. 82 mM). The whole system was minimized, then gradually heated up to 300 K at constant volume using Langevin dynamics with a dumping coefficient equal to 5 ps^{-1} . The density of the system was equilibrated at constant number of particles, pressure (1 atm) and temperature

(300 K) (NPT) ensemble for 200 ps, implementing a modified Nosé-Hoover method in which Langevin dynamics is used to control fluctuations in the barostat[179]. In both thermalisation and density equilibration, the micelle was weakly restrained using a positional harmonic force constant of 2.0 kcal/mol/Å². A further NPT equilibration was run again up to 200 ps with removing all the restraints from the micelle. The production runs were performed in NVT ensemble, using Langevin dynamics with a damping coefficient of 3 ps⁻¹ and a simulation time of 50 ns.

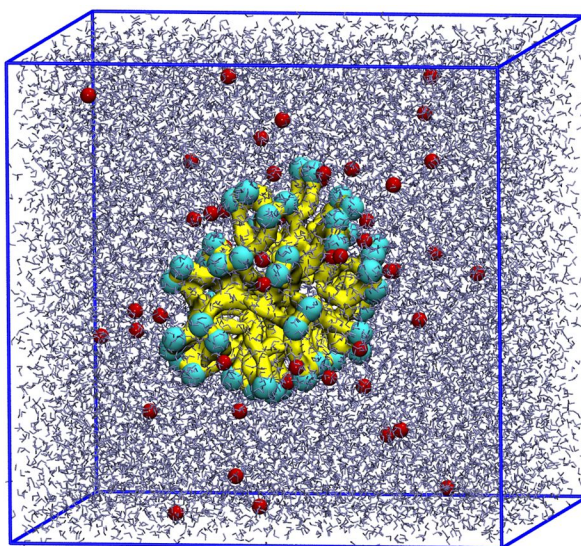


Figure V-13. Box of water with volume of $\sim 83 \times 80 \times 82 \text{ \AA}^3$ and ~ 17900 water molecules, where micelle made up of 27 gemini surfactant neutralized by 54 counterions was immersed.

In all the simulations a radial cutoff of 12.0 Å for the non-bonded interactions and a timestep of 2.0 fs for integrating the equations of motion were utilized; all the bonds involving hydrogen atoms were kept fixed at their equilibrium value. The trajectories were propagated with NAMD software and subsequently analyzed with the module *cpptraj*[180] of AmberTools13[162], VMD[163] software and GROMACS analysis tools[165].

The simulation of the diluted system was carried out with a micelle of $N = 27$ immersed in a box of volume $\sim 151 \times 148 \times 150 \text{ \AA}^3$, ~ 112000 water molecules and 54 chloride anions, which corresponds to a salt stoichiometric concentration of ca. 13.5 mM (chloride concentration of ca. 27 mM). The minimization/thermalisation/equilibration protocol was the same as above. For the simulation of the smaller micelle, $N = 15$, 30 anions were utilized to neutralize the system and the box has a volume of $\sim 66 \times 65 \times 67 \text{ \AA}^3$ and ~ 8500 water molecules. This setting corresponds to a counterion concentration of ca. 172 mM (which means a stoichiometric salt concentration equal to ca. 86 mM).

As for the evaluation of the observables, the first 5 ns of the simulations were discarded. Indeed, looking at Figure V-14, we deem the systems converged just after the first 5 ns of simulation time; whereas, in the case of the diluted system, we omitted the first 10 ns of production run.

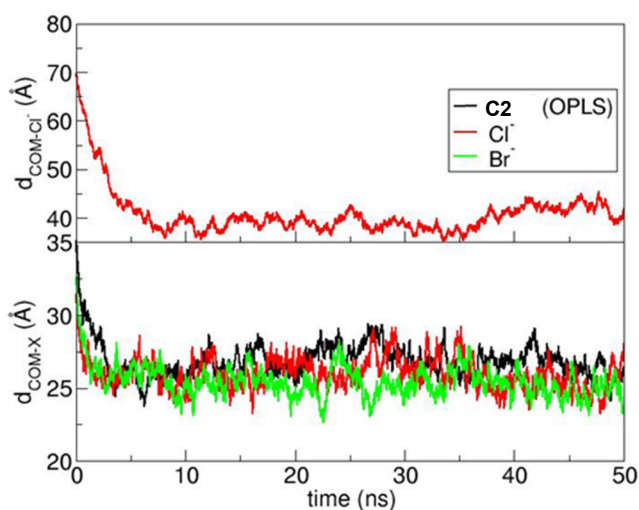


Figure V-14. Equilibration assessment on the example of C2, Cl⁻ and Br⁻ counterions.

To assess the convergence we run one more simulation up to 100 ns; after splitting this trajectory into two 50 ns sub-trajectories, we evaluated R_g , SASA and ϵ for the two halves and saw that the values were practically the same (Figure V-15).

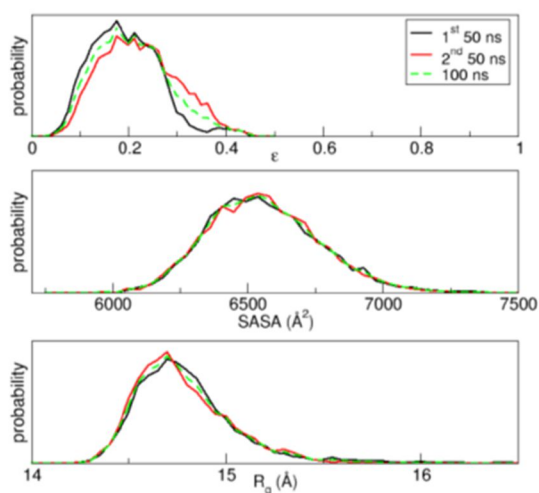


Figure V-15. R_g , SASA and ϵ evaluated for 100 ns trajectory as well as two 50 ns sub-trajectories after splitting the first one.

**Chapter VI. Rheological study of the Hofmeister effects at
semi-dilute regime**

Introduction

So far we have discussed how Hofmeister effects influence the self-assembly of 10-2-10 X gemini in aqueous solution at concentrations just above the CMC. At such concentrations gemini form mostly spherical aggregates (micelles). It was shown that nature of the counterion strongly impacts the balance of forces that contributes to the formation of the micellar aggregates. Thus, for example, the thermodynamic parameter, hydration free energy $-\Delta G_{hyd}$, which determines required energy for transfer of an anion from the ideal gas phase to the infinitely dilute solution, has significant influence on the CMC of the surfactant. For the gemini with counterions that have low $-\Delta G_{hyd}$ (e.g., TFA, Br^- , NO_3^-), formation of micellar aggregates is more favorable compared to the gemini having counterions with high values of $-\Delta G_{hyd}$ (C2, PH, F^-). For more details, see Chapter III.

In the present Chapter, we investigate how this ion specificity will impact the assembly at higher concentration. Upon increasing the surfactant concentration or adding salts, small spherical micelles grow in size and form rodlike then wormlike micelles[110, 181-184]. At high enough concentration these long and flexible wormlike micelles get entangled and behave as polymers[185, 186]. The formation of such entangled supramolecular structures increases the viscosity and elasticity of the system. Transition from dilute (growth of the micellar size is slow as a function of surfactant concentration) to semi-dilute (rapid growth of micelles) regime is characterized by the overlap concentration (Φ^*)[186-188]. Because of the significant change in the viscosity at this concentration, rheological study can be used to examine the mechanical properties of the wormlike micellar solutions.

The question we ask here is the following: if the ion specific effects that we have observed at the concentration around CMC with spherical micellar solution will have the same contribution to the self-assembly process of gemini surfactants at the higher level of system complexity (entangled wormlike micelles), or whether it would differ due to the change in balance of forces that drives the self-assembly of the amphiphiles?

1. Wormlike micelles

Wormlike micelles of cationic gemini surfactants can be easily obtained without any additives due to the packing parameter[17]. The geometry of the surfactant aggregates is determined to a certain extent by packing parameter[6], $p = v/a_0l$, where v and l are volume and extended length of the hydrophobic part respectively, and a_0 is a surface area occupied by the surfactant headgroup. For, $p = 1/3$ spherical micelles are formed; for $1/3 < p < 1/2$, cylindrical (wormlike) micelles are formed; for $1/2 < p < 1$, vesicles are formed; and for $p \sim 1$, bilayers are formed (Figure VI-1).

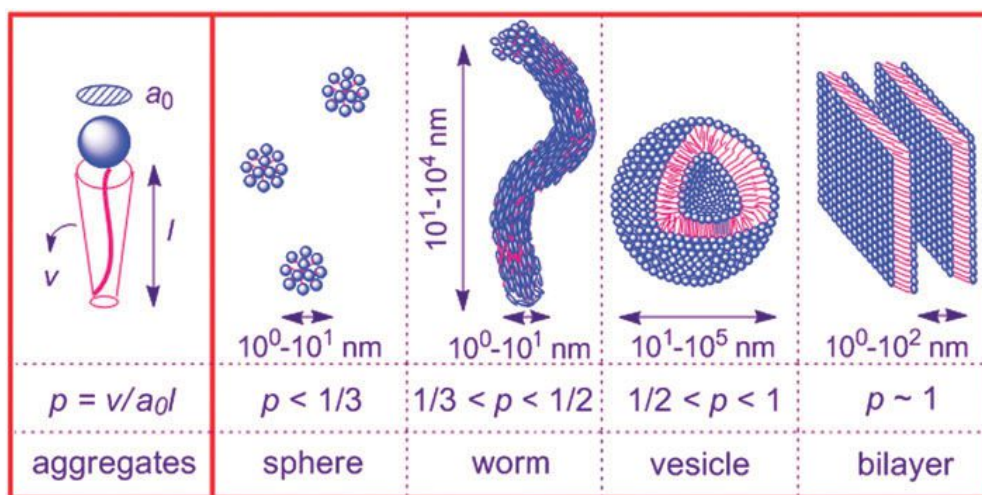


Figure VI-1. Contribution of the packing parameter to the morphology of the surfactant aggregates[189].

Gemini surfactants, having larger volume of the hydrophobic moiety than their single chain analogues, tend to form cylindrical micelles at much lower concentration[183]. Moreover, for the ionic amphiphiles the facility to form wormlike micelles would depend on the degree of ionization that determines the effective headgroup area. For the surfactants with a lower degree of ionization, the formation of wormlike micelles would be more favorable due to the screened electrostatic repulsion between the headgroups of the surfactant molecules and consequently smaller area per headgroup (a_0).

It was previously shown[187, 190] that for the salt-free solutions in dilute regime ($\Phi < \Phi^*$), the micellar length and viscosity increase slowly with increasing surfactant concentration. However, in the semi-dilute regime ($\Phi > \Phi^*$), the length of the aggregates as well as viscosity increase rapidly[191]. Entanglement of the long micellar aggregates increases the viscoelastic properties of the system, and thereby the micellar network can be characterized as the one for flexible polymers.

Nevertheless, the micellar solutions are called “living” polymer in order to differentiate them from the macromolecular polymer, due to their ability to break and recombine reversibly.

To describe more precisely micellar growth of the surfactants, we used a model proposed by Mackintosh and co-workers[187, 190]. With increasing the concentration of the surfactant in the solution (Φ), the average aggregation number (\bar{N}) of the micelles rises and can be described by a simple power law increase, with exponent 1/2:

$$\bar{N} \sim \Phi^{1/2} \quad (\text{VI-1})$$

where Φ is a volume fraction. From the thermodynamic point of view, the growth of aggregates can be characterized by several energies. For the *neutral* or highly screened micelles there are two main terms. First one is end-cap energy. Being energetically costly, it would promote formation of long aggregates, reducing amount of the end-caps. The second term is entropy of mixing. It would favor formation of many small micelles. These two competitive terms will give rise to the polydispersity of the system. Moreover, the average aggregation number of the micelles can be described as exhibiting a power law growth and will depend on the concentration as follows:

$$\bar{N} \sim \Phi^{1/2} \exp[E_c/2] \quad (\text{VI-2})$$

where \bar{N} is average aggregation number, and E_c is an end-cap energy. At the same time, viscosity according to the theory based on this growth law[192-194] is expected to be:

$$\eta \sim N\Phi^3 \sim \Phi^{3.5} \quad (\text{VI-3})$$

In the case of *ionic* surfactants, self-assembly process is more complex due to the presence of an additional thermodynamic term: electrostatic repulsion between headgroups that would favor the disassembly of micelles. In addition, due to the presence of counterions in the system we should add a new parameter, Debye screening length (κ^{-1}). This parameter would depend on the concentration and properties of the counterions that determine the degree of ionization of the micelle (α). The relationship between Debye length κ^{-1} and ionization degree in this case can be described by equation[183]:

$$\kappa^2 = 4\pi l\rho\alpha \quad (\text{VI-4})$$

where ρ is the number density of polar heads.

In *dilute regime* the micelle length is shorter than Debye screening length and the system is characterized by a slow increase in aggregates size with concentration[183]. The transition from dilute to *semi-dilute regime* occurs when the micellar length becomes comparable with the Debye length of electrostatic interactions. With increasing the concentration, the contribution of the energy promoting the breaking of the micelle (formation of end-caps) decreases due to the screening of the electrostatic interactions[17] ($\Delta E(\Phi) \sim -1/\sqrt{\Phi}$, where ΔE is a contribution from electrostatic interactions). The deviation from the growth law $\bar{N} \sim \Phi^{1/2} \exp[E_c/2]$ to $\bar{N} \sim \Phi^{1/2} \exp[\Delta E(\Phi)]$, strongly enhances the micellar growth with increasing surfactant concentration. The growth of average aggregation number could be derived from electrostatic energy as was described by Mackintosh *et al.*[187] and Safran *et al.*[195], giving:

$$\bar{N} \simeq 2\Phi^{1/2} \exp\left[\frac{1}{2}(E_c - l\alpha v^*/\sqrt{\Phi})\right] \quad (\text{VI-5})$$

where l is Bjerrum length, a is radius of rodlike micelle and v^* is an effective charge per unit length. Important to note, that aggregate growth depends on E_c and α . Due to the scaling of the micellar length, the viscosity of the system in semi-dilute regime (above Φ^*) would grow rapidly. Hence, investigating it through zero share rate viscosity and determining overlap concentration, we are able to estimate the contribution of the ion specific effects on the formation of “living” polymer.

2. Results and discussions

To determine the overlap concentration, we measured zero shear rate viscosity (η_0) of the surfactant solutions at different concentrations at 20 °C. Figure VI-2 presents the dependence of η_0 on the concentration of the surfactant in the solution for gemini with different counterions. The behavior of η_0 is characterized by rapid increase at certain concentration that depends on the counterion of the gemini surfactant. This sharp increase in viscosity indicates the transition from dilute to semi-dilute regime. In the dilute regime, the distance between micelles is relatively high (more than Debye screening length) and the size of aggregates increases slowly. After the transition to semi-dilute regime, the rate of the growth of the aggregates length increases significantly inducing the entanglement of the wormlike micelles. The crossover of these two regimes is characterized by Φ^* , that can be easily determined as an intersection of the two lines, the linear fit describing dilute regime and the linear fit describing semi-dilute regime.

It is interesting to note, that for such counterions as TFA, Br^- and NO_3^- , the transition is characterized by abrupt change in the slope, whereas for Cl^- , C2 and PH the transition is more gradual. The same behavior of the slope was observed for the conductivity measurements, where the transition from the monomers to the micellar aggregates (CMC) depends on the nature of the counterion and provides information about ionization degree of the formed micelles.

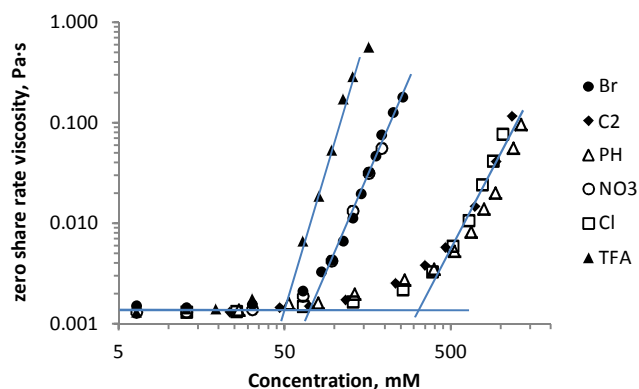


Figure VI-2. Zero shear rate viscosity as a function of surfactant concentration for 10-2-10 gemini with different counterions.

As was mentioned in the section 1, Φ^* strongly depends on the end-cap energy as well as the degree of ionization of the micelle. Since the cationic part of the salt is unchanged, E_c would not vary much for the different counterions. At the same time, the counterion nature, that determines ionization degree, would influence the micellar growth. For example, Oda *et al.*[196] showed that

for cetyltrimethylammonium salts, the observed value of Φ^* is lower for more hydrophobic counterions (*n*-heptane sulfonate and mixture of $\text{Br}^- + \text{HCN}^-$ in molar ratio 1/2) than for more hydrophilic ones (*n*-hexane sulfonate mixture of $\text{Br}^- + \text{HCN}^-$ in molar ratio 1/1). Counterions with higher degree of binding ($1-\alpha$) screen the micelle and favor the aggregate formation, whilst E_c does not strongly dependent on α . Moreover, the influence of the salt effect on the formation of wormlike micelles was investigated[85, 197-199]. Indeed, the Hofmeister effects have a significant contribution to the forces that provide aggregate growth and particularly to the electrostatic interactions. In their work, Oelschlaeger *et al.*[199] discuss the influence of added salts on the scission energy (energy required to create two end-caps). They showed that added salts have an effect on the Φ^* (trend follows Hofmeister series). However, for the investigated systems, scission energy is independent of the nature of the added salt. These findings are in agreement with the results obtained by Oda *et al.*[196].

Our results in the present case show that Φ^* for 10-2-10 gemini, as well as the CMC, depend strongly on the counterion (Table VI-1). For the 10-2-10 X where X = TFA, Br^- and NO_3^- Φ^* is 51 mM, 78 mM and 71 mM respectively, whereas for X = Cl^- , C2 and PH, it is almost 5 times higher (377 mM, 425 mM and 465 mM respectively).

Table VI-1. Values of the CMC and α_E obtained by conductivity measurements at 30 °C, and Φ^* obtained by rheological measurements at 20 °C for the 10-2-10 X gemini, where X = Br^- , Cl^- , NO_3^- , PH, C2, TFA)

Counterion	CMC, mM	α_E	Φ^* , mM
	Temperature 30°C		Temperature 20°C
NO_3	6.3	0.15	71
TFA	6.4		51
Br	6.4	0.15	78
Cl	12.4	0.21	377
C2	22.7	0.26	425
PH	26.0	0.25	465

In order to discuss these results, we will refer to the approach developed by Collins and co-workers[36]. In their review, it was shown that oppositely charged ions with equal water affinity tend to come together in solution to form contact ion pairs, whereas those with different water

affinity tend to stay apart. The affinity to the water is related to the surface charge density of the ion and hence polarizability.

We applied this concept to the system under investigation. Figure VI-3 shows the CMC and the Φ^* as function of polarizability for the 10-2-10 gemini with different counterions. All the data on this Figure could be divided into two groups. *First* group is monoatomic anions: Cl^- and Br^- . For these small ions of high charge density are not polarizable and highly hydrated. Big ions of low charge density are polarizable and poorly hydrated[36]. We expect self-assembly for the surfactant with polarizable anion at lower concentration due to its high affinity of the counterion to the headgroup. Figure VI-3 shows that for more polarizable anion Br^- (4.85 \AA^3), the CMC as well as Φ^* are lower than for the less polarizable Cl^- (3.42 \AA^3). The *second* group is polyatomic counterions: NO_3^- , C2 and PH. The situation for them is more complex. For example, polarizable and big C2 and PH have the highest values of the CMC and Φ^* . It is opposite of what we would expect. Such behavior could be explained by change in the surface charge density of the anions. It is no longer homogeneous as for the monoatomic counterions. The size and polarizability of the ion are not any more directly related to hydration of the anion. Hence, dispersion forces alone cannot describe the interactions that ensure the aggregate formation and growth; thus, other properties of the anions should be taken into account.

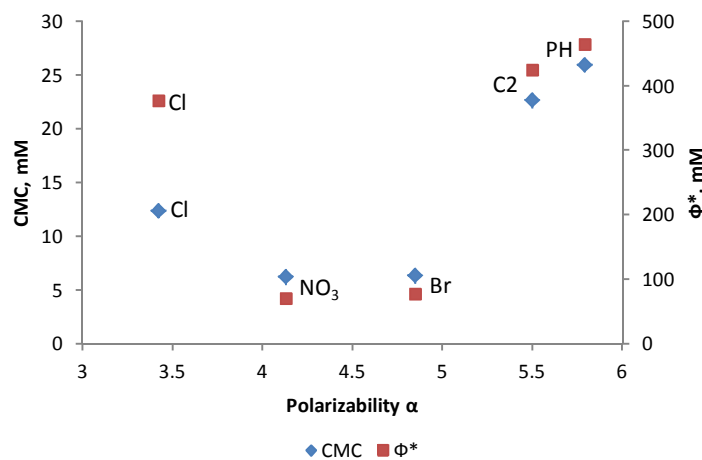


Figure VI-3. CMC and Φ^* as a function of polarizability for the 10-2-10 gemini with different counterions.

In the Chapter III we discussed that for the 10-2-10 X the CMC values correlate well with the hydration free energy and the lyotropic number. Same trend was observed for Φ^* as it can be seen in Figure VI-4.

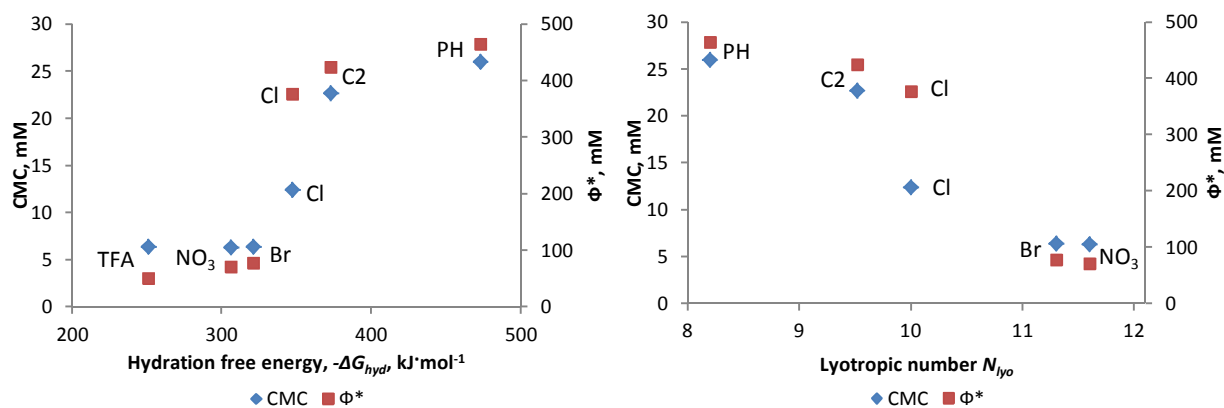


Figure VI-4. CMC and Φ^* as a function of $-\Delta G_{hyd}$ (left) and N_{lyo} (right) for the 10-2-10 gemini with different counterions.

These results indicate that the self-assembly of the surfactants in the dilute regime (formation of spherical micelles) and semi-dilute regime (formation of entangled wormlike micelles) both depend on the degree of the association between the headgroup and counterion. Stronger headgroup-counterion association, as observed for hydrophobic counterions such as NO₃⁻, Br⁻ and TFA⁻ with lower ionization degrees α_E , leads to lower repulsion between headgroups and lower interfacial curvature, and more rapid growth of the micelles, as it favors the formation of the longer cylindrical micelles. Surfactants with more hydrophilic counterions form micelles with lower charge screening, hence, higher ionization degree. This is the case for counterions such as Cl⁻, C2 and PH for which the ionization degrees of the micelles α_E are 0.21, 0.26 and 0.25 respectively. Due to the electrostatic interactions that increase the entropy of the system, aggregates grow only at higher concentration, leading to higher Φ^* . Interestingly, Φ^* value for the 10-2-10 Cl suggests that Cl⁻ is more hydrophilic anion (the value of Φ^* is closer to that of C2 than to Br⁻), whereas, the value of the CMC for the 10-2-10 Cl indicates an intermediate behavior for the Cl⁻ anion (Figure VI-4).

3. Conclusions

In this Chapter we investigated the behavior of micellar growth for 10-2-10 X gemini with different counterions ($X = \text{Br}^-$, NO_3^- , TFA, PH, Cl^- , C2) using rheology. It was shown that the nature of the counterion has a strong impact on the formation of the wormlike micelles, their further growth and formation of a network of entangled micelles. Hydrophobic counterions such as Br^- , NO_3^- and TFA are characterized by stronger association with surfactant headgroups (low α). This provides screening of the electrostatic interactions in the micellar solution at lower concentrations, decreasing the effective headgroup area and as a result favoring formation of long entangled micellar aggregates. In contrast, hydrophilic counterions such as Cl^- , PH and C2 having high α , screen micellar charge to a lower extent and exhibit micellar growth at much higher concentrations.

Results shown in Table VI-1 are consistent with the CMC and α data obtained in Chapter III. The increase of the changes in inducing micellar growth followed the same order as CMC: TFA \sim $\text{Br}^- \sim \text{NO}_3^- > \text{Cl}^- > \text{C2} > \text{PH}$. Analyzing the increase in viscosity of the system related to Φ^* , we showed that hydration free energy of the anions provides the best explanation of ion effects on the micellar solution. In addition, our results show that there are the same driving forces controlling aggregate formation at the level of spherical micelles, as well as extensive micellar growth at the level of long cylindrical micelles.

4. Experimental section

4.1. Material and methods

The 10-2-10 X with different counterions were synthesized as was described in Chapter II. The samples were prepared by weighing surfactants and adding the corresponding volume of water directly into sample vials. To get a homogeneous solution, heating at 60 °C for sufficient time and simultaneous stirring was necessary.

Measurements were performed for the following systems:

- (1) 10-2-10 Br solutions in water with surfactant concentration from 6.4 mM to 256 mM
- (2) 10-2-10 PH solutions in water with surfactant concentration from 52.8 mM to 1.32 M
- (3) 10-2-10 C2 solutions in water with surfactant concentration from 46.6 mM to 1.165 M
- (4) 10-2-10 Cl solutions in water with surfactant concentration from 12.8 mM to 1.024 M
- (5) 10-2-10 NO₃ solutions in water with surfactant concentration from 6.4 mM to 192 mM
- (6) 10-2-10 TFA solutions in water with surfactant concentration from 6.4 mM to 160 mM

The rheological measurements were performed with Rheometer HAAKE RheoStress 600 using Couette geometry. The Couette cell consisted of a 27.206 mm diameter aluminium-coated cup and a titanium rotor of diameter 25.079 mm and length 37.573 mm. The gap distance for all the measurements was chosen as 0.04 mm, temperature was set at 20 °C. HAAKE Rheo win Job Manager Ver. 4.41.0000 software was used for the data collection. For each measurement shear rate was adjusted according to the concentration. “Range calculator” from the software was used to estimate approximately the shear rate that can be applied for the certain system. The maximum waiting time was chosen as 500 s. Usually, the system reached equilibrium much faster than the set time. Before data collection was started, solution was homogenized for 300 s in order to reach the equilibrium at 20 °C.

4.2. Data analysis

The obtained plots, viscosity (η) vs shear rate ($\dot{\gamma}$) (log/log scale), were analyzed using HAAKE Rheo win Data Manager Ver. 4.41.0000. The data were extrapolated in order to obtain the zero shear rate viscosity (η_0) using the same software (Figure VI-5). There is always some deviation at the low shear rate due to the limitation of the sensitivity of the apparatus. However, it disappears with increasing the $\dot{\gamma}$. While estimating η_0 , we do not take into account the deviation at the low $\dot{\gamma}$.

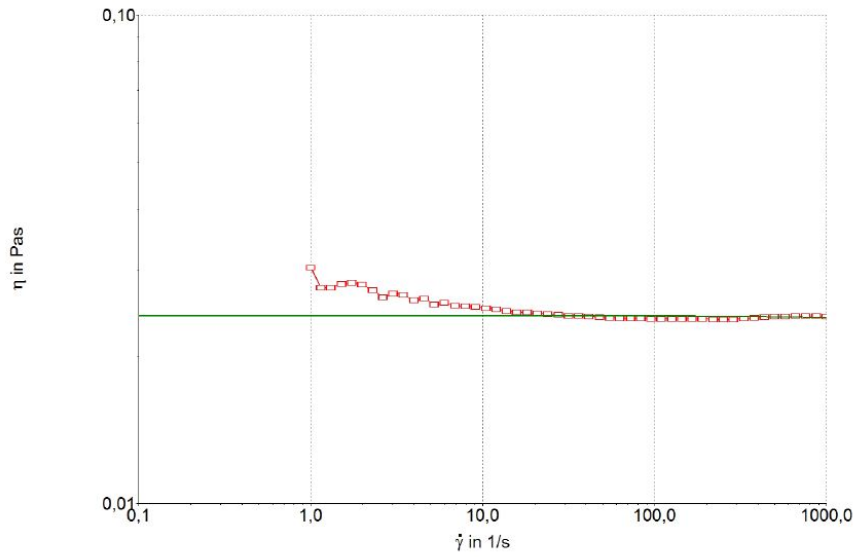


Figure VI-5. Dependence of viscosity (η) on shear rate ($\dot{\gamma}$) for 10-2-10 Cl at the concentration 768 mM obtained using Rheo win Data Manager software. Horizontal green solid line indicates the extrapolation of the viscosity to zero shear rate.

Estimated η_0 values were plotted as a function of concentration in log-log scale to obtain the overlap concentration (Φ^*). The intersection of two straight lines, at the concentrations before and after Φ^* gave as the values of overlap concentration (Figure VI-2).

Chapter VII. Impact of counterion nature on the crystal structure of cationic gemini surfactants

Some of the crystal structures of the gemini surfactants discussed in this chapter were previously obtained by Dr. Sabine Manet in our group.

Introduction

Up to now our study was focused on the ion specific effects on the self-assembly properties of cationic gemini surfactants in aqueous solution. We have clearly demonstrated that the properties of cationic surfactants in the bulk are intimately linked to counterion properties such as ion size, ion polarizability, ion hydration energy, pKa, hydration and lyotropic numbers. Even though, the hydrophilic/hydrophobic properties of anions seem to predict the assembling behaviors of the system relatively well, it still is determined by the subtle interplay between the hydration of counterions and the dissociation energies (stability of crystallinity) of the ion pair. Thus, combining the study of ion effects on the self-assembly of the gemini surfactants in the crystalline in addition to the solution state we can get better insight into the interactions controlling the ion specificity.

The counterion effects on the solubilization and melting behaviors were already reported by our group[200]. It was found that contrary to the Kraft temperature, characterizing the solubility of the ionic surfactants, the melting temperature of the crystals was higher for the small ions and decreased as the ionic radii of the counterions increase. Another important observation is that the surfactants with different counterions exhibit different melting behavior, characterizing by liquid crystal mesophases. This strongly suggests that crystalline structure strongly depends on the counterion. In this context, the single x-ray crystallography is a powerful tool to elucidate the effect of various ions on the packing of the amphiphiles at the molecular level.

Various crystal structures of gemini-type surfactants were investigated previously[201-204]. For example, Hattori *et al.*[203] showed the influence of the spacer length on the gemini 4-s-4 Br, presenting two conformation of the surfactant molecule in the crystal structures. Wei *et al.*[201] demonstrated the crystal packing for the gemini with OH group in the spacer where hydrogen bonds have a strong impact. However, the systematic study of the impact of the counterion nature on the crystalline packing is yet to be addressed.

In this final chapter we investigate the contribution of ion specificity on the self-organization of amphiphiles in crystalline structure, studying the gemini surfactants with different halide counterions. Moreover, we demonstrate how the gemini having quaternary and tertiary ammonium headgroup (the last one is characterized by proton) crystalize differently.

1. Results and discussions

1.1. Packing of gemini surfactants in the crystalline structure.

In Figure VII-1 and VII-2, single-crystal structures and the packing arrangement of n-2-n gemini (n = 10, 14, 16) with various counterions such as: Γ^- , Br^- and Cl^- as well as 10-2-10 gemini with tertiary ammonium headgroup are shown. Quaternary gemini with two halide counterions Br^- and Γ^- crystallized from different organic solvents have the same triclinic space group P-1 (Table VII-1, Figure VII-1)). The packing of the molecules driven by electrostatic and van der Waals interactions represents anti-gauche conformation, where two hydrocarbon chains lie perpendicular to the spacer and extend to opposite sides of the headgroups (for clarity see Figure VII-1 A and B). The plane defined by the C-C bonds of the two hydrocarbon chains are parallel and shifted with each other, and are perpendicular to the plane defined by the C-C bonds of the spacer. No solvent molecules are co-crystallized. Such type of molecular configuration in crystal structure for cationic gemini with halide counterions was reported previously[202, 203, 205]: Berthier *et al.*[202] and Svensson *et al.*[205] have reported the same space group (P-1) and ordering of hydrocarbon chains in anti-gauche conformation for 12-2-12 Br and 12-2-12 I respectively, crystallized from organic solvents. The Figure VII-2 shows that the packing arrangement into the crystal for the n-2-n quaternary gemini with Γ^- and Br^- as counterions are almost the same and do not depend on the chain length for $10 < n < 16$ (not presented here). In the crystal lattice, molecules are organized in parallel with interdigitated tails and headgroups are aligned with axis *b*, see Figure VII-2 A for clarity.

From the observed results, it seems that the anti-gauche conformation is energetically more favorable for the gemini with the spacer length of two and the chain length of ten or more hydrocarbons. Indeed, for the gemini with short spacer and long hydrophobic chains the steric effect and repulsive van der Waals interactions would probably favor the anti-gauche conformation. We also observed in some cases, a polymorphism for 10-2-10 I crystallized in H_2O (no solvent in the structure). Interestingly, two conformations were found in one unit cell: gauche and anti-gauche (Figure VII-1 C). Although, the single-crystals X-ray measurements were not complete due to the low stability and small size of the crystal, the analysis of the anti-gauche conformation for the molecule of 10-2-10 I indicates that they are more “open” and the alkyl chains have angle more than 90° with respect to the spacer.

In order to study the influence of the headgroup properties on the packing arrangement in the crystals, we studied the 10-2-10 gemini with tertiary ammonium headgroup denoted as 10-2-10 ter. This gemini contains a proton instead of one methyl in the headgroup. Analyzing 10-2-10 ter Br crystallized from H₂O, we obtained the same space group (triclinic P-1) and anti-gauche conformation as for the quaternary analog. However, on the Figure VII-1 clearly seen that the carbons in α and β lie down at the same plane as spacer and the angle between alkyl chains and spacer plane is more than 90°. Moreover, the position of counterions differs from the one typical for the quaternary 10-2-10 Br, why we have such changes would be discussed later. In Chapter III we mentioned that the low solubility of the tertiary gemini surfactants in water was attributed to hydrogen bonding between the hydrogens of the headgroups and the counterions. In crystal structure of 10-2-10 ter Br, crystallized from water we can clearly see that the hydrogen bonding is the main interaction that determines the location of the counterions Figure VII-2 D. Moreover, the anti-gauche conformation is round edged or wave-like compared to the one of quaternary gemini surfactants, see Figure VII-2 A. The interdigitation for the alkyl tails is not observed. So one can see that decrease in the size of the headgroups and formation of the hydrogen bonds, significantly change the shape and packing of the molecule within the crystal.

Meanwhile, orthorhombic crystals with Pbc_a space group (Table VII-1) were observed with 14-2-14 Cl co-crystallized with one water molecules per gemini. In contrast to n-2-n with Br⁻ and I⁻ counterions, 14-2-14 Cl molecules in the crystals have gauche conformation (Figure VII-1 D). The aliphatic chains lie down perpendicular to the spacer and extend in one side of the headgroups (in the same plane with respect to the spacer). The presence of water molecule in the crystals is attributed to the hygroscopic properties of the Cl⁻ anion. Being hydrophilic, probably chloride “dragged in” the water molecule from the solvent in the crystal structure. Intriguingly, the presence of water molecules changes the balance of forces controlling crystal organization from anti-gauche, as we observed for the bromide and iodide, to gauche. The water molecules favorably settle in the hydrophilic region, in the vicinity of the headgroups, and hence the conformation which has well defined hydrophilic and hydrophobic areas is more preferable. Crystal lattice for the 14-2-14 Cl is shown on the Figure VII-2 B. Since 14-2-14 Cl have gauche conformation, the way molecules arrange into the crystal is very different from those with Br⁻ or I⁻ counterions as described above. This structure is very close to lamellar phases with repeated bilayer structures and the two hydrocarbon chains are facing one another on the same side of the spacer, and they are interdigitated

and form bilayers with well-defined polar and non-polar regions, see Figure VII-2 B. The water molecules are located within the hydrophilic regions close to the headgroups.

Table VII-1. Crystallographic data for cationic gemini surfactants n-2-n with Γ^- , Br^- and Cl^- as a counterion obtained from single-crystal measurements.

	10-2-10 I (CH_3CN)	10-2-10 I (H_2O)	10-2-10 I (H_2O) polymorph.	16-2-16 I ($\text{MeOH}/$ Acetone)	10-2-10 Br (CH_3CN)	14-2-14 Br ($\text{MeOH}/$ Acetone)	14-2-14 Cl (ACN)	10-2-10 ter Br (H_2O)
Formula	$\text{C}_{13}\text{H}_{29}\text{IN}$	$\text{C}_{13}\text{H}_{29}\text{IN}$	$\text{C}_{39}\text{H}_{87}\text{I}_3\text{N}_3$	$\text{C}_{38}\text{H}_{82}\text{I}_2\text{N}_2$	$\text{C}_{13}\text{H}_{29}\text{BrN}$	$\text{C}_{34}\text{H}_{74}\text{Br}_2\text{N}_2$	$\text{C}_{34}\text{H}_{76}\text{Cl}_2\text{N}_2\text{O}$	$\text{C}_{12}\text{H}_{26.50}\text{Br}_2\text{N}_2$
FW (g-mol ⁻¹)	326.27	326.27	978.82	820.86	279.28	670.77	599.87	358.67
Temperature (K)	293	110	293	293	113	293	113	293
Crystal system	triclinic	triclinic	triclinic	triclinic	triclinic	triclinic	orthorhombic	triclinic
Space group	P-1	P-1	P-1	P-1	P-1	P1	Pbca	P-1
Z	2	2	2	2	2	1	8	2
Z'	0.5	0.5	1.5	1	0.5	1	1	0.5
a (Å)	7.2858(4)	7.2048(6)	7.945(5)	8.891(2)	6.9176(5)	6.946(1)	9.8560(6)	5.6594(3)
b (Å)	8.8012(5)	8.6132(7)	13.279(9)	13.564(4)	8.5365(6)	8.518(1)	14.4116(10)	6.20190(10)
c (Å)	14.4660(10)	13.9385(13)	25.002(15)	19.125(6)	14.5033(10)	17.117(2)	52.110(4)	22.5865(11)
α (degree)	73.270(5)	75.61(2)	93.02(4)	102.94(2)	75.50(1)	92.589(5)	90.00	94.036(9)
β (degree)	79.475(6)	80.82(2)	94.94(3)	91.77(2)	81.43(1)	94.541(4)	90.00	92.741(12)
γ (degree)	66.679(5)	67.76(2)	99.70(3)	102.51(2)	67.31(1)	113.753(4)	90.00	103.760(14)
Volume (Å ³)	813.28	773.44	2584	2187.0	763.65	920.7	7401.7	766.40
R1 [$I \geq 2\sigma(I)$]	0.0633	0.0592	0.1435	0.0877	0.0830	0.0341	0.0736	0.0525
wR2 (all data)	0.1648	0.1164	0.3432	0.3247	0.1969	0.0980	0.1860	0.1242
density	1.332	1.401	1.258	1.246	1.215	1.210	1.077	1.554
Number refl [$I \geq 2\sigma(I)$]	2158	1983	1169	2062	2144	3126	5786	2271
Number parameters	140	136	409	380	139	344	360	129
diffractometer	R-axis	FRX	FRX	R-axis	FRX	Proteum	FRX	FRX

Z- the number of patterns in the unit cell; **Z'**- the number of patterns in the asymmetric unit; **a, b, c, α , β , γ** - unit cell parameters; **R1** reliability factor³ (should be < 10%); **wR2** - weighting scheme applied to R1⁴

$$^3 R1 = \frac{\sum ||Fo| - |Fc||}{\sum |Fo|}$$

where Fo could be assimilated to experimental data (or electron density) and Fc to the calculated data (or purposed model)

$$^4 wR2 = \left[\frac{\sum [w(Fo^2 - Fc^2)^2]}{\sum [w(Fo^2)^2]} \right]^{1/2}$$

where $w = 1/[\sigma^2(Fo^2) + (aP)^2 + bP]$ where $P = (Fo^2 + 2Fc^2)/3$

where a and b are the first and the second parameter in the weighting scheme instruction

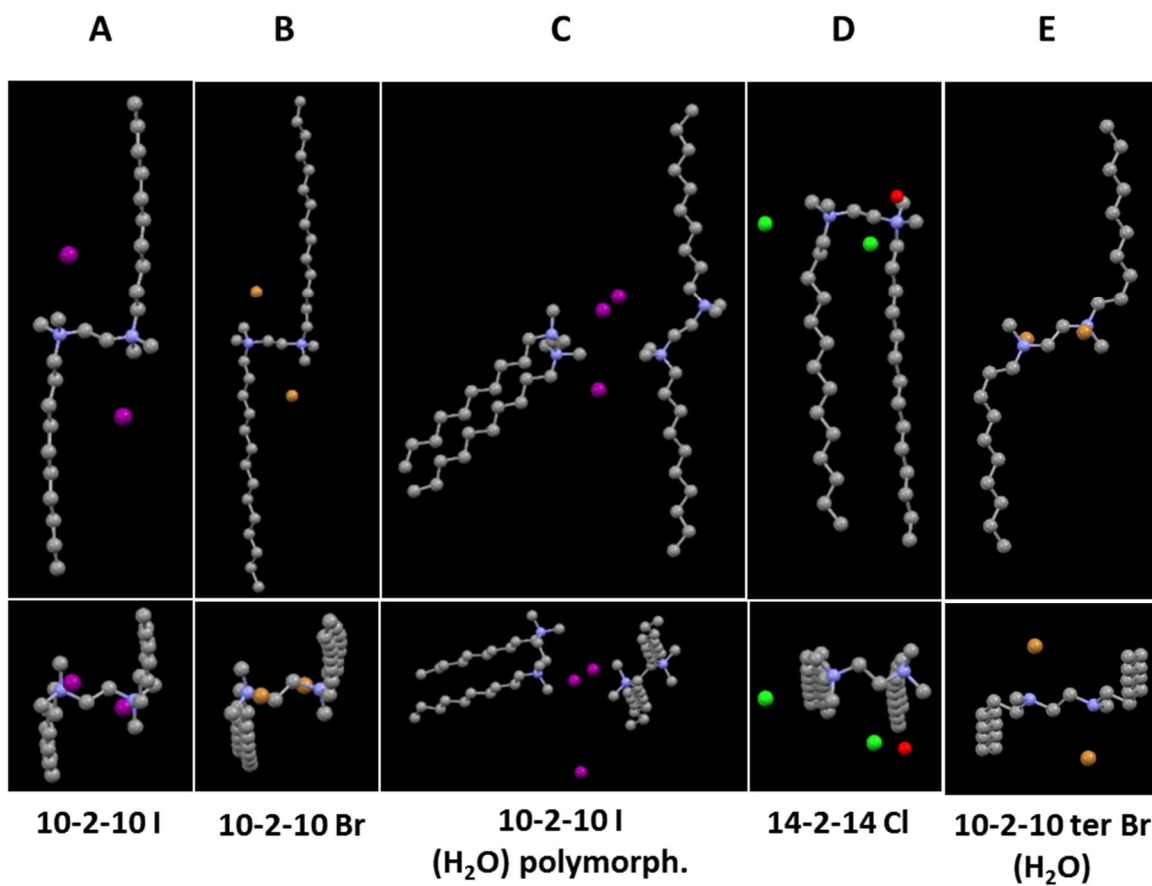


Figure VII-1. Stick and ball representation of n -2- n ($n = 10, 14, 16$) gemini found in the single-crystal structure with counterions such as: Γ^- , Br^- and Cl^- . Color code: N, C, I, Br, Cl and O atoms are in blue, grey, purple, brown, green and red respectively. Hydrogens are not presented for clarity.

The polymorphism obtained for the 10-2-10 I, when the molecule was crystallized from water is very interesting. As we mentioned previously gemini surfactants have two conformations in one crystals. Probably the way molecules aggregate in water (the hydrophobic chains hidden within the core of the micelle) favored the formation of gauche conformation in the crystalline structure even without co-localized solvent molecules. On the Figure VII-2 C it is shown how two molecules in gauche conformation are packed between layers of molecules with more “open” anti-gauche conformation, making kind of “sandwich” structure parallel axis c . Considering the bilayer motif formed with the molecules in gauche conformation, the angle of the tilt of the hydrophobic chains is higher than gauche conformation in the crystals obtained with the 14-2-14 Cl.

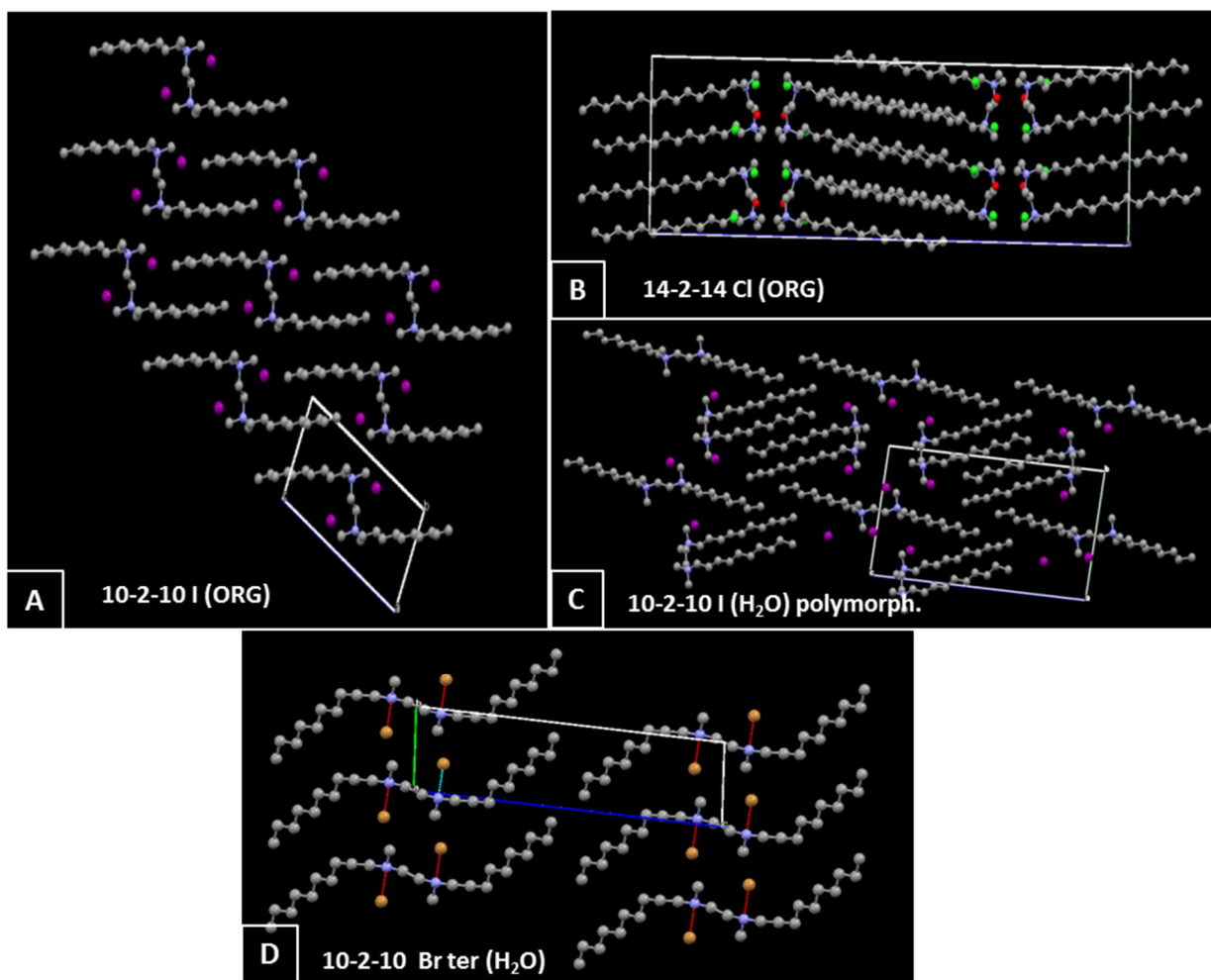


Figure VII-2. Packing arrangement of 10-2-10 I (A), 14-2-14 Cl (B) and 10-2-10 I polymorph (C) and 10-2-10 ter Br (D). View along the *a* axis. (A), (B): crystals were grown from organic solvent, CH₃CN; (C) and (D) crystal was grown from H₂O. Color code: N, C, O, I and Cl atoms are in blue, grey, red, purple and green, respectively. Hydrogen atoms were not shown for clarity. Red dash lines indicate the hydrogen bonds.

In summary, two conformations are typically observed for gemini ammonium surfactant in crystals: gauche and anti-gauche. The packing arrangement of these molecules in crystal lattice depends on the subtle balance of forces such as electrostatic interactions between headgroups and counterions (nature of counterion), presents of solvent molecules in the structure, van der Waals interactions between hydrocarbons, hydrogen bonding and the solvent from which crystals were obtained.

1.2. Distances between counterion and nitrogen of the headgroups for gemini n-2-n X, where X = I⁻, Br⁻ and Cl⁻.

To characterize the monoatomic counterion effect on the crystal structure and to compare the characteristic distances in the crystals, we focused on the quaternary gemini having counterions I⁻, Br⁻ and Cl⁻: 10-2-10 I, 16-2-16 I, 10-2-10 Br, 14-2-14 Br and 14-2-14 Cl, crystalized from organic solvents. Probably due to the high hydrophilicity of Cl⁻ in comparison with Br⁻ and I⁻ (free energies of hydration for I⁻, Br⁻, and Cl⁻ are -283, -321 and -347 kJ·mol⁻¹ respectively)[30] we could only crystalize 14-2-14 for this counterion. We compared the distances between the ammonium atom of the headgroup and the anions (X⁻-N⁺). For all the crystallized gemini surfactants, it is observed that the effect of the aliphatic chain length is negligible, whilst the types of counterions have important effect for the relative positions of counterions with respect to N atoms in the crystals, see Table VII-2.

Table VII-2. Crystallographic data for cationic gemini surfactants n-2-n with I⁻, Br⁻ and Cl⁻ as a counterion obtained from single-crystal measurements.

Counterion	Object1	Object 2	10-2-10	12-2-12	14-2-14	16-2-16	10-2-10 ter
Br	1	N	4.14	4.14	4.11		
	1	N*	4.33	4.34	4.20		3.19 HB
	1	N#	4.40	4.36	4.36		
	2	N'	4.14	4.14	4.16		
	2	N#	4.33	4.34	4.32		
	2	N*	4.40	4.36	4.35		
I	1	N	4.36			4.39	
	1	N*	4.53			4.51	
	1	N#	4.60			4.58	
	2	N'	4.36			4.39	
	2	N#	4.53			4.51	
	2	N*	4.60			4.58	

Now we will focus on 10-2-10 I, 10-2-10 Br and 14-2-14 Cl crystalized from the same solvent (CH₃CN). Using the Mercury software, we defined the positions of the halide of interest relative to its three nearest nitrogen neighbors, as shown in Figure VII-3 and summarized in Table VII-3. For 14-2-14 Cl in gauche conformation, there are two populations of Cl⁻, one located at the interface of hydrophilic part of the molecule and second one more buried in the hydrophobic layer

as you can see on the Figure VII-2 B, where the packing arrangement shown. Hence distance $\text{Cl}^- \text{-N}^+$ would be different for two Cl^- populations.

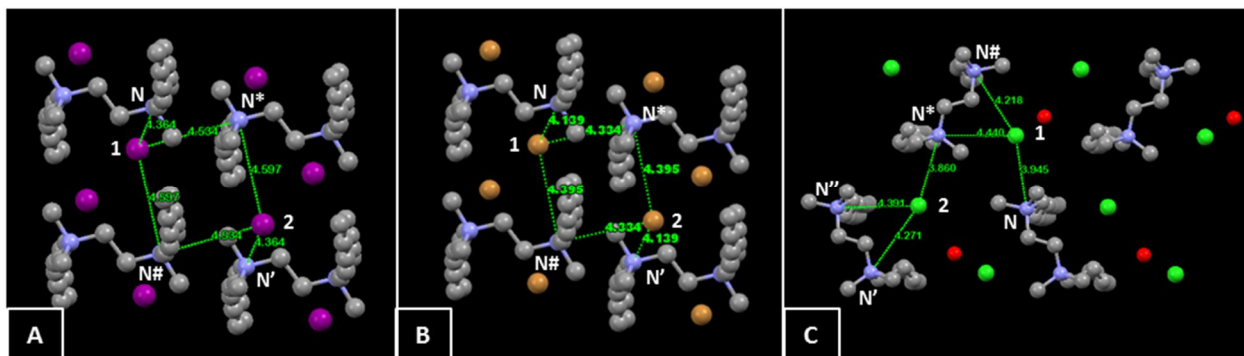


Figure VII-3. Distances between the counterion and the ammonium atom of the headgroup in the crystal structure for (A) 10-2-10 I, (B) 10-2-10 Br and (C) 14-2-14 Cl. Color code: N, C, O, I, Br and Cl atoms are in blue, grey, red, purple, brown and green respectively. Hydrogen atoms were not shown for clarity.

The summary in Table VII-3 clearly shows that Cl^- are closest to ammonium ion whereas I^- are the farthest. To get better insight into association energy between counterions and positively charged headgroups, we can look at the Coulomb interactions using rough approximations. The energy between two point charges separated by a distance r can be expressed by the following equation:

$$V(r) = \pm \frac{q_1 q_2}{4\pi\epsilon_0 r} \quad (\text{VII-1})$$

where q_1 and q_2 are two charges and ϵ_0 is the permittivity in vacuum. Since halides and headgroups of the gemini surfactants have charge equals 1 and $k_e = \frac{1}{4\pi\epsilon_0}$ is a Coulomb's constant, the energy for I^- , Br^- and Cl^- counterions can be approximated as electrostatic potential plus other contributions as follows:

$$E_I = k_e \left(\frac{1}{r_1} + \frac{1}{r_2} + \frac{1}{r_3} \right) + \dots \quad (\text{VII-2})$$

$$E_{Br} = k_e \left(\frac{1}{r_1} + \frac{1}{r_2} + \frac{1}{r_3} \right) + \dots \quad (\text{VII-3})$$

$$E_{Cl} = k_e \left(\frac{1}{r_1} + \frac{1}{r_2} + \frac{1}{r_3} \right) + \dots \quad (\text{VII-4})$$

where r_1 , r_2 and r_3 are the distances between counterion and the three closest cationic headgroups. Since other terms contribute less to the energy of the ion, these will be neglected. Then the ratio

between energy of Γ^- and Br^- can be shown as $\frac{E_{\text{Br}^-}}{E_{\Gamma^-}} = 1.05$, and the ratio between Cl^- and Br^- as $\frac{E_{\text{Cl}^-}}{E_{\text{Br}^-}} = 1.03$ for the population of the closer Cl^- and 1.02 for the other.

Previously the free energies for the formation of ion pairs of bolaform 1-2-1 X in the gas phase were calculated as X = Cl^- -158.0, Br^- -150.8, and Γ^- -142.6 kcal mol⁻¹. These values give the estimated ratio between Br^- and Γ^- as $\frac{E_{\text{Br}^-}}{E_{\Gamma^-}} = 1.06$, and between Cl^- and Br^- as $\frac{E_{\text{Cl}^-}}{E_{\text{Br}^-}} = 1.05$.

Table VII-3. Distances $\text{X}^- \text{-N}^+$ in crystal structure for n-2-n gemini with three halide counterions: Γ^- , Br^- , Cl^- .

Object1	Object2	$\Gamma^- \text{-N}^+$ for 10-2-10 Γ^- , Å	$\text{Br}^- \text{-N}^+$ for 10-2-10 Br^- , Å	Object1	Object2	$\text{Cl}^- \text{-N}^+$ for 14-2-14 Cl^- , Å
1	N	4.364	4.139	1	N	3.945
1	N*	4.534	4.334	1	N#	4.218
1	N#	4.597	4.395	1	N*	4.440
2	N'	4.364	4.139	2	N*	3.860
2	N#	4.534	4.334	2	N'	4.271
2	N*	4.597	4.395	2	N''	4.391

The very good agreement for the estimation of the cation-anion interaction in the crystals estimated above and the ion-pair free energy obtained by the DFT calculations is remarkable and gives strong evidence that n-2-n gemini molecules have stronger crystallinity in the presence of smaller anions. The ion sizes of Cl^- , Br^- and Γ^- are 1.81 Å, 1.96 Å and 2.20 Å respectively[30].

This observation is also in agreement with the melting temperature of 14-2-14 gemini which increases in the order, $\Gamma^- < \text{Br}^- < \text{Cl}^-$ as we reported previously[200].

Comparing the quaternary and tertiary ammonium gemini, we can see that for 10-2-10 ter Br^- each counterion strongly bounded to the respective nitrogen of the headgroup with hydrogen bond, the distance $\text{X}^- \text{-N}^+$ is 3.187 Å.

2. Conclusions

We have demonstrated the impact of the counterion nature on the crystalline structures of cationic gemini surfactant molecules, n-2-n (n = 10, 14, 16). A number of inter- and intra-molecular forces, such as Columbic forces, van der Waals interactions, hydrogen bonding and steric effect play important roles cooperatively and determines the molecular conformation of gemini surfactants and their packing. It was shown that the crystalline structures of gemini surfactants are roughly classified in two conformations: gauche and anti-gauche. In general, gemini n-2-n with halide counterions crystallize in gauche conformation when they are either crystallized from water or when water molecules are co-crystallized, for other cases, anti-gauche conformation energetically preferable even with solvent in the crystal structure.

We also characterized the strength of association between monoatomic counterions and positively charged nitrogens of the headgroups through distances between them. The distance for the halides follows the trend $\text{I}^- > \text{Br}^- > \text{Cl}^-$, inversely correlated to the strength of the headgroup-counterion association. Indeed, in a crystalline ordering, more hydrophilic counterions with smaller radii have stronger electrostatic interactions with the surrounding ammonium atoms than the more hydrophobic ones. Important to note, that in aqueous solution, when the molecules self-assemble into micelles, we see the opposite trend. In previous chapters we showed that Cl^- ion being the most hydrated, associate less with the interface of the micelle, where as I^- make the strong ion pairing with headgroups due to its high hydrophobicity. We demonstrated that in solution the hydration free energy of the counterion has the biggest impact on the properties of surfactant, whereas in crystals the size of an ion is the determining factor.

Finally, it was shown that for the tertiary gemini surfactants formed hydrogen bonds between the headgroup and counterion are crucial for its behavior in solid as well as liquid states (as was shown in other chapters).

3. Experimental section

3.1. Preparation of the single crystals

Single crystals of gemini 10-2-10 I, 10-2-10 Br and 14-2-14 Cl were grown from the saturated acetonitrile solution (40, 50 and 2 mg per 0.5, 0.5 and 0.25 mL respectively) by heating up (60 °C) and cooling to the room temperature and further slow evaporation until crystals would be observed. For 14-2-14 Cl evaporation was avoided in order to decrease the contact between compound and atmospheric water. Might be important to note, that for 14-2-14 Cl, a very small amount of compound was not soluble, which could favor crystals growth.

Using the same procedure single crystals were obtained from nitromethane. Note that for 14-2-14 Cl stepwise cooling from 40 to 20 °C was performed by 1 °C per day. Temperature control was done by thermostat.

Single crystals of 10-2-10 I also were obtained from H₂O by heating a C = 5 mM solution up to 60 °C and cooling it down to r. t. After few days thin needlelike crystals were formed.

Crystals of 14-2-14 Br and 16-2-16 I were obtained from vapor diffusion of acetone in saturated MeOH solution.

3.2. X-ray single-crystal diffraction.

Crystallographic data of compounds were collected with different diffractometers with a monochromatic Cu-K α radiation ($\lambda = 1.54190 \text{ \AA}$):

- (i) a FR-X Rigaku diffractometer with rotating anode, Varimax optics and a Dectris Pilatus 200K detector
- (ii) a R-Axis Rapid Rigaku MSC diffractometer with rotating anode, Varimax optics and a curved image plate detector
- (iii) a Proteum Bruker diffractometer with rotating anode, Helios optics and a Platinum CCD camera

The unit cell determination and data reduction were performed using the Crystal Clear program suite[206] or Proteum2 program suite on the full set of data. The structure was solved by direct methods and refined using Shelx 97 suite of programs[207] in the integrated WinGX system[208]. The positions of the H atoms were deduced from coordinates of the non-H atoms and

confirmed by Fourier synthesis. The non-H atoms were refined with anisotropic temperature parameters. H atoms were included for structure factor calculations but not refined.

- General conclusions -

In this work we focused on the investigation of ion specific effects on the self-assembly of cationic surfactants. We studied the effect of various counterions on the self-organization features of cationic surfactants in aqueous solution. In order to obtain a more comprehensive understanding of the effect of interfacial ionic and molecular interactions on aggregate properties, we used different approaches. Combining the investigation of physical properties of the molecular assemblies at the bulk solution level and determining interfacial water and counterion concentrations by experiment (chemical trapping) and by simulation (molecular dynamics), we demonstrated that the properties of micellar assemblies strongly depend on the type of monoatomic or polyatomic counter-anion present in solution.

- In the first Chapter we present a literature review on amphiphile molecules and their self-assembly properties into micelles in aqueous solution. In order to elucidate how counterions of the ionic surfactants can affect their micellization, we introduce ion specific effects also known as Hofmeister effects. From a historical perspective we can see how all the attempts to describe the interactions involved in Hofmeister effects by simplified theories have their limitations. Introduction of new forces that might be responsible for ion specificity was done almost every decade however there is still no general agreement as to which forces and ion properties drive the ion specific effects. Summarizing all knowledge obtained so far, it is safe to say that in addition to electrostatic and dispersion forces, one should also take into account the hydration forces that play a significant role in ion specificity.
- In Chapter II, we introduce the cationic gemini surfactants and counterions that are investigated in this study. We give the synthetic procedures used to obtain cationic surfactants with a variety of counterions.
- In Chapter III, the physical properties of the micellar solution are studied. We demonstrate how the critical micelle concentration, CMC, ionization degree and free energy of micellization of the surfactants 1) strongly depend on the ion properties such as size, polarizability, hydration free energy, hydration number, pKa of conjugated acid and lyotropic number of the counterions; 2) follow the Hofmeister series. On the contrary, the aggregation number of the micelles did not show a strong dependence on the counterion

nature. The correlation between the ion properties and the properties of aggregation showed that for monoatomic halides, the CMC depends monotonously on all these properties. In contrast, the polyatomic anions have a more complex behavior. We found that all properties of the ion influence the CMC values; however, the hydration free energy of the ions has the most obvious impact to the micellization behavior. Moreover, classifying anions according to their hydrophobic/hydrophilic properties, we see that: surfactants associated with more hydrophobic counterions, having a lower ionization degree, favor surfactant micellization. Whereas, surfactants with hydrophilic counterions, having high ionization degree, disfavor the formation of aggregates.

We also demonstrated that by changing the properties of the headgroup, we can significantly affect the order of the Hofmeister series and hence the interactions responsible for ion specific effects.

- The experimental investigation of the interfacial properties of the micelles was done by a probing technique called chemical trapping, as discussed in the Chapter IV. Using chemical trapping we demonstrated that poorly hydrated counterions are strongly associated with the headgroup and are located primary at the interfacial region of the micelle. On the other hand, the interfacial concentration of highly hydrated ions is a low and indicates low degree of counterion-headgroup binding. These results are in a good agreement with micellar physical properties in bulk solution.
- In Chapter V we introduce a computational approach based on molecular dynamic (MD) simulations applied to study the structural properties of the micelles at the atomic level. First of all, the MD simulations were used as a computational approach to investigate interfacial properties of the micelles. We found that the obtained results are coherent with the experimental results obtained by chemical trapping: the hydrophobic ions tend to associate strongly with the micelle and are primarily located in the vicinity of the headgroups forming contact ion pairs. Hydrophilic counterions, having stronger association with water, interact less with the headgroups of the micelle. In addition, it was demonstrated that anion nature affects the structural properties such as compactness, roughness and sphericity of the micelles. The micelle

with hydrophobic anions was most stabilized and least with hydrophilic anions. Moreover, we clearly showed that alkyl carboxylate counterions with increasing chain length start to penetrate the micellar hydrophobic core.

It is interesting to note that although the polarizability of the ions was not considered in the MD simulations, obtained results are in a good agreement with experimental observations.

- In Chapter VI we present a rheological study performed for wormlike micellar systems. We investigated the bulk properties of gemini having various counterions at much higher concentrations, where they form a network of entangled micelles. It was shown that the nature of the counterions strongly affects micellar growth and exhibits a similar tendency (following Hofmeister series) as was shown for spherical micelles. The hydrophobic counterions, due to their association with the headgroups, screen the micellar charge, thus favoring their growth, whereas hydrophilic ions screen micellar charge to a lower extent and exhibit micellar growth at much higher concentrations. Similarly to the CMC, the observed increase in viscosity of the system attributed to micellar growth, could be correlated with hydration free energy of anion.
- In the last Chapter, we consider the impact of the counterion nature on the crystalline structures of gemini surfactants. It was found that, contrarily to the aqueous solution, where the hydration of anions plays the crucial role, in crystals, the anions with smaller radii show a stronger association with the cationic headgroups.

Summarizing the results obtained by different approaches, we found that the ion specific effects which determine the behavior of micellar aggregates in aqueous solution strongly depend on the hydrophilic/hydrophobic properties (free energy of hydration) of the ion. It is interesting to note that the polarizability of the ions, which provides information of the dispersion forces and thus on ion specificity, seems to correlate less with the aggregation properties. Contrarily, the free energy of hydration of the ion, correlates very well with properties of surfactant aggregates. These results strongly suggest that ion hydration free energy can provide information about the ion specific effects in aqueous solution. However, note that the properties of the substrate should be taken into account not less carefully in order to predict Hofmeister effects.

- Perspectives -

The present study was focused on the fundamental century-old challenge concerning ion specificity. Our results confirmed that the properties of the cationic surfactants with soft methylated headgroups associated with different counterions follow the order in Hofmeister series. However, our preliminary observations concerning tertiary ammonium surfactants, demonstrate that slight changes in the properties of the headgroups, particularly replacement of one methyl group by a proton, resulted in the appearance new interactions that strongly changed the self-assembly of surfactants and hence the impact of counterions.

Having a comprehensive description of the ion specificity for quaternary gemini surfactants, future work can focus on a more global investigation of the systems involving the same anions but different headgroups. More work should therefore be done on tertiary ammonium surfactants in order to understand how changing the softness of the headgroup as well as introducing hydrogen bonding would influence ion specific effects. Moreover, secondary ammonium or even headgroup with another molecular structure should be investigated.

As was shown, the combination of different approaches allows to get an insight into the interactions between counterion and substrate at a molecular level. Applying different techniques, which study the system at different levels, one can obtain a better understanding of its properties and behavior. Such an approach can provide an absolutely new view on many challenges in science including ion specific effects.

– References –

1. Rosen, M.J., *Characteristic Features of Surfactants*, in *Surfactants and Interfacial Phenomena*. 2004, John Wiley & Sons, Inc. p. 1-33.
2. Romsted, L.S., *Surfactant Science and Technology: Retrospects and Prospects*. 2014: Taylor & Francis.
3. Sorrenti, A., O. Illa, and R.M. Ortuno, *Amphiphiles in aqueous solution: well beyond a soap bubble*. *Chemical Society Reviews*, 2013. **42**(21): p. 8200-8219.
4. Tanford, C., *The hydrophobic effect: formation of micelles and biological membranes*. 1973, New York: Wiley.
5. Tanford, C., *Theory of micelle formation in aqueous solutions*. *The Journal of Physical Chemistry*, 1974. **78**(24): p. 2469-2479.
6. Israelachvili, J.N., *Intermolecular and Surface Forces*. 2010: Elsevier Science.
7. Israelachvili, J.N., D.J. Mitchell, and B.W. Ninham, *Theory of self-assembly of hydrocarbon amphiphiles into micelles and bilayers*. *Journal of the Chemical Society, Faraday Transactions 2: Molecular and Chemical Physics*, 1976. **72**(0): p. 1525-1568.
8. Ramanathan, M., et al., *Amphiphile nanoarchitectonics: from basic physical chemistry to advanced applications*. *Physical Chemistry Chemical Physics*, 2013. **15**(26): p. 10580-10611.
9. Debye, P., *Note on light scattering in soap solutions*. *Journal of Colloid Science*, 1948. **3**(4): p. 407-409.
10. Debye, P., *Light Scattering in Soap Solutions*. *The Journal of Physical and Colloid Chemistry*, 1949. **53**(1): p. 1-8.
11. Ooshika, Y., *A theory of critical micelle concentration of colloidal electrolyte solutions*. *Journal of Colloid Science*, 1954. **9**(3): p. 254-262.
12. Reich, I., *Factors Responsible for the Stability of Detergent Micelles*. *The Journal of Physical Chemistry*, 1956. **60**(3): p. 257-262.
13. Halsey, G.D., *On the Structure of Micelles*. *The Journal of Physical Chemistry*, 1953. **57**(1): p. 87-89.
14. Hoeve, C.A.J. and G.C. Benson, *On the Statistical Mechanical Theory of Micelle Formation in Detergent Solutions*. *The Journal of Physical Chemistry*, 1957. **61**(9): p. 1149-1158.
15. Poland, D.C. and H.A. Scheraga, *Hydrophobic bonding and micelle stability; the influence of ionic head groups*. *Journal of Colloid and Interface Science*, 1966. **21**(3): p. 273-283.
16. Nagarajan, R. and E. Ruckenstein, *Theory of surfactant self-assembly: a predictive molecular thermodynamic approach*. *Langmuir*, 1991. **7**(12): p. 2934-2969.
17. Zana, R. and J. Xia, *Gemini Surfactants: Synthesis, Interfacial and Solution-Phase Behavior, and Applications*. *Surfactant Science*. Vol. 117. 2004, New York: Marcel Dekker.
18. Menger, F.M. and J.S. Keiper, *Gemini Surfactants*. *Angewandte Chemie International Edition*, 2000. **39**(11): p. 1906-1920.

19. Camesano, T.A. and R. Nagarajan, *Micelle formation and CMC of gemini surfactants: a thermodynamic model*. Colloids and Surfaces A: Physicochemical and Engineering Aspects, 2000. **167**(1–2): p. 165-177.
20. Hofmeister, F., *Zur Lehre von der Wirkung der Salze*. Arch. Exp. Path. Pharmacol., 1888. **24**: p. 247-260.
21. Kunz, W., P. Lo Nostro, and B.W. Ninham, *Specific ion effects in colloidal and biological systems*. Current Opinion in Colloid & Interface Science, 2010. **15**(1–2): p. 34-39.
22. Poiseuille, J., *Sur le mouvement des liquides de nature très différente dans les tubes de très petits diamètres*. Ann Chim Phys, 1847. **21**: p. 76-110.
23. Salis, A. and B.W. Ninham, *Models and mechanisms of Hofmeister effects in electrolyte solutions, and colloid and protein systems revisited*. Chemical Society Reviews, 2014. **43**(21): p. 7358-7377.
24. Kunz, W., *Specific Ion Effects*. 2010: World Scientific Publishing Company.
25. Pegram, L.M. and M.T. Record, *Hofmeister Salt Effects on Surface Tension Arise from Partitioning of Anions and Cations between Bulk Water and the Air–Water Interface*. The Journal of Physical Chemistry B, 2007. **111**(19): p. 5411-5417.
26. Weissenborn, P.K. and R.J. Pugh, *Surface Tension and Bubble Coalescence Phenomena of Aqueous Solutions of Electrolytes*. Langmuir, 1995. **11**(5): p. 1422-1426.
27. Robertson, B.T., *Contributions to the Theory of the Mode of Action of Inorganic Salts upon Proteins in Solution*. The Journal of Biological Chemistry, 1911. **9**(3): p. 303-326.
28. Loeb, J., *THE PROTEINS AND COLLOID CHEMISTRY*. Science, 1920. **52**(1350): p. 449-456.
29. Adamson, A., *A textbook of physical chemistry*. 2012: Elsevier Science.
30. Yitzhak, M., *Ion Properties*. 1997: New York : Marcel Dekker.
31. Jones, G. and M. Dole, *THE VISCOSITY OF AQUEOUS SOLUTIONS OF STRONG ELECTROLYTES WITH SPECIAL REFERENCE TO BARIUM CHLORIDE*. Journal of the American Chemical Society, 1929. **51**(10): p. 2950-2964.
32. Cox, W.M. and J.H. Wolfenden, *The Viscosity of Strong Electrolytes Measured by a Differential Method*. Proceedings of the Royal Society of London A: Mathematical, Physical and Engineering Sciences, 1934. **145**(855): p. 475-488.
33. Marcus, Y., *Effect of Ions on the Structure of Water: Structure Making and Breaking*. Chemical Reviews, 2009. **109**(3): p. 1346-1370.
34. Jenkins, H.D.B. and Y. Marcus, *Viscosity B-Coefficients of Ions in Solution*. Chemical Reviews, 1995. **95**(8): p. 2695-2724.
35. Gurney, R.W., *Ionic processes in solution*. 1953: McGraw-Hill.
36. Collins, K.D., G.W. Neilson, and J.E. Enderby, *Ions in water: Characterizing the forces that control chemical processes and biological structure*. Biophysical Chemistry, 2007. **128**(2–3): p. 95-104.
37. Smith, J.D., R.J. Saykally, and P.L. Geissler, *The Effects of Dissolved Halide Anions on Hydrogen Bonding in Liquid Water*. Journal of the American Chemical Society, 2007. **129**(45): p. 13847-13856.

38. Zhang, Y. and P.S. Cremer, *Interactions between macromolecules and ions: the Hofmeister series*. Current Opinion in Chemical Biology, 2006. **10**(6): p. 658-663.
39. Sala, J., E. Guardia, and J. Marti, *Specific ion effects in aqueous electrolyte solutions confined within graphene sheets at the nanometric scale*. Physical Chemistry Chemical Physics, 2012. **14**(30): p. 10799-10808.
40. Barthel, J., H. Krienke, and W. Kunz, *Physical Chemistry of Electrolyte Solutions: Modern Aspects*. 1998: U.S. Government Printing Office.
41. Berry, R.S., S.A. Rice, and J. Ross, *Physical Chemistry*. 2000: Oxford University Press.
42. Ninham, B.W. and P.L. Nostro, *Molecular Forces and Self Assembly: In Colloid, Nano Sciences and Biology*. 2010: Cambridge University Press.
43. Wang, Z.-G., *Fluctuation in electrolyte solutions: The self energy*. Physical Review E, 2010. **81**(2): p. 021501.
44. Wang, R. and Z.-G. Wang, *Effects of image charges on double layer structure and forces*. The Journal of Chemical Physics, 2013. **139**(12): p. 124702.
45. Boström, M. and B.W. Ninham, *Dispersion Self-Free Energies and Interaction Free Energies of Finite-Sized Ions in Salt Solutions*. Langmuir, 2004. **20**(18): p. 7569-7574.
46. Boström, M. and B.W. Ninham, *Contributions from Dispersion and Born Self-Free Energies to the Solvation Energies of Salt Solutions*. The Journal of Physical Chemistry B, 2004. **108**(33): p. 12593-12595.
47. Rashin, A.A. and B. Honig, *Reevaluation of the Born model of ion hydration*. The Journal of Physical Chemistry, 1985. **89**(26): p. 5588-5593.
48. MacDonald, J.R., *Comparison and discussion of some theories of the equilibrium electrical double layer in liquid electrolytes*. Journal of Electroanalytical Chemistry and Interfacial Electrochemistry, 1987. **223**(1–2): p. 1-23.
49. Grahame, D.C., *The Electrical Double Layer and the Theory of Electrocapillarity*. Chemical Reviews, 1947. **41**(3): p. 441-501.
50. Bockris, J.O., et al., *On the Structure of Charged Interfaces*. Proceedings of the Royal Society of London A: Mathematical, Physical and Engineering Sciences, 1963. **274**(1356): p. 55-79.
51. Burt, R., G. Birkett, and X.S. Zhao, *A review of molecular modelling of electric double layer capacitors*. Physical Chemistry Chemical Physics, 2014. **16**(14): p. 6519-6538.
52. Ninham, B.W. and V.A. Parsegian, *Electrostatic potential between surfaces bearing ionizable groups in ionic equilibrium with physiologic saline solution*. Journal of Theoretical Biology, 1971. **31**(3): p. 405-428.
53. Parsons, R., *The electrical double layer: recent experimental and theoretical developments*. Chemical Reviews, 1990. **90**(5): p. 813-826.
54. Derjaguin, B. and L. Landau, *Theory of the stability of strongly charged lyophobic sols and of the adhesion of strongly charged particles in solutions of electrolytes*. Progress in Surface Science, 1993. **43**(1–4): p. 30-59.
55. Verwey, E.J.W. and J.T.G. Overbeek, *Theory of the stability of lyophobic colloids*. 1948, Amsterdam: Elsevier.

56. Pashley, R.M., et al., *Direct measurements of surface forces between bilayers of double-chained quaternary ammonium acetate and bromide surfactants*. The Journal of Physical Chemistry, 1986. **90**(8): p. 1637-1642.
57. Tsao, Y.H., et al., *Osmotic stress measurements of dihexadecyldimethylammonium acetate bilayers as a function of temperature and added salt*. Langmuir, 1993. **9**(1): p. 233-241.
58. Shubin, V.E. and P. Kékicheff, *Electrical Double Layer Structure Revisited via a Surface Force Apparatus: Mica Interfaces in Lithium Nitrate Solutions*. Journal of Colloid and Interface Science, 1993. **155**(1): p. 108-123.
59. Israelachvili, J.N. and R.M. Pashley, *Measurement of the hydrophobic interaction between two hydrophobic surfaces in aqueous electrolyte solutions*. Journal of Colloid and Interface Science, 1984. **98**(2): p. 500-514.
60. Ninham, B.W. and D.F. Evans, *The Rideal Lecture. Vesicles and molecular forces*. Faraday Discussions of the Chemical Society, 1986. **81**(0): p. 1-17.
61. Dzyaloshinskii, I.E., E.M. Lifshitz, and L.P. Pitaevskii, *The general theory of van der Waals forces*. Advances in Physics, 1961. **10**(38): p. 165-209.
62. Kunz, W., P. Lo Nostro, and B.W. Ninham, *The present state of affairs with Hofmeister effects*. Current Opinion in Colloid & Interface Science, 2004. **9**(1–2): p. 1-18.
63. Ninham, B.W. and V. Yaminsky, *Ion Binding and Ion Specificity: The Hofmeister Effect and Onsager and Lifshitz Theories*. Langmuir, 1997. **13**(7): p. 2097-2108.
64. Boström, M., D.R.M. Williams, and B.W. Ninham, *Surface Tension of Electrolytes: Specific Ion Effects Explained by Dispersion Forces*. Langmuir, 2001. **17**(15): p. 4475-4478.
65. Boström, M., D.R.M. Williams, and B.W. Ninham, *Ion Specificity of Micelles Explained by Ionic Dispersion Forces*. Langmuir, 2002. **18**(16): p. 6010-6014.
66. Boström, M., D.R.M. Williams, and B.W. Ninham, *The Influence of Ionic Dispersion Potentials on Counterion Condensation on Polyelectrolytes*. The Journal of Physical Chemistry B, 2002. **106**(32): p. 7908-7912.
67. Collins, K.D., *Why continuum electrostatics theories cannot explain biological structure, polyelectrolytes or ionic strength effects in ion–protein interactions*. Biophysical Chemistry, 2012. **167**(0): p. 43-59.
68. Jungwirth, P. and D.J. Tobias, *Specific Ion Effects at the Air/Water Interface*. Chemical Reviews, 2006. **106**(4): p. 1259-1281.
69. Lund, M., R. Vacha, and P. Jungwirth, *Specific Ion Binding to Macromolecules: Effects of Hydrophobicity and Ion Pairing*. Langmuir, 2008. **24**(7): p. 3387-3391.
70. Mason, P.E., et al., *Specificity of Ion–Protein Interactions: Complementary and Competitive Effects of Tetrapropylammonium, Guanidinium, Sulfate, and Chloride Ions*. The Journal of Physical Chemistry B, 2009. **113**(10): p. 3227-3234.
71. Horinek, D., S.I. Mamatkulov, and R.R. Netz, *Rational design of ion force fields based on thermodynamic solvation properties*. J. Chem. Phys., 2009. **130**: p. 124507.
72. Lund, M., L. Vrbka, and P. Jungwirth, *Specific Ion Binding to Nonpolar Surface Patches of Proteins*. Journal of the American Chemical Society, 2008. **130**(35): p. 11582-11583.
73. Vlachy, N., et al., *Hofmeister series and specific interactions of charged headgroups with aqueous ions*. Advances in Colloid and Interface Science, 2009. **146**(1–2): p. 42-47.

74. Yang, Z., *Hofmeister effects: an explanation for the impact of ionic liquids on biocatalysis*. Journal of Biotechnology, 2009. **144**(1): p. 12-22.
75. Paterová, J., et al., *Reversal of the Hofmeister Series: Specific Ion Effects on Peptides*. The Journal of Physical Chemistry B, 2013. **117**(27): p. 8150-8158.
76. Vrbka, L., et al., *Specific Ion Effects at Protein Surfaces: A Molecular Dynamics Study of Bovine Pancreatic Trypsin Inhibitor and Horseradish Peroxidase in Selected Salt Solutions*. The Journal of Physical Chemistry B, 2006. **110**(13): p. 7036-7043.
77. Collins, K.D., *Ions from the Hofmeister series and osmolytes: effects on proteins in solution and in the crystallization process*. Methods, 2004. **34**(3): p. 300-311.
78. Vrbka, L., et al., *Quantification and rationalization of the higher affinity of sodium over potassium to protein surfaces*. Proceedings of the National Academy of Sciences, 2006. **103**(42): p. 15440-15444.
79. Jungwirth, P. and B. Winter, *Ions at Aqueous Interfaces: From Water Surface to Hydrated Proteins*. Annual Review of Physical Chemistry, 2008. **59**(1): p. 343-366.
80. Leontidis, E., et al., *Effects of Monovalent Anions of the Hofmeister Series on DPPC Lipid Bilayers Part II: Modeling the Perpendicular and Lateral Equation-of-State*. Biophysical Journal, 2007. **93**(5): p. 1591-1607.
81. Ruckenstein, E. and H. Huang, *Specific ion effects on double layer forces through ion hydration*. Colloids and Surfaces A: Physicochemical and Engineering Aspects, 2014. **459**(0): p. 151-156.
82. Song, J., et al., *Ion specific effects: decoupling ion-ion and ion-water interactions*. Physical Chemistry Chemical Physics, 2015. **17**(13): p. 8306-8322.
83. Willott, J.D., et al., *Anion-Specific Effects on the Behavior of pH-Sensitive Polybasic Brushes*. Langmuir, 2015. **31**(12): p. 3707-3717.
84. Lima, F.S., et al., *Effect of Counterions on the Shape, Hydration, and Degree of Order at the Interface of Cationic Micelles: The Triflate Case*. Langmuir, 2013. **29**(13): p. 4193-4203.
85. Alkschbirs, M.I., et al., *Effects of some anions of the Hofmeister series on the rheology of cetyltrimethylammonium-salicylate wormlike micelles*. Colloids and Surfaces A: Physicochemical and Engineering Aspects, 2015. **470**(0): p. 1-7.
86. Zana, R., *Surfactant solutions: new methods of investigation*. 1987: M. Dekker.
87. Edlund, H., A. Sadaghiani, and A. Khan, *Phase Behavior and Phase Structure for Catanionic Surfactant Mixtures: Dodecyltrimethylammonium Chloride–Sodium Nonanoate–Water System*. Langmuir, 1997. **13**(19): p. 4953-4963.
88. Koehler, R.D., S.R. Raghavan, and E.W. Kaler, *Microstructure and Dynamics of Wormlike Micellar Solutions Formed by Mixing Cationic and Anionic Surfactants*. The Journal of Physical Chemistry B, 2000. **104**(47): p. 11035-11044.
89. Oelschlaeger, C., et al., *Synergistic effects in mixed wormlike micelles of dimeric and single-chain cationic surfactants at high ionic strength*. Eur. Phys. J. E, 2003. **11**(1): p. 7-20.
90. Manet, S., et al., *Counteranion Effect on Micellization of Cationic Gemini Surfactants 14-2-14: Hofmeister and Other Counterions*. Langmuir, 2010. **26**(13): p. 10645–10656.
91. Mittal, K.L. and H.R. Anderson, *Acid-Base Interactions: Relevance to Adhesion Science and Technology*. 1991: Taylor & Francis.

92. Williams, R.J., J.N. Phillips, and K.J. Mysels, *The critical micelle concentration of sodium lauryl sulphate at 25° C*. Trans. Faraday Soc., 1955. **51**: p. 728-737.
93. Fujiwara, M., et al., *A temperature study on critical micellization concentration (CMC), solubility, and degree of counterion binding of α -sulfonatomyristic acid methyl ester in water by electroconductivity measurements*. Colloid and Polymer Science, 1997. **275**(5): p. 474-479.
94. Garcia-Mateos, I., M. Mercedes Velazquez, and L.J. Rodriguez, *Critical micelle concentration determination in binary mixtures of ionic surfactants by deconvolution of conductivity/concentration curves*. Langmuir, 1990. **6**(6): p. 1078-1083.
95. Manabe, M., et al., *Effect of alkanols on intermicellar concentration and on ionization of micelles*. Journal of Colloid and Interface Science, 1987. **115**(1): p. 147-154.
96. Pérez-Rodríguez, M., et al., *A Comparative Study of the Determination of the Critical Micelle Concentration by Conductivity and Dielectric Constant Measurements*. Langmuir, 1998. **14**(16): p. 4422-4426.
97. Carpena, P., et al., *Problems Associated with the Treatment of Conductivity–Concentration Data in Surfactant Solutions: Simulations and Experiments*. Langmuir, 2002. **18**(16): p. 6054-6058.
98. Galgano, P.D. and O.A. El Seoud, *Micellar properties of surface active ionic liquids: A comparison of 1-hexadecyl-3-methylimidazolium chloride with structurally related cationic surfactants*. Journal of Colloid and Interface Science, 2010. **345**(1): p. 1-11.
99. Kumar, B., et al., *Effect of short chain length alcohols on micellization behavior of cationic gemini and monomeric surfactants*. Journal of Molecular Liquids, 2012. **172**(0): p. 81-87.
100. Sugihara, G., et al., *An electroconductivity study on degree of counterion binding or dissociation of α -sulfonatomyristic acid methyl ester micelles in water as a function of temperature*. Colloid and Polymer Science, 1997. **275**(8): p. 790-796.
101. Evans, H.C., *Alkyl Sulphates. Part I. Critical Micelle Concentrations of the Sodium Salts*. J. Chem. Soc., 1956: p. 579-586.
102. Shanks, P.C. and E.I. Franses, *Estimation of micellization parameters of aqueous sodium dodecyl sulfate from conductivity data*. The Journal of Physical Chemistry, 1992. **96**(4): p. 1794-1805.
103. Zana, R., *Critical Micellization Concentration of Surfactants in Aqueous Solution and Free Energy of Micellization*. Langmuir, 1996. **12**(5): p. 1208-1211.
104. Morris, D.F.C., *Lyotropic numbers of the formate and acetate ions and related thermodynamic properties*. Recueil des Travaux Chimiques des Pays-Bas, 1959. **78**(3): p. 150-160.
105. Marcus, Y., *Ions in Water and Biophysical Implications: From Chaos to Cosmos*. 2014: Springer Netherlands.
106. Voet, A., *Quantative Lyotropy*. Chemical Reviews, 1937. **20**(2): p. 169-179.
107. Huc, I. and R. Oda, *Gemini surfactants: studying micellisation by ^1H and ^{19}F NMR spectroscopy*. Chemical Communications, 1999(20): p. 2025-2026.
108. Clint, J.H., *Surfactant Aggregation*. 1992: Blackie.

109. Li, X., et al., *Dynamic and Static Light Scattering Studies on Self-Aggregation Behavior of Biodegradable Amphiphilic Poly(ethylene oxide)–Poly[(R)-3-hydroxybutyrate]–Poly(ethylene oxide) Triblock Copolymers in Aqueous Solution*. The Journal of Physical Chemistry B, 2006. **110**(12): p. 5920-5926.
110. Debye, P. and E.W. Anacker, *Micelle Shape from Dissymmetry Measurements*. The Journal of Physical Chemistry, 1951. **55**(5): p. 644-655.
111. Yu, L., et al., *Determination of critical micelle concentrations and aggregation numbers by fluorescence correlation spectroscopy: Aggregation of a lipopolysaccharide*. Analytica Chimica Acta, 2006. **556**(1): p. 216-225.
112. Zana, R., *Dimeric (Gemini) Surfactants: Effect of the Spacer Group on the Association Behavior in Aqueous Solution*. Journal of Colloid and Interface Science, 2002. **248**(2): p. 203-220.
113. Barhoum, S. and A. Yethiraj, *An NMR study of macromolecular aggregation in a model polymer-surfactant solution*. The Journal of Chemical Physics, 2010. **132**(2): p. -.
114. Bales, B.L., et al., *Precision Relative Aggregation Number Determinations of SDS Micelles Using a Spin Probe. A Model of Micelle Surface Hydration*. The Journal of Physical Chemistry B, 1998. **102**(50): p. 10347-10358.
115. Alargova, R.G., et al., *Micelle Aggregation Numbers of Surfactants in Aqueous Solutions: A Comparison between the Results from Steady-State and Time-Resolved Fluorescence Quenching*. Langmuir, 1998. **14**(19): p. 5412-5418.
116. Wattebled, L., et al., *Aggregation Numbers of Cationic Oligomeric Surfactants: A Time-Resolved Fluorescence Quenching Study*. Langmuir, 2006. **22**(6): p. 2551-2557.
117. Wilk, K.A., et al., *Fluorescence probe studies upon microenvironment characteristics and aggregation properties of gemini sugar surfactants in an aquatic environment*. Journal of Photochemistry and Photobiology A: Chemistry, 2011. **219**(2–3): p. 204-210.
118. Reekmans, S., et al., *Change in the Micellar Aggregation Number or in the Size Distribution? A Dynamic Fluorescence Quenching Study of Aqueous Cetyltrimethylammonium Chloride*. Langmuir, 1993. **9**: p. 2289-2296.
119. Infelta, P.P., *Fluorescence quenching in micellar solutions and its application to the determination of aggregation numbers*. Chemical Physics Letters, 1979. **61**(1): p. 88-91.
120. Gehlen, M.H. and F.C. De Schryver, *Time-resolved fluorescence quenching in micellar assemblies*. Chemical Reviews, 1993. **93**(1): p. 199-221.
121. Infelta, P.P., M. Gratzel, and J.K. Thomas, *Luminescence decay of hydrophobic molecules solubilized in aqueous micellar systems. Kinetic model*. The Journal of Physical Chemistry, 1974. **78**(2): p. 190-195.
122. Tachiya, M., *Application of a generating function to reaction kinetics in micelles. Kinetics of quenching of luminescent probes in micelles*. Chemical Physics Letters, 1975. **33**(2): p. 289-292.
123. Boens, N., et al., *Simultaneous analysis of single-photon timing data with a reference method: Application to a poisson distribution of decay rates*. Chemical Physics, 1988. **121**(2): p. 199-209.

124. Singh, J., et al., *Aggregate Properties of Sodium Deoxycholate and Dimyristoylphosphatidylcholine Mixed Micelles*. The Journal of Physical Chemistry B, 2008. **112**(13): p. 3997-4008.
125. Phillips, J.N., *The energetics of micelle formation*. Transactions of the Faraday Society, 1955. **51**(0): p. 561-569.
126. DeLisi, R., S. Milioto, and R. Triolo, *Heat capacities, volumes and solubilities of pentanol in aqueous alkyltrimethylammonium bromides*. Journal of Solution Chemistry, 1988. **17**(7): p. 673-696.
127. Kalyanasundaram, K., *Photochemistry in Microheterogeneous Systems*. 2012: Elsevier Science.
128. Lide, D.R., *CRC Handbook of Chemistry and Physics, 85th Edition*. 2004: Taylor & Francis.
129. Coury, L., Current separations, 1999. **18**: p. 91-96.
130. Romsted, L.S., *Reactions and Synthesis in Surfactant Systems*. Surfactant Science (Book 100). 2001: J. Texter Ed.; Marcel Dekker: New York. 265-294.
131. Geng, Y., et al., *Origin of the Sphere-to-Rod Transition in Cationic Micelles with Aromatic Counterions: Specific Ion Hydration in the Interfacial Region Matters*. Langmuir, 2005. **21**(2): p. 562-568.
132. Geng, Y., L.S. Romsted, and F. Menger, *Specific Ion Pairing and Interfacial Hydration as Controlling Factors in Gemini Micelle Morphology. Chemical Trapping Studies*. Journal of the American Chemical Society, 2006. **128**(2): p. 492-501.
133. Menger, F.M., et al., *Interfacial Composition of Gemini Surfactant Micelles Determined by Chemical Trapping*. Langmuir, 2000. **16**(23): p. 9095-9098.
134. Texter, J., *Reactions And Synthesis In Surfactant Systems*. 2001: Taylor & Francis.
135. Galli, C., *Radical reactions of arenediazonium ions: An easy entry into the chemistry of the aryl radical*. Chemical Reviews, 1988. **88**(5): p. 765-792.
136. Szele, I. and H. Zollinger, *Dediazoniation of Arenediazonium Ions in Homogeneous Solution. Part XII. Solvent effects in competitive heterolytic and homolytic dediazoniations*. Helvetica Chimica Acta, 1978. **61**(5): p. 1721-1729.
137. Zollinger, H., *Diazo chemistry: aromatic and heteroaromatic compounds*. 1994: VCH.
138. Reichardt, C., *Solvents and Solvent Effects in Organic Chemistry*. 2006: Wiley.
139. Chaudhuri, A., et al., *Arenediazonium salts: new probes of the interfacial compositions of association colloids. I. Basic approach, methods, and illustrative applications*. Journal of the American Chemical Society, 1993. **115**(18): p. 8351-8361.
140. Jencks, W.P., *Ingold Lecture. How does a reaction choose its mechanism?* Chemical Society Reviews, 1981. **10**(3): p. 345-375.
141. Romsted, L.S., *Do Amphiphile Aggregate Morphologies and Interfacial Compositions Depend Primarily on Interfacial Hydration and Ion-Specific Interactions? The Evidence from Chemical Trapping*. Langmuir, 2007. **23**(2): p. 414-424.
142. Menger, F.M. and C.E. Portnoy, *Chemistry of reactions proceeding inside molecular aggregates*. Journal of the American Chemical Society, 1967. **89**(18): p. 4698-4703.
143. Bunton, C.A., et al., *Ion binding and reactivity at charged aqueous interfaces*. Accounts of Chemical Research, 1991. **24**(12): p. 357-364.

144. Cuccovia, I.M., et al., *New Method for Estimating the Degree of Ionization and Counterion Selectivity of Cetyltrimethylammonium Halide Micelles: Chemical Trapping of Free Counterions by a Water Soluble Arenediazonium Ion*. Langmuir, 1997. **13**(4): p. 647-652.
145. Soldi, V., et al., *Arenediazonium Salts: New Probes of the Interfacial Compositions of Association Colloids. 6. Relationships between Interfacial Counterion and Water Concentrations and Surfactant Headgroup Size, Sphere-to-Rod Transitions, and Chemical Reactivity in Cationic Micelles†*. Langmuir, 2000. **16**(1): p. 59-71.
146. Romsted, L.S. and J. Yao, *Arenediazonium Salts: New Probes of the Interfacial Compositions of Association Colloids. 4.1-3 Estimation of the Hydration Numbers of Aqueous Hexaethylene Glycol Monododecyl Ether, C12E6, Micelles by Chemical Trapping*. Langmuir, 1996. **12**(10): p. 2425-2432.
147. Lo Nostro, P. and B.W. Ninham, *Hofmeister Phenomena: An Update on Ion Specificity in Biology*. Chemical Reviews, 2012. **112**(4): p. 2286-2322.
148. Hegarty, A.F., in *The Chemistry of the Diazonium and Diazo Groups*, S. Patai, Editor. 1978, John Wiley & Sons: New York. p. 511-591.
149. Banerjee, R., P. Kumar Das, and A. Chaudhuri, *Interfacial indazolization: novel chemical evidence for remarkably high exo-surface pH of cationic liposomes used in gene transfection*. Biochimica et Biophysica Acta (BBA) - Biomembranes, 1998. **1373**(2): p. 299-308.
150. Allen, M.P. and D.J. Tildesley, *Computer simulation of liquids*. 1987: Clarendon press, Oxford.
151. Petrenko, R. and J. Meller, *Molecular Dynamics*, in *eLS*. 2001, John Wiley & Sons, Ltd.
152. Tian, P., *Molecular dynamics simulations of nanoparticles*. Annual Reports Section "C" (Physical Chemistry), 2008. **104**(0): p. 142-164.
153. van Gunsteren, W.F. and H.J.C. Berendsen, *Computer Simulation of Molecular Dynamics: Methodology, Applications, and Perspectives in Chemistry*. Angewandte Chemie International Edition in English, 1990. **29**(9): p. 992-1023.
154. Schwierz, N., D. Horinek, and R.R. Netz, *Reversed Anionic Hofmeister Series: The Interplay of Surface Charge and Surface Polarity*. Langmuir, 2010. **26**(10): p. 7370-7379.
155. Zhang, Y. and P.S. Cremer, *The inverse and direct Hofmeister series for lysozyme*. Proc Natl Acad Sci U S A, 2009. **106**(36): p. 15249-53.
156. Oda, R., et al., *Molecular Organization of Gemini Surfactants in Cylindrical Micelles: An Infrared Dichroism Spectroscopy and Molecular Dynamics Study*. Langmuir, 2002. **18**(25): p. 9659-9667.
157. Bruce, C.D., et al., *Molecular Dynamics Simulation of Sodium Dodecyl Sulfate Micelle in Water: Micellar Structural Characteristics and Counterion Distribution*. The Journal of Physical Chemistry B, 2002. **106**(15): p. 3788-3793.
158. Storm, S., et al., *Molecular Dynamics Simulation of SDS and CTAB Micellization and Prediction of Partition Equilibria with COSMOmic*. Langmuir, 2013. **29**: p. 11582-11592.
159. Schwierz, N., D. Horinek, and R.R. Netz, *Anionic and Cationic Hofmeister Effects on Hydrophobic and Hydrophilic Surfaces*. Langmuir, 2013. **29**(8): p. 2602-2614.
160. Marcus, Y., *Ionic radii in aqueous solutions*. Chemical Reviews, 1988. **88**(8): p. 1475-1498.

161. Jensen, K.P. and W.L. Jorgensen, *Halide, Ammonium, and Alkali Metal Ion Parameters for Modeling Aqueous Solutions*. Journal of Chemical Theory and Computation, 2006. **2**(6): p. 1499-1509.
162. Case, D.A., et al., *Amber12*. University of California, San Francisco, 2012.
163. Humphrey, W., A. Dalke, and K. Schulten, *VMD - Visual Molecular Dynamics*. J. of Molec. Graphics, 1996. **14**: p. 33-38.
164. <http://csb.stanford.edu/~koehl/ProShape/protsurf.php>.
165. Hess, B., et al., *GROMACS 4: Algorithms for Highly Efficient, Load-Balanced, and Scalable Molecular Simulation*. J. Chem. Theory Comput., 2008. **4**: p. 435-447.
166. <http://isaacs.sourceforge.net/phys/rdfs.html>.
167. Vanommeslaeghe, K. <http://mackerell.umaryland.edu/~kenno/cgenff/>.
168. Vanommeslaeghe, K., E.P. Raman, and A.D. MacKerell, *Automation of the CHARMM General Force Field (CGenFF) II: Assignment of Bonded Parameters and Partial Atomic Charges*. Journal of Chemical Information and Modeling, 2012. **52**(12): p. 3155-3168.
169. Evans, D.F., D.J. Mitchell, and B.W. Ninham, *Ion Binding and Dressed Micelles*. J. Phys. Chem., 1984. **88**: p. 6344-6348.
170. Gunnarsson, G., B. Joansson, and H. Wennerstroem, *Surfactant association into micelles. An electrostatic approach*. The Journal of Physical Chemistry, 1980. **84**(23): p. 3114-3121.
171. Bockris, J.O. and A.K.N. Reddy, *Modern Electrochemistry I*. Vol. 1. 1997: Plenum Press: New York.
172. Srinivasan, V. and D. Blankschtein, *Effect of Counterion Binding on Micellar Solution Behavior: 1. Molecular-Thermodynamic Theory of Micellization of Ionic Surfactants*. Langmuir, 2003. **19**: p. 9932-9945.
173. Jorgensen, W.L., D.S. Maxwell, and J. Tirado-Rives, *Development and Testing of the OPLS All-Atom Force Field on Conformational Energetics and Properties of Organic Liquids*. Journal of the American Chemical Society, 1996. **118**(45): p. 11225-11236.
174. Chen, J. and B.L. Trout, *Computational Study of Solvent Effects on the Molecular Self-Assembly of Tetrolic Acid in Solution and Implications for the Polymorph Formed from Crystallization*. J. Phys. Chem. B, 2008. **112**: p. 7794-7802.
175. MacKerell, A.D., et al., *All-Atom Empirical Potential for Molecular Modeling and Dynamics Studies of Proteins†*. The Journal of Physical Chemistry B, 1998. **102**(18): p. 3586-3616.
176. Klauda, J.B., et al., *Update of the CHARMM All-Atom Additive Force Field for Lipids: Validation on Six Lipid Types*. The Journal of Physical Chemistry B, 2010. **114**(23): p. 7830-7843.
177. Kim, J., et al., *Comparative ab initio study of the structures, energetics and spectra of $X^-(H_2O)_n=1-4$ [$X=F, Cl, Br, I$] clusters*. The Journal of Chemical Physics, 2000. **113**(13): p. 5259-5272.
178. Martínez, L., et al., *PACKMOL: A package for building initial configurations for molecular dynamics simulations*. Journal of Computational Chemistry, 2009. **30**(13): p. 2157-2164.
179. Feller, S.E., et al., *Constant pressure molecular dynamics simulation: The Langevin piston method*. J. Chem. Phys., 1995. **103**(11).

180. Roe, D.R. and T.E.C. Iii, *PTRAJ and CPPTRAJ: Software for Processing and Analysis of Molecular Dynamics Trajectory Data*. J. Chem. Theory Comput., 2013. **9**(7): p. 3084-3095.
181. Porte, G., J. Appell, and Y. Poggi, *Experimental investigations on the flexibility of elongated cetylpyridinium bromide micelles*. The Journal of Physical Chemistry, 1980. **84**(23): p. 3105-3110.
182. Imae, T. and S. Ikeda, *Sphere-rod transition of micelles of tetradecyltrimethylammonium halides in aqueous sodium halide solutions and flexibility and entanglement of long rodlike micelles*. The Journal of Physical Chemistry, 1986. **90**(21): p. 5216-5223.
183. Kern, F., et al., *Dynamic Properties of Salt-Free Viscoelastic Micellar Solutions*. Langmuir, 1994. **10**(6): p. 1714-1723.
184. Hassan, P.A., J. Narayanan, and C. Manohar, *Vesicles and worm-like micelles: Structure, dynamics and transformations*. Current Science, 2001. **80**(25): p. 980.
185. Rehage, H. and H. Hoffmann, *Viscoelastic surfactant solutions: model systems for rheological research*. Molecular Physics, 1991. **74**(5): p. 933-973.
186. Zana, R. and E.W. Kaler, *Giant Micelles: Properties and Applications*. 2007: CRC Press.
187. Mackintosh, F., S. Safran, and P. Pincus, *Equilibrium size distribution of charged 'living' polymers*. J. Phys.: Condens. Matter, 1990. **2**: p. 359-364.
188. Ying, Q. and B. Chu, *Overlap concentration of macromolecules in solution*. Macromolecules, 1987. **20**(2): p. 362-366.
189. Chu, Z., C.A. Dreiss, and Y. Feng, *Smart wormlike micelles*. Chemical Society Reviews, 2013. **42**(17): p. 7174-7203.
190. Mackintosh, F., S. Safran, and P. Pincus, *Self-Assembly of Linear Aggregates: the Effect of Electrostatics on Growth*. Europhys. Lett., 1990. **12**: p. 697-702.
191. Oda, R., et al., *Direct Evidence of the Shear-Induced Structure of Wormlike Micelles: Gemini Surfactant 12-2-12*. Langmuir, 1997. **13**(24): p. 6407-6412.
192. Cates, M.E., *Reptation of living polymers: dynamics of entangled polymers in the presence of reversible chain-scission reactions*. Macromolecules, 1987. **20**(9): p. 2289-2296.
193. Cates, M.E., *Theory of the Viscosity of Polymeric Liquid Sulfur*. Europhys. Lett., 1987. **4**: p. 497-502.
194. Cates, M.E., *Dynamics of living polymers and exible surfactant micelles : scaling laws for dilution*. J. Phys. France, 1988. **49**: p. 1593-1600.
195. Safran, S.A., et al., *Growth of charged micelles*. J. Phys. France, 1990. **51**(6): p. 503-510.
196. Oda, R., et al., *Effect of the Lipophilicity of the Counterion on the Viscoelasticity of Micellar Solutions of Cationic Surfactants*. Langmuir, 1998. **14**(16): p. 4364-4372.
197. Abezgauz, L., et al., *Effect of Hofmeister anions on micellization and micellar growth of the surfactant cetylpyridinium chloride*. Journal of Colloid and Interface Science, 2010. **342**(1): p. 83-92.
198. Macias, E.R., et al., *Effect of ionic strength on rheological behavior of polymer-like cetyltrimethylammonium tosylate micellar solutions*. Soft Matter, 2011. **7**(5): p. 2094-2102.
199. Oelschlaeger, C., P. Suwita, and N. Willenbacher, *Effect of Counterion Binding Efficiency on Structure and Dynamics of Wormlike Micelles*. Langmuir, 2010. **26**(10): p. 7045-7053.

200. Manet, S., et al., *Effect of Hofmeister and Alkylcarboxylate Anionic Counterions on the Krafft Temperature and Melting Temperature of Cationic Gemini Surfactants*. Langmuir, 2013. **29**(11): p. 3518-3526.
201. Wei, Z., et al., *Crystalline structures and mesomorphic properties of gemini diammonium surfactants with a pendant hydroxyl group*. Journal of Colloid and Interface Science, 2011. **354**(2): p. 677-685.
202. Berthier, D., et al., *From Chiral Counterions to Twisted Membranes*. Journal of the American Chemical Society, 2002. **124**(45): p. 13486-13494.
203. Hattori, N., et al., *Crystal structures of bis(quaternaryammonium bromide) surfactants, ethanediyl-1,2-bis(butyldimethylammonium bromide) dihydrate and propanediyl-1,3-bis(butyldimethylammonium bromide)*. Journal of Molecular Structure, 1998. **471**(1–3): p. 13-18.
204. Oda, R., et al., *Molecular Structure of Self-Assembled Chiral Nanoribbons and Nanotubules Revealed in the Hydrated State*. Journal of the American Chemical Society, 2008. **130**(44): p. 14705-14712.
205. Svensson, P.H., M. Gorlov, and L. Kloo, *Dimensional Caging of Polyiodides*. Inorganic Chemistry, 2008. **47**(24): p. 11464-11466.
206. Rigaku, *CrystalClear-SM Expert 2.1*. 2013: Tokyo, Japan.
207. Sheldrick, G., *A short history of SHELX*. Acta Crystallographica Section A, 2008. **64**(1): p. 112-122.
208. Farrugia, L.J., *WinGX suite for small-molecule single-crystal crystallography*. Journal of Applied Crystallography, 1999. **32**(4): p. 837-838.

La présente étude est une approche holistique axée sur l'étude des effets spécifiques d'ions sur les propriétés d'auto-assemblage de tensioactifs cationiques gemini. Notre objectif principal étant l'étude de l'effet de divers contre-ions sur les caractéristiques d'auto-assemblage de tensioactifs cationiques en solution aqueuse. Afin d'obtenir une vision plus complète de l'effet des interactions ioniques et moléculaires à l'interface sur les propriétés globales, nous avons utilisé des approches différentes. Nous avons combiné une étude expérimentale portant sur les propriétés en solution (concentration micellaire critique, degré d'ionisation, nombre d'agrégation, etc.), avec des approches centrées sur l'étude des propriétés micellaires interfaciales en analysant les concentrations des contre-ions et de l'eau de façon expérimentale (piégeage chimique) et informatique (simulations de dynamique moléculaire). En outre, nous avons étudié l'impact de la nature des contre-ions sur la croissance des micelles géantes par rhéologie. En plus de l'examen des propriétés de tensio-actifs en solution, les effets spécifiques d'ions sur les structures cristallines des agents tensioactifs gemini ont été étudiés.

Nous avons trouvé que les effets d'ions spécifiques qui déterminent le comportement des agrégats micellaires de gemini cationiques d'ammonium quaternaire dans des solutions aqueuses dépendent fortement de l'énergie libre d'hydratation des contre-ions, en d'autres termes, sur leur propriétés hydrophile / hydrophobe. Contrairement à la solution aqueuse, dans les cristaux, la taille de l'ion devient le facteur déterminant. La comparaison des résultats obtenus pour un même système en solution aqueuse et à l'état solide a montré l'importance des interactions ion-eau dans les effets spécifiques d'ions. Cependant, il faut noter que les propriétés du substrat (les gemini dans notre cas) doivent être prises en compte non moins soigneusement afin de prédire complètement les effets Hofmeister.

Mots-clés: effets spécifiques d'ions, auto-assemblage, tensioactifs gemini, micellisation, propriétés d'interface, piégeage chimique, simulations de dynamique moléculaire, rhéologie, micelles géantes, structure cristalline

The present study is a holistic approach focused on the investigation of ion specific effects on the self-assembly properties of cationic gemini surfactants. Our main focus was on the effect of various counterions on the self-organization features of cationic surfactants in aqueous solution. In order to obtain a more comprehensive understanding of the effect of interfacial ionic and molecular interactions on aggregate properties we used different approaches. We combined an experimental study focused on the bulk solution properties (critical micelle concentration, ionization degree, aggregation number, etc.), with approaches focused on investigating the interfacial micellar properties by analyzing the interfacial counterion and water concentrations, experimentally (chemical trapping) and computationally (molecular dynamic simulations). Moreover, the impact of counterion nature was investigated by studying the growth of wormlike micelles using rheology. Besides the examination of the surfactants properties in solution, the ion specific effects on the crystalline structures of gemini surfactants were studied.

We found that ion specific effects which determine the behavior of micellar aggregates of cationic quaternary ammonium gemini in aqueous solutions strongly depend on the free energy of hydration of the counterions, in others words, on their hydrophilic/hydrophobic properties. Contrarily to aqueous solution, in crystals, the size of the ion becomes the determining factor. Comparison of the results obtained for the same system in aqueous solution and in solid state showed the importance of ion-water interactions in ion specific effects. However, one should note that the properties of substrate (the gemini in our case) should be taken into account not less carefully in order to fully predict Hofmeister effects.

Keywords: ion specific effects, self-assembly, gemini surfactants, micellization, interfacial properties, chemical trapping, molecular dynamic simulations, rheology, wormlike micelles, crystal structure